DEVELOPMENT OF A KINETIC MODEL FOR STEERABLE CATHETERS FOR MINIMALLY INVASIVE SURGERY

A Thesis Submitted to the

College of Graduate Studies and Research

In Partial Fulfillment of the Requirements

For the Degree of Doctor of Philosophy

In the Division of Biomedical Engineering

University of Saskatchewan

Saskatoon

By

XIAOHUA HU

PERMISSION TO USE

In presenting this thesis in partial fulfillment of the requirements for a Postgraduate degree from the University of Saskatchewan, I agree that the Libraries of this University may make it freely available for inspection. I further agree that permission for copying of this thesis in any manner, in whole or in part, for scholarly purposes may be granted by the professor or professors who supervised my thesis work or, in their absence, by the Chair of the Division or the Dean of the College in which my thesis work was done. It is understood that any copying or publication or use of this thesis or parts thereof for financial gain shall not be allowed without my written permission. It is also understood that due recognition shall be given to me and to the University of Saskatchewan in any scholarly use which may be made of any material in my thesis.

Requests for permission to copy or to make other use of material in this thesis in whole or part should be addressed to:

Chair of the Division of Biomedical Engineering
University of Saskatchewan
57 Campus Drive
Saskatoon, Saskatchewan, S7N 5A9, Canada

ABSTRACT

The steerable catheters have demonstrated many advantages to overcome the limitations of the conventional catheters in the minimally invasive surgery. The motion and force transmission from the proximal end to distal tip of the catheter have significant effects to the efficiency and safety of surgery. While the force information between the catheter and the body (e.g., vessel) can be obtained by mounting sensors on the distal tip of the catheter, this would be more intrusive and less reliable than the one without the sensors, which is described in this disseration. In addition, the small diameters of the catheters may also restrict the idea of mounting sensors on the distal tip. The other approach to obtain the force information is to infer it from the information outside the body. This will demand an accurate mathematical model that describes the force and motion relation called kinetic model, and unfortunately, such a kinetic model is not available in the literature.

In this dissertation, a kinetic model for steerable catheters is presented wich captures the following characteristics of the steerable catheter, namely (1) the geometrical non-linear behavior of the catheter in motion, (2) the deformable pathway, (3) the friction between the catheter and the pathway, and (4) the contact between the catheter and pathway. A non-linear finite element system (SPACAR) was employed to capture these characteristics. A test-bed was built and an experiment was carried out to verify the developed kinetic model.

The following conclusions can be drawn from this dissertation: (1) the developed kinetic model is accurate in comparison with those in literature; (2) the Dahl friction model, the LuGre friction model and the simplified LuGre friction model are able to capture the friction behavior between the catheter and the pathway but the Coulomb friction model fails (as it cannot capture the hysteresis property which has a significant influence on the behavior of the catheter); (3) the developed kinetic model has the potential of being used to optimize the design and operation of steerable catheters with several salient findings that (3a) the maximal contact force between the

catheter and the pathway occurs on the tip of the distal part or the connecting part between the distal part and catheter body of the catheter and (3b) the rigidity and length of the distal part are crucial structural parameters that affect the motion and force transmission significantly.

There are several contributions made by this dissertation. In the field of the steerable catheter, biomechanics and bio-instrumentation, the contributions are summarized in the following: (1) the approach to develop the kinetic model of the steerable catheter in a complex work environment is useful to model other similar compliant medical devices, such as endoscope; (2) the kinetic model of the steerable catheter can provide the force information to improve the efficiency and safety of MIS (minimally invasive surgery) and to realize the "doctor-assisted" catheter-based MIS procedure; (3) the kinetic model can provide accurate data for developing other simplified models for the steerable catheters in their corresponding work environments for realizing the robotic-based fully automated MIS procedure. (4) The kinetic model of the steerable catheter and the test-bed with the corresponding instruments and methods for the kinetic and kinematic measurements are a useful design validation in the steerable catheter technology as well as for the training of physicians to perform the catheter-based interventional procedure by adding more complex anatomic phantoms. In the field of continuum manipulator and continuum robots, the approach to develop the kinetic model is useful to model other manipulators and robots, such as snake-like robots.

ACKNOWLEDGEMENTS

Before starting this dissertation, I want to first acknowledge and thank many people that have made it possible by contributing their support in many different ways during this precious journey.

First, I would like to express my deepest gratitude to my supervisor and close friend, Professor Wenjun (Chris) Zhang, whose understanding, encouragement, support, expertise and guidance let me to walk through the darkest period of my life and complete this dissertation. I have been greatly influenced and inspired by his enthusiasm and dedication to his work and his guidance to the young generation. I really appreciate him for all of what he did for me.

I am also deeply thankful to my co-supervisor, Dr. Yigang Luo, whose expertise and guidance on the clinical feedback of this research and other projects. He provided warm-hearted care and advice on my father's disease. I would like to thank my advisory committee members: Professor Madan M. Gupta, Professor Fangxiang Wu and Professor Mohamed Boulfiza, for patiently reading this work and giving me valuable advices and suggestions.

I would also like to thank Dr. Lin Cao, Dr. Jaap P. Meijaard (Delft University of Technology, Netherlands), Professor Arend Schwab (Delft University of Technology, Netherlands) and Dr. Harm ten Hoff (BayLink LLC, San Francisco, USA), for their help and support on using Spacar; Mr. Doug Bitner and Mr. Louis Roth, for their technical support on mechanical experiments.

I would also like to thank my friends for their encouragements and inspirations: Professor Daniel Chen, Professor Changli Liu, Ms. Annie Meng, Forrest Zhang, Olivia Wang, Zhen Wang, Ying Yan, Yu Cao, Mark Li, Jingyang Peng, Gary Huang, Dong He, Lina Zhang, Bing Zhang, Rain Zhao, Wubin Cheng, Tan Zhang, Wenjun Lin, Amy Zhang, Chunyu Zhou, Ming Zhu, Any Chen and Rob Arthur etc.

I would like to express my deepest gratitude to my father Mr. Zhengxing Hu, mother Ms. Fangxue Ding, wife Cynthia Zhang, sister Chuanxiang Hu, brother-in-law Zhihu Wu, parents-in-law Ms. Shumei Luo and Mr. Shaonian Zhang for their endless love, support and understanding. Special thanks go to my friends Haiyan Zhang and Jiale Hou for their help and encouragement.

I also acknowledge the financial support from China Scholarship Council (CSC), University of Saskatchewan Ph.D. Graduate Scholarship and National Natural Science Foundation of China for fundamental research funding (Funding No.: 51375166) that provided partial financial support for this dissertation research.

DEDICATION

This dissertation is dedicated to my father Mr. Zhengxing Hu and mother Ms. Fangxue Ding.

谨以此文献于我的父亲胡正兴先生和母亲丁方学女士。

TABLE OF CONTENTS

LIST OF TABLES

LIST OF FIGURES

LIST OF ABBREVIATIONS

CFTM	Catheter Force and Torque Monitor
CGCI	Catheter Guidance, Control and Imaging-Maxwell
CMOS	Complementary Metal Oxide Semiconductor
CP	Connecting Part
CPF	Conducting Polymer Fibers
CT	Computerized Tomography
D-H	Denavit-Hartenberg
DOF	Degree of Freedom
FEM	Finite Element Method
F-S	Frenet-Serret
HPV	High-Pass Valve
ICPF	Ionic Conducting Polymer Film
IPMC	Ionic Polymer Metal Composite
LPV	Low-Pass Valve
MIS	Minimally Invasive Surgery
MRI	Magnetic Resonance Imaging
PRB	Pseudo-Rigid-Body
RFA	Radiofrequency Ablation
RMSE	Root-Mean-Square-Error
SMA	Shape Memory Alloy
SPE	Solid Polymer Electrolyte

CHAPTER 1 INTRODUCTION

This dissertation presents a study of the kinetic modeling of the steerable catheter by considering complex interactions between the catheter and the pathway for minimally invasive surgery (MIS). This chapter introduces the background and motivation of the dissertation research and describes the specific objectives. After that, there is an organization of the dissertation.

1.1 Background and motivation

MIS utilizes image-guided procedures to diagnose and treat diseases in nearly every organ system, and MIS has revolutionized surgery in the last two decades. Using imaging modalities physicians obtain images which are then used to direct interventional instruments throughout the body. These procedures are usually performed by using endoscopies, needles and narrow tubes also called catheters, rather than by making large incisions into the body as in traditional open surgery. By minimizing the physical trauma to the patient, MISs can reduce infection rate and recovery time considerably and it can also allow shortening the hospital stay of the patients.

1.1.1 Conventional catheters and their limitations

One of the common tools used in MIS, in particular in interventional radiology, is the catheter which is a long, thin and flexible tube or wire. The catheter is inserted into the vascular system, gastrointestinal tract, airway and man-made pathway for diagnosis and treatment. Currently, the majority of MIS procedures are performed by using manually deflectable catheters. These manually-operated catheters have a limited range of motion and flexibility, and much rely on an operator's skill and experience to maneuver the catheter tip and to maintain stability at the target site. The complexity of the anatomy of the target site and the lack of information of the contact force are responsible for the difficulties in operation in terms of dexterity, safety and stability

(inappropriately leading to failures of the operation).

The conventional catheter is made by a range of polymers, including silicone rubber, nitinol, nylon, polyurethane, and polyethylene terephthalate latex, and thermoplastic elastomers. Silicone is one of the most common choices because it is inert and unreactive to body fluids and a range of medical fluids with which it might come into contact.

The typical procedure for catheterization is as follows: a guidewire is inserted into the arterial puncture. A catheter then passes over the guidewire and is pushed into the artery. Once the catheter reaches the target position, the guidewire is then removed. Sometimes, a catheter is directly inserted to the target site. The imaging devices make the vessels and catheters show up on the x-ray fluoroscopy or ultrasound images during catheterization.

In order to pass the intersections of vessels, the physician has to pre-shape the distal tip of catheter or guidewire. The shape of catheter is initially in a "best guess" based on the anatomy and the operator's experience. Several commonly used diagnostic peripheral catheters are shown in Figure 1.1, in which, the tips of catheters are pre-shaped to various shapes in order to pass the complex anatomy of blood vessels. For a sharp angle of the intersection of vessel, some complex procedures and techniques have to be performed. For instance, the physician uses the "Waltman Loop" technique which is shown in Figure 1.2 (Worthington-Kirsch et al., 2002), catheterizing the ipsilateral internal iliac artery. The physician usually tries several times to pull back, rotate and push forward the catheter until the distal tip reaching the target site. The procedure of this kind will not only increase time and thus radiation dose to patients but also will increase the risk of catheter-induced complications such as spasm or dissection.

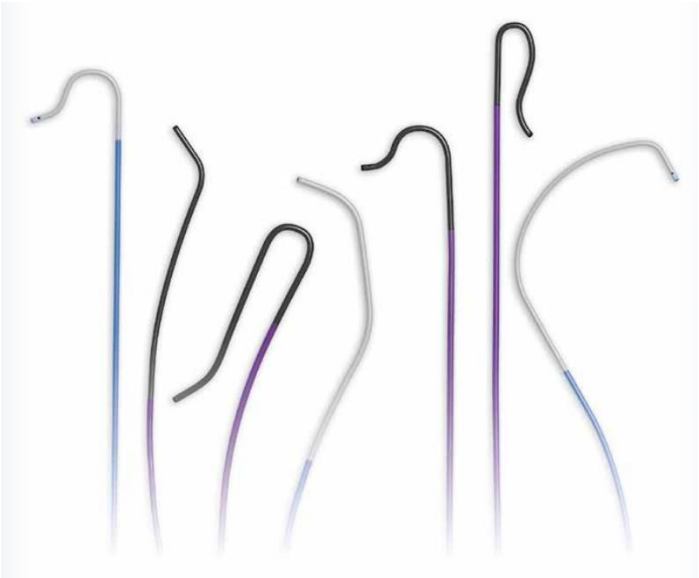

Figure 1.1. Diagnostic Peripheral Catheters made by Merit Medical OEM Inc. (Available at: http://meritoem.com/files/documents/brochures/CathetersExtrusionsFB.pdf)

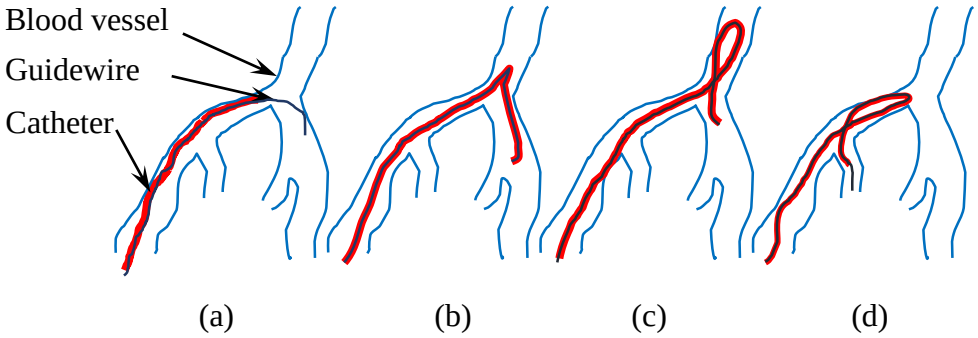

Figure 1.2. "Waltman Loop" Technique. Reprinted with kind permission from Worthington-Kirsch et al. (2002): (a) A catheter is advanced into the contralateral iliac artery and a guidewire positioned with its tip at the aortic bifurcation. (b) The catheter and wire are advanced together as the catheter is rotated. (c) The catheter forms a loop in the distal aorta. (d) The looped catheter can then be directed into the ipsilateral iliac artery with the use of a soft guidewire.

Conventional catheters have a limited range of motion and flexibility and rely on the operator's skill and experience to manoeuvre the catheter tip and maintain stability at target sites. The successful catheterization with conventional catheters largely depends on making the right decisions and on manual dexterity. Due to the complexity of the anatomy of the target vessel, the

catheter distal tip is difficult to gain access to certain target sites. ***The main drawbacks*** of the conventional catheter are as follows: *(1) catheterization navigation, and (2) steering force transmission from the proximal tips to the distal tips*.

There are two problems with conventional catheters regarding the catheterization navigation. *The first problem* is the uncertainty of the maneuver at the T cross intersection. Figure 1.3 shows the situation where B direction is desired, but actually the catheter may move along A direction. *The second problem* is the tip of catheter may hook in the small branch pathway.

Another problem is that the force transmission of the catheter from the proximal end activated by physicians to the distal tip meets some uncertainties. The catheters with the pre-curved distal tips move forward and backward into vascular system, gastrointestinal tract and airway by means of translation and rotation applied by physicians out of patients. The catheters inside the body have to deal with the contact and friction between the catheter and pathway, and resistance force by blood if the catheter in the blood vessel, and the movement of the patient. The input force cannot be completely transmited to the distal tips by flexible catheters with 1~5 mm diameters and nearly 1 m long.

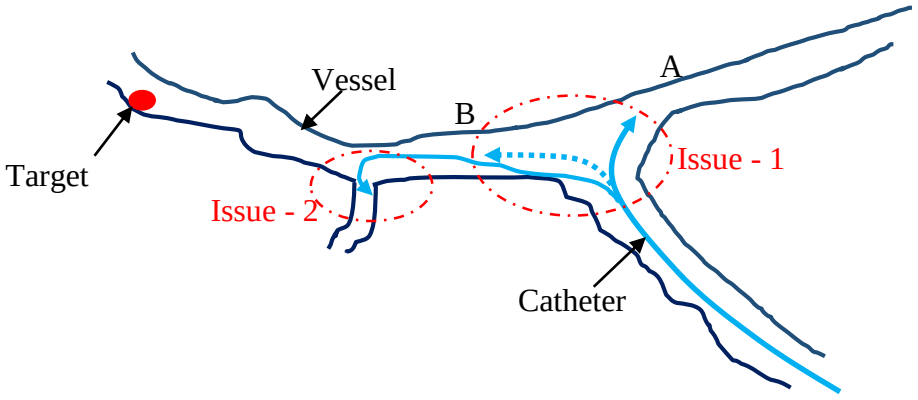

Figure 1.3. Navigation challenges during catheterization

1.1.2 Steerable catheters

To overcome the foregoing limitations of the conventional catheters, various steerable catheters are developed. The steerable catheter means that the deflection of the distal tip can be controlled

by operators outside the human body. A typical tendon-driven steerable catheter with its control unit is shown in Figure 1.4, in which the distal tip of the catheter can be deflected into two directions by a pair of tendons. The steerable catheters have shown many advantages compared with the conventional catheters. The main advantages of steerable catheters are improved the accessibility to difficult anatomy and catheter stability, reduced the fluoroscopy times and decreased the total radiation exposure of both patients and physicians (Di Biase et al. 2009, Miyazaki et al. 2010, Ullah et al. 2014, Aagaard at el. 2015).

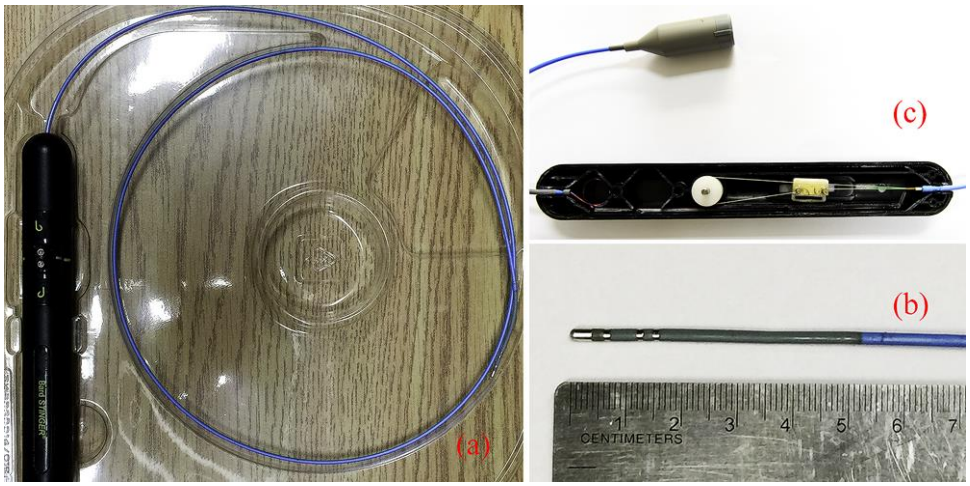

Figure 1.4. Bard Stinger Radiofrequency Ablation (RFA) Catheter and its control unit (a: catheter with control unit; b: distal tip of catheter; c: inside of the control unit)

The technology for steerable catheters has been advanced greatly in the past decade. Some commercial products of steerable catheters and robotic catheters are available, such as Polaris X™ Steerable Diagnostic Catheters (Boston Scientific Inc., Marlborough, USA), Artisan Extend Control Catheter (Hansen Medical Inc., Mountain View, USA), and Niobe® Magnetic Navigation System (Stereotaxis Inc., St. Louis, USA). A number of minimally invasive clinical applications benefit from steerable catheters, including cardiac surgery (Boston Scientific 2016, Hansen Medical 2016a, Stereotaxis 2016), vascular surgery (Jeon et al. 2012, Ikuta et al. 2012, Hansen Medical 2016b), aneurysm surgery (Guo et al. 1995, Bailly et al. 2005, Bailly et al. 2011), neurosurgery (Szewczyk et al. 2011, Butler et al. 2012), arthroscopy (Dario et al. 2000. Kutzer et al. 2011) and intrauterine fetal surgery (Harada et al. 2006, Zhang et al. 2009) and so on. Each application of the steerable catheter requires the customization of design.

1.1.3 Force sensing of the steerable catheters

The force information of the steerable catheter, in particular, the force at the distal tip, is a key factor to ensure safety and efficiency in the catheter-based surgeries (Yokoyama et al. 2008, Di Biase et al. 2009a). Force applied at the distal tip of the catheter has to be controlled in a certain range, e.g., 0.2-0.3 N for the effective catheter ablation of arrhythmias (Di Biase et al. 2009b). A large contact force between the distal tip of the catheter and the pathway may cause injury, e.g., perforation and popping in surgery. A small contact force may affect the efficacy and stability of the surgery, even leading to failure of operation. The force information can be obtained by a force sensor mounted at the distal tip of the catheter directly. Recently, the steerable catheters with force sensors integrated at the distal tip have been developed (Yokoyama et al. 2008, Di Biase et al. 2009b, Biosense Webster 2016, Hansen Medical 2016a). However, this procedure would be quite intrusive and less reliable. This is limited by the small diameters of the catheters and applications, i.e., the MRI compatibility in MRI working environment. In addition, these catheters must be integrated with their interfaces, and this causes a noticeable cost. The prices of these catheter systems integrated with force sensors are usually significantly higher than those of the catheters without force sensors. This is one of the major concerns for the wider use of these catheters with the integrated force sensor, since the catheters are for one time use only.

The other way to obtain the force information is to mount force sensors at the proximal end of the catheter which are outside the human body and then to infer the force information between the catheter and its working environment from the information of input force obtained by the force sensors using a kinetic mathematical model of steerable catheter. The basic idea of the force estimation is close to the idea of "intrinsic force sensing" in the context of continuum manipulators (Xu and Simaan 2008). Several mathematical models are developed in literature, e.g., the energy method based model developed by Xu and Simaan (2008, 2010), the pseudo-rigid-body (PRB) based models developed by Ganji et al. (2009) and Khoshnnam et al. (2012, 2015), etc. Webster and Jones (2010) presented a review of modeling of constant curvature continuum robots, which includes many different types of steerable catheters. There are two main issues for the current mathematical models. One issue is that most of the models are based on the assumption of constant

curvature in absence of external constraints, which compromises the accuracy of the models (Webster and Jones 2010, Jung et al. 2011, Khoshnam et al. 2015). In actuality, curvature variations are existed along the length of the catheter, which are further caused by the friction forces and contact forces. The other issue is that these models are developed in a free space. The free space assumption is apparently far away from the actual situation which involves the contact and friction between the catheter and pathway. Consideration of these factors in building a mathematical model for kinetics of the catheter is the motivation of this dissertation.

The overall objective of this dissertation study was to develop a kinetic model of the steerable catheter by considering the interaction between the catheter and pathway. The benefits of such a model are: (1) to facilitate in developing a new operation procedure, (2) to facilitate the optimal design of the existing catheter system, (3) to facilitate the design of new catheter systems, and (4) to facilitate the development of virtual reality-based surgical simulators for training of physicians.

1.2 Objectives and scope

To achieve the foregoing overall objective, the following three specific objectives were defined.

Objective 1: To develop a kinetic model for the steerable catheter to describe the motion and force transmission of the catheter in its pathway by considering (1) the geometrical non-linear behavior of the catheter in motion, (2) the deformable pathway, (3) the friction between the catheter and the pathyway, and (4) the contact between the catheter and pathway. It is noted that the driving force applied by the physician is obtained by the force sensor mounted at the proximal end of the catheter which is outside the human body.

Objective 2: To set up an experimental test-bed to validate the kinetic model. This objective can be further divided into two more specific objectives: (2a) to set up a test-bed to estimate the parameters of the model; (2b) to set up a test-bed which can measure all required information and to validate the model.

Objective 3: To explore the applications of the kinetic model in terms of the investigation of the

behaviors of the steerable catheter during catheterization and the benefits for new design and optimal design of steerable catheters.

The purpose of this dissertation is to prove the effectivenss of a methodology for builing a kinetic model that capture the four characteristics of the catheter, as mentioned before. The methodology includes the application of a finite element approach with its program system SPACAR, modeling of the contact and friction between the catheter and pathway. Owing to this purpose, a 2D experimental test-bed was constructed in assisting the model development and model validation. The reason to start with the 2D system instead of the 3D system is because of (1) low computational cost with a 2D system and (2) easy extension of a 2D finite element model (e.g., planar beam element) to a 3D finite element model (e.g. spatial beam element) with SPACAR. Further, in Objective 1, the information of the driving force on the catheter is from the physicians is assumed known.

1.3 Organization of dissertation

This dissertation is composed of six chapters.

Chapter 1 gives an introduction to this research, including the background, issues to motive the present research and research objectives with scope.

Chapter 2 presents a literature review on the classification various steerable catheters and the associated kinetic models, providing the understanding of the background of steerable catheters and the challenges in constructing a kinetic model. This chapter also elaborated on the suitability of taking the finite element method as a tool for constructing the kinetic model of steerable catheters.

Chapter 3 presents the development of a kinetic model of the steerable catheter and the pathway by considering their interaction. The movement of a steerable catheter in a pathway is a complex engineering phenonmenon, involving many factors such as the structure and stiffness and damping of the catheter of itself, the structure and stiffness and damping of the pathway, interaction between the catheter and the pathway (friction and contact mechanics). All these factors have been captured

in the kinetic model as developed in this dissertation.

Chapter 4 presents the experimental validation of the kinetic model of the steerable catheter. An experimental test-bed of the steerable catheter was developed. The parameters in the model of the catheter as well as the model of the pathway were determined by the experiments. Several groups of experiments and simulations were performed to validate the developed kinetic model. The validity and reliability of the model were discussed as well.

Chapter 5 presents the analysis of the kinetic model of the steerable catheter with the aim to give the rationale for the development of the kinetic model (in Chapter 3), including (1) the number of finite elements used to model the whole catheter and (2) the choice of a proper friction model.

Chapter 6 presents the application of the kinetic model of the steerable catheter, particularly studying three important parameters that would affect the motion and force transmission signficiantly and the safety of the MIS. These parameters are: (1) the maximal contact force between the steerable catheter and the inner wall of the pathway was analysed; (2) the structure of the steerable catheter with different bending rigidities and different lengths of the distal part.

Chapter 7 gives the conclusions drawn from the results obtained, summarizes the contributions of the dissertation, and recommends the future research work.

A part of the content in Chapter 2 has been documented in a paper: Hu, X.H., Cao, L., Luo, Y.G., & Zhang, W.J., “Steerable Catheters for Minimally Invasive Surgery: A Review”, in submissioin to *Medical Engineering & Physics*. A part of the contents of Chapter 3 and Chapter 4 has been documented as a paper: X.H. Hu, L. Cao, Y.G. Luo, C.L. Liu & W.J. Zhang, “A Kinetic Model for Steerable Catheters Considering Their Interaction with Pathways”, in submission to *IEEE Transactions on Robotics.*

CHAPTER 2 STEERABLE CATHETERS FOR MINIMALLY INVASIVE SURGERY: LITERATURE REVIEW

2.1 Introduction

This chapter presents a review of the literature in relation to the steerable catheters and their modeling approaches. Section 2.2 provides a full background on steerable catheters, in which, steerable catheters are classified into four main groups based on the actuation mechanisms: (1) tendon driven catheters, (2) magnetic navigation catheters, (3) self-bending catheters (shape memory effect catheters, steerable needles, concentric tubes, conducting polymer driven catheters and hydraulic pressure driven catheters) and (4) hybrid actuation catheters, and the advantages and limitations of each of them are commented and analyzed. Section 2.3 discusses the typical modeling approaches for the kinematics and kinetics of the steerable catheter, including Denavit-Hartenberg (D-H) conversion, Frenet-Serret (F-S) conversion and exponential coordinates methods for kinematic modelling, and classical Bernoulli-Euler beam theory, pseudo-rigid-body (PRB) models, energy methods, Cosserat rod theory, lumped-parameter modeling approach and finite element methods (FEM) for kinetic modeling. The advantages and limitations of these methods with respect to the modeling requirements are analyzed. Section 2.4 summarizes the review and discusses the need and urgency of this dissertation research. There is a revisit of the specific objectives as proposed in Chapter 1 and justifies that the geometrically non-linear FEM is the best choice and most suitable tool for modeling the steerable catheter to interact with its working environment for this research.

2.2 Classification of steerable catheters

The steerable catheters can be considered as continuum manipulators. A continuum

manipulator can be defined as a continuously deformable manipulator made by elastic materials, which does not contain rigid links. Continuum manipulators are similar to, but distinct from hyper-redundant manipulators which contain many short (infinite) and rigid links. By comparing with hyper-redundant manipulators, continuum manipulators are inherently compliant and articulate due to elastic deformation. Details of the continuum manipulators are referred to the review articles (Robinson and Davies 1999, Webster and Jones 2010, Walker 2013).

Steerable catheters have different requirements than other applications of continuum manipulators, and these requirements are: (1) The diameter of catheters is strictly limited due to their working environments (e.g., vascular system, gastrointestinal tract, airway or man-made pathway, e.g., inner pathway of endoscopy); (2) The catheter should have a high dexterity to be navigated to the target place in the "channel"; (3) The catheter should have a certain stiffness to perform complex tasks and had better have a force feedback control. The high contact force or torque would provoke injuries, while the low contact force may not perform complex tasks well and/or not have sufficient the tip stability of a catheter; (4) Material should be biocompatible and sterilizable; (5) Material should be soft to have a good compliance with the biological environment; (6) Material should be magnetic resonance imaging (MRI) compatibility (if the catheter is used in MRI system); (7) The cost of catheters is a concern.

Steerable catheters can be categorized based on several different criteria. The first criterion is the actuation mechanism, and based on this criterion steerable catheters are categorized into (1) tendon-driven catheters, (2) magnetic navigation catheters, (3) self-bending catheters and (4) hybrid actuation catheters. The second criterion is the section of actuation, and based on this criterion, steerable catheters are categorized into (1) single-section and (2) multi-section. The third criterion is the workspace, and based on this criterion, steerable catheters are categorized into (1) planar and (2) spatial. The detailed information of several typical steerable catheters can be found in Table 2.1. In the following, categorization of steerable catheters based on the actuation mechanism principle will be discussed in detail, including a comparison of several types of steerable catheters.

2.2.1 Tendon-driven steerable catheters

One of the frequently driven principles to construct lightweight and small size steerable catheters is the use of one or several antagonistic tendons to control the orientation of distal tips of steerable catheters. Most of them share a single backbone (which is an elastic structure) that supports tendons and delivers substances. This backbone is made of a variety of materials, such as springs, elastic tubes and braided polymer tubes. Among these materials, the super-elastic material nitinol (NiTi) alloy is often used. One of the primary structural features of the backbone is with a laser-machined slotting pattern to achieve a desired stiffness and direction of bending along the axis of the backbone. Tendons are placed at equally spaced intervals along with the catheter backbone and as such, the whole catheter has its shape to approximate a circular arc. The tendons at the proximal end of the catheter are controlled with a control unit which is further controlled by operators. The schematic diagram of the actuation mechanism of tendon-driven steerable catheter is illustrated in Figure 2.1.

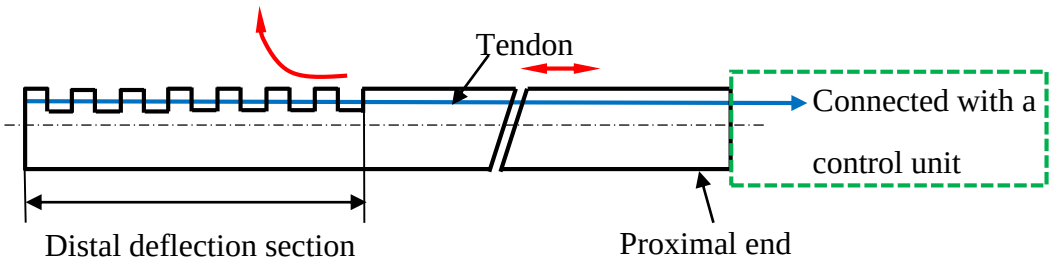

Figure 2.1. Schematic diagram of the structure of the tendon-driven steerable catheter.
(The red arrows indicate the movement of tendon and the deflection of the distal section.)

2.2.1.1 Single-section catheters

The steerable catheters have two categories: single-section and multi-section. Single-section tendon-driven catheters can have one to four tendons. The locations of tendons in the manipulator are shown in Figure 2.2. The simplest tendon-driven catheter is composed of the backbone and one or two tendons, e.g., Polaris X™ Steerable Diagnostic Catheter (single tendon) and SteeroCath-Dx™ Bidirectional Steerable Diagnostic Catheter (a pair of tendons)

by Boston Scientific Inc. (Boston Scientific, 2016). The similar design of steerable catheters can be found in (Ganji and Janabi-Sharifi 2009, Khoshnam et al. 2012, Khoshnam et al. 2015).

For both the diagnosis and radiofrequency ablation (RFA) steerable catheters, there is no central open lumen (inner channel) in the catheter system. In order to insert a particular surgery tool through a catheter, some tendon-driven steerable catheters with a central open lumen are developed. Kutzer et al. (2011) and Murphy et al. (2013) presented a tendon-driven cannula with a large open lumen used to remove the osteolysis formed behind the acetabular shell of primary total hip arthroplasties (Figure 2.3, Left). It has a 5.99 mm-outer-diameter and 5 mm-inner-diameter nitinol tubes as a backbone which is cut into many interlocked slots. Two channels which are cut axially through the outer wall of the backbone spaced 180° apart. Two driven cables are threaded through the channels to bend the distal tip. Penning et al. (2011) presented a prototype of the catheter which consists of four articulation tendons and a flexible machined Teflon spine (Figure 2.3, Right). The tendons are enclosed in a polyester mesh sleeve to hold the control wires to the catheter body. The catheter is driven by a Continuum Robotics Electromechanical System Testbed which consists of four servo motors to independently control each tendon, and a linear actuator to control the insertion of the catheter.

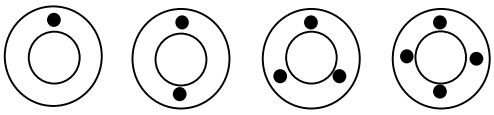

(a) (b) (c) (d)

Figure 2.2. Location and number of tendons in tendon-drive catheters.

(a) The catheter is driven by one tendon and examples can be found in (Khoshnam et al. 2012, Guo et al. 2011, Khoshnam et al. 2015, Boston Scientific, 2016); (b) The catheter is driven by a pair of tendons which are placed in 180° and examples can be found in (Ganji and Janabi-Sharifi 2009, Kutzer et al. 2011, Waston 2013); (c) The catheter is driven by three tendons placed 120° apart and example can be found in (Degani et al. 2006, Xu and Simaan 2008); (d) The catheter is driven by four orthogonally spaced tendons and examples can be found in (Harada et al. 2006, Camarillo et al. 2008, Penning et al. 2011).

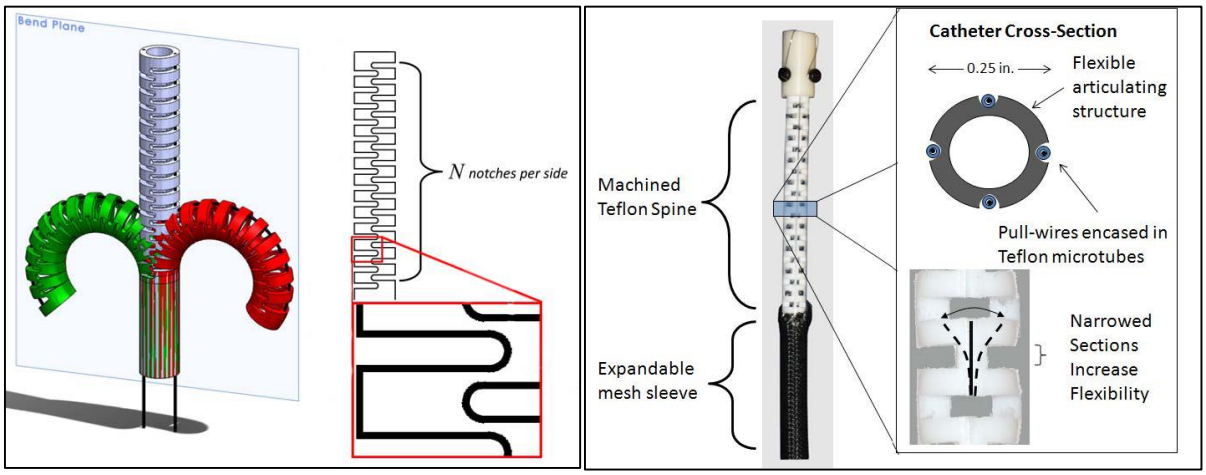

Figure 2.3. Steerable catheters with an open lumen.

(Left: The cannula driven by two tendons with an open lumen was designed by Kutzer et al. (2011). Reprinted with kind permission, from (Kutzer et al. 2011) © 2011 IEEE. Right: The catheter driven by four tendons with an open lumen was designed by Penning et al. (2011). Reprinted with kind permission, from (Penning et al. 2011) © 2011 IEEE.

One sophisticated and commercially available tendon-driven steerable catheter system is the Sensei X Robotic Catheter System for cardiac surgery by Hansen Medical Inc. (Kanagaratnam et al. 2008, Carlson & Barbagli 2013), and this catheter system is an electromechanical master/slave system that remotely controls a steerable guide catheter positioning within the heart. The system is composed of three components that are connected: the physician's workstation, remote catheter manipulator and steerable guide catheter (Artisan® Extend Control Catheter). There are two force sensors in the distal tip of catheter to get the force information to the physicians. The steerable catheter was described in detail by Camarillo et al. (2008a, 2008b). It is a 3.8 mm diameter catheter for cardiovascular surgery. It has a super-elastic NiTi spine as central backbone for articulation inside the catheter. The catheter is controlled by four equally spaced tendons that lie approximately on its perimeter within polyimide sheath to allow for low friction. The tendons are restrained by a braid of stainless steel flat wire. The inner and outer diameters of the catheter are lined with laminated plastics for medical use. Four tendons are controlled by four DC motors with encoder feedback.

The aforementioned tendon-driven steerable catheters have an entire backbone. The stiffness

of the catheter cannot be changed during the operation. Several steerable catheters with a group of backbones connected in series are developed. Such a catheter may be called a discrete catheter system. The discrete backbone system is composed of a chain of segments connected by joints e.g., spherical joint; see Figure 2.4 and 2.5 for examples. Figure 2.4 shows a highly articulated robotic probe for minimally invasive cardiac surgery developed by (Degani et al. 2006). It consists of two concentric tubes. Both tubes consist of rigid cylindrical links connected by spherical joints which can rotate 15º range which are assembled four cables, three for the outer tube (120º apart) and one for the inner tube. It is noted that both orientations and stiffness can be controlled through the three cables. When the cables are relaxed, the tubes become limp, and vice versa. Figure 2.5 shows a bending manipulator of 2.4 mm in diameter with a centrally inserted laser fiber (0.7 mm in diameter) for intrauterine fetal surgery developed by (Harada et al. 2006). The distal tip of manipulator is composed of cylindrical parts with four holes and spheres with a hole. They are assembled by four wires and a central tool. The number of joints can be changed according to the stiffness of the centrally inserted tool. The four wires are controlled by two ultrasound motors.

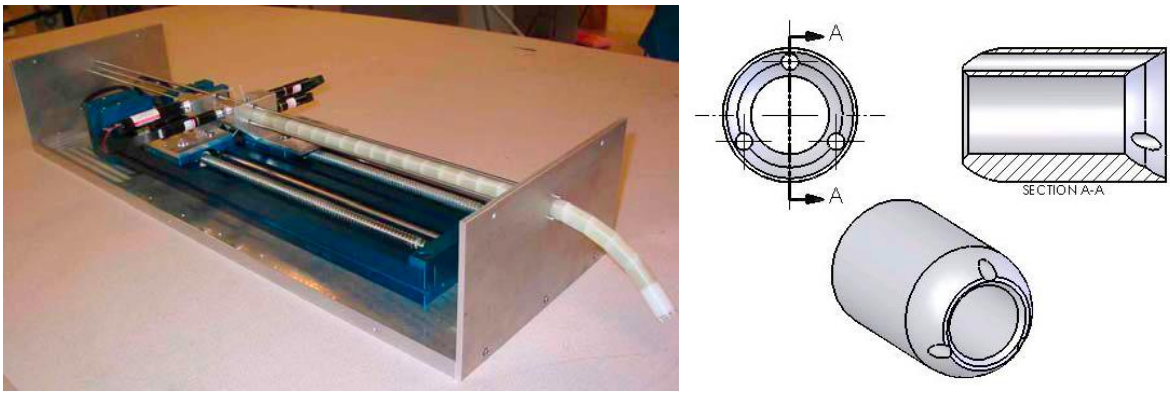

Figure 2.4. Steerable catheters with a discrete backbone (Degani et al. 2006) (Left: entire steerable catheter system; Right: single link of the backbone). Reprinted with kind permission, from (Degani et al. 2006) © 2006 IEEE.

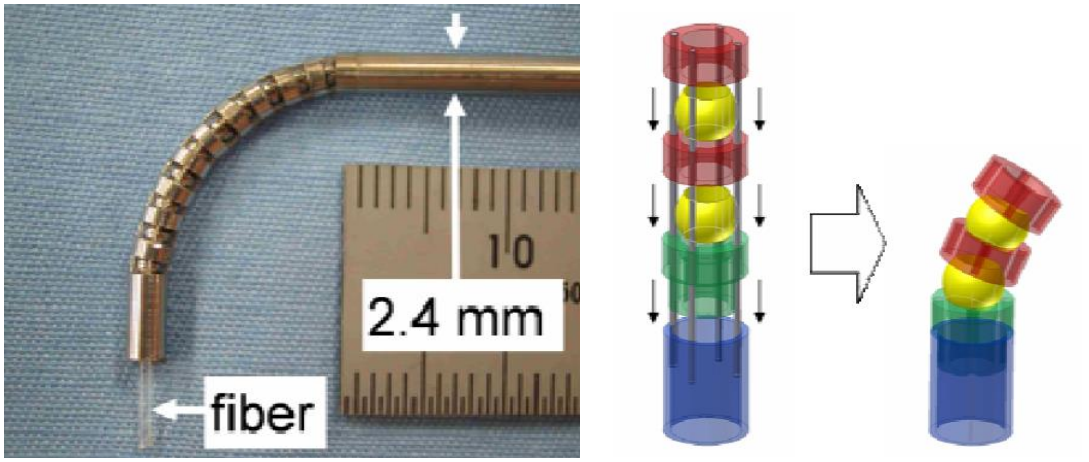

Figure 2.5. Bending laser manipulator developed by Harada et al. (2006). (Left: prototype of the manipulator; Right: bending mechanism). Reprinted with kind permission, from (Harada et al. 2006) © 2006 IEEE.

The steerable catheter with a multi-backbone is developed by eliminating the backlash, enhancing down-scalability, and improving payload. The steerable catheter with multi-backbone is typically composed of several parallel elastic rods or tubes. Xu and Simaan (2008) reported a single-section continuum robot for minimally invasive surgery. It has four super-elastic NiTi tubes as its backbones. One primary backbone is centrally located and is attached to the base disk and end disk. Three identical secondary backbones are equidistant from each other and serve as driven tendons. Each secondary backbone is actuated in push–pull mode by an actuation rod. A multi-section multi-backbone continuum robot was further developed in the Simaan's research group as well (Simaan et al. 2009, Xu and Simaan 2010), which will be discussed later.

2.2.1.2 Multi-section catheters

In order to provide a sufficient number of degrees of freedom (DOF) or workspace size for tasks, many steerable catheters are required to have multi-section. Each section is steered by a group of tendons separately. The number of tendons for the distal section may not be the same with the number of tendons for the proximal section. For the multi-section tendon-driven catheter, the way of sections coupling is quite important which is critical to its dexterity and

diameters. Usually, there are two ways for sections coupling: co-placed and distributed (Figure 2.6). To compare with the independent coupling of sections, the co-placed coupling of section has potential to reach smaller diameters. However, the deflection of the distal section usually affects the deflection of the proximal section. The distributed coupling of sections has more dexterity and the distal section potentially has more degrees of freedom.

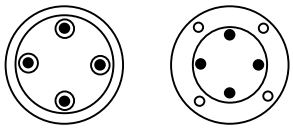

Figure 2.6. The ways of sections coupling (Left: co-placed; Right: distributed). For the co-placed coupling of sections, the tendons for the proximal section share the pathways with the tendons for the distal section in the part of proximal section; examples can be found in (Simaan et al. 2009, Xu and Simaan 2010). For the distributed coupling of sections, the tendons for each section have their independent pathways; examples can be found in (Camarillo et al. 2009, Carroll et al. 2011, Carlson and Barbagli 2013).

Camarillo et al. (2009) described a catheter with two articulating sections and two tendons per section arranged antagonistically from the distal to proximal. The way of how the sections are coupled is the distributed one. Carlson and Barbagli (2013) presented a two-section catheter. Each section is controlled by four orthogonal tendons. The way of sections coupling is distributed. Xu and Simaan (2010) presented a three sections multi-backbone continuum robot for minimally invasive surgery. The structure of each section is the same as their single section multi-backbone continuum robot (Xu and Simaan 2008). The way of sections coupling is co-placed. Backbones of the proximal and middle sections are concentric NiTi tubes, while the backbones of the distal section are NiTi beams, which pass through the backbone tubes of the second segment.

Tendon-driven catheters have simple structures and can be steered remotely easily. Due to the actuation mechanism, the structure is relatively bulky to small size catheters, in particular, for multi-sections catheters. The diameter of catheter is restrained. The friction between tendon and guide channel makes compensation in control to be a challenge. The control unit should avoid

slack tendons during articulation. Tendons may cause backlash which affects the moment and force delivered to the joint as well.

2.2.2 Magnetic navigation catheters

In the magnetic navigation technique, the catheters with magnetic distal tips are steered within the patient. Several large magnets placed on either side of the patient which can generate a magnetic field. Physicians can control the distribution of magnetic field to deflect the distal tips of catheters within the patient to the desired direction.

The commercially available products for magnetic navigation catheters include Niobe® ES magnetic navigation system (Stereotaxis, St. Louis, MO, USA) (Stereotaxis 2016) and Catheter Guidance, Control and Imaging-Maxwell (CGCI) (Magnetecs, Inglewood, CA, USA) (Magnetecs 2016). Niobe® ES magnetic navigation system is designed to make the treatment of complex cardiac arrhythmias safe and effective (Figure 2.7) (Stereotaxis 2016; Ernst et al. 2004). There are two permanent magnets to generate a uniform magnetic field (0.08 T) in this system. The distal tip of catheter is embedded with a small permanent magnet which interacts with the magnetic field. The intensity magnetic field is controlled by adjusting the relative position of two permanent magnets. The insertion or retraction of the catheter is controlled by a catheter manipulator. Operators steer the catheter fully automatically by a joystick or mouse based on the image feedbacks by the user interface. The system proved a safe and effective tool in the treatment of supraventricular and ventricular arrhythmias based on the clinical feedbacks (Erni et al. 2004; Pappone et al. 2006; Arya et al. 2008; Kim et al. 2008; Wood et al. 2008; Chun et al. 2010; Proietti et al. 2013). The main advantages for remote magnetic navigation are the reduced fluoroscopy time and the low chance of complication. The drawback is the increased total procedural time.

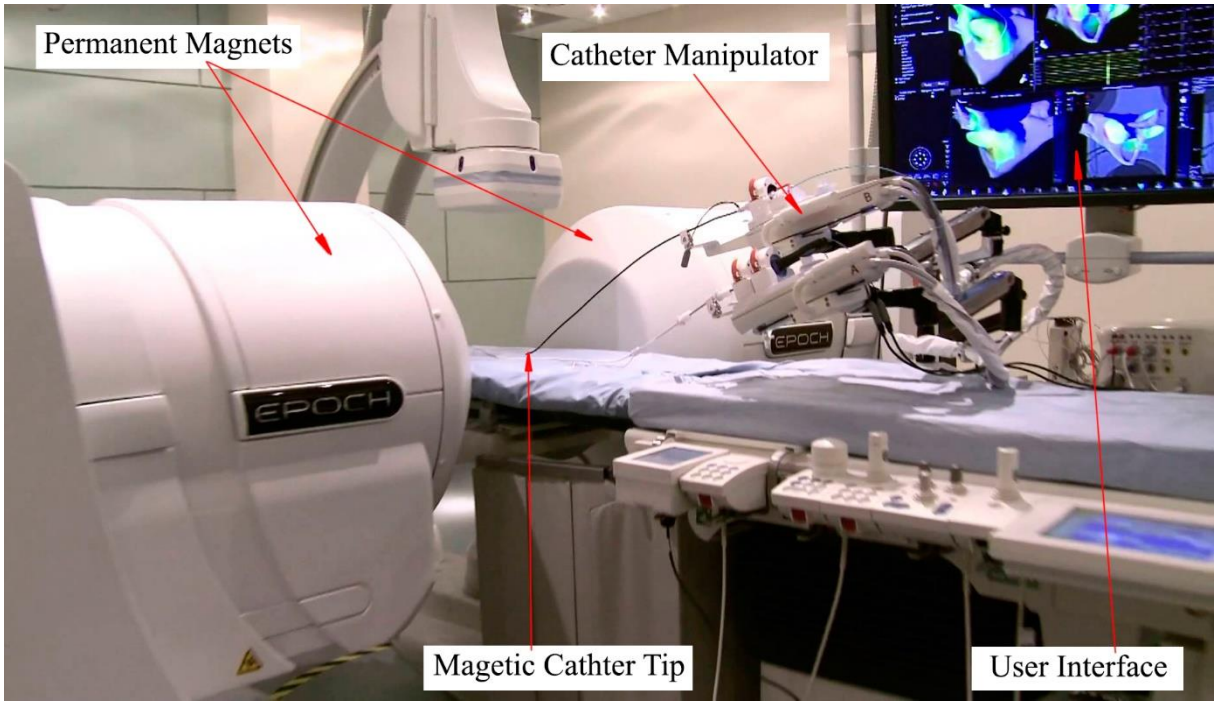

Figure 2.7. Niobe® ES magnetic navigation system.

(Available at: http://www.stereotaxis.com/products/epoch/)

Besides the magnetic fields generated by permanent magnets, they can be generated by electromagnets as well (Nguyen et al. 2010, Faddis et al. 2002, Govari et al. 2011, Jeon et al. 2012). Stereotaxia Inc. designed a similar magnetic navigation system as Niobe® ES magnetic navigation system in the early stage named Telstar (Faddis et al. 2002). Its magnetic field is generated by 3 orthogonal electromagnets. Directional catheter navigation is accomplished by generating a desired magnetic field vector. Nguyen et al. (2010) presented the CGCI system for cardiac surgery. The system consists of eight coil-core electromagnets arranged semi-spherically around the chest on a standard fluoroscopy table. They can generate approximately 15 cm, with a maximal uniform magnetic field strength of 0.14 T. The variance of magnetic field in terms of magnitude and direction is greatly improved. The nearly real time control of catheter tip can be achieved. Jeon et al. (2012) developed a catheter system to steer and unclog the catheter by magnetic torque and force. The catheter is composed of a flexible tube with a rotatable drill tip at the distal tip which is a permanent magnet. The magnetic field is generated by two types of magnetic coils: uniform coils and gradient coils. The magnetic torque and force can be independently controlled. To compare with the magnetic fields generated by permanent

magnets, they have two advantages: (1) they can increase the stability and contact force of distal tips by increasing the strength of the magnetic fields; (2) The system can continuously and rapidly shape and reshape of the magnetic fields which provides instantaneously transmitted changes to the tip of the magnetized catheter leading to nearly real-time remote navigation.

Another way of magnetic navigation is guiding the catheter inside a magnetic resonance imaging (MRI) system. Gosselin et al. (2011) presented a catheter and a guidewire with ferromagnetic heads steered by applying magnetic gradients inside a MRI system. However, two ferromagnetic spheres introduce undesired dipole-dipole interactions. Gudino et al. (2011) reported that a microcathter was steered inside a MRI system. The tip of the catheter was built an array of steering coils. Similar studies can also be found in (Liu and Cavusoglu 2014, Hetts et al. 2013). The coil activation times and optimization of the catheter design including use of MRI appropriate materials are necessary for safe remote control magnetic catheter guidance (Hetts et al. 2013).

The permanent magnets control the magnetic field by changing the relative position and cannot be switched off, which may cause a safety problem. The electromagnets control the magnetic field by controlling the current and relative position, and can be switched off. Control of electromagnets is easier to implement in most cases and faster in comparison with the position and orientation control needed for permanent magnets (Faddias et al. 2002; Nguyen et al. 2010, Erni et al. 2013). However, such a magnet shows a hysteresis non-linear behavior. Since the catheters are only steered by the magnetic force in most of systems, the horizontal bending angle and vertical deflection of the catheters cannot be controlled independently. Another problem is that the catheter can only have a single-section which may not be enough to complete some complex tasks.

2.2.3 Self-bending catheters

Self-bending catheters are made by some flexible materials including shape memory alloy (SMA), hydraulic bellows, and conducting polymers which can be bent continuously from the

interaction in the backbone itself, not from other external mechanisms (i.e., tendon and magnetic field).

SMAs, especially nitinol, have super-plasticity, biocompatible, high recoverable strains, good kink resistance, good steer-ability and torque-ability, and can be made in a very small diameter (under 1mm) that makes them an ideal candidate for the guide-wires or catheters for MIS (Duerig et al. 1999; Morgan 2004). The catheters made by the SMA can be categorized into two types in terms of the actuation mechanism: one is shaped by using the shape memory effect, and the other is shaped by using its super-plasticity known as steerable needles and concentric tubes.

2.2.3.1 Shape memory effect catheters

This type of catheters is actuated by SMA actuators using the shape memory effect. The SMAs can transform between the stiff austenite phase and the martensite phase to generate force and deformation induced by the temperature. After being plastically deformed in its low temperature martensite phase, the SMA material can recover strains up to 8% when heated to austenite (Tung et al. 2008). The catheter bends and shrinks due to the force generated by SMA actuators when heated. Once the temperature is back to the initial state, the catheter and SMA actuators recover to initial state as well due to the elasticity. The structure of SMAs can be wires, coils and carved tubes.

Dario et al. (1991) designed a catheter tip actuated by four SMA wires (90º apart) placed into the wall of catheter. Four optical fiber sensors are placed into the wall as well in order to get feedback information. The SMA wires are heated and cooled by circulating fluid through the same lumens in which the SMA wires are located. Takizawa et al. (1999) presented a catheter actuated by three SMA wires (120º apart) with 1.5 mm diameter. Tactile sensors are developed and installed on the tip of catheter. It takes around 2 seconds to achieve the maximum bending angle 45º. Jayender et al. (2008, 2009) developed an active catheter actuated by three SMA wires spaced at 120º. These wires are micro-welded to stainless steel pads which are glued to

the central catheter to be a multi-section catheter to obtain varying bending angles. The catheter with SMA wires is packaged to avoid any injury of the vessel wall by the heat. Two similar active catheters for neuroradiology and their optimal design process can be found in (Szewczyk et al. 2011).

Using SMA wires can facilitate the miniaturization of catheter. It can produce large forces but only generate a short displacement. In order to obtain large displacements (thus large bending angles) and quick response, micro SMA coils are used as actuators. The catheters are composed of multi-links to produce an enough bending angle. Lim et al. (1995, 1996) developed a multi-link active catheter with the 2.8 mm diameter. It consists of several links and joints made of SMA actuators. Three SMA coils are located at nearly 120º apart and heated by electrical current. The SMA actuators can be heated directly. However, they have low resistances (10 Ω). They proposed an indirect heating method using nickel thin film deposited on a parylene coated SMA actuators (200 Ω). The maximum bending angle is 13º. Haga et al. (1998, 2000) presented three active catheters whose diameters are less than 2 mm, which are actuated by series of distributed SMA coils. The first catheter consists of many distributed link-joint units and the diameter is 1.2 mm. Three groups of SMA coils are fixed at equivalent angles between two links and one joint. When the SMA coils are heated by an electrical current above a certain transition temperature, it shrinks and bends the catheter. The maximum bending angle is 11º under 80 mA input current. The other two catheters eliminate the link-joint units and the SMA actuators are fixed on the inner tube with adhesive materials. One has the liner coil outside the SMA actuators, and the other has the liner coil inside the SMA actuators. The liner coil is used as an electrical common ground and both terminals of each joint are connected to this liner coil. Their bending angles can achieve 45º under 120 mA input current and 90º under 80 mA input current respectively. They also develop a guide wire with only 0.5 mm diameter (Haga et al. 2002). It can bend to one direction using one meandering SMA actuator and a stainless coil spring. It bends over 60º under 50 mA input current.

One problem in catheters actuated by multi-link SMAs is that too many lead wires are required to control the SMA actuators. The total number of lead wires required is at least equal to that

of the SMA actuators. Park and Esashi (1999) described a multilink active catheter with an integrated Complementary Metal Oxide Semiconductor (CMOS) interface circuit for communication and control within a 2.0 mm diameter (Figure 2.8). The lead wires are reduced to 3. Three SMA actuators are fixed between the links 120º apart with 3% deformation strain. The catheter bends due to SMA actuators recovering their original shapes heated by the electric current. The maximum bending angle is 51º under 100 mA input current.

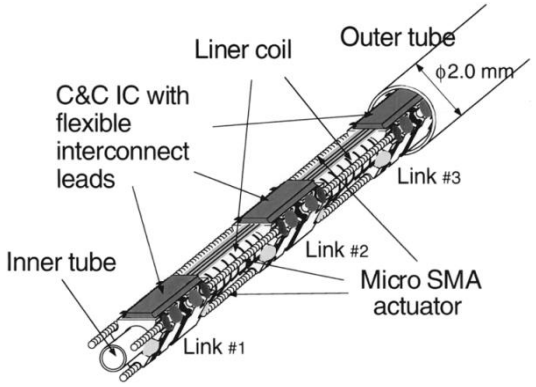

Figure 2.8. Overall structure of catheter developed by Park and Esashi (1999). Reprinted with kind permission, from (Park and Esashi 1999) © 1999 IEEE.

In order to achieve relative large actuation force and displacement of SMA actuators, several carved tubes of SMA actuators are developed. Tung et al. (2007, 2008) developed an actuator made from laser machining SMA tubes with 1.5 mm long and 1.27 mm diameter for use in an active steerable catheter (Figure 2.9). It can produce larger force (1-2 N) and displacement (20% elongation) to compare with SMA wires and coils. The 180º turn can be achieve by 9 actuators with 20º of bending each.

Although SMA actuators offer a compact alternative to conventional actuators, SMA actuators have several drawbacks: (1) they have relatively low machinability and need some special manufacturing processing, i.e. laser machining; (2) the active catheters usually need several linked SMAs, which requires many lead wires to control the SMA actuators and makes the system more complex; (3) compared with the tendon-driven catheters and magnetic catheters, SMA actuators generate lower force which may not complete complex task; (4) the heat by the

SMA actuators may cause a big problem in terms of safety. SMA actuators require to be heated by the current and makes removing heat to be quite challenging. A high temperature may cause the injury of cells or tissue; (5) they have non-linear behavior of strain to input current or temperature. SMAs have a hysteresis characteristic as a result of which their control can be difficult (Jayender et al. 2008, 2009).

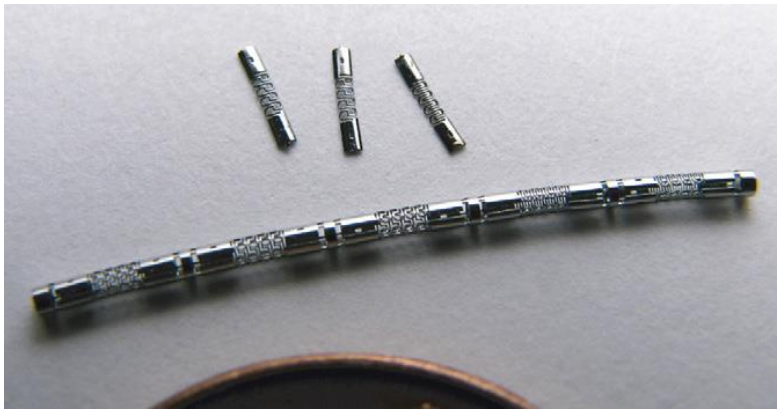

Figure 2.9. Laser machining SMA actuators by Tung et al. (2008). Reprinted with kind permission from (Tung et al. 2008) © 2008 Elsevier.

2.2.3.2 Steerable needles and concentric tubes

Besides utilizing the shape memory effect of SMA actuators to drive the catheter, the catheter made by SMAs can be shaped by pre-bent utilizing their super-plasticity and high recoverable strains, known as flexible needles (Webster et al. 2005, 2006 & 2007, Alterovitz et al. 2005 & 2008, Abayazid et al. 2013) and concentric tubes (Webster 2007; Webster et al. 2009; Dupont et al. 2010; Gosline et al. 2012).

The needles can be steered through certain curved trajectories inside soft tissue in various ways. Abolhassani et al. (2006) provided a survey regarding needle insertion into soft tissue. One way to steer this kind of needle is to make the needles with beveled tips and steer them using the asymmetric forces of a beveled tip. The bevel tips of flexible needles can be bent due to tip asymmetric when they contact the tissue during insertion. The bevel tip can be reoriented by rotation, and then push it forward until achieving the target (Figure 2.10). The needle will follow

the insertion path when retracted. It is noticed that the steerable needles cannot be operated as a manipulators in free space.

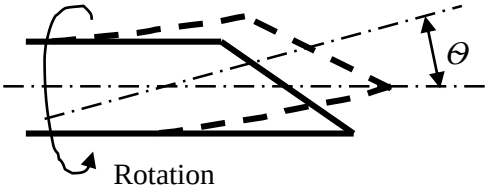

Figure 2.10. Movement of the bevel tip of needle.

Webster et al. (2005, 2006) presented a flexible needle made by nitinol and two systems for steerable needle insertion. The bevel steering effect is enhanced due to the material is more flexible. Then a robot actuates the needle with kinematic model based control techniques through rotation and translation. The kinematics-based model is limited since it did not account for needle–tissue interaction along the length of the needle. Alterovitz et al. (2005, 2008) developed a 2D planning algorithm for insertion of a flexible needle with a bevel tip into soft tissue with obstacles. The interaction between needle and soft tissue are modeled by finite element method, and this was used in the planner to account for tissue deformation. Golzman and Shoham (2007) presented a robotic system for steering the flexible needles in soft tissue in real-time closed-loop control. The planned needle-tip trajectory avoids the obstacle and hits the targets by given a target and possible obstacle locations. Duindam et al. (2010) presented a constant-time 3D motion planning algorithm for flexible needles using geometric inverse kinematics. Abayazid et al. (2013) presented an ultrasound images guided control system to robotically steer a needle made by nitinol with an asymmetric tip. They use both kinematics-based model and kinetics of needle-tissue interaction model to predict the needle deflection.

The concentric tubes made by flexible tubes can be steered as well. When a curved elastic tube is inserted inside other elastic tubes, their shapes are decided by mutually resultant curvature because they have the same stiffness. By translation and rotation of the tubes with respect to each other, their curvatures and overall length of tubes can be varied. The tubes are typically made by nitinol in its super-elastic phase. They can be made into desired shapes by heat

treatment before assembly. To compare with other types of steerable catheters, the concentric tubes are relatively new and have been investigated in the past ten years. The investigations of concentric tubes were started and mainly conducted by two research groups simultaneously, Webster et al. (2009) and Dupont et al. (2010). A review of the state of the art of concentric tubes can be found in (Gilbert et al. 2013).

Webster et al. (2007, 2009) presented an active cannula made by nitinol, which is composed of three telescoping, concentric and pre-curved tubes (Figure 2.11). The diameter of largest section is 2.4 mm and the diameter of smallest section is 0.8 mm. Each tube has a translation and rotation degree of freedom. A three tube, six-DOF actuation unit was developed to control the concentric tubes. Other important achievements regarding design, modeling and control of concentric tubes by their research group can be found in (Rucker & Webster 2009, Rucker et al. 2010, Burgner et al., Gilbert et al. 2013, Burgner et al. 2014).

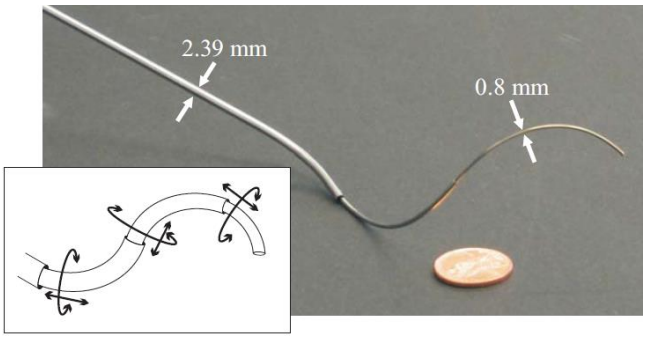

Figure 2.11. Active cannula made of superelastic Nitinol tubes (Webster et al. 2009).

Dupont et al. (2010) developed a concentric tube robot composed of three pre-curved nitinol tubes, which is similar to the active cannula by Webster et al. (2009). The diameter for the largest section is 2.77 mm and the smallest section is 1.85 mm. A tele-operation system is developed to achieve the real-time position control of tubes based on the forward kinematics and inverse kinematics models. Gosline et al. (2012) used this concentric tube robot to percutaneously access the right atrium and to deploy a tissue approximation device to complete intracardiac beating-heart surgery. Other important achievements regarding design, modeling

and control of concentric tubes by their research group can be found in (Bedell et al. 2011, Mahvash & Dupont 2011, Arabagi 2013).

Xu et al. (2012, 2013) presented a concentric tube robot composed of two nitinol tubs. The outer tube was fixed and the inner tube was rotated. The position of the distal tip can be obtained from an electromagnetic tracking system. A fast torsionally compliant kinematic model using global variables and model based control method were developed.

To compare with other types of robotic catheters, the concentric tubes are more flexible and smaller in terms of diameters. They do not utilize the shape memory effect (which can avoid heat problem). Additional sections can be easily added by increasing the number of tubes, which is often challenging to add additional bending sections to other robotic catheters. Furthermore, the lumen of concentric tubes can provide addition tubes or control wires for the tools mounted at the distal tips. However, it has several limitations. The selection of the initial curvature of each tube is an important design consideration (Webster 2007). Small radii of pre-curvature are easily to negotiate tighter turns within anatomy. However, too small radii may cause tube damage. In addition, it requires more complex control methods to be steered accurately.

2.2.3.3 Conducting polymers driven catheters

Catheters actuated by conducting polymers have shown some promise. The principle of the conducting polymer is as this. When the polymer is doped electrochemically, ions are driven into the polymer causing expansion of the volume of polymers and further generating bending displacement, and vice versa. The conducting polymers are controlled by electric signals at low voltage (under 2 V), and of easy miniaturization due to its simple structure particularly when the polymer is in fluids (Smela, 2003). The tip of catheters, which is based on the principle of conducting polymers, can be bent when an electrical potential in the electrolyte environment is applied.

Guo et al. (1995) proposed three micro catheters with active guide-wire that has two bending

degrees of freedom actuated by an Ionic Conducting Polymer Film (ICPF). The basic structure of the catheter is shown in Figure 2.12. The bending principle is that an ICPF fixed at the distal tip of guide-wire can be bent under a voltage input. Two lead wires are used for supplying electric energy to the ICPF. The diameters of these micro catheters are 1 mm, 1.3 mm and 2 mm, respectively. The ICPF actuator has fast response, driven by low voltage (2 V) to compare with the SMA in the wet condition without electrolysis and heat, safety in body (Oguro et al. 1993). The maximum bending angle is 41º with a distal displacement of 10 mm.

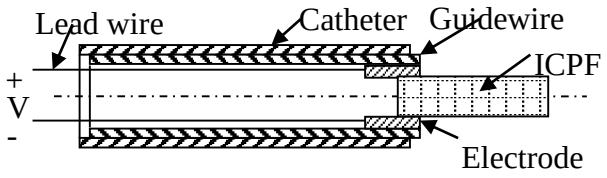

Figure 2.12. Basic structure of micro catheter developed by Guo et al. (1995). Reprinted with kind permission, from (Guo et al. 1995) © 1995 IEEE.

Santa et al. (1996) proposed two active catheters with 0.8 mm diameters by polypyrrole conducting polymer and an ionic conductor solid polyelectrolyte as ionic reservoir. In one catheter, two groups of conducting polymer actuators in the form of thin strips with a solid polymer electrolyte (SPE), respectively, are inserted in the catheter wall. In the other catheter, the wall of the catheter is made of conducting polymer fibers (CPF) embedded in a SPE elastromeric matrix (50% SPE and 50% CPF). The maximum bending angles (with a distal placement of 7.4mm) are 28º and 24º, respectively. One drawback is that the stiffness of SPE is too low.

Sewa et al. (1998) presented a gold chemically plated perfluorocarboxylic acid film for catheter system. The polymer can be bent 90º with 8 mm distal tip displacement under 2V input voltage in water. The polymer also shows durability more than 10 million cycles. Alici et al. (2006) proposed a conducting polymer actuator which has potential to be a bending tip of the steerable catheter. The electrolyte layer in the middle is polyvinylidine fluoride which is clamped by two polymer polypyrroles as the electroactive components. The thin layers of platinum are coated to polypyrroles to increase the conductivity. The maximum bending angle for the actuator strip

with length of 10 mm, the width of 1 mm and the thickness of 0.21 mm can be over 90º under 1V input voltage. However, the maximum output force at the tip is only 0.006 N under 1 V input voltage.

Fang et al. (2009) developed an active guide-wire for cardiac catheterization by using ionic polymer metal composites (IPMCs). A pair of parallel IPMCs is fixed at the distal tip of guide-wire, in particular, one serving as an actuator and the other serving as a sensor. The control signal consists of high and low frequencies. The low frequency signal makes the IPMC to deform and change its surface electrical resistance, while the high frequency signal retains the deformation information. By utilizing a lock-in amplifier to demodulate the high frequency signal, the deformation can be measured.

The main drawback of conducing polymers is of relatively low response and the nonlinearity due to their actuation principle, i.e. hysteresis and back relaxation. This is a challenge to the control system for this type of actuators.

2.2.3.4 Hydraulic pressure driven catheters

Another actuation principle is that the catheters are composed of one or several hydraulic bellows and the distal tips are steered by hydraulic pressure of bellows. The variation of hydraulic pressure inside the bellows modifies their lengths and, therefore, the bending of the catheter.

Haga et al. (2005) developed a catheter of 0.94 mm in diameter, actuated by the hydraulic suction mechanism for intravascular MIS. The catheter is made of Nitinol tube covered by a silicone rubber tube (Figure 2.13), in which, the nitinol tube is cut of a line of rings with connecting beams. The catheter is filled with water and its bending angle is controlled by the suction of water.

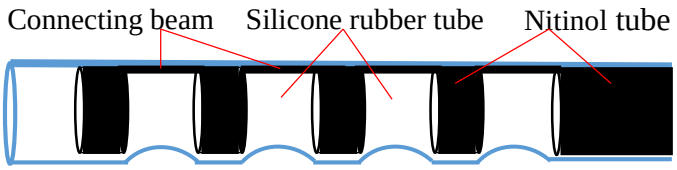

Figure 2.13. Structure of the catheter developed by Haga et al. (2005). Reprinted with kind permission, from (Haga et al. 2005) © 2005 IEEE.

Bailly et al. (2005) proposed a two-section catheter called MALICA for the endovascular treatment of aortic aneurysm. The structure of catheter consists in two bases interconnected by three 120º positioned bellows. The actual prototype has a diameter of 4.9 mm, a length of 20 mm, and a working channel of 2 mm diameter and includes two spacer disks for each section (Figure 2.14). The pressure variation inside the bellows leads to the variation in their length, which then induces the bending of the device. This section structure is modular, which can easily build a multi-section catheter. Bailly et al. (2011) proposed a catheter as well. The distal platform of catheter is driven by three completely stress-free electrodeposited nickel bellows which are actuated by hydraulic pressure. To prevent bellows from buckling while maintaining a sufficient bending, two intermediate spacer disks are used.

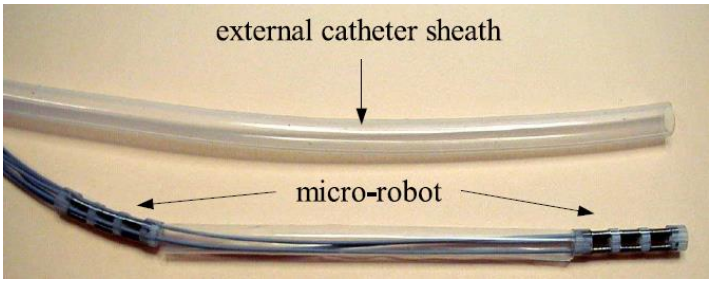

Figure 2.14. Prototype of two-section catheter developed by Bailly et al. (2005). Reprinted with kind permission from (Bailly et al. 2005) © 2005 IEEE.

Ikeuchi and Ikuta (2009) presented micro active catheter with 0.3 mm diameter using membrane micro emboss following excimer laser ablation process. A bellows at the tip is composed of a series of folded micro-chambers connected by micro-channels. The bellows can be bent on one side by hydraulic pressure within 0º to 180º.

Ikuta et al. (2012) proposed a two-section hydraulic pressure driven active catheter (Figure 2.15). They use two valves with different range of pressures to control two sections sharing common bellows. Each section has a bellows-shaped bending actuator and a micro valve to control the opening and closing the channels respectively, in particular, a low-pass valve (LPV) and a high-pass valve (HPV). Each section can be bent when the bellows is expanded by the normal saline which is not harmful for the patients in the event of the leak.

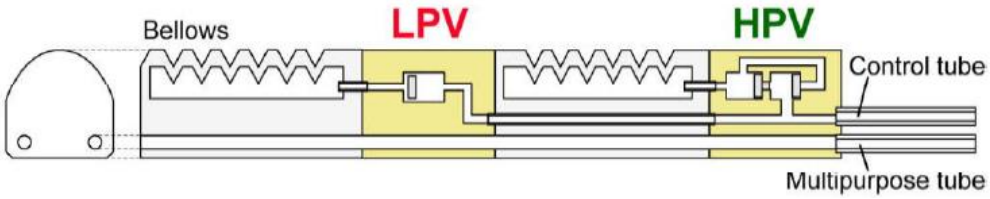

Figure 2.15. Hydraulic pressure driven active catheter developed by Ikuta et al. (2012). Reprinted with kind permission from (Ikuta et al. 2012) © 2012 IEEE.

The catheter driven by hydraulic pressure is safer than other types of catheters and retreated quickly due to its actuation principle. Nevertheless, it shows some drawbacks. The output force is relatively small which cannot complete some complex tasks. It needs bellows and micro-valves to control the hydraulic pressure that may be bulky for catheters and need relatively complex fabricating techniques. It may have leakages and cause pressure losses which limit efficiency.

2.2.4 Hybrid actuation catheters

Combination of the aforementioned two actuation catheters (Section 2.2.1 and Section 2.2.3, respectively) into a new multi-section catheter called hybrid actuation catheter is promising to achieve a relative compact structure with small size and easy control. Details for engineering hybridization principle can be found from (Zhang et al., 2010).

Butler et al. (2012) presented a robotic endoscopy for MIS, which is composed of a steerable concentric tube manipulator and an exoskeleton designed to contain and manipulate a manual

endoscope (Figure 2.16). The system consists of five segments. Part A is the initial portion of scope neck with rigid torsion. Part B is the bending section which is controlled by tendons. Part C is a short, straight and rigid section which houses the tip optics and the steerable concentric tube (Part D). The concentric tube can be rotated and translated with stiffness dominated by the scope. Part E is a straight mono-polar cautery wire device with stiffness dominated by the concentric tube.

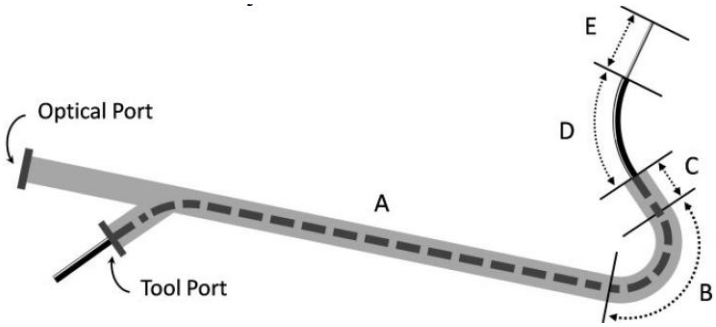

Figure 2.16. Schematic diagram of robotic endoscopy developed by Butler et al. (2012). Reprinted with kind permission from (Butler et al. 2012) © 2012 IEEE.

The Magellan^{TM} robotic catheters designed and manufactured by Hansen Medical Inc. (2016b) have three sections for peripheral vascular interventions (Figure 2.17). Based on the diameters of the proximal part of the catheters, Magellan^{TM} robotic catheters have three different sizes: 6 Fr, 9 Fr and 10 Fr. The middle section and proximal section are driven by a group of tendons separately. The distal section is pre-curved nitinol guide wire. The distal tip can be rotated and pre-curved by the middle section. To compare with the robotic endoscopy by Butler et al. (2012), the maneuverability is improved with cost of tendon-driven sections size.

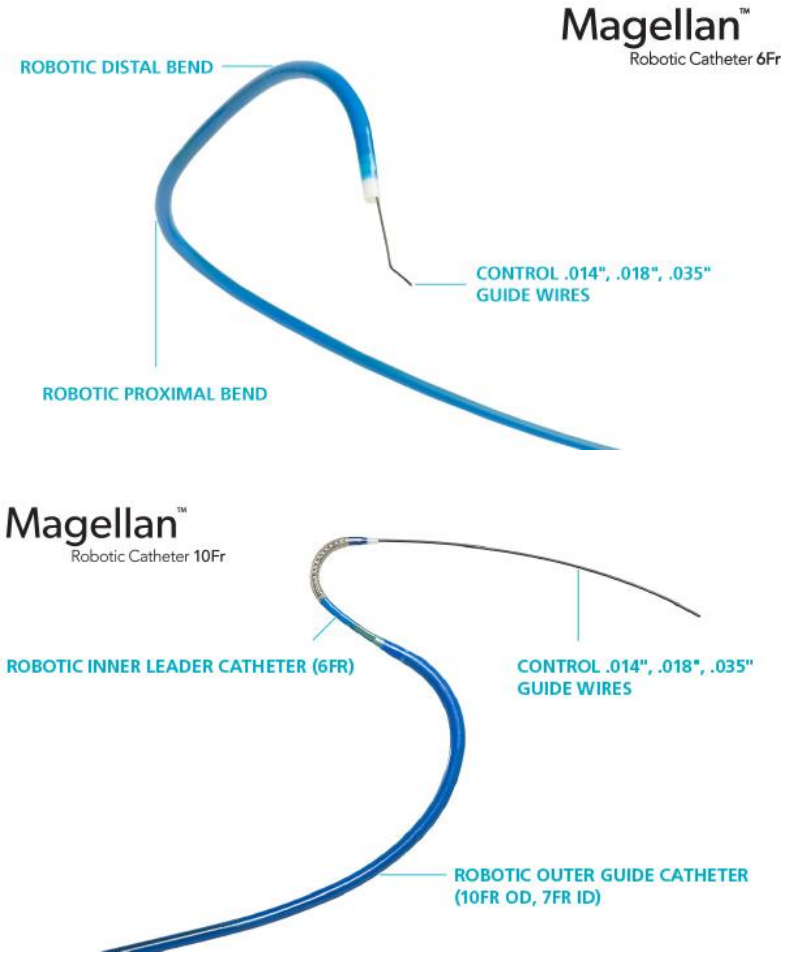

Figure 2.17. Magellan™ Robotic Catheters.

(Upper: Magellan™ 6 Fr Robotic Catheter, available at: http://www.hansenmedical.com/us/en/ vascular/magellan-robotic-catheters/magellan-10fr-robotic-catheter; Down: Magellan™ 10 Fr Robotic Catheter, available at: http://www.hansenmedical.com/us/en/ vascular/magellan-robotic-catheters/magellan-10fr-robotic-catheter).

Table 2.1 Comparisons of some typical steerable catheters in the literature

Author (year)	Actuation principle	Section	DOF	Bending Angle	Sections coupling	Distal tip force	Application	Outer Diameter (mm)
Guo et al. (1995)	Conducting polymer	1	2	42.3º	N/A	x	Aneurysm surgery	2
Santa (1996)	Conducting polymer	1	2	28º	N/A	x	General MIS	0.8
Lim et al. (1995, 1996)	SMA	2	4	13º	Co-placed	x	General MIS	2.8
Haga et al. (1998, 2000, 2002)	SMA	1	2	90º	N/A	Sensors	General MIS	1.4
Park and Esashi (1999)	SMA	2	4	51º	Co-placed	Sensor	General MIS	2
Takizawa et al. (1999)	SMA	1	2	45º	N/A	Sensor	Cerebral surgery	1.5
Jayender et al. (2009)	SMA	2	4	24.7º	Co-placed	Model	Cardiac surgery	1.5
Szewczyk et al. (2011)	SMA	1	2	70º	N/A	x	Neuroradiology	1.2
Bailly et al. (2005)	Hydraulic	2	4	90º	Independent	x	Aneurysm surgery	4.9
Bailly et al. (2011)	Hydraulic	1	2	90º	N/A	x	Aneurysm surgery	4.9
Ikuta et al. (2012)	Hydraulic	2	2	170º	Co-placed	x	Endovascular surgery	3
Degani et al. (2006)	Tendon	1	3	90º	Independent	x	Cardiac surgery	12
Harada et al. (2006) Zhang et al. (2009)	Tendon	1	2	40º	N/A	x	Intrauterine fetal surgery	2.4
Xu and Simaan (2010)	Tendon	3	6	90º	Co-placed	Model	General MIS	7.5
Kutzer et al. (2011)	Tendon	1	1	135º	N/A	x	Removal of osteolysis	5.99
Penning et al. (2011)	Tendon	1	3	180º	N/A	x	Cardiac surgery	6.35
Camarillo et al. (2009)	Tendon	2	4	90º	Independent	x	Cardiac surgery	4

Table 2.1 Comparisons of some typical steerable catheters in the literature (continued)

Author (year)	Actuation principle	Section	DOF	Bending Angle	Sections coupling	Distal tip force	Application	Outer Diameter (mm)
Jeon et al. (2012)	Magnetic	1	2	45º	N/A	x	Endovascular surgery	2
Niobe II system (Stereotaxis 2016)	Magnetic	1	2	120º	N/A	Sensor	Cardiac surgery	2.67
Webster et al. (2006)	Pre-bent	1	2	N/A	N/A	x	General MIS	0.7
Webster et al. (2009)	Pre-bent	3	6	N/A	Co-placed	x	General MIS	0.8(d)//2.39(p)
Dupont et al. (2010)	Pre-bent	3	5	N/A	Co-placed	x	General MIS	1.85(d)/2.41(m) /2.77(p)
Abayazid et al. (2013)	Pre-bent	1	2	N/A	N/A	Model	General MIS	0.5
Butler et al. (2012)	Tendon & Pre-bent	3	6	-/-/180º, 100º (p)	Independent	x	Neurosurgery	1(d)/1.3(m)/ 3.7(p)
Magellan^{TM} robotic catheter (Hansen Medical 2016b)	Tendon & Pre-bent	3	6	-/180º(m)/ 90º(p)	Independent	sensors	Peripheral vasculature	1(d)/2.13(m)/ 3.25(p)

Note:

(1) ‘x’ means unavailable;

(2) (d) means the distal section; (m) means the middle section; (p) means the proximal section.

2.2.5 Discussion

From the above discussion, each type of steerable catheters has advantages and disadvantages. Comparison of different types of steerable catheters will be presented in this part, in particular, from the aspects of maneuverability, performance, size of catheter, safety, and cost.

2.2.5.1 Maneuverability and performance

The maneuverability includes navigation and capability of being used for complex tasks. The navigation mainly refers to the control of bending angle. If the bending angle is controlled more easily and faster with a larger amplitude, the maneuverability is better. The catheters driven by tendons or hydraulic pressure can easily control the bending angle by adjusting the tendons or hydraulic pressure (the bending angle up to 180^{o} can be achieved). The friction between the tendons and pathway, backlash and slack of tendons can affect the control of tip in the tendon-driven catheter significantly. The magnetic catheter can achieve a large bending angle. The catheters driven by SMA actuators and conducting polymers can only achieve a relatively small bending angle compared with the foregoing three types of catheters. The maneuverability of pre-curved nitinol catheters is relatively poor, as the catheters are not articulated in terms of their structure.

For the capability that a catheter can be used for performing complex tasks, there are the following factors: the output force, accuracy of maneuver, DOF and workspace of catheter. If its output force is large and accurate with a sufficient number of DOFs and a sufficiently large workspace, the catheter can achieve performing complex tasks. The tendon-driven catheters have a good accuracy and a fast maneuver speed in comparison with the other types of catheters, and it can also generate a large force. This performance result is due to a high rigidity of the system and a fast response control system. The response of magnetic navigation catheter systems cannot reach too fast when the magnetic field is generated by permanent magnets. A delay occurs between designation of the magnetic field vector and catheter movement (Faddias et al. 2002; Nguyen et al. 2010). The hysteresis should be taken into account in control in this kind of catheters. The output force can be controlled by the strength of the magnetic field. The catheter driven by hydraulic pressure and pre-curved nitinol catheter are inherently more compliant, which restricts their output force and

stability. Catheters actuated by SMAs and conducting polymers rely on their materials. These materials show significant nonlinearities, i.e. hysteresis and time-varying mechanical characteristics, which are challenging for control. Accuracy of the maneuver is low with SMAs but the output force is high and the maneuver range is large. Catheters actuated by conducting polymers have a fast response.

The DOFs and workspace are basic requirements for catheter systems. The magnetic catheters have a limited workspace and DOF due to the single-section structure. There is an approach to combining several catheters in operation to increase the DOFs and workspace. For instance, Simaan et al. (2009) proposed a three arms robot with three distal dexterity units which serve like three tendon-driven steerable catheters for MIS of the throat, in particular, two for manipulation and one for suction. In the magnetic navigation catheters system, two or more catheters cannot be steered in the magnetic field simultaneously, because two or more catheter tips interfere with each other by the magnetic fields. The other types of catheters can avoid this problem.

2.2.5.2 Size of the catheter

For MIS surgery, the small diameter of catheter is one of the basic requirements. The size depends on the structure and fabricating process of catheter. The tendon-driven catheter has one or several tendons which transmit the input force to the distal tip remotely. The tendons must have sufficient stiffness to overcome the friction between the tendons and channels. They cannot be made in very small diameters in terms of reliability, which causes bulky catheters. This drawback may be amplified during increasing the sections which needs more tendons. Although the hydraulic pressure driven catheters have one or several hydraulic bellows, the size of catheters can be controlled very small. It can be multi-section without increasing the hydraulic bellows by using different pressure valves. The steerable catheters driven by SMAs, conducting polymers share some common features, that is, the actuators fixed at the distal tip and using several thin lead wires for power supply. COMS interface circuit can reduce the lead wires. This kind of catheters can be made in very small size. The magnetic catheter is embedded a small magnetic tip at the distal tip only. They do not contain any other wires or channels which make them with small diameters. The pre-curved flexible nitinol catheter is the same as conventional catheters or micro-catheter in terms

of structure. They can be fabricated in very small diameters.

2.2.5.3 Safety

Safety is one of the important factors for medical devices. A catheter must be maneuvered without causing any complications, such as perforation. One factor that affects the safety is the stiffness of catheters. The tendon-driven catheters are relative rigid, which has a potential risk of perforation. To avoid this, the accurate force feedback information has to be monitored during the operation. Various force sensors are developed and installed at the distal tips of catheters. However, the force sensors cannot be as reliable as haptic feeling of physicians. Magnetic navigation catheters and conducting polymers driven catheters can be made by very soft catheters with small size and relatively rigid distal tips. These catheters and hydraulic pressure driven catheters are inherently more compliant, so unlikely causing perforation. It is worth to mention that one of the main advantages for magnetic navigation catheter systems is reducing the complications from the clinical feedbacks using Niobe systems. However, the complication is not reduced by using Sensei X Robotic Catheter System, or even higher than manual operations based on the clinical reports, which may be caused by the relatively higher rigidity.

All the factors which may affect safety should be taken into account. The catheters actuated by shape memory effects driven by electrical power need attention. They may cause the overheat problem as well. To compare with this type of catheter, the catheters driven by conducting polymers with small voltage (under 1V) are safer. The driven liquid for pressure driven catheters is usually of physiological saline, which is not harmful to patients. In the magnetic navigation catheter system, the permanent magnets control the magnetic field by changing the relative position and cannot be switched off, which may cause the safety problem.

2.2.5.4 Cost

The cost of medical devices is an essential concern both for physicians and patients, in particular for single-used catheters. The expensive price of the catheter will restrict its wide clinical applications. Among all the steerable catheter systems, the most expensive one is the magnetic

navigation catheter system. The cost includes robotic system and operation environment. Installing a magnetic navigation catheter system may require that the catheter system be equipped with steel plates and specialized equipment to prevent the magnetic fields from interfering with other equipment. Such installations can be costly and time consuming. Other types of the catheters do not have special operation environment requirements, compatible and portable for existing operation rooms. The catheters actuated by shape memory effects, conducting polymers and hydraulic pressure require relatively complex fabricating techniques which may increase the cost. The tendon-driven catheters and pre-covered SMAs are inexpensive to compare with others.

2.3 Modeling of steerable catheters

The purpose of modeling is of two-fold. The first purpose is to optimize the existing design and to facilitate the new design. The second purpose is to improve the real-time control of the operation. In this section, some typical approaches to model the kinematics and kinetics of steerable catheters are discussed.

2.3.1 Kinematic modeling

A kinematic model describes the shape and motion of steerable catheters. Developing an accurate kinematic model of steerable catheters is a challenge due to the complexity of the elastic interaction. Unlike the kinematics of traditional rigid-link manipulators whose pose of any point on the manipulators can be fully defined by the link lengths and joint angles, the inherent compliance of steerable catheters requires to take into account the elasticity. An accurate model has to consider actuation force and torque applied to the catheters coupled with environmental interaction force. Solving these problems is a necessary first step towards the practical implementation, particularly in robotic systems.

2.3.1.1 Models of piecewise constant curvature

For modeling different types of steerable catheters, different types of steerable catheters share common assumptions and approaches. One common assumption is the constant-curvature

approximation due to the simplifications of kinematic modeling. The piecewise constant-curvature assumption means that an entire manipulator is composed of a number of mutually tangent curved segments and each segment has a constant curvature along its length. The position and orientation of the manipulator can be described by the curvature, angle and length of each segment from a set of configuration coordinates along the backbone to that point. Usually, a single constant curvature segment is used for each actuation segment of the manipulator, i.e., only one constant curvature segment is used for the distal dip of the single section steerable while two constant curvature segments are used for the proximal actuation segment and the distal actuation segment (respectively) in the two-section steerable catheter.

Based on the assumption of constant curvature, the kinematic models of steerable catheters can be derived from Denavit-Hartenberg (D-H) conversion (Ganji and Janabi-Sharifi, 2009, Khoshnam et al. 2015), exponential coordinates (Sears and Dupont 2006, Webster et al. 2009), and Frenet-Serret (F-S) conversion (Rucker and Webster 2009, Rucker et al. 2010a, Rucker et al. 2010b, Burgner-Kahrs et al. 2014). Webster and Jones (2010) presented a review of kinematic modeling of constant curvature continuum robots, which includes many different types of steerable catheters and demonstrates that several different modeling approaches can obtain a common result for piecewise constant-curvature kinematics under the same coordinate.

The D-H conversion is one of the most popular methods for the kinematics of the conventional rigid-link manipulators. In this method, a series of homogeneous transformations generated from standard D–H parameters are used to describe the kinematics of a series of rigid links connected by different types of joints (Bi et al. 2002). This method was also implemented to steerable catheters to use virtual rigid links to approximately represent the continuous structures (Ganji and Janabi-Sharifi 2007, Ganji and Janabi-Sharifi 2009, Khoshnam et al. 2015). Typically, a single section steerable catheter can be decomposed into three segments based on D-H conversion: the catheter body section, distal deflection section and end-effector section. Based on these three virtual rigid links coordinates relations, the D-H parameters table can be obtained and the kinematic transformation is constructed. In order to get more accurate prediction model, Khoshnam et al. (2015) further decomposed the deflection section into three segments based on the experimental observation of the deflection of a single section steerable catheter.

The exponential coordinates based on Lie Group theory is also a useful tool to represent the kinematics of steerable catheters, in particular, concentric tubes (Webster et al. 2006, Sears and Dupont 2006, Webster et al. 2009). The overall tubes shape locally is assumed to minimize the stored total elastic energy in the system which is used to find the equilibrium equations. The kinematics of concentric tubes is calculated by finding local minimum elastic energy based on the equilibrium equations and the shape of the end effector is defined by the arc parameters and the product of exponentials formula as described in (Murray et al. 1994). To compare with Sears and Dupont's (2006) model, Webster et al. (2009) used the way to model the kinematics of concentric tubes with consideration of torsional effects.

The F-S conversion provides a good way to derive the kinematics of piecewise constant curvature manipulators. Differential calculus, in particular, F-S conversion provides a tool to describe the static and dynamic behavior of non-linearly elastic rod (Antman, 1995). The F-S equations parameterize a curve in terms of arc length by defining a local coordinate which moves along the curve in terms of tangent vector and normal vector in planar case. The local coordinates along the curve can be obtained by integrating the tangent vector. The detailed derivation can be found in (Hannan and Walker, 2003). It can also be extended to 3-D situation (Bailly et al. 2011). Before using the F-S conversion, the basic strategy is also minimization of the total elastic energy stored in a collection of pre-shaped elastic tubes to determine the equilibrium equations. The applications in steerable catheters can be found in (Rucker and Webster 2009, Rucker et al. 2010a, Rucker et al. 2010b, Bailly et al. 2011, Burgner-Kahrs et al. 2014).

2.3.1.2 Models of variable curvature

The constant curvature has to be used carefully since this assumption may not be accurate in applications with uncertain constraints (Webster and Jones 2010, Jung et al. 2011, Khoshnam et al. 2015). Recently, efforts in steerable catheters adopting the variable curvature kinematic framework which does not conform accurately to constant curvature configurations have been made (Dupont et al. 2010, Rucker et al. 2010, Rucker and Webster 2011, Kutzer et al. 2011, Segreti et al. 2012, Murphy et al. 2013, Burgner-Kahrs et al. 2014).

The variable-curvature kinematics of the steerable catheters typically comprises a position vector with a rotation matrix which evolves along the arc length to express the backbone pose as a function of arc length. Two differential equations are used to represent the kinematics of the steerable catheter. One is that the position vector with respect to the arc length is the differential equations of the rotation matrix and velocity vector. The other is that the rotation matrix with respect to the arc length is the rotation matrix and curvature vector. The curvature vector is the derivative with respect to the arc length. Generally, the numerical integration methods have to be employed to solve these differential equations from the base to the distal tip of the catheter. The direct numerical integration methods are generally recommended. In a direct integration method, the system of equations of motion is integrated by a step-by-step numerical procedure. No transformation of the equations of motion is needed prior to integration and using difference formulas that involve one more increments of time usually approximates time derivatives.

2.3.2 Kinetic modeling

The force information of steerable catheters is important to ensure safety and efficiency. The force information can be obtained by mounting sensors at the distal tip of the catheter to measure the contact force directly. However, this procedure would be intrusive and less reliable. In addition, this is limited by the small diameters of the catheters and applications, e.g., the MRI compatibility. The other way to obtain the force information is deriving from a mathematical model and force information on the catheter but outside the human body.

The steerable catheter is a long, thin and flexible body, which does not have distinct joints and segments. The kinetics of steerable catheters has been studied with the following approaches: classical Bernoulli-Euler beam theory (Camarillo et al. 2008, Camarillo et al. 2009, Ganji et al. 2009, Khoshnam 2012), pseudo-rigid-body (PRB) models (Ganji et al. 2009, Khoshnnam et al. 2012, Khoshnnam et al. 2015), energy methods (Tunay 2004 & 2011, Xu and Simman 2008 & 2010, Webster et al. 2009, Rucker et al. 2010, Rucker and Webster 2011), Cosserat rod theory (Jones et al. 2009, Rucker et al. 2010b, Tunay 2011, Xu and Patel 2012), lumped-parameter modeling approach (Glozman and Shoham 2007, Reed et al. 2009, Jung et al. 2011, Jung et al.

2014) and finite element methods (FEM) (Alterovitz et al. 2005, Alterovitz et al. 2008, Chentanez et al. 2009).

Bernoulli-Euler beam theory is a direct analytical way to analyze a cantilevered beam undergoing large deflection which is similar to the deflection of steerable catheter. The piecewise constant curvature assumption is used in this method. The bending follows the classical Bernoulli–Euler equation which states that the bending moment is proportional to the beam curvature. Direct applications of beam theory can be found in (Camarillo et al. 2008, Camarillo et al. 2009, Ganji et al. 2009, Khoshnam 2012).

PRB models introduced by Howell (2001) are used to approximately predict the large deflection of flexible cantilever beam subjecting to tip loads since they significantly reduce the number of degrees of freedom compared with the finite element method. The PRB models are based on the Bernoulli-Euler beam theory and constant curvature assumption. In the PRB model, the flexible beam is approximated with two or more rigid links pivoted together with torsional springs. The joints and springs represent the deformations and stiffness of the material respectively. Based on the numbers of joints and segments used in the model, the PRB models have different topologies which were summarized and compared by Venkiteswaran and Su (2015). Ganji et al. (2009) and Khoshnam et al (2012) presented mechanics models to predict the contact force of the distal tip based on the deflections of the distal tip of the steerable catheter by using the PRB model with two rigid links connected by one pivot. Based on the deflection experiment results, Khoshnam et al (2015) further extended this PRB model to the PRB 3R model which has four rigid links connected with each other by three pivots. The detail information of the PRB 3R model can be found in (Su, 2009).

Energy methods is a powerful tool to model the kinetics of steerable catheters. One of sophisticated energy methods is the principle of virtual work. Xu and Simaan (2008, 2010) analyzed the intrinsic wrench sensing capabilities of a multi-backbone multi-section tendon driven manipulator based on the principle of virtual work under the constant curvature assumption. In their model, the ratio of the gravitational energy to elastic energy is a function of bending angle by given a circular bending shape of a continuum manipulator. Tunay (2004 & 2011) developed a mechanical model for

magnetic navigation catheters steered in the externally applied magnetic fields based on the principle of stationary potential energy. In their model, the potential energy consists of the strain energy of the catheter body and deformed tissue and the magnetic potential energy. Minimum elastic energy was also used to model the kinetics of both the constant curvature and variable curvature models for concentric tubes in (Webster et al. 2009, Rucker et al. 2010, Rucker and Webster 2011). The overall tubes shape locally is assumed to minimize the stored total elastic energy in the system which is used to find the equilibrium equations.

Cosserat rod theory is a well-known approach to model and simulation of slender elastic objects. A comprehensive discussion of this theory can be found in (Antoman 1995). In Cosserat rod theory, the elastic rod is regarded as a long and thin deformable body, its length larger than the cross-section area. The rod is defined as the continuous point-mass (also called the element). When the Lagrange equation of motion is applied to the rod, its large bending and twisting deformations can be captured. The steerable catheters are good examples of Cosserat rods and their kinetic models can follow the notation and formulation from Cosserat rod theory. Applications of Cosserat rod theory can be found in guide wire and catheter insertion simulation (Tang et al. 2012), tendon driven catheter (Jones et al. 2009, Rucker and Webster 2011), magnetic navigation catheter (Tunay 2011), and concentric tubes (Xu and Patel 2012, Xu et al. 2013, Rucker et al. 2010b, Burgner-Kahrs et al. 2014). In some cases, the Cosserat rod theory needs to be coupled with other models to account for the unique structure of steerable catheters (Jones et al. 2009, Rucker and Webster 2011). It is noted that the distributed force and moments along the rod are discarded in Cosserat rod theory.

Lumped-parameter modeling approach for the steerable catheter is the extension of dynamics of a lumped-mass system. In this approach, the lumped-parameter model uses virtual finite discretized mass points which are connected with each other with spring and damper to capture the dynamics. The governing equations of the system can be obtained from energy method or Newtown-Euler equations with considering of the internal and external forces which are iterated element by element. Jung et al. (2011, 2014) modeled the dynamics of the tendon driven steerable catheter in free space with considering the internal friction between the tendons and sheathes. The friction is modeled by a modified Dahl friction model coupled with the well-known Capstan equation. Glozman and

Shoham (2007) modelled the steerable needle contact with the tissue. The contact force between the needle and the tissue is modeled as a combination of lateral virtual springs distributed along the needle curve plus friction forces tangent to the needle. Reed et al. (2009) used the similar way to model the steerable needle contact with the tissue. The contact between the needle and tissue is modeled as a virtual spring-damping system.

Finite element method (FEM) can solve the mechanics of the steerable catheter with high -fidelity. The FEM analyses the physics of an elastic material by employing the principle of virtual work. It is based on the continuum mechanics. The general dynamic equilibrium equation of the linear FEM is represented as (Bathe 1996)

$$M\ddot{U} + C\dot{U} + KU = R \tag{2.1}$$

where *M* is the mass matrix of elements, *C* the damping matrix of elements; *K* the stiffness matrix of elements, *R* the resultant force and torque applied to the elements, and *U* the displacements matrix of elements which is corresponding to the *R*. The linear FEM is based on the assumption that the boundary conditions remain unchanged. This assumption is reflected in the use of constant constraint relations for the complete response. If the boundary conditions are changed, the response is linear only prior to the change in boundary condition.

The nonlinear FEM can take into account the material nonlinearity that is the nonlinear stress-strain behavior given by the constitutive relation and geometrical nonlinearity which includes large displacement, large rotations and large strain (Zhang and van der Werff 1998, Bonet and Wood 2008, Ghali 2008, Cheng et al. 2013). The general dynamic equilibrium equation of the nonlinear FEM can be derived based on the Equation (2.1) using iterative procedures. The mass matrix and damping matrix are independent with time. The stiffness matrix should be updated in each step. The stiffness at time *t* is modified as

$$K^t = {K_E}^t + {K_G}^t \tag{2.2}$$

where K_E is the linear elastic stiffness matrix, and K_G is nonlinear stiffness matrix which depends on the geometry and initial stress. The dynamic equilibrium equation of the nonlinear FEM is represented as

$$M\ddot{U}^{t+\Delta t} + C\dot{U}^{t+\Delta t} + \left(K_E^t + {K_G}^t\right)U^{t+\Delta t} = R^{t+\Delta t} \tag{2.3}$$

The FEM has shown its efficiency to model the continuum manipulators, in particular, in the contact situation. Applications can be found in the flexible needle to contact with the soft tissue (Alterovitz et al. 2005, Alterovitz et al. 2008, Chentanez et al. 2009), flexible surgical instrument inside the endoscopy (Khatait et al. 2013, Khatait et al. 2014), catheter to contact with blood vessel (ten Hoff 1993, Cotin et al. 2005, Duriez et al. 2006, Lenoir et al. 2006), colonoscope to interact with the colon (Cheng et al. 2013).

2.3.3 Discussion

The modeling the kinematics and kinetics of steerable catheters is the tradeoff between the model accuracy and computational expense. Based on the accuracy of the models, these models may be roughly classified into low-fidelity models and high-fidelity models. The models based on the piecewise constant curvature assumption are characterized as low-fidelity models. The reason is that the piecewise constant curvature assumption ignores the curvature variations along the length of the manipulator caused by the friction forces, gravity, and contact forces. The variable curvature models (e.g., Cosserat rod theory model and FEM model) are categorized into high-fidelity models since the curvature of the manipulator is varied due to the applied forces. Of course, the computational efficiency for these models is usually low.

Based on the modeling theory, some models based on the virtual rigid links, e.g., kinematic model based on D-H conversion, the kinetics models based on PRB models and lumped-parameter models have relatively high computational efficiency. They use a well-known standardized approach which is modular and have relatively simple structures. Sometimes, it is easier to work with other models by considering more complicated phenomena such as friction and contact. For instance, the lumped-parameter model can consider the nonlinear friction behavior incorporating with the Dahl friction models and Capstan equations (Jung et al. 2014). However, the main drawbacks of these models are poor accuracy, since they are not built upon elasticity theory. The models based on the elasticity theory and variable curvature can offer general framework. The governing equations are solved by numerical integration methods with high order. The accuracy of these models is greatly improved.

For the aforementioned models, most of the models are developed in free-space, which means they do not consider the interaction with their work environments. However, in many medical applications, the initial free-space catheter models need to be coupled with the environmental interaction models. For instance, the friction and contact between catheters and pathways should be taken into account during the catheter based surgeries. If the catheters go through blood vessels, the fluid dynamics should be taken into account. The steerable needle models based on the lumped-parameter modeling approach take into the consideration of the contact with the tissue (Glozman and Shoham 2007, Reed et al. 2009). However, as discussed before, these models are low-fidelity models. To compare with other methods, the FEM has shown its efficiency to model the continuum manipulators coupled with the environments by considering complex phenomena, e.g., external loads, friction behavior and contact situations.

2.4 Conclusion

The efforts of many researchers have led to significant achievements in the design, applications and analysis for the steerable catheter over the last decade. The classifications of steerable catheters based on the actuation mechanisms were reviewed. The classifications provide insight into the technical aspects behind the core aspects of steerable catheters, e.g., maneuverability and performance, possibility for miniaturization, safety and cost. Typical methods for kinematic and kinetic modeling of the steerable catheter were discussed. It can be anticipated that increasing steerable catheters would provide more promising benefit for both surgeons and patients with the less invasive access pathways and manipulation possibilities in the future.

The above review has shown some opportunities for further research on the design and modeling to advance the steerable catheter technology. (1) *Design and optimization*: the diversity of the medical applications with their specific requirements provides a wide research ground for the design of steerable catheter with its end-effector. The main design concerns of a steerable catheter are the miniaturization, workspace, maneuverability and stability which are physically related to its diameter, stiffness, actuation sections and length of each actuation segment. In other words, the design of a steerable catheter is a trade-off among these four design parameters. For this reason, the optimization of steerable catheters needs to be done. Optimization puts a high demand on

accuracy of the model for kinetics, and therefore, development of a more accurate model for steerable catheters is an emerging research area. (2) *Modeling*: variable curvature models coupled with the working environment are potentially an active research area. As discussed in Section 2.3, most of the modeling approaches for steerable catheters are based on the constant curvature assumption in free-space. However, in many medical applications, the catheter has to interact with the soft tissue in a complex way. These models based on the constant curvature approximation are no longer accurate. It requires more accurate variable curvature models coupled with the working environment by considering various complicated nonlinear behaviors. Among these modeling approaches, the nonlinear FEM is the best choice and most suitable tool to model the kinetics of the steerable catheters to interact with its work environment.

CHAPTER 3 THE KINETIC MODEL OF STEERABLE CATEHTERS

3.1 Introduction

In order to get the motion and force transmission of distal tip of the steerable catheter to ensure efficiency and safety, a kinetic model of the catheter coupled with the environmental interaction forces should be developed. The steerable catheter is a long, thin and flexible body which does not have joints and segments. It can be bent at any point, in particular, at the distal deflecting part of the catheter. The steerable catheter is under large deformation during the MIS procedures. The steerable catheter moves with respect to the interaction force between the catheter and the inner wall of the pathway by the external force from the physician. The pathway is a curved flexible object. The large deformation and interaction forces between the catheter and inner wall of the pathway need to be taken into account. The deformation of the catheter as well as pathway and their interaction show a high nonlinearity.

In this chapter, a kinetic model of steerable catheters with consideration of the aforementioned characteristics of a steerable catheter system is presented, which provides the information of both motion and force of the steerable catheter such as the shape of catheter, interaction force between the catheter and the pathway. The model of the steerable catheter is presented in Section 3.2. The model of the pathway is presented in Section 3.3. The contact model for the interaction between the steerable catheter and the pathway with consideration of friction behaviors is presented in Section 3.4. A summary is given in Section 3.5.

3.2 Model development for the steerable catheter

As discussed previously in Section 2.3, several methods are available for modeling a steerable catheter and FEM is the best choice and most suitable tool to model the kinetics of the steerable

catheters to interact with its work environment. In this study, FEM was chosen as a tool to model the steerable catheter in the pathway. In particular, the steerable catheter was modeled as a series of planar flexible beam elements connecting with each other by shared common nodes. The elongation and orientation deformations of the beam can well capture a complete deformation of the catheter. The detailed description of the planar flexible beam element will be discussed later.

The schematic diagram of the model of the steerable catheter to interact with the curved pathway is shown in Figure 3.1. The entire length of the catheter was presented by an assembly of these beam elements. The origin of the global coordinate system, *O*, was set at the middle point of the proximal end of the pathway. Node 1 represents the distal tip of the steerable catheter. It is noted that the beam elements representing the distal deflecting part of the catheter and the catheter body should be defined separately, due to the significant differences of mechanical properties of the two parts. The lengths of the beam elements used to define the distal deflecting part of the catheter have to be much shorter since this part is much more flexible than the catheter body. In addition, it is usually under large deflection during the navigation and operation of the catheter. This will be discussed in detail in the simulation part of the model.

Two assumptions were made in the model development, which are as follows:

(1) The mechanical property, such as the density of mass, flexural rigidity and damping, of each segment of the distal part of the steerable catheter is considered to be the same. It is noted that in reality, the electrodes and end-effector with their electrical wires inside the catheter are distributed over the distal part and they can affect the mechanical properties of the distal part. Modeling the entire distal part with several segments allows for consideration of this distribution.

(2) The mechanical property of each segment of the catheter body part of the steerable catheter is considered to be the same in the density of mass, flexural rigidity and damping. It is noted that in general, the entire catheter body may have non-uniform geometry and material, so modeling the entire body with several segments allows for consideration of this non-uniformity in mechanical properties.

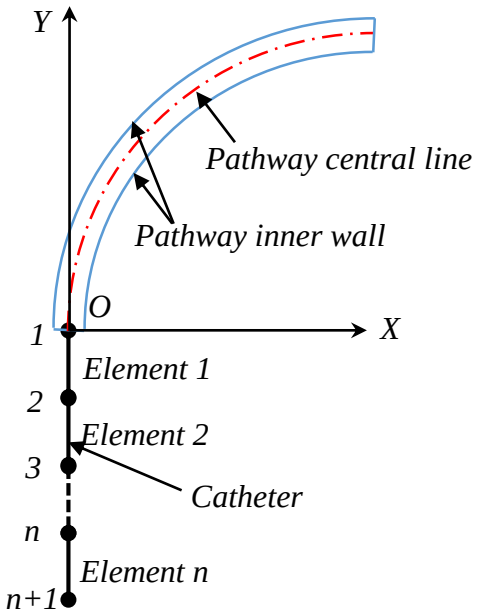

Figure 3.1. Schematic diagram of the model of the steerable catheter interacting with the curved pathway

3.2.1 Planar flexible beam element

The planar flexible beam element is shown in Figure 3.2. The beam element has two end nodes, note *p* and note *q*. The configuration of the beam element is described by two position vectors $\boldsymbol{x^p}$ and $\boldsymbol{x^q}$ of the end note *p* and note *q*. Each position vector has two Cartesian coordinates and one orientation coordinate. The angular orientations of orthogonal vectors $\boldsymbol{n_x}$ and $\boldsymbol{n_y}$ are attached to the end notes. Vector $\boldsymbol{n_x}$ is directly along the beam element axis and vector $\boldsymbol{n_y}$ is perpendicular to the beam element axis in undeflected state. The local coordinate at each node ($\boldsymbol{n_x}$, $\boldsymbol{n_y}$) is transformed to the global coordinate system by the two planar rotation matrices $\boldsymbol{R}^p$ and $\boldsymbol{R}^q$ with the angles of ϕ^p and ϕ^q respectively. Vector $\boldsymbol{x}^{(k)}$ of the *k* element coordinates is given by (Jonker 1997)

$$\boldsymbol{x}^{(k)} = \begin{bmatrix} \boldsymbol{x^p} \\ \boldsymbol{x^q} \end{bmatrix} = [x^p, y^p, \phi^p \,|x^q, y^q, \phi^q\,]^T \tag{3.1}$$

where the (x^p, y^p) and (x^q, y^q) are the Cartesian coordinates representing the positions of the element in the global coordinate system, and ϕ^p and ϕ^q are the orientation coordinates representing the orientations of the nodes, respectively.

The beam element's elongation deformation ε_1 and bending deformation parameters ε_2 and ε_3, can be represented in terms of the coordinates as follows:

$$\varepsilon_1^{(k)} = D_1^{(k)}\left(x^{(k)}\right) = \sqrt{(x^q - x^p)^2 + (y^q - y^p)^2} - l_0^{(k)} \tag{3.2}$$

$$\varepsilon_2^{(k)} = D_2^{(k)}\left(x^{(k)}\right) = (x^q - x^p)sin\phi^p - (y^q - y^p)cos\phi^p \tag{3.3}$$

$$\varepsilon_3^{(k)} = D_3^{(k)}\left(x^{(k)}\right) = -(x^q - x^q)sin\phi^q + (y^q - y^p)cos\phi^q \tag{3.4}$$

where $l_0^{(k)}$ is the original length of the element; the analytical functions $D_1^{(k)}\left(x^{(k)}\right)$, $D_2^{(k)}\left(x^{(k)}\right)$ and $D_3^{(k)}\left(x^{(k)}\right)$ are the deformation or form functions. The geometric meaning of bending deformation parameters ε_2 and ε_3 are shown in Figure 3.2.

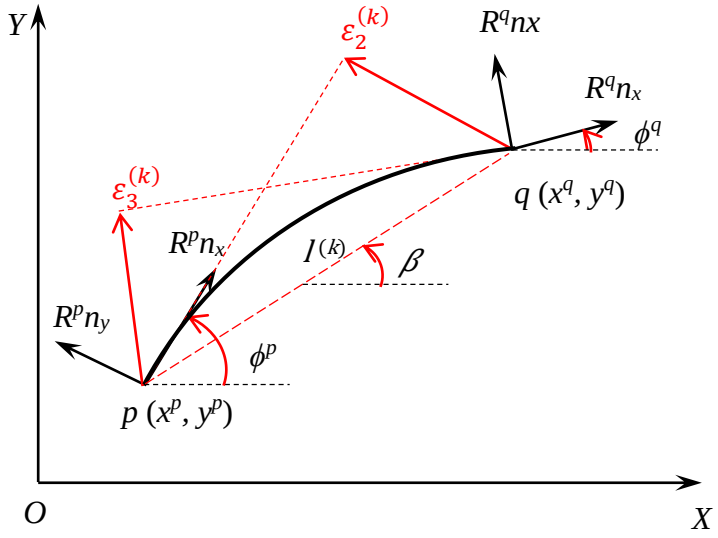

Figure 3.2. Schematic diagram of the planar flexible beam element

3.2.2 Kinematic analysis

The kinematic analysis of the steerable catheter concerns with the configuration of the system which can be obtained by the assembly of the beam elements. These beam elements are connected by shared common nodes. The configuration of the steerable catheter is described by a set of nodal coordinates $\boldsymbol{x^{(k)}}$ and deformation parameters $\boldsymbol{\varepsilon^{(k)}}$. The nodal coordinate $\boldsymbol{x}$ of the whole system is defined by

$$\boldsymbol{x} = [x_1, x_2, x_3, \ldots, x_n]^T \tag{3.5}$$

The set is a collection of all nodes in a set of elements to model the target system. The deformation parameter set or vector $\boldsymbol{e}$ can be described by the nodal coordinate set or vector $\boldsymbol{x}$ as follows

$$\boldsymbol{e} = \boldsymbol{D}(\boldsymbol{x}) \tag{3.6}$$

where **D** is a set of all deformation functions. Both constraints and inputs imposed by the environment the catheter system interacts can be defined on the node coordinates and/or deformation parameters. Based on the constraints and inputs, the nodal coordinates are classified into three groups: $\boldsymbol{x}^{(0)}$, $\boldsymbol{x}^{(m)}$, $\boldsymbol{x}^{(c)}$, and the deformation parameters are classified into three groups as well: $\boldsymbol{e}^{(0)}$, $\boldsymbol{e}^{(m)}$, $\boldsymbol{e}^{(c)}$. The definitions of these groups are listed in Table 3.1. The objective of kinematic analysis is to solve the equations for the $\boldsymbol{x}^{(c)}$ and $\boldsymbol{e}^{(c)}$ based on the governing equations by letting $\boldsymbol{e}^{(c)}$ be zero, given the independent generalized coordinates $\boldsymbol{q}$ which is defined as

$$\boldsymbol{q} = \left[\boldsymbol{x}^{(m)}, \boldsymbol{e}^{(m)}\right]^T \tag{3.7}$$

The solution can be represented by the following functions

$$\boldsymbol{x} = \boldsymbol{\mathcal{F}}^{(x)}(\boldsymbol{q}) \tag{3.8}$$

$$\boldsymbol{e} = \boldsymbol{\mathcal{F}}^{(e)}(\boldsymbol{q}) \tag{3.9}$$

Equation (3.8) and (3.9) are called the geometric transfer functions which express both the configuration and deformation state of the system. The velocity vectors $\dot{\boldsymbol{x}}$ and $\dot{\boldsymbol{e}}$ can be derived by differentiating Equation (3.8) and (3.9) with respect to time, namely

$$\dot{\boldsymbol{x}} = \boldsymbol{D}\boldsymbol{\mathcal{F}}^{(x)}(\boldsymbol{q}) \cdot \dot{\boldsymbol{q}} \tag{3.10}$$

$$\dot{\boldsymbol{e}} = \boldsymbol{D}\boldsymbol{\mathcal{F}}^{(e)}(\boldsymbol{q}) \cdot \dot{\boldsymbol{q}} \tag{3.11}$$

where $\boldsymbol{D}\boldsymbol{\mathcal{F}}^{(x)}(\boldsymbol{q})$ and $\boldsymbol{D}\boldsymbol{\mathcal{F}}^{(e)}(\boldsymbol{q})$ are the derivative functions of $\boldsymbol{\mathcal{F}}^{(x)}(\boldsymbol{q})$ and $\boldsymbol{\mathcal{F}}^{(e)}(\boldsymbol{q})$ at $\boldsymbol{q}$, respectively. The accelerations can be derived by differentiating Equation (3.10) and (3.11) with respect to time, namely

$$\ddot{\boldsymbol{x}} = \left(\boldsymbol{D}^{(2)}\boldsymbol{\mathcal{F}}^{(x)}(\boldsymbol{q}) \cdot \dot{\boldsymbol{q}}\right)\dot{\boldsymbol{q}} + \boldsymbol{D}\boldsymbol{\mathcal{F}}^{(x)}(\boldsymbol{q}) \cdot \ddot{\boldsymbol{q}} \tag{3.12}$$

$$\ddot{\boldsymbol{e}} = \left(\boldsymbol{D}^{(2)}\boldsymbol{\mathcal{F}}^{(e)}(\boldsymbol{q}) \cdot \dot{\boldsymbol{q}}\right)\dot{\boldsymbol{q}} + \boldsymbol{D}\boldsymbol{\mathcal{F}}^{(e)}(\boldsymbol{q}) \cdot \ddot{\boldsymbol{q}} \tag{3.13}$$

The kinematic analysis is performed by solving the geometric transfer functions which are usually nonlinear. They are solved iteratively using the Newton-Raphson method.

Table 3.1 Definition of the nodal coordinates and deformation parameters

Parameters	Definition
$\boldsymbol{x}^{(0)}$	boundary conditions of the coordinates
$\boldsymbol{x}^{(m)}$	independent generalized nodal coordinates (inputs)
$\boldsymbol{x}^{(c)}$	calculated dependent coordinates
$\boldsymbol{e}^{(0)}$	zero deformation parameters
$\boldsymbol{e}^{(m)}$	independent generalized deformation parameters (inputs)
$\boldsymbol{e}^{(c)}$	calculated dependent deformation parameters

3.2.3 Dynamic analysis

The dynamic analysis of the steerable catheter can be performed based on the principle of virtual power with consideration of the inertia/stiffness/damping properties of the steerable catheter and then the beam elements that cover the catheter. The force and bending moments acting on the beam element are shown in Figure 3.3. The nodal forces $\boldsymbol{F}^p\left(F_x^p,\ F_y^p\right)$, $\boldsymbol{F}^q\left(F_x^q,\ F_y^q\right)$ and bending moments T^p, T^q are acting at each node. With nodal froces $\boldsymbol{F}^{(k)} = [F_x^p,\ F_y^p, T^p, F_x^q,\ F_y^q, T^q]^T$ and nodal velocities $\dot{\boldsymbol{x}}^{(\boldsymbol{k})} = \begin{bmatrix}\dot{\boldsymbol{x}}^{\boldsymbol{p}} \\ \dot{\boldsymbol{x}}^{\boldsymbol{q}}\end{bmatrix} = \left[\dot{x}^p, \dot{y}^p, \dot{\phi}^p \ \middle| \dot{x}^q, \dot{y}^q, \dot{\phi}^q\ \right]^T$, the equilibrium equation of the beam element can be interpreted by (Jonker 1997)

$$\begin{bmatrix} 1 & 0 & 0 \\ 0 & 1 & -1 \\ 0 & l^{(k)} & 0 \\ 1 & 0 & 0 \\ 0 & -1 & 1 \\ 0 & 0 & -l^{(k)} \end{bmatrix} \begin{bmatrix} \sigma_1^{(k)} \\ \sigma_2^{(k)} \\ \sigma_3^{(k)} \end{bmatrix} = \begin{bmatrix} F_x^p \\ F_y^p \\ T^p \\ F_x^q \\ F_y^q \\ T^q \end{bmatrix} \tag{3.14}$$

where $\sigma_1^{(k)}$, $\sigma_2^{(k)}$ and $\sigma_3^{(k)}$ are the generalized stresses. The generalized stresses are calculated based on the Kelvin-Voigt model (Aarts et al. 2011). From Equation (3.14), the nodal forces can be calculated by

$$\boldsymbol{F}^{(k)} = [-\sigma_1^{(k)}, \sigma_2^{(k)} - \sigma_3^{(k)}, \sigma_2^{(k)} l^{(k)}, \sigma_1^{(k)}, \sigma_3^{(k)} - \sigma_2^{(k)}, -\sigma_3^{(k)} l^{(k)}]^T \tag{3.15}$$

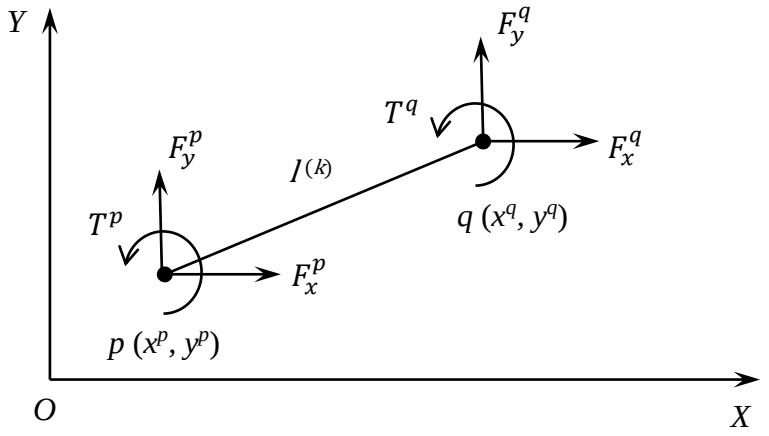

Figure 3.3. Forces and bending moments of a planar beam element

The stiffness properties of the flexible beam elements are described by the stiffness matrices $S^{(k)}$ relating to the stresses and deformations, which are expressed by (Jonker 1997)

$$S^{(k)} = \begin{bmatrix} \frac{E^{(k)}A^{(k)}}{l^{(k)}} & 0 & 0 \\ 0 & 4\frac{E^{(k)}I^{(k)}}{(l^{(k)})^3} & -2\frac{E^{(k)}I^{(k)}}{(l^{(k)})^3} \\ 0 & -2\frac{E^{(k)}I^{(k)}}{(l^{(k)})^3} & 4\frac{E^{(k)}I^{(k)}}{(l^{(k)})^3} \end{bmatrix} \tag{3.16}$$

where $E^{(k)}$ is the Young's modulus; $A^{(k)}$ is the cross sectional area; and $I^{(k)}$ is the second moment of inertia. The stress parameters $\sigma^{(k)}$ are represented by

$$\sigma^{(k)} = S^{(k)}\varepsilon^{(k)} \tag{3.17}$$

where

$$\sigma^{(k)} = \begin{bmatrix} \sigma_1^{(k)} \\ \sigma_2^{(k)} \\ \sigma_3^{(k)} \end{bmatrix} \text{ and } \varepsilon^{(k)} = \begin{bmatrix} \varepsilon_1^{(k)} \\ \varepsilon_2^{(k)} \\ \varepsilon_3^{(k)} \end{bmatrix} \tag{3.18}$$

The inertia properties of the distributed mass of the beam elements in this thesis are described by the consistent mass matrices $M^{(k)}$ which are expressed by (Jonker 1997)

$$M^{(k)} = \frac{m^{(k)}l_o^{(k)}}{420}\begin{bmatrix} 156I & 22l_o^{(k)}\dot{R}^p n_x & 54I & -13l_o^{(k)}\dot{R}^q n_x \\ 22l_o^{(k)}\dot{R}^p n_x & 4(l_o^{(k)})^2 & 13l_o^{(k)}n_x^T\dot{R}^p & -3(l_o^{(k)})^2 n_x^T\dot{R}^p\dot{R}^q n_x \\ 54I & 13l_o^{(k)}n_x^T\dot{R}^p & 156I & -22l_o^{(k)}\dot{R}^q n_x \\ -13l_o^{(k)}\dot{R}^q n_x & -3(l_o^{(k)})^2 n_x^T\dot{R}^p\dot{R}^q n_x & -22l_o^{(k)}\dot{R}^q n_x & 4(l_o^{(k)})^2 \end{bmatrix} \tag{3.19}$$

The global mass matrix *M* can be obtained by assembling the consistent mass matrices. According to the principle of virtual power for the external forces, including the inertial forces and the stress vector σ, the equation of motion of the system can be obtained (Jonker 1997)

$$\langle (\boldsymbol{F}, \boldsymbol{M}\ddot{\boldsymbol{x}}), \boldsymbol{\delta \dot{x}} \rangle = \langle \boldsymbol{\sigma}, \boldsymbol{\delta \dot{e}} \rangle \tag{3.20}$$

where *F* is the global nodal force vector which including nodal forces and inertia forces, , $\delta \dot{x}$ and $\delta \dot{e}$ virtual velocities.

By differentiating the geometric transfer fucntions Equations (3.10) and (3.11), $\delta \dot{x}$ and $\delta \dot{e}$ can be obtained

$$\boldsymbol{\delta \dot{x}} = \boldsymbol{D\mathcal{F}^{(x)}(q)} \cdot \delta \dot{\boldsymbol{q}} \tag{3.21}$$

$$\boldsymbol{\delta \dot{e}} = \boldsymbol{D\mathcal{F}^{(e)}(q)} \cdot \delta \dot{\boldsymbol{q}} \tag{3.22}$$

Substitution of Equations (3.10), (3.11), (3.12), (3.13), (3.21), and (3.22) into Equation (3.20) yields the equations of motion

$$\left[\boldsymbol{D\mathcal{F}^{(x)}(q)^T M \mathcal{F}^{(x)}}\right]\ddot{\boldsymbol{q}} = D\mathcal{F}^{(x)}(\boldsymbol{q})^{\boldsymbol{T}}\left[\boldsymbol{F} - \boldsymbol{M}\left(\boldsymbol{D^2\mathcal{F}^{(e)}(q)} \cdot \dot{\boldsymbol{q}}^{\boldsymbol{2}}\right) + \boldsymbol{D\mathcal{F}^{(x)}(q)} \cdot \ddot{\boldsymbol{q}}\right] - \boldsymbol{D\mathcal{F}^{(e)}(q)} \cdot \boldsymbol{\sigma} \tag{3.23}$$

The details of the planar flexible beam element, kinematic analysis and dynamic analysis refer to (Van der Werff 1977, Jonker 1997).

3.2.4 Numerical integration method

The equations of kinematic analysis and dynamic analysis of the FEM model of the steerable catheter are solved numerically in commercial FEM software – SPACAR in Matlab environment. The SPACAR program is based on the non-linear FEM (as presented above), which is capable of analysing the multi-DOF mechanisms with flexible links and treat the general case of the coupled large displacement motion and small elastic deformation. The analysis is performed by solving the non-linear equations of motion or by using the perturbation method. Various types of integrators are available in the SPACAR program, which include various explicit, semi-implicit and implicit methods (Aarts et al., 2011). The integrator with its initial time step and error tolerance significantly affects the convergence, stability, accuracy and computational time of the model in the simulation. The small error guides the integration method towards choosing sufficiently small time steps needed for the stability and convergence. The error tolerance is used to control the step size in each

step of integration. The larger values may cause the system no convergence, unstable and lower the accuracy, while the smaller values improve the accuracy with but increasing the computational time. The explicit fifth-order Runge-Kutta integrator with variable step size was used for solving the problem in this thesis. An initial time step of $1x10^{-5}$ s was chosen. An absolute error tolerance and relative error tolerance of $5x10^{-8}$ were used for the integrator.

3.3 Model of the insertion pathway of the catheter

During the MIS operation, the inner wall of the pathway deforms in a complex way due to the interaction force with the catheter, although the pathway is constrained by the soft tissues. However, the dynamic behavior of the pathway is not significant compared with the steerable catheter. In this thesis, the centerlines of the pathway were assumed to be fixed and the inner walls of pathway can be deformed during the interaction with the steerable catheter. The deformation of wall of the pathway can be defined by the wall stiffness and damping ratio, and the input force imposed from the catheter.

In real surgical situation, the geometric information of the pathway can be obtained by medical images, i.e., CT scan and ultrasound, which can be quite complex. In this study, in order to increase the computational efficiency, the pathway is simplified as a series of piecewise constant curvature flexible tubes. Each segment of flexible tube has a uniform inner diameter and a wall thickness. The geometric behavior of each segment of tube was defined by the centreline of tube with its inner diameter d_i. The centerlines can be represented by a straight line, a circular arc, and sinusoid curve, etc. The entire pathway was combined by these different geometric shapes connected with each other. The connection of two segments of centerlines is represented by sharing the same tangents at the connecting joint by two segments. The centerlines were represented by $l_i = [x_i, y_i]^T$, where, i is the i^{th} segment, which indicates the coordinates of points of the centerlines in the global coordinate. The original point of the global coordinate was defined at the enter point of the pathway.

Figure 3.4 illustrates a part of a curved pathway whose centerline is composed by an arc $\widehat{BC}$ of 90 degree with the radius of R_i and two straight lines AB and CD at both ends of the arc. The center point of the arc is at $O_i(x_o, y_o)$. The geometric information of this pathway can be defined by the

vectors $\overrightarrow{OA}$, $\overrightarrow{OO_i}$, $\overrightarrow{OB}$, $\overrightarrow{OC}$ and $\overrightarrow{OD}$ with inner diameter d_i and arc radius R_i. Each point $l_i = [x_i, y_i]^T$ on the global coordinate can be defined by the given geometric information of each segment.

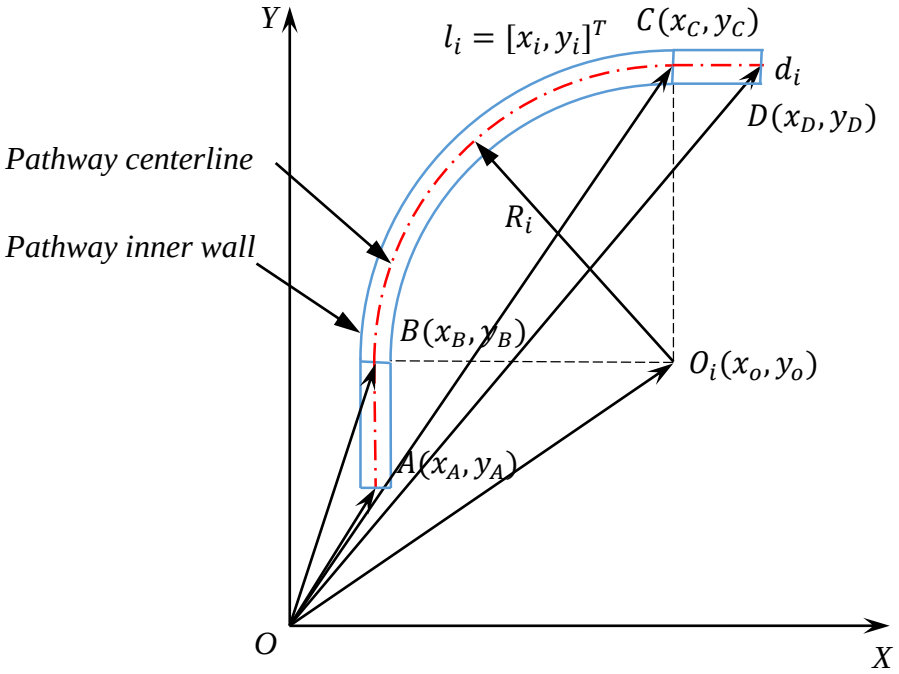

Figure 3.4. Schematic diagram of a part of curved pathway

3.4 Contact model between the catheter and the pathway

In this section, the contact model between the steerable catheter and the pathway is illustrated. Contact forces computed from the contact model will be applied to the kinetics model of the steerable catheter in order to solve the force-motion equations in Section 3.2. In this study, the hydrodynamic drag force in the pathway is not considered because it is very small and can be off-set by a proper operation (e.g., insertion of more force).

In this study, the contact force between the beam elements (which represent the steerable catheter) and the inner wall of the pathway is defined at the nodes of beam elements. As the nodes of beam elements deviate from the centerlines and contact with the inner wall of the pathway, the contact forces applied at the nodes are equivalent to the elastic forces of the wall deformations which are related to the depths and speeds of the penetration of nodes. The forces and velocities on the nodes

of beam elements interact with the inner wall of the pathway are analyzed, as shown in Figure 3.4. Besides the proximal end input node, the forces applied at other nodes of elements contact with the pathway are mainly contact force and friction force. The contact force F_n is in the normal direction of the contact point on the curved pathway. Its direction can either point out from the center point of the curve or be opposite. The friction force F_f is always along the tangent direction of the contact point and its direction is always opposite to the tangent direction of the nodal motion at the contact point. Therefore, the resultant force $\boldsymbol{F}$ applied at the node during interaction is represented by

$$\boldsymbol{F} = \boldsymbol{F_n} + \boldsymbol{F_f} \tag{3.24}$$

The instantaneous velocity vector $\boldsymbol{v}$ of the node in the contact point, it can be represented as

$$\boldsymbol{v} = \boldsymbol{v_n} + \boldsymbol{v_t} \tag{3.25}$$

where $\boldsymbol{v_n}$ is the decomposition velocity on the normal direction of contact point and $\boldsymbol{v_t}$ is the decomposition velocity on the tangent direction of contact point.

3.4.1 Contact between the steerable catheter and pathway

In order to obtain the contact force, the contact situation of each node of a beam element has to be determined by the normal distance x_n between the centerline and the displacement of each node in each small time step. It is easy to understand that if the normal distance is larger than the inner radius of the pathway, the node contact with the inner wall of the pathway. From Figure 3.5, the normal distance x_n can be obtained by

$$x_n = \left|\overrightarrow{O_\iota P} - \overrightarrow{O_\iota C_\iota}\right| \tag{3.26}$$

where vectors $\overrightarrow{O_\iota P}$ and $\overrightarrow{O_\iota C_\iota}$ are given by

$$\overrightarrow{O_\iota P} = \overrightarrow{OO_\iota} - \overrightarrow{OP} \tag{3.27}$$

$$\overrightarrow{O_\iota C_\iota} = \overrightarrow{OO_\iota} - \overrightarrow{OC_\iota} \tag{3.28}$$

Based on the normal distance x_n, there are three categories of regions for the beam element inside in the pathway (ten Hoff 1993), which are shown in Figure 3.4:

(1) No contact zone: when x_n is smaller than the inner radius r_i of the pathway, there is no contact at all.

(2) Transitional contact zone: when x_n increases to r_i, the node of beam element starts to contact with the inner wall of the pathway. The transitional contact zone is such that x_n is between the r_i and r_a, which makes the computational force continuously increase.

(3) Full contact zone: when x_n is larger than r_a, the node of beam is in full contact with the inner wall of the pathway.

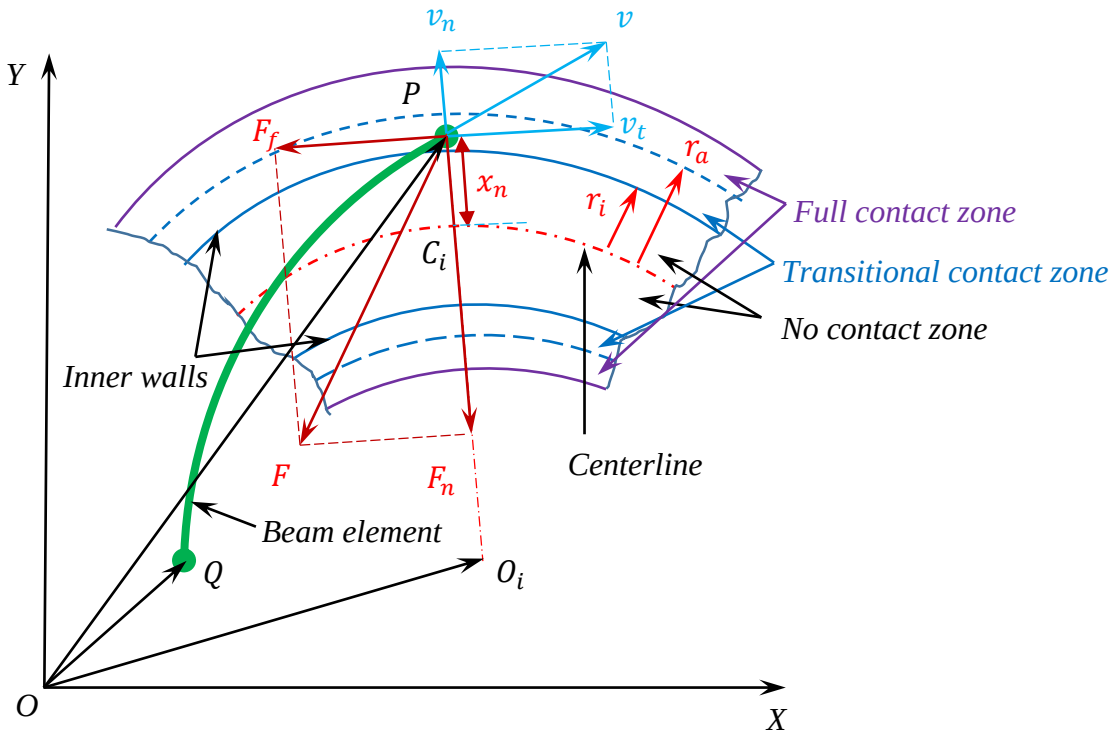

Figure 3.5. Force and velocity applied on the node *P* at the contact point.

The normal contact force F_n in different regions is given by (ten Hoff 1993, Khatait et al. 2014)

$$F_n = \begin{cases} 0 & if\ x_n < r_i \\ \frac{k_p(x_n - r_i)^2}{2(r_a - r_i)} + \frac{[3(r_a - r_i) - 2(x_n - r_i)^2](x_n - r_i)^2}{(r_a - r_i)^3} c_p v_n & if\ r_i \le x_n \le r_a \\ \frac{1}{2} k_p (2x_n - r_i - r_a) + c_p v_n & if\ x_n > r_a \end{cases} \quad (3.29)$$

where k_p and c_p are the stiffness and damping coefficient of the wall of the pathway. In this study, the contact model has been converted to the discrete form during the iterative computational steps in FEA. At a particular *t* step, Equation (3.29) can be expressed as

$$F_n(t) = \begin{cases} 0 & if\ x_n(t) < r_i \\ \frac{k_p(x_n(t)-r_i)^2}{2(r_a-r_i)} + \frac{[3(r_a-r_i)-2(x_n(t)-r_i)^2](x_n(t)-r_i)^2}{(r_a-r_i)^3} c_p v_n(t) & if\ r_i \le x_n(t) \le r_a \\ \frac{1}{2}k_p(2x_n(t) - r_i - r_a) + c_p v_n(t) & if\ x_n(t) > r_a \end{cases} \quad (3.30)$$

3.4.2 Friction model

When the steerable catheter contacts the inner wall of pathway, the friction force will play an important role. Each contact point of the catheter with the pathway has a friction state, either stick or slip, due to the maneuvering force which is applied at the proximal end of the catheter by physicians. The stick state is a static friction state, in which there is no relative motion of the contact point between the catheter and pathway. The slip state is a dynamic friction state, in which, the relative motion between the catheter and pathway occurs along the tangential direction. In different friction states, the friction has different characteristics. The friction states between the catheter and pathway have to be transformed because the maneuvering force is not continuous during the navigation of the steerable catheter in surgeries. From the static friction to dynamic friction, it shows Stribeck effect and pre-sliding behaviors. The Stribeck effect is such that the friction force decreases when the sliding velocity is increased from the static friction to dynamic friction. The pre-sliding behavior is such that the asperities on two contact surfaces will experience deformation that results in the pre-sliding motion when the external force is not large enough to overcome the stationary friction. It also shows the viscous friction and hysteresis behaviors with a flexible object inserting into a pathway (Wang and Yan 2009, Khatait et al. 2014).

A large number of friction models have been developed in the literature. A comprehensive comparison of the typical friction models can be found in (Liu et al. 2015, Kang 2007). Ideally, a comprehensive friction model which can capture all these friction characteristics should be used to describe the friction behaviors between the steerable catheter and pathway. However, a comprehensive friction model which has relatively complex structures and parameters could largely decrease the computational efficiency. Three typical friction models are discussed in detail: Coulomb friction model, Dahl friction model and LuGre friction model. Based on the accuracy and computational efficiency of applications, a simplified LuGre friction model is proposed and mainly used in this study.

3.4.2.1 Coulomb friction model

The first classical friction model is Coulomb friction model which is widely used due to its simplest structure. In the Coulomb friction model, the friction force is proportional to the normal load and its direction is along the opposite direction of velocity. The mathematic form of Coulomb friction force F_c can be represented as

$$F_c = \mu F_n \tag{3.31}$$

where μ is the Coulomb friction coefficient, and F_n is the normal load between the two contact surfaces. In this study, the contact model is converted to the discrete form during the iterative computational steps in FEA. At a particular *t* step, Equation (3.31) can be expressed as

$$F_c(t) = \mu F_n(t) \tag{3.32}$$

The normal contact force $F_n(t)$ can be obtained from Equation (3.32). Coulomb friction is unable to capture some friction characteristics: Stribeck effect, pre-sliding behaviors, viscous friction and hysteresis, due to its simplicity.

3.4.2.2 Dahl friction model

Another commonly used friction model with simple structure is Dahl friction model. The Dahl friction model models the friction force as a function of the relative displacement of the two contact surfaces, taking the following form (Olsson et al. 1998)

$$\frac{dF_f}{dx} = \sigma_0 (1 - \frac{F}{F_c} sgn\dot{x})^{\alpha} \tag{3.33}$$

where F_f is the friction force, x the relative displacement between the two contact surfaces, σ_0 the contact stiffness coefficient, F_c the Coulomb friction force, $\dot{x}$ the relative velocity between the two contact surfaces, and α a parameter to determine the shape of the stress-strain curve. $\alpha = 1$ is the most commonly used in the literature. In this study, the value of α is taken 1 as well. In the time domain, the Equation (3.33) can be derived as

$$\frac{dF_f}{dt} = \frac{dF_f}{dx} \cdot \frac{\mathrm{d}x}{dt} = \sigma_0 (1 - \frac{F_f}{F_c} sgn\dot{x}) \frac{\mathrm{d}x}{dt} \tag{3.34}$$

Then, the Dahl friction force can be expressed as

$$F_f = \sigma_0 z \tag{3.35}$$

$$\dot{z} = \dot{x}(1 - \frac{F_f}{F_c} sgn\dot{x}) \tag{3.36}$$

where z is defined as average displacement of elastic component. In this study, the friction model has to be transformed to the discrete form during the iterative computational steps in FEA. At a particular *t* step, Equation (3.35) and (3.36) can be expressed by the parameters in currents step at time *t* and previous step at time (*t-1*) by the following forms

$$F_f(t) = \sigma_0 z(t) \tag{3.37}$$

$$\dot{z} = \frac{z(t)-z(t-1)}{\Delta t} = v_t(t)(1 - \frac{F_f(t)}{F_c(t)} sgnv_t(t)) \tag{3.38}$$

Then $z(t)$ in the Equation (3.37) can be derived based on the Equation (3.38) as

$$z(t) = v_t(t)\Delta t \left(1 - \frac{F_f(t)}{F_c(t)} sgnv_t(t)\right) + z(t-1) \tag{3.39}$$

where the Coulomb friction force can be obtained by Equation (3.26), and tangential velocity $v_t(t)$ at each contact point can be obtained based on the FEM of the steerable catheter. By given $z(0) = 0$ at the initial time step, the friction force at each contact point can be obtained by Equation (3.37) and (3.39).

The Dahl friction model shows its efficiency and to capture the hysteresis behavior of a tendon sliding in a sheath in a robotic catheter model (Jung et al. 2011). However, it cannot describe the viscous friction and Stribeck effect due to its simplicity. In addition, to compare with Coulomb friction model, by using Dahl friction model, the initial step and error tolerances used in the simulation of FEM of steerable catheter should be decreased with the consideration of the stability and convergence. This can increase the computational time.

3.4.2.3 LuGre friction model

One of comprehensive friction models to capture all the friction characteristics mentioned before is LuGre friction model which is the extension Dahl friction model. The mathematic form of LuGre friction model is given by (Kang 2007, Canudas de Wit *et al*. 1995)

$$F_f = \sigma_0 z + \sigma_1 \dot{z} + \sigma_2 \dot{x} \tag{3.40}$$

$$\dot{z} = \dot{x}(1 - \frac{\sigma_0 z}{|F_c|} sgn\dot{x}) \tag{3.41}$$

where F_f is the friction force, x the relative displacement between the two contact surfaces, σ_0 the contact stiffness coefficient, σ_1 the damping coefficient, σ_2 the viscous friction coefficient, F_c the Coulomb friction force, z the average displacement of elastic component and $\dot{x}$ the relative velocity between the two contact surfaces.

In this study, the LuGre friction model have been converted to the discrete form during the iterative computational steps in FEA. At a particular *t* step, Equation (3.40) and (3.41) can be expressed by the parameters in currents step at time *t* and previous step at time (*t-1*) by the following forms

$$F_f(t) = \sigma_0 z(t) + \sigma_1 \dot{z}(t) + \sigma_2 v_t(t) \tag{3.42}$$

$$\dot{z}(t) = \frac{z(t)-z(t-1)}{\Delta t} = v_t(t)\left(1 - \frac{\sigma_0 z(t)}{|F_c(t)|} sgn v_t(t)\right) \tag{3.43}$$

Then $z(t)$ in the Equation (3.42) can be derived based on the Equation (3.43) as

$$z(t) = v_t(t)\Delta t\left(1 - \frac{\sigma_0 z(t)}{|F_c(t)|} sgn v_t(t)\right) + z(t-1) \tag{3.44}$$

During the iterative computational steps, each step size is quite small ($1\text{x}10^{-5}$ used in simulation part), $z(t) \approx z(t-1)$ can be obtained, then Equation (3.44) can be written as

$$z(t) = v_t(t)\Delta t\left(1 - \frac{\sigma_0 z(t-1)}{|F_c(t)|} sgn v_t(t)\right) + z(t-1) \tag{3.45}$$

where the Coulomb friction force can be obtained by Equation (3.26), and tangential velocity $v_t(t)$ at each contact point can be obtained based on the FEM of the steerable catheter. By given $z(0) = 0$ at the initial time step, the friction force at each contact point can be obtained by Equations (3.42), (3.44) and (3.45).

LuGre friction model is able to describe more friction behaviors and gets more accurate result. However, to compare with Coulomb friction model and Dahl friction model, by using LuGre friction model, the initial step and error tolerances used in the simulation of FEM of steerable catheter should be further decreased with the consideration of the stability and convergence. This can increase the computational time. Some other comprehensive friction models may be able to predict more accurate results, i.e., the elastoplastic friction model (Dupont et al. 2000) which is the extension of LuGre friction model and Leuven friction model (Swevers et al. 2000) which can improve the hysteresis behavior of the friction predicted by LuGre friction model, but they have more complicated structures which can further decrease the computational efficiency. In this study,

these friction models with more complicated structures are not considered due to the consideration of the computational efficiency.

In this study, the deformations of steerable catheter and pathway are in the elastic phase which leads to $\dot{z} = \dot{x}$. Equation (3.40) can be reduced to

$$F_f = \sigma_0 z + (\sigma_1 + \sigma_2)\dot{z} \tag{3.46}$$

where $(\sigma_1 + \sigma_2)$ is a constant coefficient and it can be denoted as σ_1 simply. The following simplified LuGre friction model can be obtained

$$F_f = \sigma_0 z + \sigma_1 \dot{z} \tag{3.47}$$

Based on above discussion, the discrete form of this simplified LuGre friction model can be represent as

$$F_f(t) = \sigma_0 z(t) + \sigma_1 \dot{z}(t) \tag{3.48}$$

where $\dot{z}(t)$ and $z(t)$ are given by Equation (3.44) and (3.45). The simplified LuGre friction model can improve the computational efficiency to compare with LuGre friction model. Its accuracy is higher than Coulomb friction model and Dahl friction model. It will be mainly used in this study.

3.5 Conclusion

In this chapter, the model of the steerable catheter and the model of the pathway were presented. For the steerable catheter model, the planar beam element was employed. Each planar beam element has two translational coordinates and two rotational coordinates, which describe and update the deformation and motion of the element in the global coordinate. Each element is connected by sharing common node to represent the assembled steerable catheter. It is noted that the beam elements used to represent the distal deflection part and catheter body were defined separately. In order to model the pathway, the geometric information and mechanical properties were defined. The geometric information was modeled by the centerline of each segment with the inner diameter. The deformation of wall of pathway was defined by the wall stiffness and damping ratio, and the input force by the catheter. The interaction between the steerable catheter and pathway was described by adding the contact model and friction models. Coulomb friction model, Dahl friction model, LuGre friction model and simplified LuGre friction model and their discrete forms used in finite element computation were described. Based on the accuracy and computational

efficiency of applications, the simplified LuGre friction model was chosen for the problem in this study.

CHAPTER 4 EXPERIMENTAL VALIDATION OF THE KINETIC MODEL

4.1 Introduction

This chapter provides a description of the validation of the developed kinetic model described in the last chapter. The validation was performed on a built steerable catheter test-bed. A transparent flexible pre-shaped PVC tube was used to model the pathway in the test-bed. Various groups of experiments were performed to estimate the parameters of the steerable catheter and pathways which were used in the simulation. In this study, an experimental test-bed of the steerable catheter interacting with the pathway was built. The input of the kinetic model of the steerable catheter is the external force applied by the physician, and the outputs of the kinetic model include the motion of the catheter and the output force of the distal tip of the catheter. The test-bed is able to collect the information of the motion and force of the catheter during experiments, sufficient for the kinematics and dynamics of the catheter.

This chapter is organized as follows. Section 4.2 presents the experimental test-bed constructed in this study, including instruments, sensors and data acquisitions. Section 4.3 presents several groups of experiments to estimate the mechanical properties of the catheter and pathways. Section 4.4 presents the comparison of the experimental results and simulation results. Discussions and conclusions of the developed kinetic model and experiments are given in Section 4.5 and Section 4.6, respectively.

4.2 Experimental setup

An experimental setup of the steerable catheter was developed to validate the model. In general, the test-bed with comprehensive data collection was developed that was comprised of a 7F B Curve Stinger™ Ablation Catheter (Bard® Electrophysiology Division C.R. Bard, Inc., Lowell, MA),

PVC tubes which were used to be the phantom of the pathway, catheter force and torque monitor (abbreviation: CFTM), flexible force sensor (Tekscan Inc., Boston, MA), coordinate papers and a computer with the interfaces of data acquisition of two types of force sensors. The details of each apparatus are described as follows:

(1) The 7F B curve Stinger™ Ablation Catheter is composed by two main parts: the catheter and the control unit, which are shown in Figure 4.2. There is a 52 mm at length of deflecting part at the distal end of catheter. It has three diagnosis electrodes and one radio frequency electrode. The catheter distal tip can be deflected in two directions, which is remotely controlled by the control unit through a pair of fine steer wires.

(2) Various stiffness and diameters of the transparent PVC tubes were used to be the phantom of pathways, for instance, blood vessels. The PVC tubes were fixed on the coordinate papers with 1 mm resolution, which can read the displacement of the distal tip by a camera. The tube was pre-curved to be a 90° circular arc with the radius of 0.2 m. The distal end (10 mm) and proximal end (50 mm) of the tube kept straight which makes the catheter insertion smooth.

(3) The CFTM is a handheld force/torque measuring attachment which can be mounted on the catheter body, and provides a real-time feedback on the force and torque applied by hand during experiments. It was used to collect the input force and torque in this study. The CFTM was assembled by an ATI Nano43 Transducer (ATI Industrial Automation, Apex, NC), a catheter fixed part and a handle which are shown in Figure 4.3. The Nano43 Transducer is a small 6-axis force/torque transducer. The force range 18 N and torque range 250 Nmm with the resolution of 1/256 N in force and 0.05 Nmm in torque was used in this setup. It allows the catheter body and catheter fixed part to pass through its center hole. The transducer was calibrated by the manufacturer. The Nano43 Transducer was supplied power by a power amplifier (Model: FTIFPS1, ATI Industrial Automation, Apex, NC). The data was collected by a 16-bits data acquisition board (Model: NI USB-6210, National Instruments™, Austin, TX) to the computer. The sampling rate was set to 500 Hz and the averaging level was set to 10, which could reduce the noise signal by averaging each 10 signals. The real sampling frequency was 50 Hz.

(4) The flexible force sensor is a paper-thin 0.203 mm FlexiForce® B201 sensor (Tekscan® Inc. Boston, MA) with an accuracy level of ± 3% by controlled procedures to calibrate. The

FlexiForce® B201 sensors include the following three force ranges: low 0-11 N, medium 0-667 N and high 0-4448 N. In this study, the low range sensor was used. The force sensor was connected with a plastic Economical Load and Force (ELF) handle. The plastic ELF™ handle contained data acquisition electronics with USB connection and interface to B201 sensors (Figure 4.1). Patented electronics allow operators to optimize the performance of the ELF system over a selected force/load range. The electronics adjust the device sensitivity to best fit the dynamic range of the specific application. This allows to "fine tune" FlexiForce® sensors for optimal performance. The flexible force sensor was used to measure the normal contact force between distal tip of catheter and target site in the experiments. Before using this sensor, the calibrating procedures of this flexible force sensor were taken which were as follows: a) inserting the catheter to the pathway (PVC tube) to let the distal tip contact with FlexiForce® sensor; b) pushing the catheter and adjusting the sensitivity to 18 to get the optimal results which allow to measure the normal contact force in proper level; c) calibrating the sensor by preloading the known weights which were measured by the electronic balance (12.203 g, 25.367 g, 50.607 g, 70.102 g, 88.984 g, 100.939 g, 111.862 g, 128.912 g). The acceleration of gravity was 9.8 kg/N. The normal force readings were logged at a sampling frequency of 50 Hz which was synchronized with the ATI Nano43 Transducer.

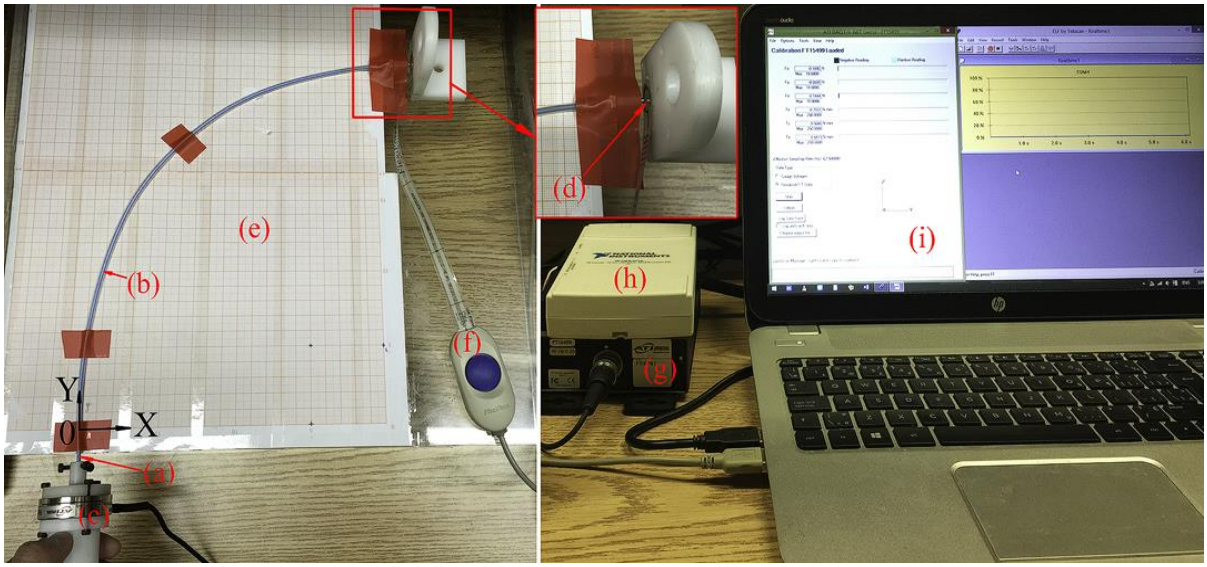

Figure 4.1. Experimental setup for validating the kinetic model of the steerable catheter (a: steerable catheter; b: PVC tube; c: catheter force monitor; d: FlexiForce® B201 sensor; e: coordinate paper; f: plastic ELFTM handle; h: DAQ board; g: Power amplifier; i: computer)

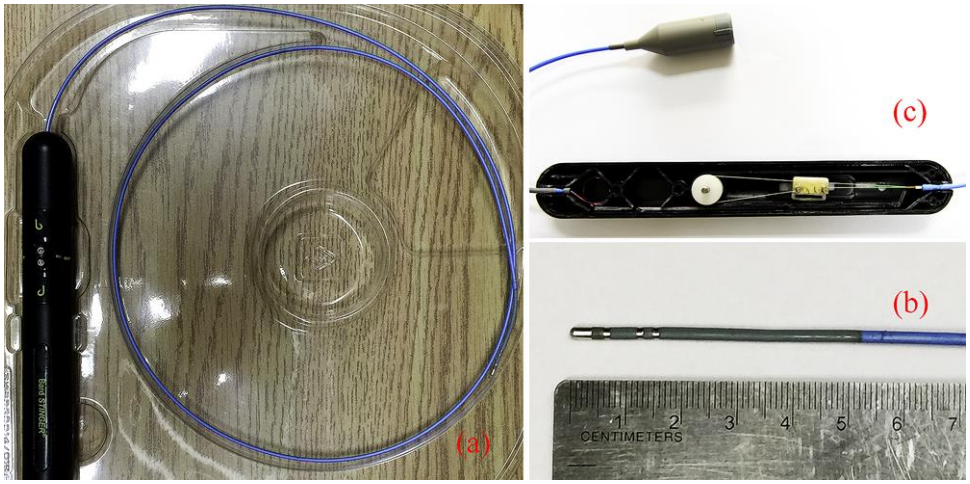

Figure 4.2. Bard Stinger Ablation Catheter and its control unit

(a: catheter with control unit; b: distal tip of catheter; c: inside of the control unit)

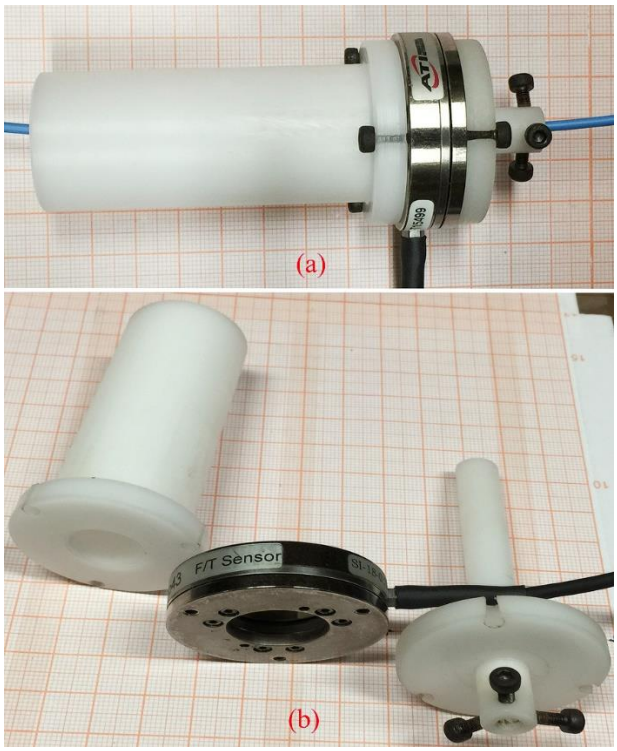

Figure 4.3. Catheter force and torque monitor (CFTM)

(a: assembled CFTM; b: unassembled CFTM)

4.3 Experimental estimation of the parameters of the kinetic model

In Chapter 3, the kinetic model of the steerable catheter was developed. In order to validate this kinetic model, the input parameters related to the mechanical properties of the steerable catheter and PVC tube were identified in this study by conducting several groups of experiments in this part. These parameters were used in the kinetic model simulation in SPACAR software later.

4.3.1 Experimental estimation of the stiffness and flexural rigidity of the catheter and tube

4.3.1.1 Experimental design and methods

The apparatus for the estimation of the flexural rigidity and stiffness of the steerable catheter and tube pathways was the Texture Analyzer (Texture Technologies Corp, Hamilton, MA). The experimental setup was shown in Figure 4.4. A test-rig with the 30 mm span for the three-point bending test of catheter body and catheter distal deflecting part which is 52 mm in length from the distal tip (Figure 4.5), and 50 mm span for the three-point bending test of the tubes (Figure 4.4) was set up. They were mounted on the Texture Analyzer testing machine as shown in Figure 4.4. The 7F B Curve Stinger™ Ablation Catheter and PVC tubes samples (phantom of the pathway) were placed and supported by the rig as shown in Figure 4.4 and Figure 4.5. As such, the catheter and PVC tubes were supported by two support frames which have a span L of 30 mm and 50 mm respectively, and a load F was put on the mid-point to produce a displacement δ. The flexural rigidity EI was calculated by

$$EI = FL^3/48\delta \tag{4.1}$$

The stiffness k was calculated by

$$k = F/\delta \tag{4.2}$$

where the stiffness k can be represented by

$$k = 48EI/L^3 \tag{4.3}$$

Here, the assumption that the relation between the stress and strain is linear is reasonable when the catheter and tubes were under small deflection.

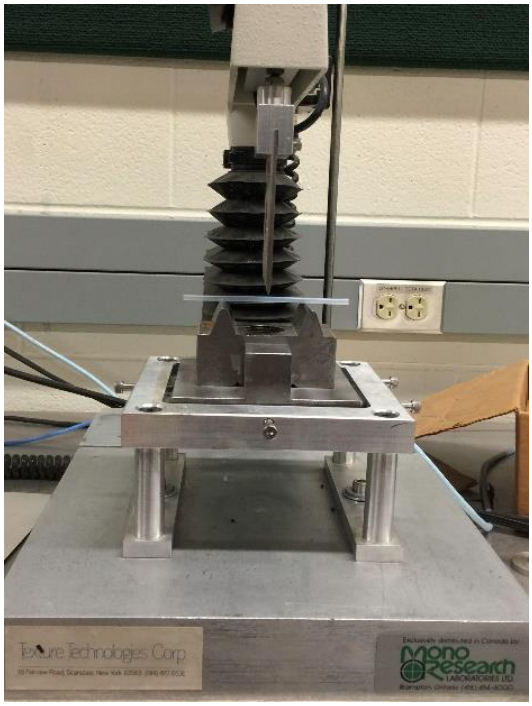

Figure 4.4. Experimental test-bed for the bending test

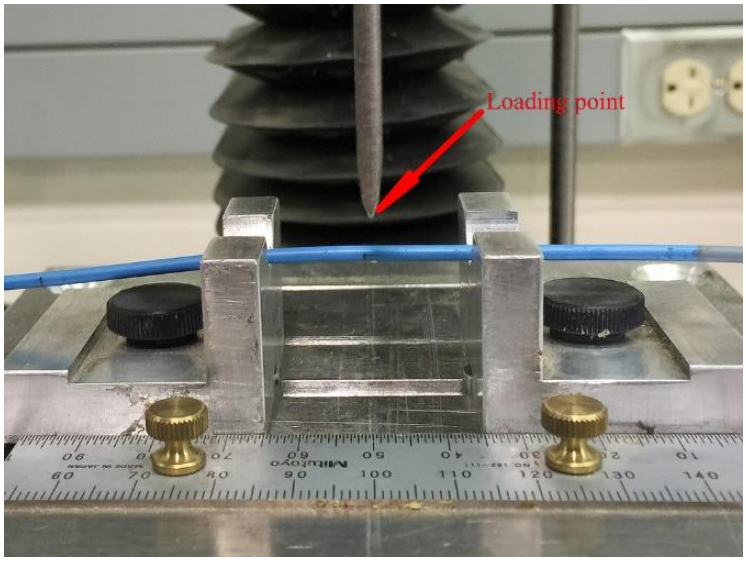

Figure 4.5. Three-point testing rig for the Bard Stinger Ablation Catheter

Several remarks were taken during the tests: (1) the Texture Analyzer was placed horizontally to ensure the bending of catheter and tubes was only occurred in the horizontal plane; (2) The maximum displacement δ was set to 5 mm which could prevent large deformation of the catheter and tubes; (3) the stiffness at each segment of the distal deflecting part of catheter was assumed to

be the same. In these measurements, the following procedures were taken in the room temperature 21 ºC:

(1) Setting the span of the rig to 30 mm, placing the catheter distal deflecting part (from 0 mm to 52 mm) to test rig and applying the load to the middle point of the distal deflecting part of the catheter. This test was repeated 6 times. 5 groups of experimental results were used for the calculation of the stiffness and bending rigidity, while one group of experimental results which was relatively largest deviation was abandoned.

(2) Placing the catheter body to the rig and testing the catheter body. The loading points were set along the catheter body length from the tip of catheter with 10 cm, 20 cm, 30 cm, 40 cm. 50 cm, respectively. Each test was repeated 4 times. 3 groups of experimental results in each test were used for the calculation of the stiffness and bend rigidity, while one group of experimental results which was relatively largest deviation was abandoned.

(3) Adjusting the span of the rig to 50 mm and testing the tube samples which were 10 cm in length. The loading points were set in the middle points of tube samples. Each test was repeated 6 times. 5 groups of experimental results were used for the calculation of the stiffness and bending rigidity, while one group of experimental results which was relatively largest deviation was abandoned.

4.3.1.2 Experimental results

The result of the bending test of the distal deflecting part of the steerable catheter is shown in Figure 4.6. From the information presented in Figure 4.6, the stiffness with root-mean-square-errors (RMSEs) which are used to measure the goodness of fit can be calculated which is shown in Table 4.1. The comparsion of the experimental results of first group bending test and fitting results is shown in Figure 4.7. Then, the flexural rigidity was calculated based on Equation (4.3), which is shown in Table 4.1 as well. The average stiffness k and average flexural rigidity EI in the five groups of experiments were calculated.

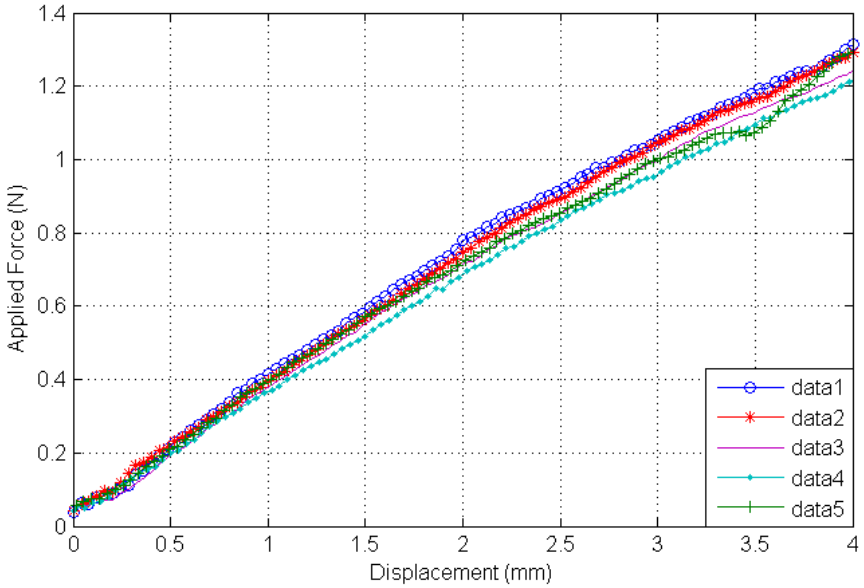

Figure 4.6. Experimental results of the bending tests of the distal deflecting part of Bard Stinger Ablation Catheter.

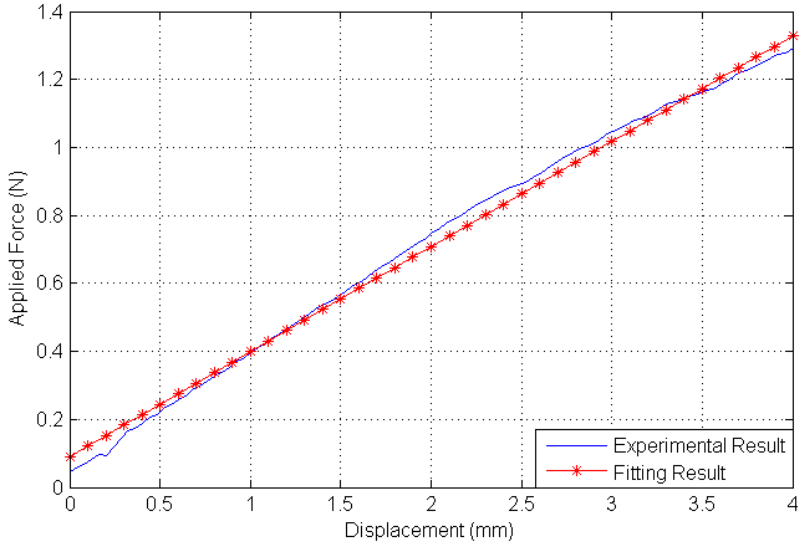

Figure 4.7. Comparsion of the experimental results of the first group bending test and fitting results of the distal deflecting part of Bard Stinger Ablation Catheter

Figure 4.8 shows one group of the load-deformation relation of the catheter body in the bending tests with the loading point being at 20 cm away from the distal tip of the catheter. The stiffness and flexural rigidity of the catheter body can be calculated based on the experimental results. The

stiffness and flexural rigidities of the catheter at different loading points with RMSEs were shown in Table 4.2. The average stiffness and flexural rigidities of catheter body were calculated based on these experimental results which are given in Table 4.2 as well.

Table 4.1. Estimated results of the stiffness based on the experimental results of the five groups

Experiments Group #	Stiffness k (N/mm)	RMSE	EI (N.mm^2)
1	0.3092	0.02998	173.925
2	0.3146	0.03566	176.9625
3	0.302	0.03135	169.875
4	0.2942	0.02275	165.4875
5	0.3021	0.0271	169.93125
Average	0.30442		171.2363

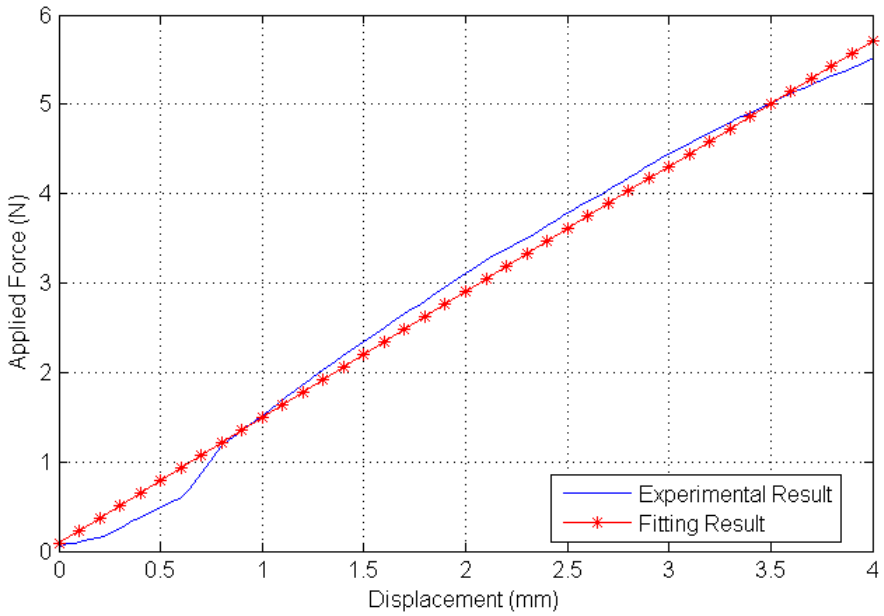

Figure 4.8. Load-deflection relation of the catheter body with the loading point being at 20 cm away from the distal tip of the Bard Stinger Ablation Catheter

Figure 4.9 shows the measured flexural rigidities of the whole catheter corresponding to the loading points with the confidence level of 95%. From this figure it can be seen that the EI varies along the

catheter length, which suggests that there is a locational effect on flexural rigidity. The flexural rigidity of distal deflecting part is quite smaller than the flexural rigidity of catheter body. The flexural rigidity of catheter distal deflecting part 171.2363 N.mm^2 and the average flexural rigidity of catheter body 734.4 N.mm^2 are used in the next simulation part.

Table 4.2. Estimated results of the stiffness based on the 5 group experimental results

Experiments Group #	Stiffness k (N/mm)	RMSE	EI (N.mm^2)
10 cm way, group 1	1.18	0.4202	663.75
10 cm way, group 2	1.299	0.2263	730.6875
10 cm way, group 3	1.24	0.1976	697.5
20 cm way, group 1	1.396	0.2006	785.25
20 cm way, group 2	1.336	0.1285	751.5
20 cm way, group 3	1.406	0.183	790.875
30 cm way, group 1	1.327	0.2186	746.4375
30 cm way, group 2	1.33	0.1755	748.125
30 cm way, group 3	1.358	0.1513	763.875
40 cm way, group 1	1.344	0.2796	756
40 cm way, group 2	1.338	0.1994	752.625
40 cm way, group 3	1.303	0.2616	732.9375
50 cm way, group 1	1.2	0.316	675
50 cm way, group 2	1.321	0.1305	743.0625
50 cm way, group 3	1.206	0.2406	678.375

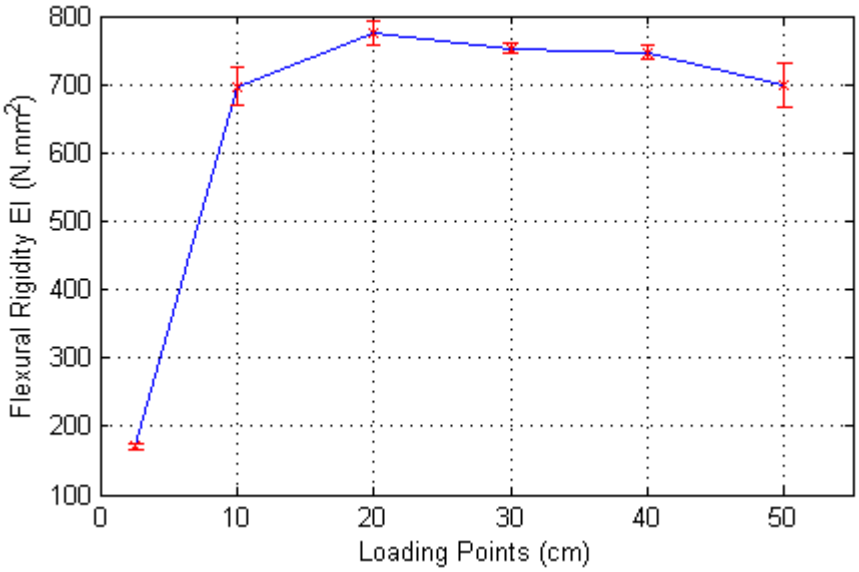

Figure 4.9. Flexural rigidities with 95% confidence interval bars of the Bard Stinger Ablation Catheter

For the three-point-bending tests of different types of PVC tubes, only one type of tube is taken as an example here. The inner diameter of this tube is 1.3 mm with the wall thickness of 0.35mm. The relation between the load and deformation in one group of experiment is shown in Figure 4.10. It is noted that the deformation of the PVC wall is quite small during the insertion or retraction of the catheter. The deformation of tube between 0 to 1.5 mm was used to calculate the stiffness and flexural rigidity of tube. The stiffness with RMSEs were calculated which is shown in Table 4.3. The comparsion of the experimental results of first group bending test and fitting results is shown in Figure 4.10. Then, the flexural rigidity was calculated which is shown in Table 4.3 as well. The average stiffness 0.62268 N.mm and average flexural rigidity 1621.563 $N.mm^2$ in the five groups of experiments were calculated, which were used in the next simulation part.

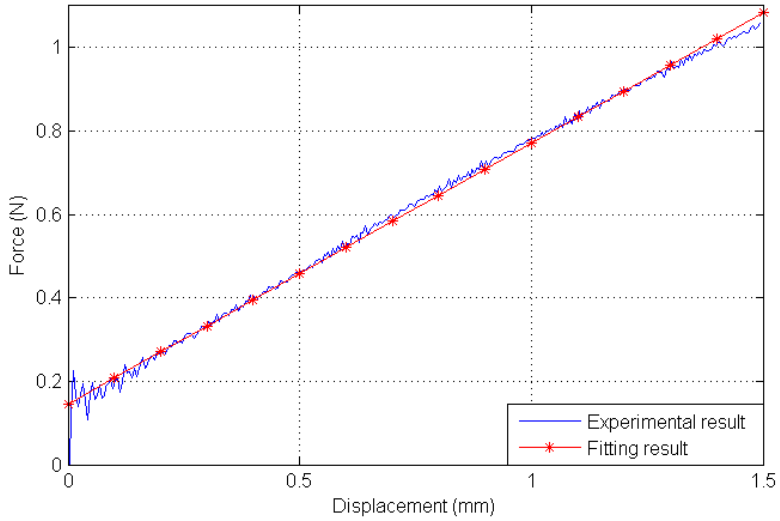

Figure 4.10. The comparsion of the experimental results of first group bending test and fitting results.

Table 4.3. The estimated results of the stiffness based on the 5 group experimental results

Experiments Group #	Stiffness k (N/mm)	RMSE	EI (N.mm^2)
1	0.6253	0.01936	1628.3854
2	0.624	0.02145	1625
3	0.6226	0.2046	1621.3541
4	0.6285	0.02155	1636.7188
5	0.613	0.02111	1596.3542
Average	0.62268		1621.563

4.3.2 Experimental estimation of the damping of the catheter and tube

4.3.2.1 Rayleigh Damping

Damping is the dissipation of energy from a vibration structure. A commonly used mechanism regarding the damping is the so-called “viscous damping” which is represented by the following equation

$$F_d = c\dot{x} \tag{4.4}$$

where

F_d: the damping force;

c: the viscous damping coefficient;

$\dot{x}$: the instantaneous velocity.

To the best of author's knowledge, it is difficult to determine the damping coefficient of a continuum manipulator which is a complex multiple degree-of-freedom (DOF) system experimentally. In addition, the damping coefficient has to be updated according to the structure of the steerable catheter inside the pathway during the insertion and retraction of catheter in the pathway. The common and efficient way to determine the damping is through an equivalent Rayleigh Damping which represents the damping to be a linear combination of mass (M) and stiffness (K)

$$C = \alpha M + \beta K \tag{4.5}$$

where α and β are the pre-defined constants which can be determined by experiments. The Rayleigh Damping is applied to both viscously and non-viscously damped multiple DOF systems (Adhikari, 2001). The efficiency of applying the Rayleigh Damping to the continuum manipulators was successfully validated in the literature, i.e., colonoscope (Cheng et al., 2013) and embolization coil (Dequidt et al., 2008). The Rayleigh Damping was used for the steerable catheter and pathway in this thesis.

Chowdhury & Dasgupta (2003) proposed a rational method to estimate the values of α and β in Equation (4.5) for systems with large DOF. The Rayleigh Damping coefficients can be reduced to the following form

$$2\zeta_i\omega_i = \alpha + \beta{\omega_i}^2 \tag{4.6}$$

where ω_i and ζ_i are the natural frequency and damping ratio respectively in the ith mode. The damping ratio in the ith mode can be represented by

$$\zeta_i = \frac{\alpha}{2\omega_i} + \frac{\beta\omega_i}{2} \tag{4.7}$$

A typical example of the relation between the natural frequency and its corresponding damping ratio is shown in Figure 4.11, where α and β are 0.3864 and 0.0162 respectively (Cheng, 2014). From Figure 4.11, it can be seen that the curve shows significant non-linearity when the natural frequency is from 0 to 5 rad/sec, and the curve shows very good linearity beyond this range. Due to the linear relationship between the natural frequency and damping ratio, the natural frequency

ζ_i in i[th] mode can be estimated based on a set of values of natural frequency $\omega_1, \omega_2, \omega_3, \ldots, \omega_m$ and their corresponding damping ratio $\zeta_1, \zeta_2, \zeta_3, \ldots, \zeta_m$ in the different modes (Chowdhury & Dasgupta, 2003)

$$\zeta_i = \frac{\zeta_m - \zeta_1}{\omega_m - \omega_1}(\omega_i - \omega_m) + \zeta_m \tag{4.8}$$

where $m < i \leq 2.5m$. Based on the above set of data, the β can be calculated by

$$\beta = \frac{2\zeta_m\omega_m - 2\zeta_{2.5m}\omega_{2.5m}}{{\omega_m}^2 - {\omega_{2.5m}}^2} \tag{4.9}$$

Based on Equation (3.6) and (3.9), the α is obtained by

$$\alpha = 2\zeta_m\omega_m - \beta{\omega_m}^2 \tag{4.10}$$

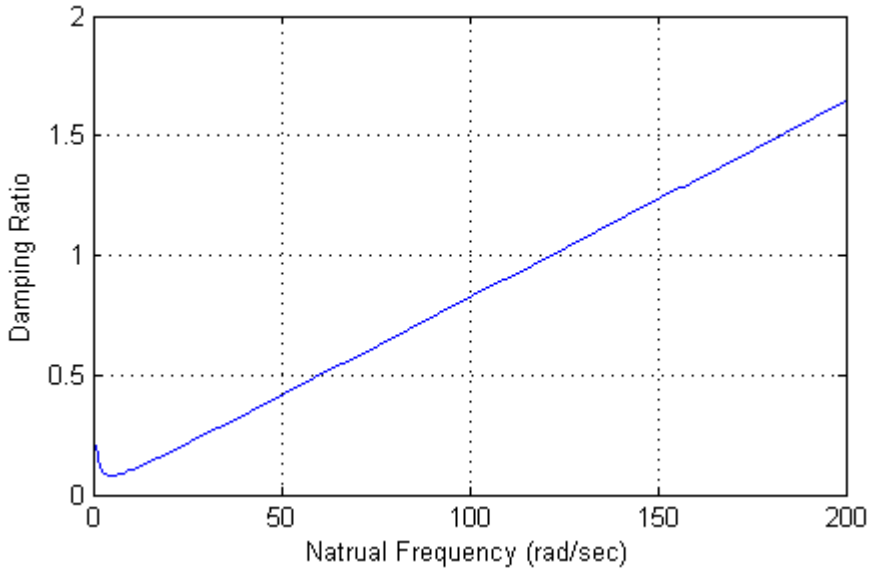

Figure 4.11. Relation between the natural frequency and its corresponding damping ratio of a CF-Q160L colonoscope based on the experimental results in (Cheng, 2014) with kind permission

In this study, this method was used to estimate the Rayleigh Damping coefficients based on the modal analysis which is the most popular and efficient method to solve engineering dynamic problems.

4.3.2.2 Experimental setup and methods

There are two assumptions for the modal parameters of the catheter and tube in the testing:

(1) The damping in each segment of the distal deflecting part of catheter is the same. The reason for this assumption is related to the fact that the four electrodes with their wire inside of catheter distribute at the distal deflecting part which may affect the damping in each segment.
(2) The external forces such as the steering force applied on the proximal end of catheter, and the contact force between the catheter and pathway had no effect on the modal parameters of the catheter and tubes. This assumption is further reaspoanble for the setup where the catheter was a cantilever beam (Figure 4.13). More specific reasons are for this set up: (i) the real situation is that the distal tip is not always constrainted and it slides along the pathway; (ii) all the parameters as determined on the test-bed will be further refined with system identification technique (as the damping parameters are related to the mass and stiffness); (iii) the whole process is a trial-and-error process.

The forced vibration test-bed was set up, which is shown in Figure 4.12. The catheter and tubes were glued on the fixed platform which is fixed on the top of a shaker. The pseudo random vibration signal from 0 to 200 Hz is generated by the Signal Analyzer Unit (Type 2035, Brüel & Kjær Sound and Vibration Measurement A/S, Montreal, Quebec) through a power amplifier (Type 2706, Brüel & Kjær Sound and Vibration Measurement A/S, Montreal, Quebec) to the shaker. The displacement of fixed platform of shaker and the displacement of catheter distal tip were measured by two laser interferometry sensors (LTC-300-200-SA, MTI Instruments Inc., Albany, NY) with the range of ±100 mm, resolution of ±20 μm and spot size of 130 μm. Both sensors are interfaced to the Signal Analyzer Unit by two A/D convertors (DSP-Lambda 30-24, TDK-Lambda Americas Inc., National City, CA) respectively.

For the catheter tip bending part tests which is 52 mm at length, the catheter was glued at 50 mm away from the distal tips during the forced vibration tests, and the displacement of the catheter distal tip was measured (Figure 4.12). For the catheter body tests, the catheter body were glued at 150 mm away from the distal tips during the tests, and the displacement of the catheter body distal end which is 50 mm way from the distal tip of catheter was measured (Figure 4.13). For other tubes tests, the tubes were glued at 100 mm away from the distal tips during the tests, and the displacement of the tube distal tip was measured.

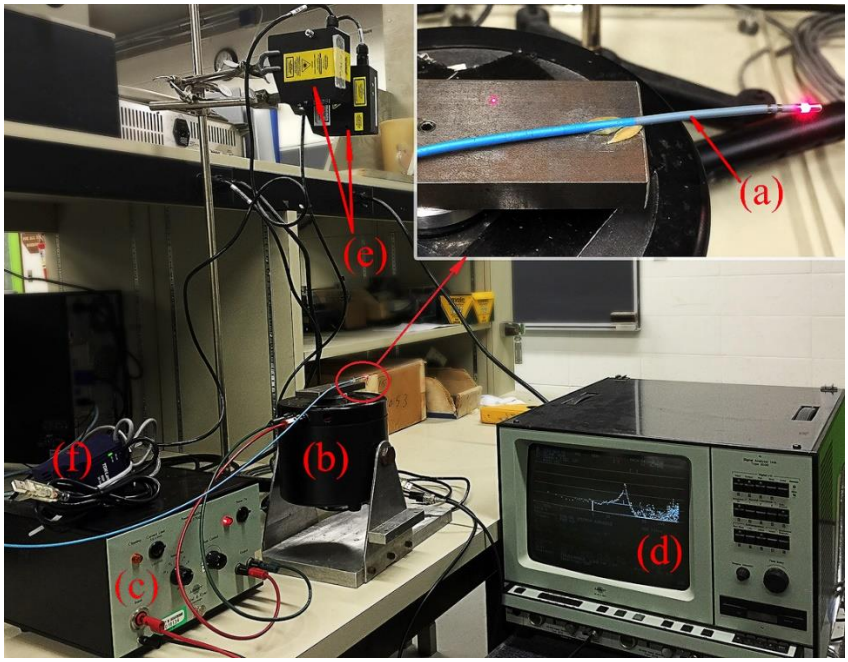

Figure 4.12. Test-bed for vibration tests of catheter distal tip
(a: Catheter; b: Shaker; c: Power amplifier; d: Signal Analyzer Unit; e: Laser interferometry sensors; f: A/D convertors)

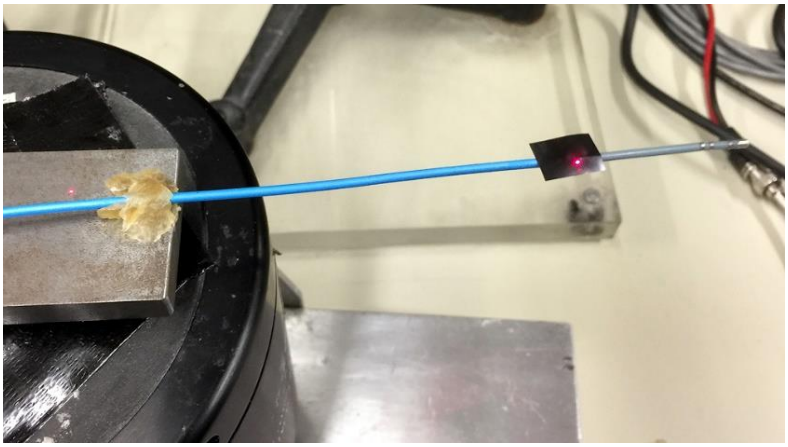

Figure 4.13. Measuring points for the vibration tests of body of the Bard Stinger Ablation Catheter.

4.3.2.3 Experimental results

In this section, the experimental results obtained from the forced vibration tests of catheter distal bending part, catheter body and tubes are described. Figure 4.14 shows a group of experimental

results of the displacement transmissibility ratio versus frequency of the distal deflecting part of the catheter. The ratio of the displacement of the distal tip of the catheter to the displacement of the top of shaker is defined as the displacement transmissibility ratio (T_r). This displacement ratio can be found by (Guo et al., 2010)

$$T_r = \sqrt{\frac{1+(2\zeta\lambda)^2}{(1-\lambda^2)^2+(2\zeta\lambda)^2}} \tag{4.11}$$

where λ and ζ are the frequency ratio and the damping ratio respectively. λ is defined as

$$\lambda = \frac{\omega_s}{\omega_c} \tag{4.12}$$

where ω_s and ω_c are the frequency of the shaker and the frequency of the catheter respectively. When the system resonances ($\omega_c = \omega_s$) take place, the damping ratio ζ can be calculated by Equation (4.11)

$$\zeta = \frac{1}{2}\sqrt{\frac{1}{{T_r}^2-1}} \tag{4.13}$$

The experimental results of different groups of forced vibration tests are shown in Figure 4.14, Figure 4.15 and Figure 4.16, respectively. Based on the experimental results, the damping ratios of different modal analysis were calculated. The relations between the natural frequencies and corresponding damping ratios in each group of experiments are shown in Table 4.4, Table 4.5 and Table 4.6 respectively. It notes that only first two modes of catheter distal deflecting part were obtained in the experiments. The reason is that the length of the deflecting part of catheter is limited which is not enough to get more modes during forced vibration tests with the input frequency between 0 to 200 Hz.

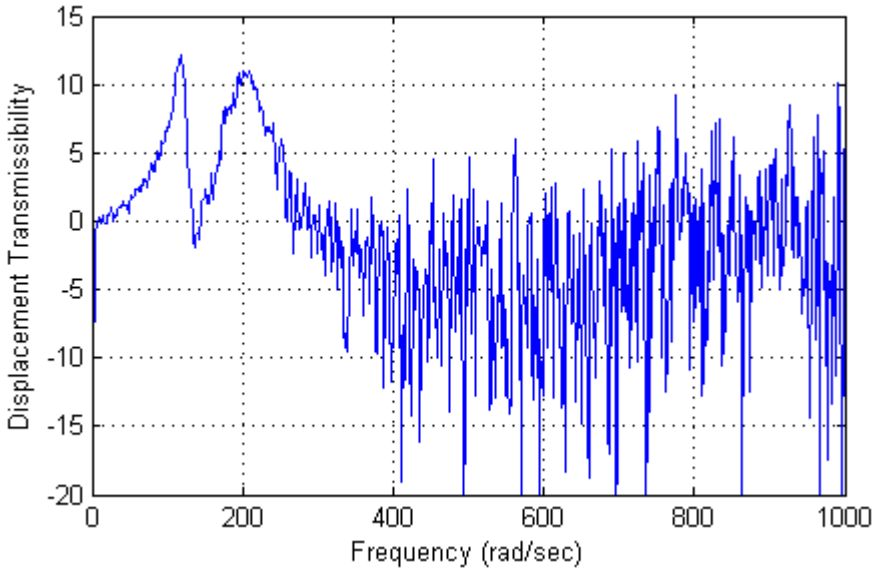

Figure 4.14. Relation between the frequency and the displacement transmissibility ratio of the distal deflecting part of the Bard Stinger Ablation Catheter

Table 4.4. Relation between the natural frequency and damping ratio for the first few modes of the distal deflecting part of the Bard Stinger Ablation Catheter

Resonance Frequency (rad/sec)	Damping Ratio
117.8096 (0*)	0.0413 (0.000161)
200.5382 (1.4810)	0.0464 (0.000536)

* The number in parenthesis indicates the standard deviations.

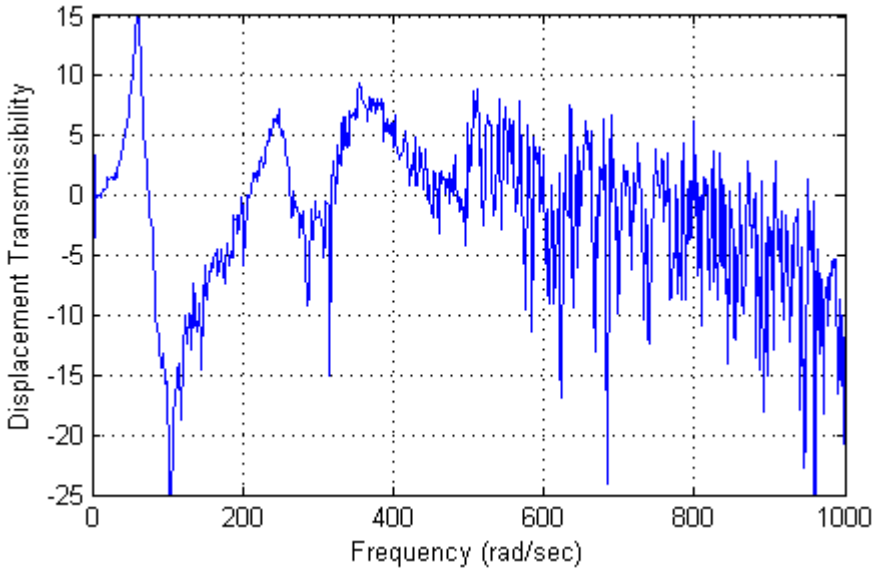

Figure 4.15. Relation between the frequency and the displacement transmissibility ratio of the catheter body of Bard Stinger Ablation Catheter

Table 4.5. Relation between the natural frequency and damping ratio for the first few modes of the catheter body of Bard Stinger Ablation Catheter

Resonance Frequency (rad/sec)	Damping Ratio
59.6902 (0*)	0.0341 (0.000574)
247.8715 (0.6283)	0.0662 (0.004724)
358.7696 (4.6172)	0.0524 (0.003197)

* The number in parenthesis indicates the standard deviations.

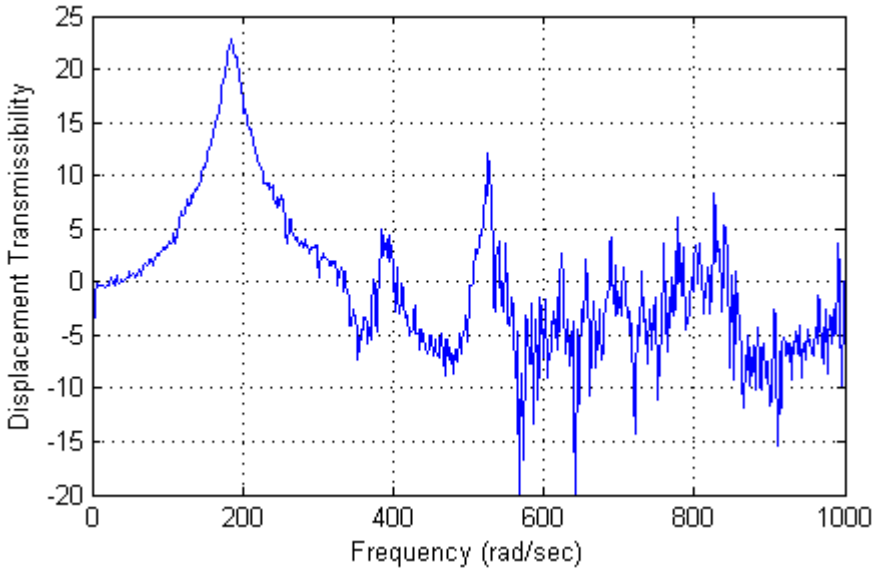

Figure 4.16. Relation between the frequency and the displacement transmissibility ratio of the tube sample

Table 4.6. Relation between the natural frequency and damping ratio for the first few modes of the tube sample

Resonance Frequency (rad/sec)	Damping Ratio
183.783 (0*)	0.0216 (0.000161)
383.5881 (0.6283)	0.1039 (0.002957)
527.473 (0.6286)	0.0359 (0.002963)

* The number in parenthesis indicates the standard deviations.

In order to calculate the damping ratios in higher modes of each testing object (the distal deflecting part of catheter, the catheter body and the tube sample), a few natural frequencies in higher modes of each testing object should be found. Their natural frequencies in high modes can be obtained using the FEM models of each object. MATLAB codes for the estimations of their natural frequencies can be found in Appendix B. The results of the first ten natural frequencies for each testing object are shown in Figure 4.17, Figure 4.18 and Figure 4.19, respectively.

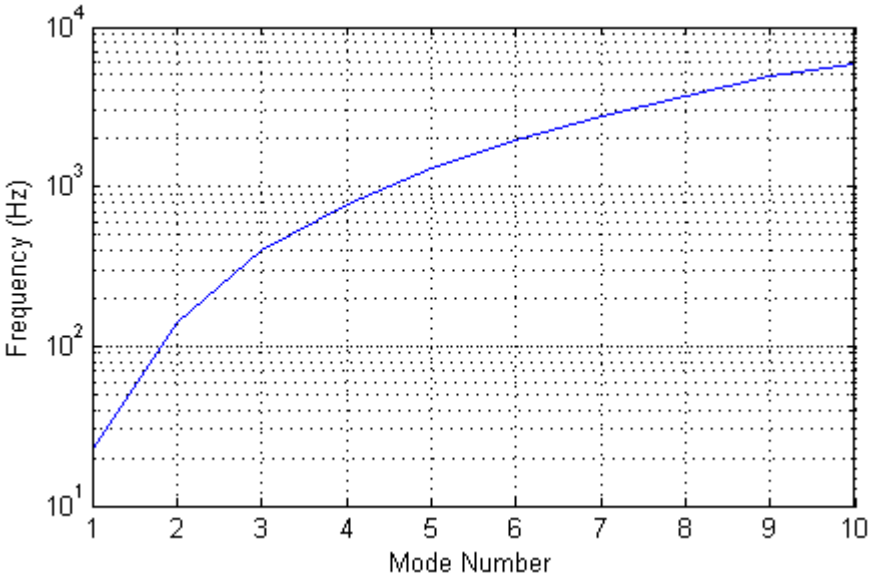

Figure 4.17. First ten natural frequencies of the distal deflecting part of Bard Stinger Ablation Catheter calculated by the FEM model

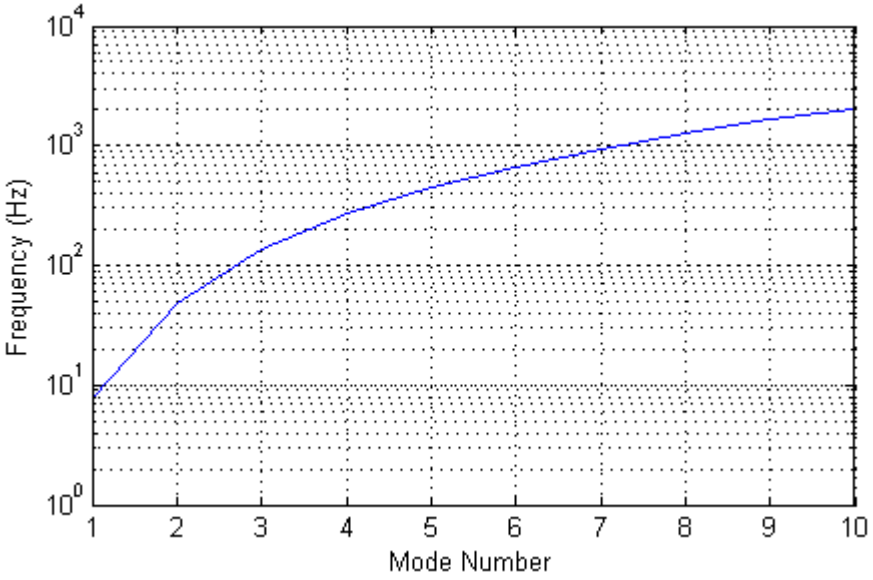

Figure 4.18. First ten natural frequencies of the catheter body of Bard Stinger Ablation Catheter calculated by the FEM model

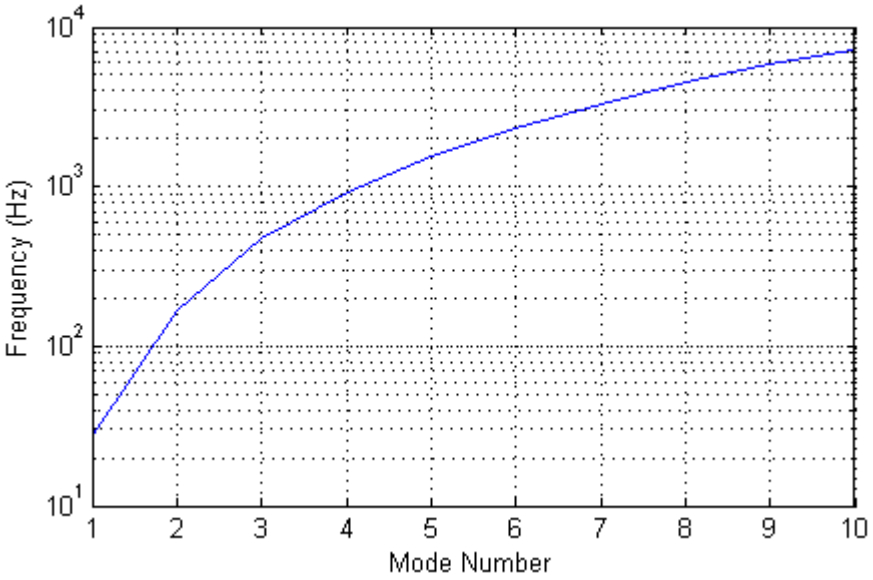

Figure 4.19. First ten natural frequencies of the tube sample calculated by the FEM model

4.3.2.4 Calculation of the Rayleigh Damping coefficients

Based on the damping ratios in the first few modes obtained from the experiments, and the first ten natural frequencies obtained from the FEM models, the damping ratios in higher modes of each testing object can be extrapolated using Equation (4.8).

The damping ratios in higher modes of 3, 4 and 5 of the distal deflecting part of the catheter are calculated by

$$\zeta_3 = \frac{\zeta_2 - \zeta_1}{\omega_2 - \omega_1}(\omega_3 - \omega_2) + \zeta_2 = 0.05733 \tag{4.14}$$

$$\zeta_4 = \frac{\zeta_2 - \zeta_1}{\omega_2 - \omega_1}(\omega_4 - \omega_2) + \zeta_2 = 0.07368 \tag{4.15}$$

$$\zeta_5 = \frac{\zeta_2 - \zeta_1}{\omega_2 - \omega_1}(\omega_5 - \omega_2) + \zeta_2 = 0.09564 \tag{4.16}$$

Based on the above data, the β can be calculated by Equation (4.9)

$$\beta = \frac{2\zeta_2\omega_2 - 2\zeta_5\omega_5}{{\omega_2}^2 - {\omega_5}^2} = 0.0000227 \tag{4.17}$$

The α is obtained by Equation (4.10)

$$\alpha = 2\zeta_2\omega_2 - \beta{\omega_2}^2 = 64.4146 \tag{4.18}$$

Now, the Rayleigh Damping of the deflecting part of the catheter can be represented as

$$C = 64.4146M + 0.0000227K \tag{4.19}$$

The damping ratios in higher modes of 4 and 5 of the catheter body can be obtained by

$$\zeta_4 = \frac{\zeta_2 - \zeta_1}{\omega_2 - \omega_1}(\omega_4 - \omega_2) + \zeta_2 = 0.2379 \tag{4.20}$$

$$\zeta_5 = \frac{\zeta_2 - \zeta_1}{\omega_2 - \omega_1}(\omega_5 - \omega_2) + \zeta_2 = 0.3761 \tag{4.21}$$

The Rayleigh Damping of the catheter body can be represented as

$$C = 15.4374M + 0.000268K \tag{4.22}$$

The damping ratios in higher modes of 4 and 5 of the tube can be obtained by

$$\zeta_4 = \frac{\zeta_2 - \zeta_1}{\omega_2 - \omega_1}(\omega_4 - \omega_2) + \zeta_2 = 0.5441 \tag{4.23}$$

$$\zeta_5 = \frac{\zeta_2 - \zeta_1}{\omega_2 - \omega_1}(\omega_5 - \omega_2) + \zeta_2 = 0.8985 \tag{4.24}$$

The Rayleigh Damping of the tube can be represented as

$$C = 11.4701M + 0.000185K \tag{4.25}$$

4.3.3 Experimental estimation of the friction coefficient

4.3.3.1 Friction equation for estimating the friction coefficient

The friction coefficient μ between the catheter and pathway plays an important role during the force transmission from the proximal end of catheter body to the distal tip of catheter during the insertion and retraction. The well-known relation between the input and output tensions (F_{in} and F_{out}) including friction force in the circumstance of a flexible string around a certain angle (θ) circle arc is the capstan friction equation (Attaway, 1999)

$$\frac{F_{in}}{F_{out}} = e^{\mu\theta} \tag{4.26}$$

The friction coefficient μ can be further calculated by

$$\mu = \left[\ln\left(\frac{F_{in}}{F_{out}}\right)\right]/\theta \tag{4.27}$$

By using the capstan friction equation to estimate the friction coefficient, two assumptions were made: (1) while applying the input force at the proximal end, the deformation of the tube (which is a π/2 circle arc) can be neglected; (2) the compression deformation of the catheter in the axial direction can be neglected. The first assumption can be achieved by fixing each segment of the

tube firmly during the testing. The second assumption can be evaluated by the compression deformation ratio (r) which is defined as the total compression deformation (δ) over the total testing length of catheter (L). The strain for the catheter under a simple compression force (F) can be calculated by

$$\varepsilon = \frac{F}{AE} \tag{4.27}$$

where A is the area of the cross section of the catheter, and E is the modulus of elasticity of the catheter. The compression deformation ratio (r) can be calculated by

$$r = \frac{\delta}{L} = \frac{\varepsilon_{tip} L_{tip} + \varepsilon_{body} L_{body}}{L_{tip} + L_{body}} \tag{4.28}$$

where ε_{tip} and ε_{body} are the strains of the distal deflecting part and body part of the catheter, respectively; L_{tip} and L_{body} are the lengths of the distal deflecting part and body part of the catheter, respectively. Based on the bending rigidity of the distal deflecting part and body part of the catheter obtained experimentally, the relation between the compression deformation ratio and the compression force for the length of 450 mm can be obtained, which is shown in Figure 3.20. From the result shown in Figure 3.20, the compression deformation of the catheter is quite small when the input force is under 3 N. The second assumption is reasonable. In this study, the capstan friction equation was used to estimate the friction coefficient between the catheter and pathway (or tube). A series of experiments were carried out to estimate the friction coefficient.

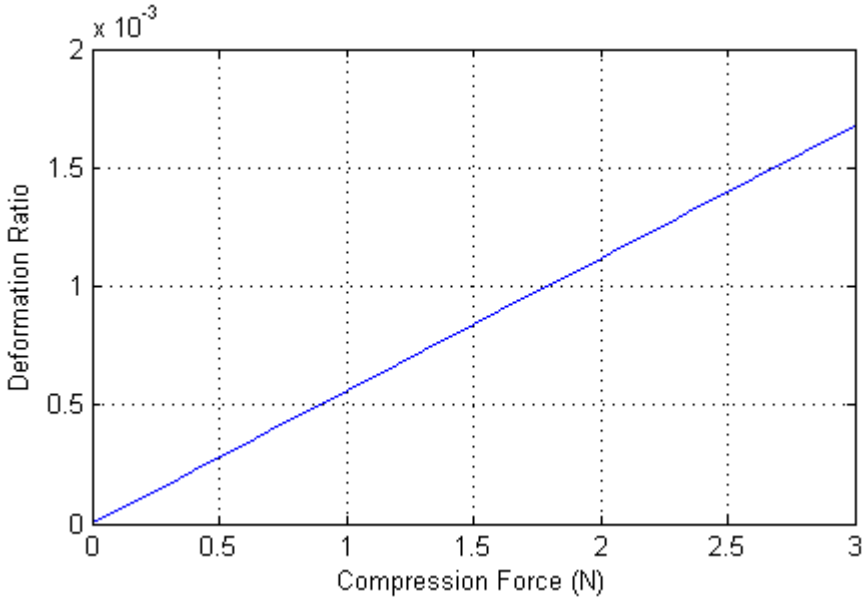

Figure 4.20. Relation between the compression force and the deformation ratio of the Bard Stinger Ablation Catheter

4.3.3.2 Experimental setup and method

The experimental setup for estimating the friction coefficient between the catheter and tube is shown in Figure 4.1. The following procedures were taken:

Step 1: Set the sampling frequency of two force sensors at 50 Hz, two stream data were collected by the same computer-based on time-stamped synchronization.

Step 2: Insert the catheter to make the distal tip of the catheter the 1~2 mm distance from the flexible force sensor by the CFTM and the resetting two force sensors to be 0.

Step 3: Measure the input force and contact force of the distal tip. Gradually increase the input force with the CFTM which was hold by one hand up to about 1.2 N. During the operation, the CFTM was steered to only have the input force along the central line direction of the straight part of tube. This can be achieved by monitoring the other force and torque components at the input end to make them close to 0. The input force was recorded by the ATI Nano 43 Transducer. The contact force between the distal tip of the catheter and target site was recorded by the flexible force sensor.

Step 4: Stop measuring the input force and contact force, and retract the catheter.

Step 5: Repeat Step 1 to Step 4 above, and there were 9 groups of the experiments in total.

4.3.3.3 Experimental results

An example of the measured input force is shown in Figure 4.21 (unfiltered data). An example of the measured contact force is shown in Figure 4.22 (unfiltered data). The original experimental data have significant noise signals which affect the analysis of the results. Particularly, there are two types of noise signals: (1) the noise signal caused by the force sensors; (2) the disturbance of the input force caused by the tremor of the hand in operation. Compared with the first type of noise signal, the second type of noise signal is more significant as shown in Figure 4.21 and Figure 4.22.

A 1-D filter was designed with a window size of 100 for processing the signals. This filter can be used to find a running average of experimental results which can reduce the disturbance caused by the input force. The detailed information of the 1-D filter refers to (Oppenheim et al., 1989).

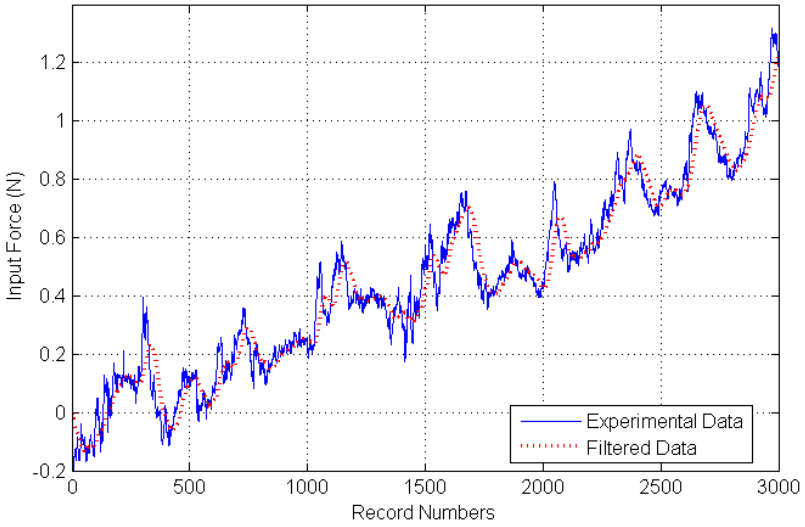

Figure 4.21. Primary input force applied by hand

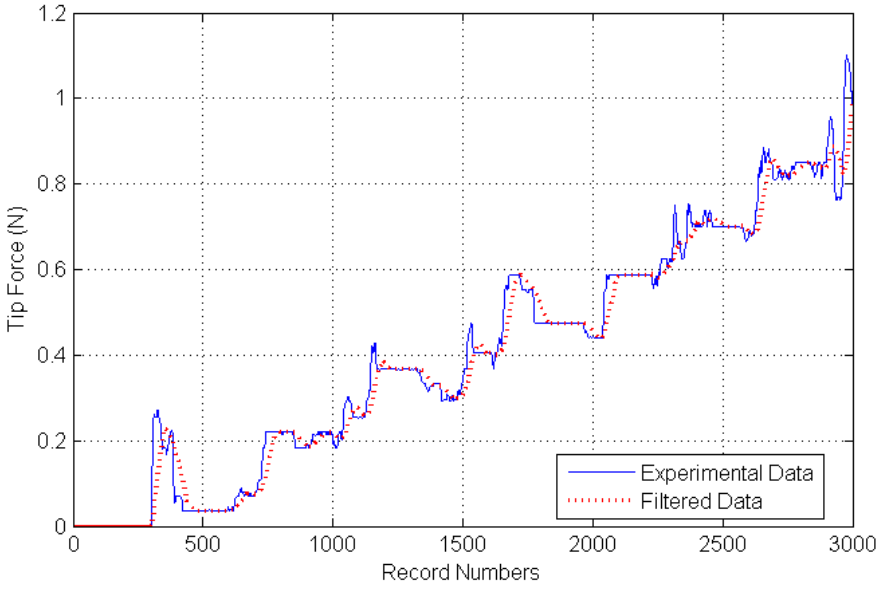

Figure 4.22. Primary contact force of the distal tip

The average value of the experimental data of the 9 groups with 95% confidence interval is shown in Figure 4.24. Based on the experimental results, the ratio between the input force and output force

($\frac{F_{in}}{F_{out}}$) was estimated to be 0.8277 with a bias -0.1048, and the RMSE was 0.06015. The friction coefficient μ was further calculated to be 0.1204. The fitting result is shown in Figure 4.24.

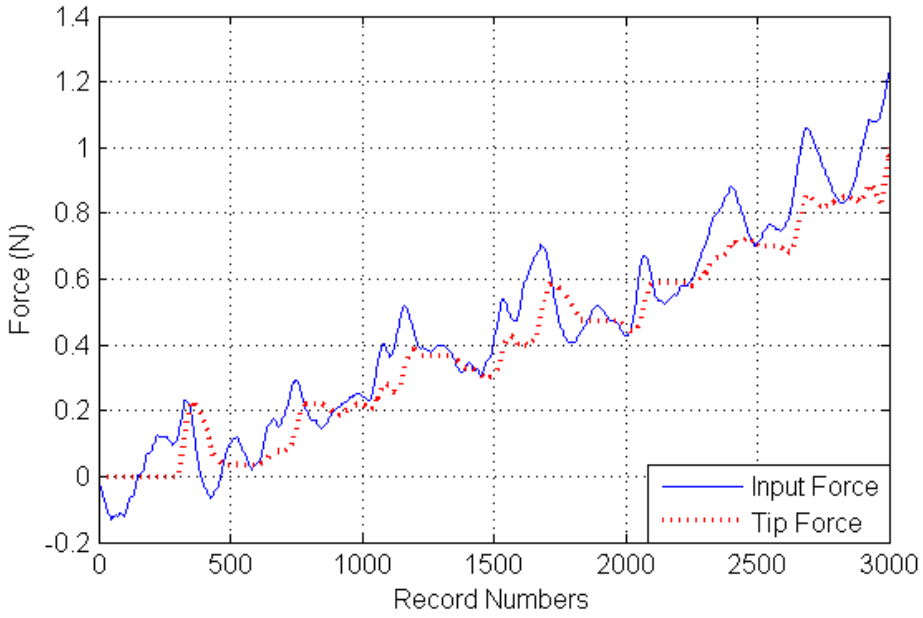

Figure 4.23. Synchronized data between filtered input force by hand and filtered contact force of the distal tip

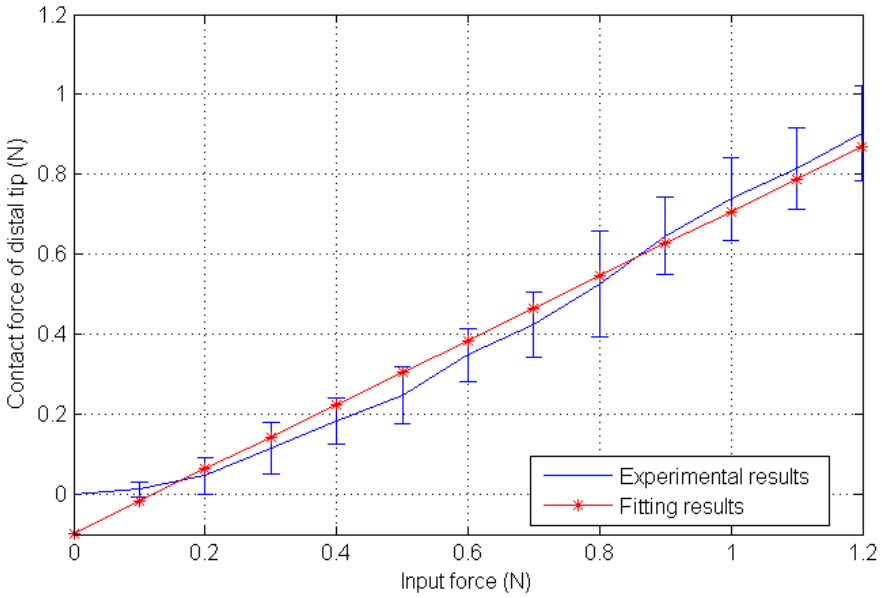

Figure 4.24. Comparison of the experimental results with 95% confidence interval bars and fitting results.

4.4 Comparison of the experimental results and simulation results

Various experiments were performed on the test-bed described in Section 4.2 to compare with the simulation results of the kinetic model of the steerable catheter with consideration of the interaction with the pathway. Both the experiments and simulations of the steerable catheter contain two parts to simulate a whole process of a catheter based surgery: navigation part and operation part. The navigation part concerns the insertion of the steerable catheter to navigate the distal tip of the catheter to a target place. The operation part concerns keeping the distal tip of the catheter at the target place firmly to complete a surgery task (e.g., delivering an agent to stop bleeding).

4.4.1 Experiment

The following procedures were taken:
Step 1: Get the geometric shape of the pathway by recording the centerline of the pathway.

Step 2: Set the sampling frequency of two force sensors at 50 Hz, two streams of data were collected by the same computer based on the time-stamped synchronization. Reset the two force sensors to be 0.

Step 3: Insert the catheter to the pathway gradually and slowly until the distal tip of the catheter out of the pathway. The displacement of the distal tip and the entire configuration of the catheter inside the pathway were recorded. During the insertion of the catheter, the input force was applied with the CFTM.

Step 4: Measure the input force and contact force of the distal tip. Gradually increase the input force with the CFTM which was hold by one hand up to about 1.2 N. Then gradually decrease the input force to 0. During the operation, the CFTM was steered to only have the input force along the central line direction of the straight part of the tube. This can be achieved by monitoring the other force and torque components at the input end to make them close to 0. The input force was recorded with the ATI Nano 43 Transducer. The contact force between the catheter distal tip and

target site was recorded with the flexible force sensor.

Step 5: Retract the catheter.

Step 6: Repeat Step 2 to Step 5. There were 9 groups of the experiments in total.

In above experimental steps, Step 1 to Step 3 belong to the navigation part and Step 4 to the operation part.

4.4.2 Simulation

The kinetic model of the steerable catheter interacting with the pathway was implemented in the SPACAR program through several user-defined routines in MATLAB environment. The model of the steerable catheter was completely instantiated by its initial geometric information of the structure, mechanical properties information with the user-defined contact force and input information. With consideration of the accuracy of the model and the computation efficiency, 12 beam elements were used to model the steerable catheter in total, in which 3 beam elements to model the distal deflecting part and 9 beam elements to model the catheter body. The reason to choose these numbers of elements will be discussed in detail in the next section. The axial deformation of each beam element was neglected in order to improve the computational efficiency. This is reasonable because the axial deformation of the steerable catheter is quite small (less than 0.17 % of the total length of catheter) under a small input force which is no more than 3 N (also see the discussion in Section 3.3.3).

The tube was pre-curved to be a 90° circular arc with radius of 200 mm (Figure 4.25). The distal end (10 mm) and proximal end (50 mm) of the pathway kept straight to make the catheter insertion smooth. The curved pathway had the circular cross-section with the inner radius $r_a = 1.3\,mm$ at which the transition zone starts. The radius of the full contact zone was defined as $r_b = 1.8\,mm$. The mechanical properties of the pathway including the stiffness and damping were defined with the parameters estimated in Section 4.3. The Coulomb friction coefficient in the simplified LuGre friction model was estimated as 0.2014. Based on our previous study regarding friction models

(Liu et al. 2015) and comparing with friction force predicted by Coulomb friction model during simulations, σ_0 and σ_1 used were chosen as 300 N/mm, and 1 Ns/mm, respectively.

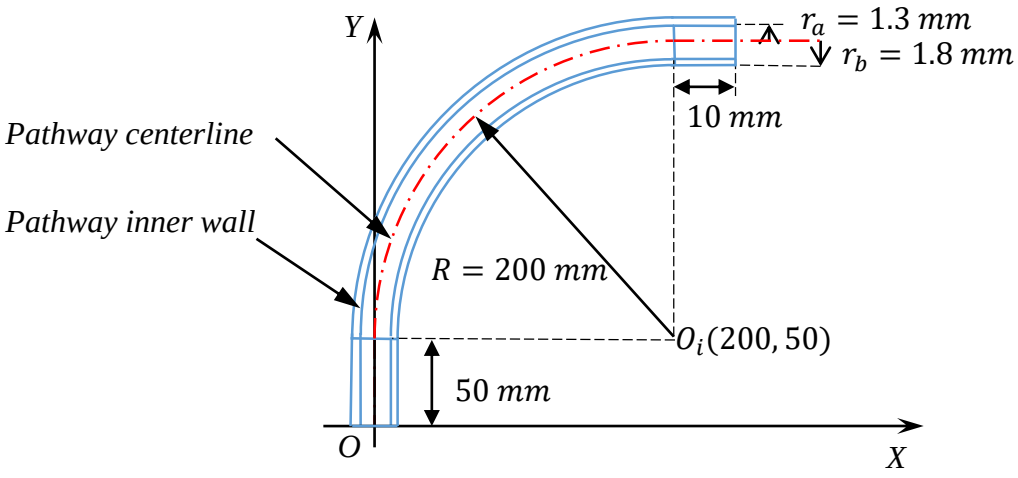

Figure 4.25. Schematic diagram of the curved pathway

The entire simulation includes two parts as well to match with these two parts of experiments: insertion and operation which are described as follows:

(1) In the simulation of the insertion of the steerable catheter, the initial geometry of the structure is defined by the determination of these nodes coordinates of these elements in the global coordinate which is shown in Figure 3.1. The initial material properties of the steerable catheter are defined with the parameters estimated in Section 4.3. An input motion with a constant velocity 0.010 m/s, is applied at the proximal end of the catheter until the distal tip of the catheter is out of the distal end of the pathway. MATLAB codes can be found in Appendix C.

(2) In the simulation of the operation, the steerable catheter body is inserted inside the pathway completely and the distal tip is out of the pathway in the insertion part. The initial geometry of the curved structure is defined by the nodes coordinates of the elements in the results of insertion simulation. The initial stress/load is defined as well in this part of simulation. The reason is that the catheter has large deformation after the insertion simulation. The initial generalized stress of each element is given by the generalized stresses in the results of insertion simulation. The generalized stresses are calculated based on the Kelvin-Voigt model; for the detail information, please refer to (Aarts et al. 2011). The node 1 which is the

distal tip is fixed during simulation. A sinusoidal input motion is applied at the proximal end of the catheter as follows,

$$x(t) = Asin(\omega t) + D \tag{4.29}$$

where A is the amplitude of the motion, ω the parameter related to input frequency, and D is the displacement of the proximal end of the catheter which is determined at the end of insertion simulation. In this study, A is chosen as 9 mm, which could make the largest input force around 1.2 N in accordance with the largest input force in experimental results. In order to observe the hysteresis behavior caused by friction clearly, ω is chosen as 4π rad/s. The velocity and acceleration of the input motion can be derived from Equation (4.29), which are as follows, and MATLAB codes can be found in Appendix D.

$$\dot{x}(t) = A\omega cos(\omega t) \tag{4.30}$$

$$\ddot{x}(t) = -A\omega^2 sin(\omega t) \tag{4.31}$$

4.4.3 Comparison of the experimental and simulation results

In the navigation part, the comparison of the displacements of the distal tip of the steerable catheter between the experimental results and simulation results is shown in Figure 4.26. In general, the simulation results show good agreements with the experimental results during the insertion of the catheter. The largest errors are at the beginning segment of the curved pathway. A more detailed comparison of the displacements of the distal tip of the steerable catheter between the experimental results and simulation results is shown in Figure 4.27. In Figure 4.27, the green lines are the initial positions of the inner walls of the pathway. It can be seen that the displacements of the distal tip of the catheter are out of the initial positions of the inner walls of the pathway, which reflects the deformation of the inner walls of the pathway. The RMSE were used to measure the differences between the experimental results and simulation results. The RMSE between the experimental and simulation results was calculated as 1.0698 mm.

In the experiments of the operation part, an example of the input force measured is shown in Figure 4.28 (unfiltered data). An example of the contact force measured is shown in Figure 4.29 (unfiltered data). A 1-D filter was designed with a window size of 100 for processing the signals to reduce the noise signals (see Section 4.3.3). The filtered signals are shown in Figure 4.28 and Figure 4.29.

The synchronized filtered data between input force by hand and the contact force of the distal tip is shown in Figure 4.30. The average value of the 9 groups of the experimental data with 95% confidence interval is shown in Figure 4.32. The synchronized simulation results of the input force and contact force of the distal tip is shown in Figure 4.31. Figure 4.32 shows a comparison between the simulation and experimental results of the relation between the input force and contact force of the distal tip of the catheter. Both the experimental results and simulation results show the hyteresis behavior of frcition clearly. The RMSE between the experimental and simulation result was calculated as 0.0678 N. The experimental results and simulation results show a very good agreement when the input force does not exceed 0.4 N based on the error bars on the experimental result, which was calcauted based on the 95% confidence interval. The allowable error with the 95% confidence interval is 0.05, and this error is acceptable considering the facts that (i) the the input force does not exceed 0.4 N and (ii) the contact force between the heart tissue and the catheter tip should be ranged from 0.2 to 0.3 N for an effective catheter ablation of arrhythimas (Di Biase et al. 2009b).

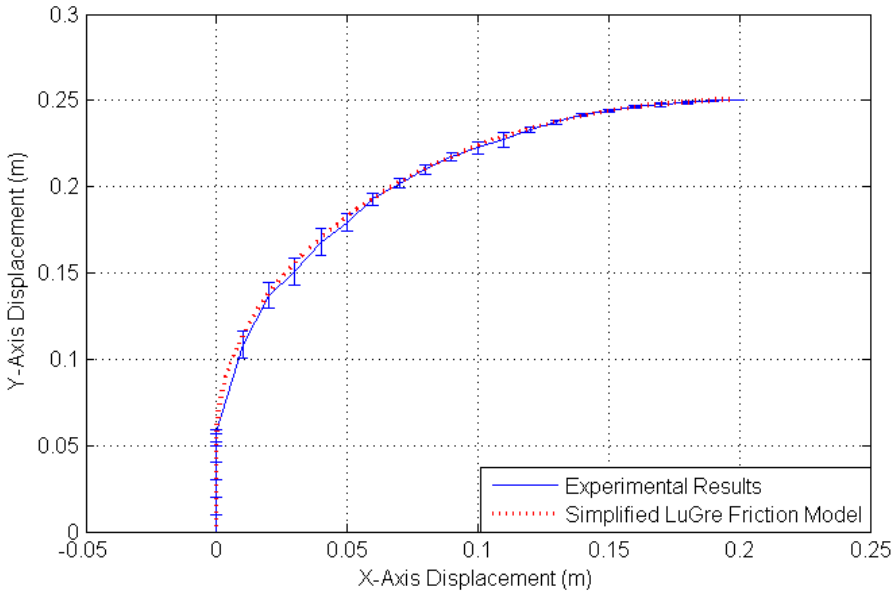

Figure 4.26. Comparison between the simulation and experimental results of the displacement of the distal tip of the steerable catheter in the pathway

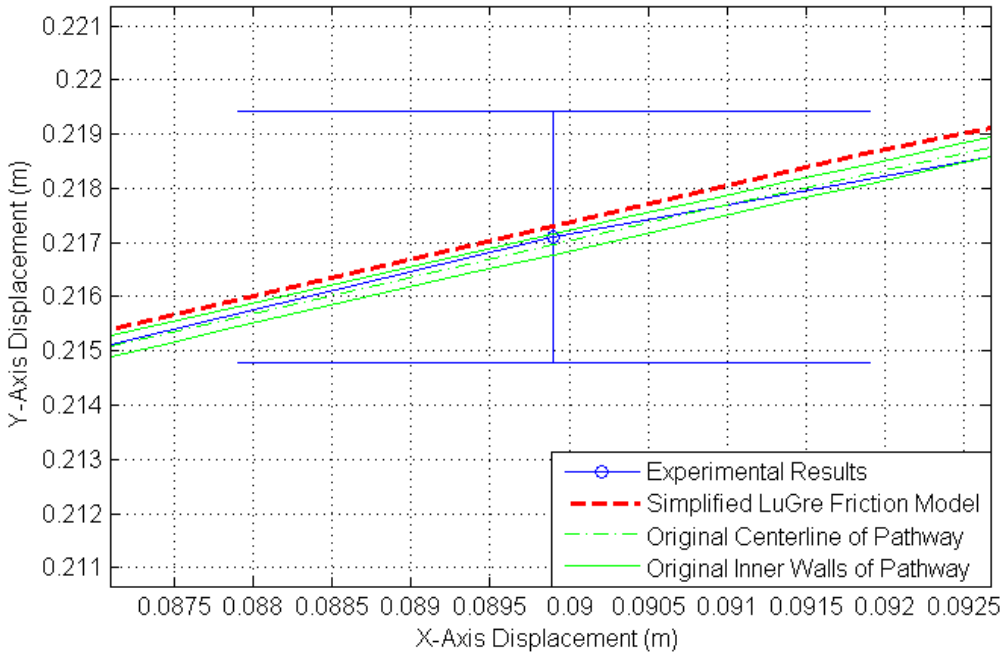

Figure 4.27. Detail view of the comparison between the simulation and experimental results of the displacement of the distal tip of the steerable catheter in the pathway

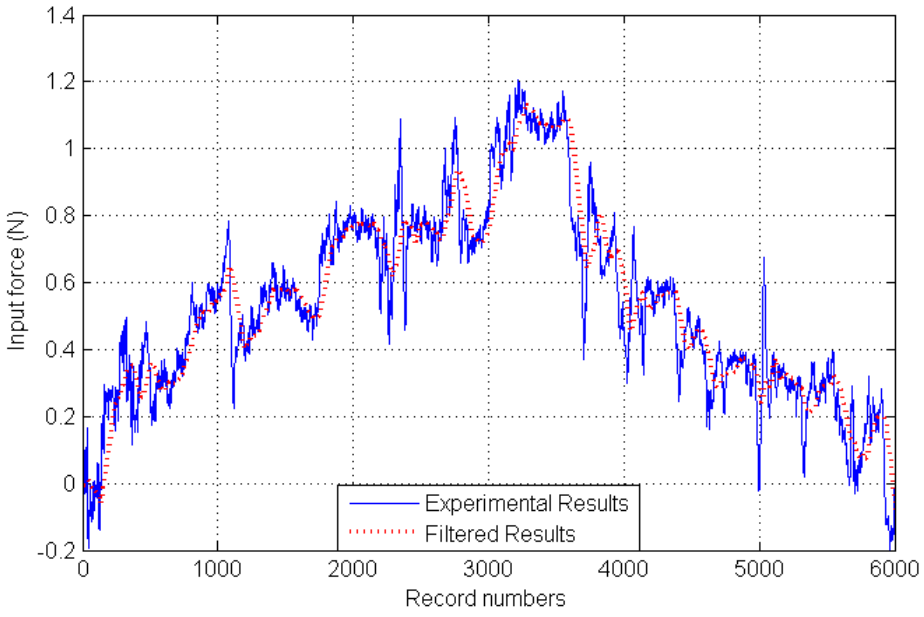

Figure 4.28. Primary input force applied by hand

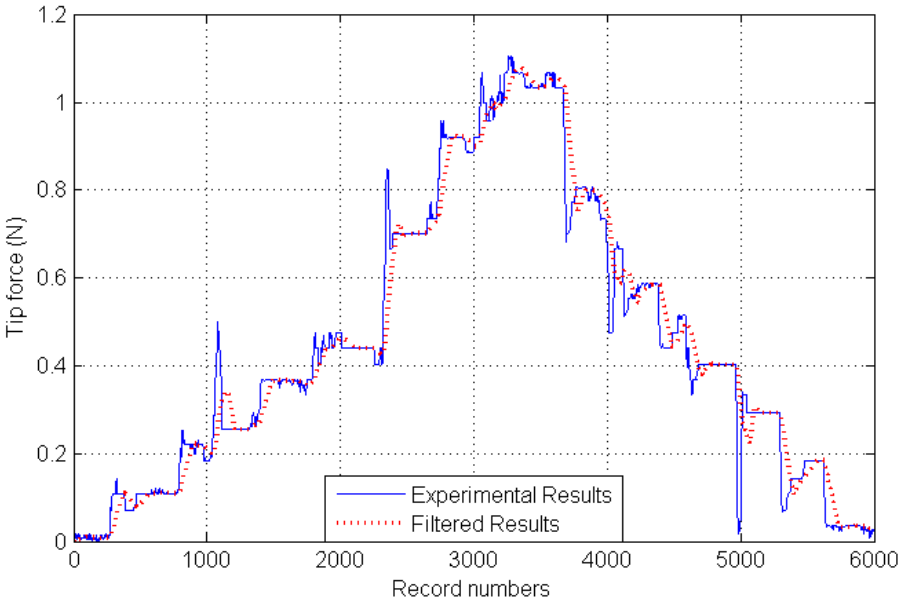

Figure 4.29. Primary contact force of the distal tip of the catheter

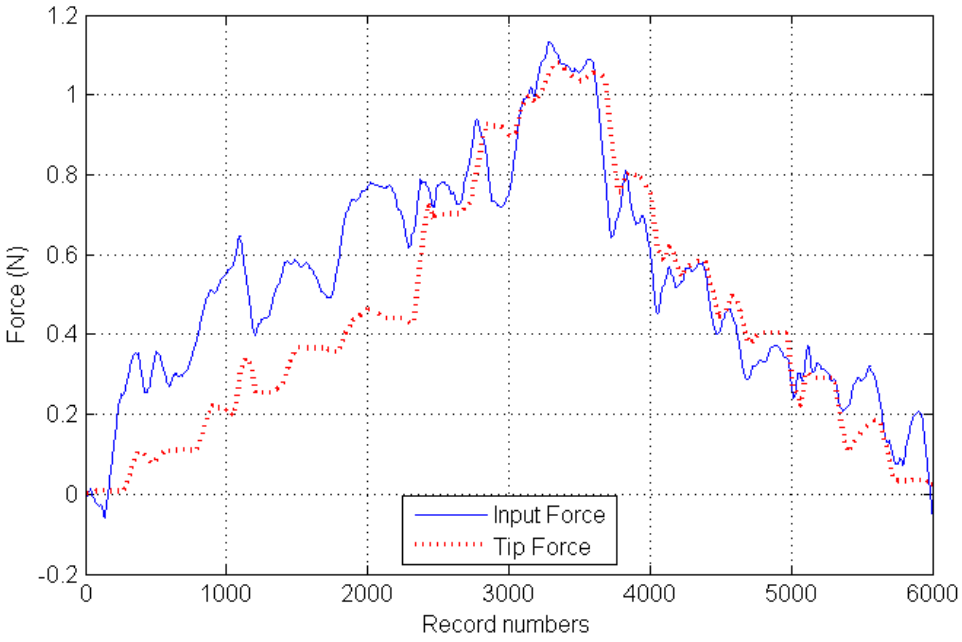

Figure 4.30. Synchronized data between filtered input force by hand and filtered contact force of the distal tip

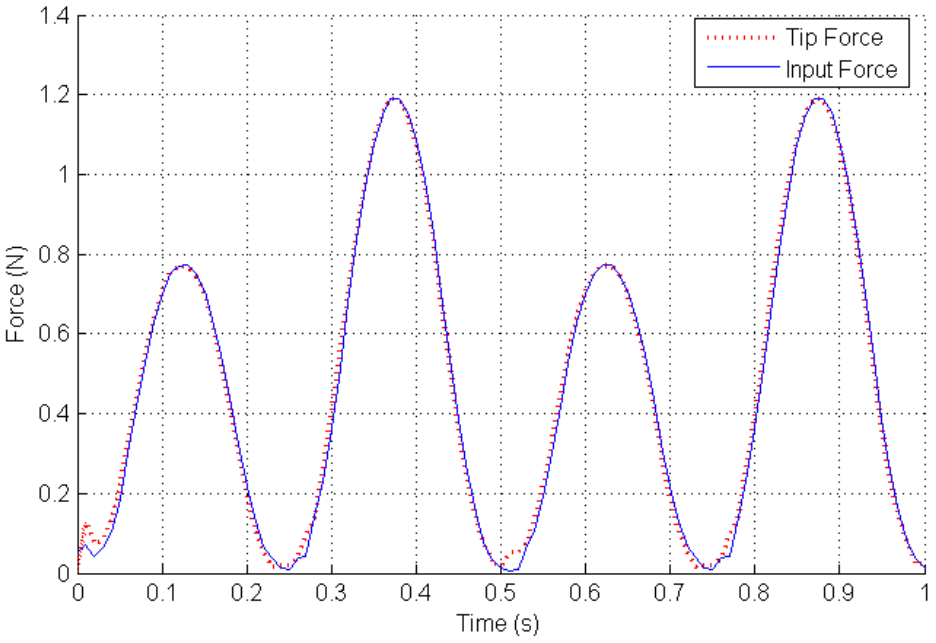

Figure 4.31. Synchronized data between input force and contact force of the distal tip in simulation results

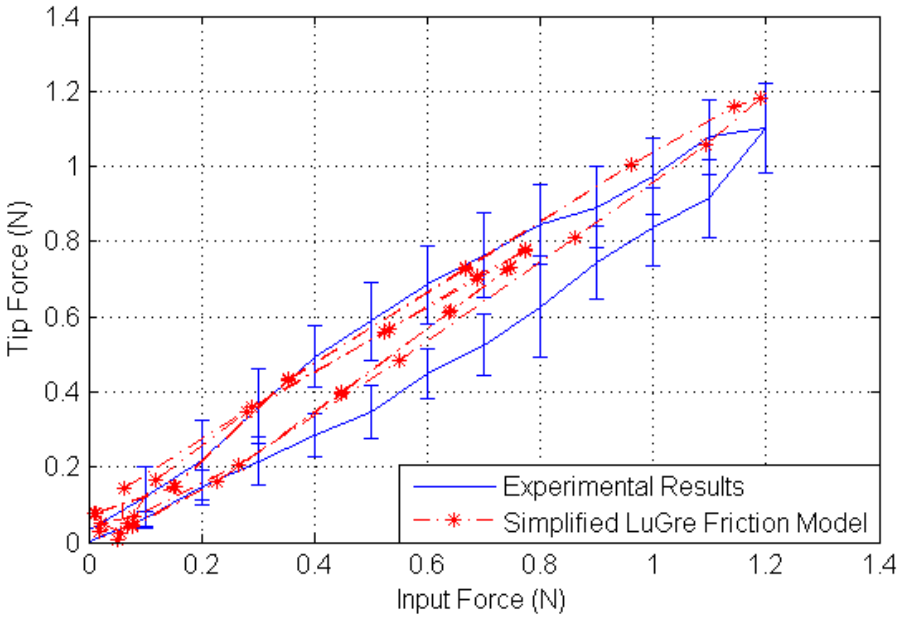

Figure 4.32. Comparisons between the simulation and experimental results of the relation between the input force and output force of the distal tip of the catheter

4.5 Discussion

From the comparison of the experimental and simulation results, there is a good agreement in the displacements of the distal tip of the catheter and the force relationship between the input force and contact force of the distal tip of the steerable catheter. The reason for some errors in terms of the motion and force transmissions is discussed below.

The main reason for the measured uncertainty error of the displacement of the distal tip of the steerable catheter lies in the measurement method which was based on the coordinate paper with 1 mm resolution. This resolution caused errors during the experiment because the deformation of the flexible tube was quite small in the transverse section, which was difficult to be captured with such a small resolution. The subsequent processing of the displacement data could further cause measurement errors. The displacements of the distal tip were transferred to numerical data by measuring the center points of the distal tip of the catheter in a series of pictures taken during the experiments. Furthermore, the errors generated from the model assumption are inevitable due to the assumption of the fixed centerline of the pathway. In the current experiment, the centerline of the pathway had slightly movement due to the interaction force between the catheter and inner walls of the pathway.

The main reason for the measured errors of the input force and contact force of the distal tip of the catheter was the jittery data of the CFTM and flexible force sensor. The measurement errors were shown with the error bar in each figure. The jittery data was caused by two types of noise signals: (1) the noise signal caused by the force sensors; (2) the disturbance of the input force caused by the tremor of hand, though some noise signals were reduced by digital filters. In addition, the repeatability during the experiment caused errors since the input force was applied by hand. Furthermore, the uncertainty of the clearance between the catheter and pathway may cause errors. It can be seen that there were relatively large errors during the increase of the input force while there were relatively small errors during the decrease of the input force. The input force needed to adjust the clearance at first.

4.6 Conclusion

The chapter presented the validation of the kinetic model of the steerable catheter developed in Chapter 3. A test-bed of the steerable catheter was developed, which made it possible to measure the motion and force transmission during the procedure of the catheter interacting with the pathway. The parameters in the model of the catheter as well as the model of the pathway were determined by the experiments. Several groups of experiments and simulations were performed to validate the developed kinetic model. Overall, there is a good agreement between the experimental and simulation results. The simplified LuGre friction models used in the simulations enabled to capture the friction behavior between the catheter and the inner walls of the pathway. It shows the hysteresis behavior of the friction clearly. The FEM model of the steerable catheter is reliable in terms of accuracy. The errors generated were analyzed from the sources such as on the measurement errors, the model assumptions and the inaccurate parameters of the mathematical model.

CHAPTER 5 ANALYSIS OF THE KINETIC MODEL

5.1 Introduction

In Chapter 3, a kinetic model of the steerable catheter interacting with its work environment was developed, and the model was validated in Chapter 4. The accuracy of the kinetic model depends on the following variables: (1) the number of finite elements and (2) the friction model. Though in Chapter 3, decisions on these variables were made, no comprehensive discussion of the rationale for these decisions was given. In this chapter, this shortcoming is remedied. The organization of this chapter is as follows. In Section 5.2, the best number of finite elements to model the steerable catheter is discussed. In Section 5.3, the best friction model to model the steerable catheter is discussed. Section 5.4 is a conclusion.

5.2 The best number of finite elements for the kinetic model

The navigation of the steerable catheter is regarding the insertion of the catheter through the pathway to the target sites. The material properties and geometry of the steerable catheter as well as the pathway are defined with the parameters defined in Section 3.4.2. An input motion with a constant velocity 0.010 m/s is applied at the proximal end of the catheter until the distal tip of the catheter is out of the end of the pathway. In Chapter 3 and Chapter 4, 12 beam elements were used to model the steerable catheter, in which 3 beam elements are used to model the distal part and 9 beam elements are used to model the catheter body part. The simplified LuGre friction model was taken to model the friction between the catheter and the pathway. In this friction model, there are two parameters σ_0 and σ_1 and they were chosen to be 300 N/mm, 1 Ns/mm, respectively.

The number of beam elements has significant effects on the accuracy of the kinetic model of the steerable catheter as well as the computational efficiency. Figure 5.1 shows a comparison of the forces exerted on the distal tip and the force exerted on the connecting part (CP) which lies in

between the distal tip and catheter body of the catheter with different numbers of elements. The total numbers of elements 9, 12 and 15 were tried. The case with 9 elements shows a significant deviation from both the case with 12 elements and the case with 15 elements in terms of the force at the distal tip and the CP. The forces with 12 elements and 15 elements are quite close to each other. But the computational time with 15 elements is much longer than that with 12 elements. Therefore, 12 elements were used to model the steerable catheter.

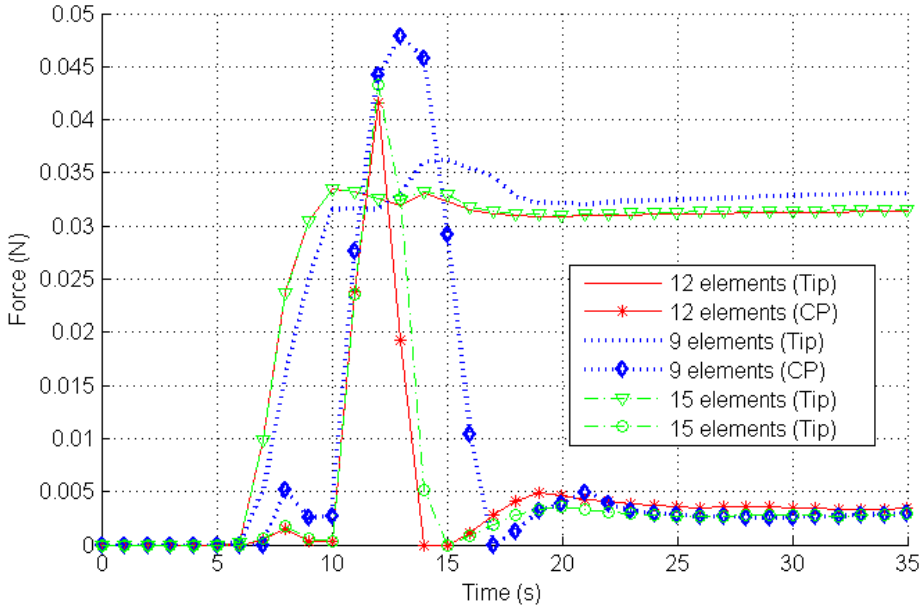

Figure 5.1. Comparison of different numbers of elements used to model the steerable catheter

Figure 5.2 shows a comparison of the different numbers of elements for the distal part of the steerable catheter with the total number of elements unchanged (12 in this case). The numbers to define the distal part of the catheter are 2, 3 and 4. The result of the reference model is with the total number of elements being 15. It can be seen from Figure 5.2 that the case with 2 elements for the distal part in the model and with 12 elements in total has a relatively large deviation, and thus this case was dropped off. The computation efficiency with 4 elements for the distal part of the catheter and with 12 elements in total is the lowest among all these cases, and thus this case was dropped off as well. Therefore, the case with 3 elements and 12 elements in total was eventually used for the distal part of the catheter in the kinetic model.

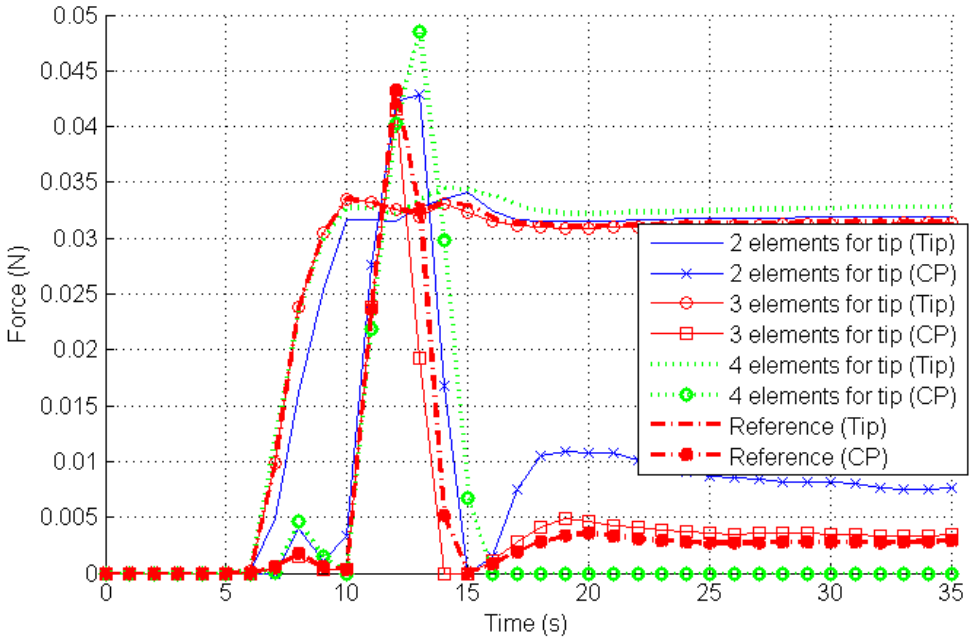

Figure 5.2. Comparison of different numbers of elements for the distal deflection part of the steerable catheter

It is noted that the total number of the beam elements to define the steerable catheter depends on the complexity of the shape of the pathway. If the shape of the pathway is more complex, more beam elements are needed to model the catheter. It is clear that the larger the the curvature of the pathway, the shorter the beam element (especially for the distal part of the catheter) and the number of elements is higher. The length ratio (l_e/R_{min}) for the distal part and catheter body of the catheter was found as an important parameter, where l_e and R_{min} are the length of element and the minimal radius of the curvature of the pathway, for determining the number of elements for the distal part and catheter body, respectively. In this study, the length ratios for the distal deflection part and catheter body were 0.0833 and 0.1944 (respectively). The length of the elements in the kinetic model can be estimated based on the length ratio and the minimal radius of the curvature of the pathway. The number of elements in the kinetics model can be further determined based on the length of the element and the total length of the steerable catheter. For instance, in this study the minimal radius of the curvature of the pathway was 200 mm and the lengths of the distal part and catheter body were 50 mm and 350 mm respevtively. The lengths of elments for the distal part and catheter body were calculated as 16.66 mm and 38.88 mm respectively. The numbers of elements

for the distal part and catheter body can be further calculated as 3 and 9 respectively.

5.3 The best friction model for the kinetic model

In Section 3.4.2, several typical friction models including Coulomb friction model, Dahl friction model, LuGre friction model and simplified LuGre friction model were discussed in detail. In this section, a comparison of the four friction models potentially used in the kinetic model of the steerable catheter is discussed. The Coulomb friction coefficient was estimated to be 0.1204. Based on our previous study regarding friction models (Liu et al. 2015) and comparing with the friction force predicted by the Coulomb friction model in simulations, σ_0, σ_1, and σ_2 used in Dahl friction model, LuGre friction model and simplified LuGre friction model were chosen to be 300 N/mm, 1 Ns/mm and 1 Ns/mm, respectively.

In the navigation part, a comparison of the experimental and simulation results for the displacement of the distal tip of the steerable catheter are shown in Figure 5.3. A more detailed comparison of the displacements of the distal tip of the steerable catheter between the experimental results and simulation results using the four friction models is shown in Figure 5.4. It can be seen that the displacements of the distal tip of the catheter with each friction model are out of the initial positions of the inner walls of the pathway, which reflects the deformation of the inner walls of the pathway.

It is noted that Figure 5.3 and Figure 5.4 are not intended to give the information regarding how accurate a friction model is. For accuracy, the RMSEs were used. The RMSEs of the displacements of the distal tip of the catheter with the different friction models are calculated and shown in Table 5.1.

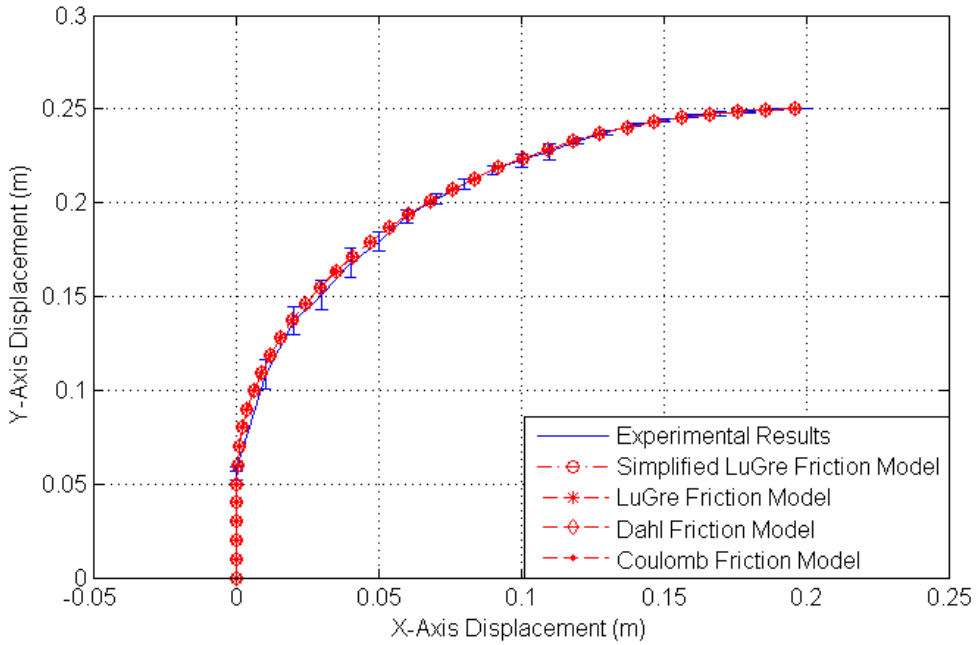

Figure 5.3. Comparison between the simulation and experimental results of the displacement of the distal tip of the steerable catheter in the pathway

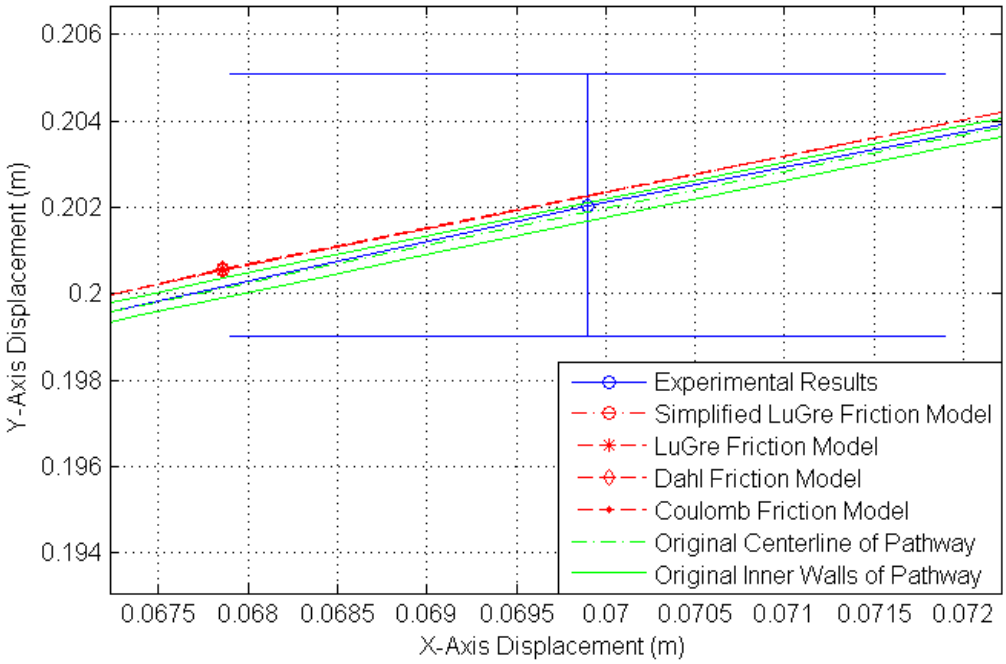

Figure 5.4. Detailed comparison of the simulation and experimental results of the displacement of the distal tip of the steerable catheter in the pathway

Table 5.1. Summary RMSEs of the displacements of the distal tip of the catheter with different friction models

Friction Model	Coulomb Friction Model	Dahl Friction Model	LuGre Friction Model	Simplified LuGre Friction Model
RMSE (mm)	1.0708	1.0706	1.0515	1.0698

Figure 5.5 shows comparisons of the simulation and experimental results for the relation between the input force and contact force of the distal tip of the catheter. The experimental results are the average values of the experimental data from 9 groups with the 95% confidence interval. The simulations were carried out by using the four friction models separately. The RMSEs of the relation between the input force and contact force of the distal tip of the catheter with different friction models were calculated and shown in Table 5.2.

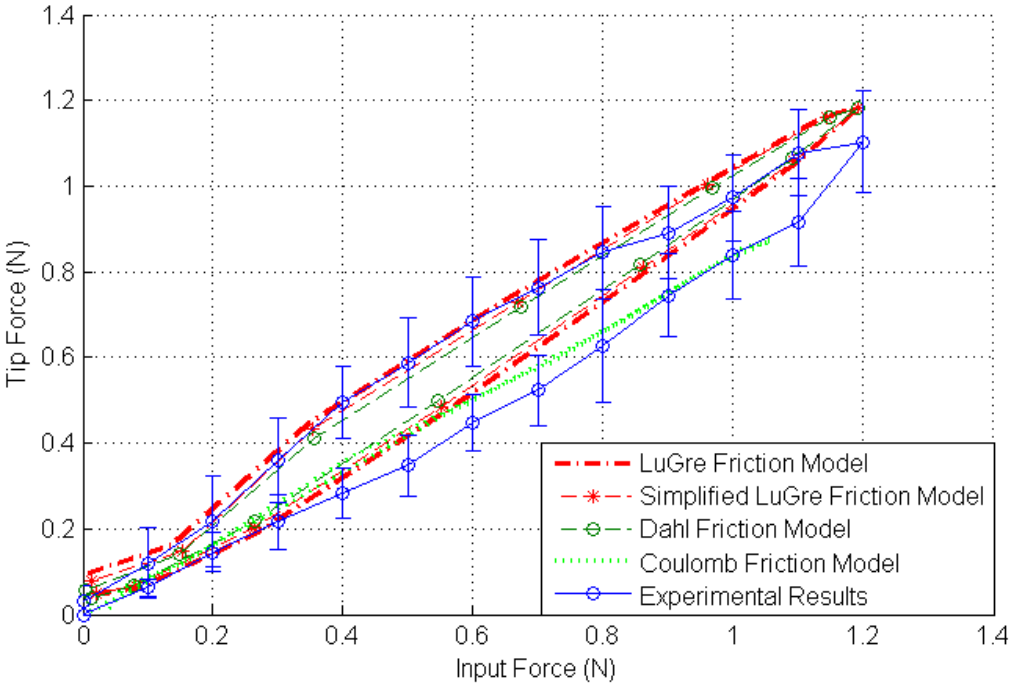

Figure 5.5. Comparisons between the simulation and experimental results of the relation between the input force and output force of the distal tip of the catheter

Table 5.2. Summary RMSEs of the relation between the input force and the force of the distal tip of the catheter with different friction models

Friction Model	Coulomb Friction Model	Dahl Friction Model	LuGre Friction Model	Simplified LuGre Friction Model
RMSE (N)	0.0995	0.0744	0.0634	0.0678

Figure 5.6 shows comparisons of the displacements of the distal tip of the catheter under the same sinusoidal input motion applied at the proximal end of the catheter. The simulation results were predicted by the kinetic model of the steerable catheter by using the four friction models separately. During the simulations, the node of the distal tip of the catheter was released. It can be seen that the simplified LuGre friction model, LuGre friction model, Dahl friction model can predict the hysteresis behavior clearly while the Coulomb friction model cannot predict the hysteresis.

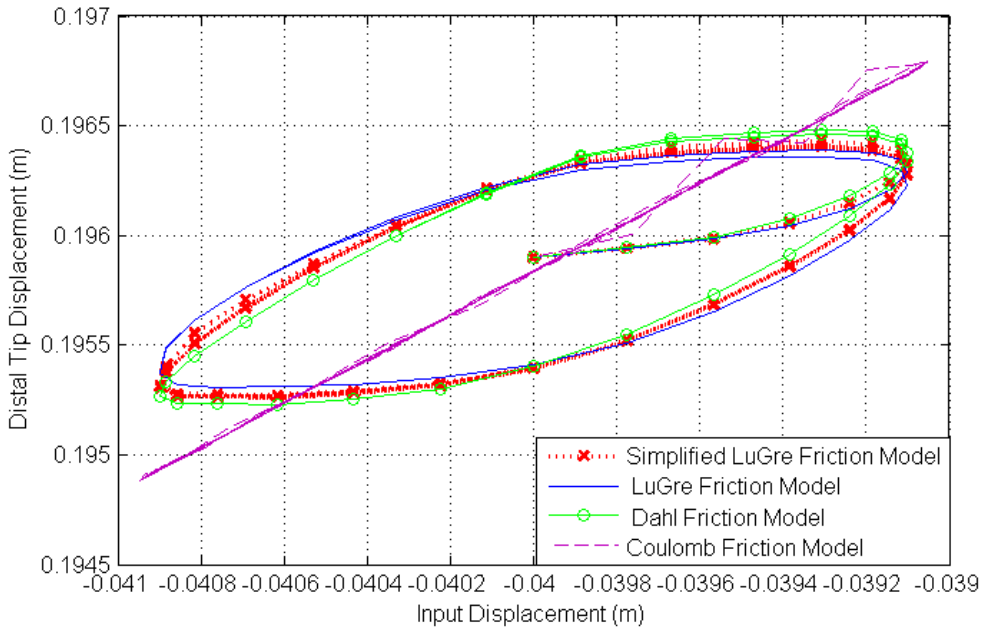

Figure 5.6. Comparison of the displacements of the distal tip of the catheter under sinusoidal inputs predicted by four different friction models

On a general note, all of the four friction models (Coulomb friction model, Dahl friction model, LuGre friction model and simplified LuGre friction model) with the contact model are able to

predict the motion and force transmission of the steerable catheter under the constraint of the pathway. From Table 5.1, it can be seen that the RMSEs in the simulation with each friction model are quite close in terms of predicting the displacement of the distal tip of the catheter. The LuGre friction model is slightly more accurate than the other friction models while the Coulomb friction model is slightly more inaccurate than the other friction models. Table 5.2 shows the errors of the predicted contact force of the distal tip with each friction model. Among the friction models, the LuGre friction model is the best one while the Coulomb friction model is the worst one in terms of the accuracy. The main reason for this result could be such that the Coulomb friction model cannot capture the hysteresis behaviour while other three friction models can capture the hysteresis behaviour.

5.4 Conclusion

In this chapter, an analysis of the kinetic model of the steerable catheter was carried out. In particular, the numbers of beam elements used to model the distal deflection part and catheter body were discussed. The length ratios for the distal deflection part and catheter body in the particular test-bed in this study were 0.0833 and 0.1944 (respectively), which is one of the bases for determining the numbers of elements for the distal deflection part and catheter body (respectively). The kinetic models of the steerable catheter with four friction models (Coulomb friction model, Dahl friction model, LuGre friction model and simplified LuGre friction model) were compared, giving the evidence that the LuGre friction model is the best one while Coulomb friction model is the worst one in terms of the accuracy.

CHAPTER 6 APPLICATIONS OF THE KINETIC MODEL

6.1 Introduction

Ideally, for a different MIS procedure, there should be a different design and operation of the catheter. The main concerns of design and operation of the steerable catheter for a specific medical task are: safety, workspace, maneuverability and stability. These concerns are further related to the maximal contact force between the catheter and tissues, and the structure of the steerable catheter especially the actuation section and its stiffness property. In this chapter, several important parameters with the structure of the catheter and its operation are discussed in order to provide the knowledge for further improvement of the design and operation of the catheter. These parameters are: (1) the length of the actuation section, (2) the stiffness of the catheter, and (3) the maximal contact force between the catheter and the inner wall of the pathway. As such, this chapter is organized as follows. Section 6.2 discusses the maximal contact force between the catheter and the inner wall of the pathway. Section 6.3 discusses how the bending stiffness of the steerable catheter affects the interaction behavior between the catheter and the pathway. Section 6.4 discusses how the length of the distal part of the steerable catheter affects the performance of the MIS procedure. Conclusions are given in Section 6.5.

6.2 The maximal contact force between the catheter and pathway

The contact forces between the steerable catheter and the inner wall of pathway affect the safety of surgery. Higher force exerted on the catheter may cause injury or perforation. The level of the maximum contact forces provides a guideline to the designer for the steerable catheter.

Figure 6.1 shows the forces exerted at the first four nodes of the catheter during the insertion stage in the pathway. The forces applied at the other nodes can be obtained through the same way. Node

1 lies in the distal tip of the catheter and Node 4 lies in the connecting part (CP) between the distal part and catheter body part. The force applied at the distal tip of the catheter started to increase dramatically when the distal tip moved to the curved pathway and contacted with the inner wall of the pathway. The forces on Node 2 and Node 3 are smaller than those on Node 1 and Node 4. It is noted that the largest force applied at the nodes is at the beginning of contact between Node 4 and the inner wall of the pathway. This situation is reasonable because the stiffness of the catheter body is much higher than the distal part of the catheter. The distal tip of the catheter and CP should be paid more attention in design, as these two parts have a higher chance to cause the perforation of the walls of the pathway than other parts of the catheter.

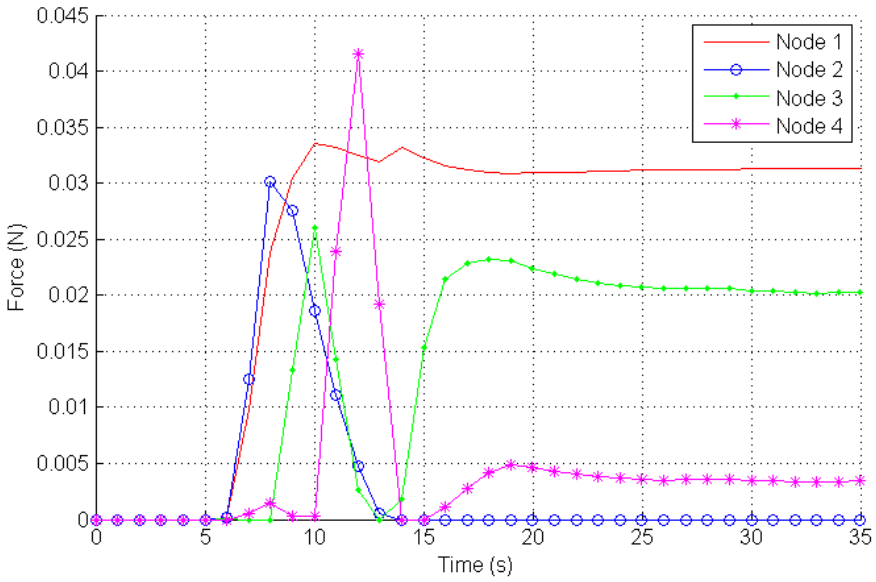

Figure 6.1. Forces exerted at the first four nodes during the insertion stage of a MIS procedure

6.3 Bending stiffness of the steerable catheter

The stiffness is one of the key factors to be considered in design of a steerable catheter. A steerable catheter with high stiffness may have good force and motion transmissions from the proximal end to the distal end and this can further improve the maneuverability and stability, but it may have large interaction forces between the catheter and pathway (or tissue) which could cause a safety issue. A steerable catheter with lower stiffness may not be able to complete certain tasks. In this section, the stiffness of the steerable catheter, effecting the motion and force transmission inside

the pathway, is analysed. The stiffness of the steerable catheter is related to both the bending rigidity of the distal part and the bending rigidity of the catheter. A certain desired bending rigidity can be determined by carefully choosing the materials and cutting slotting patterns along the length of the backbone of the steerable catheter.

Four groups of simulations with different bending rigidities of the distal part and catheter body were carried out. The input parameters are shown in Table 6.1. For Group 4, the catheter body is a variable stiffness catheter. Each segment has the same length but with a different bending rigidity.

Table 6.1. Bending rigidities used for four groups of simulation

Simulation Groups	Group 1	Group 2	Group 3	Group 4
Distal Part EI ($N.mm^2$)	171.2363	100	171.2363	100
Catheter Body EI ($N.mm^2$)	734.04	734.04	500	300, 400, 500, 600

Figure 6.2 shows a comparison of contact forces among different bending rigidities of the distal part and catheter body of the steerable catheter. It shows that the bending rigidity of the distal part affect the contact forces significantly while the bending rigidity of the catheter body does not affect the contact forces significantly. The contact forces decrease when the bending rigidity of the distal part of the catheter is smaller. Among the four groups of simulations, the variable stiffness steerable catheter (Group 4) shows the smallest contact forces. The catheter body with the variable stiffness largely reduces the contact force at the CP of the catheter.

The bending rigidities of the distal part and catheter body affect the motion and force transmission as well. Figure 6.3 and 6.4 show a comparison of the motion and force transmission among different bending rigidities of the distal part and catheter body of the steerable catheter. The bending rigidity affect the motion transmission more significantly than the force transmission. From Figure 6.3, it is noted that the result of Group 3 shows the least hysteresis while the result of Group 4 shows the worst hysteresis. The bending rigidities of the distal part and catheter body cannot be too small, as otherwise the maneuverability of the catheter at the insertion stage will be reduced; in addition, the small rigidity of the distal part and catheter body part may also decrease the operation efficiency and even cause the failure in performing a certain task.

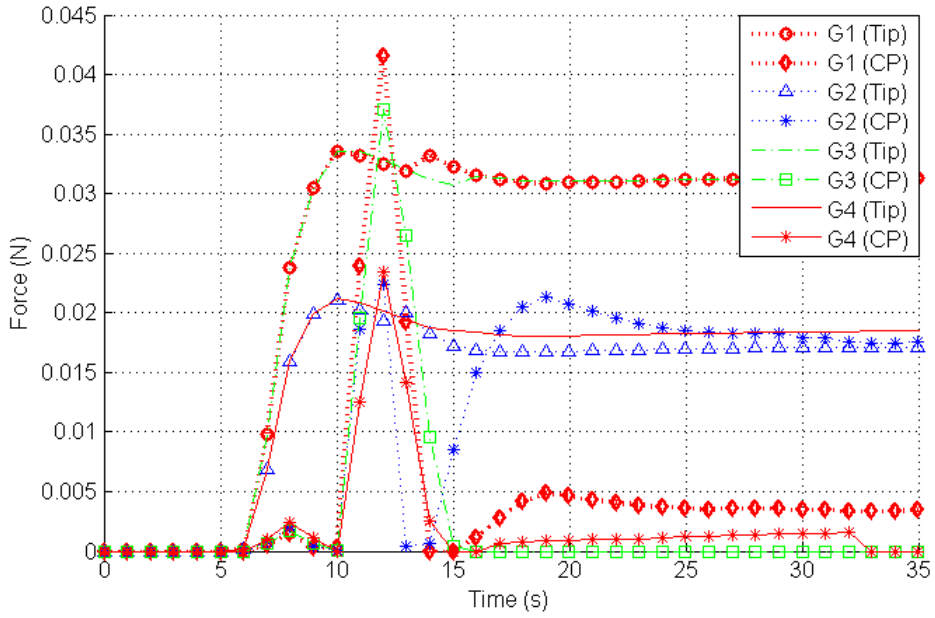

Figure 6.2. Comparison of contact forces among different bending rigidities of the distal tip and catheter body of the steerable catheter

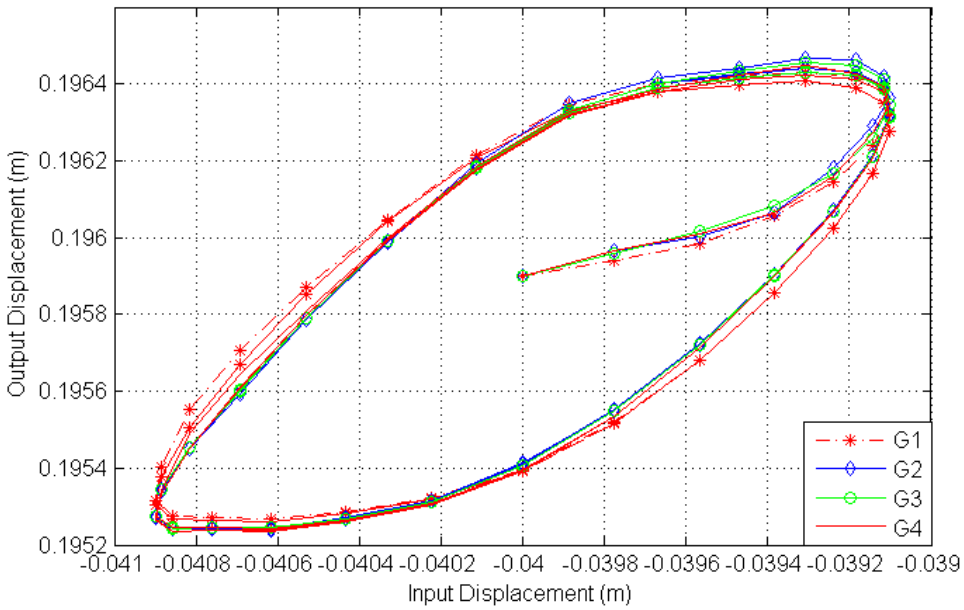

Figure 6.3. Comparison of motion transmission among different bending rigidities of the distal tip and catheter body of the steerable catheter

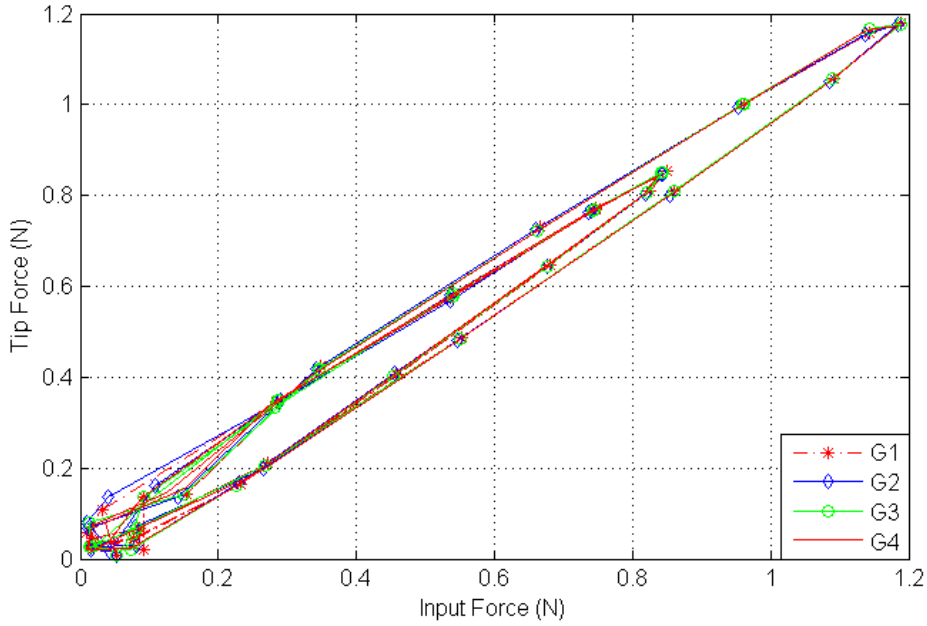

Figure 6.4. Comparison of force transmission among different bending rigidities of the distal tip and catheter body of the steerable catheter

6.4 Length of the distal part of the steerable catheter

The length of the actuation section of the steerable catheter may affect the workspace, marnuerablility and stability of the catheter. A catheter with a long actuation section may have a large workspace, but it may decrease the stability. The length of the actuation section is the length of the distal part of the steerable catheter. In this section, the effect of different lengths of the distal part of the steerable catheter on the force and motion transmission is investigated.

Three groups of simulations with different lengths of the distal part of the steerable catheters were carried out. The lengths of the distal part of the catheter used in three groups of simulations are 30 mm, 50 mm and 70 mm, respectively. Figure 6.5 shows a comparison of the contact forces with different lengths of the distal part of the steerable catheters. It shows that the length of the distal part affects the contact force significantly. The contact force increases with the shortening of the length of the distal part of the catheter.

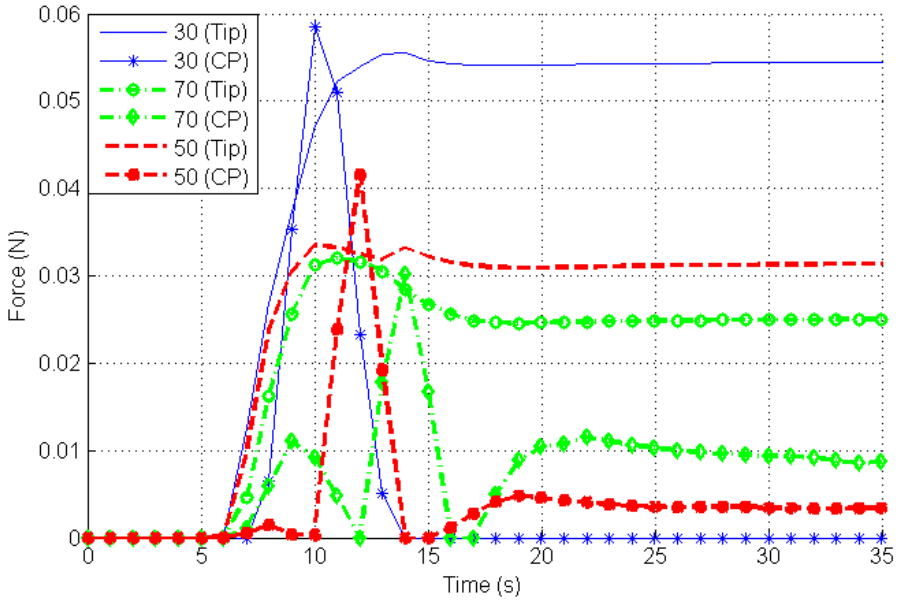

Figure 6.5. Comparison of different lengths of the distal deflection part of the steerable catheter

Figure 6.6 and 6.7 show comparisons of the motion and force transmission among different lengths of the distal part of the steerable catheter. The length of the distal part affects the motion transmission more significantly than the force transmission. From these two figures, it can be found that that the hysteresis is reduced by changing the length of the distal part. In three groups of simulation, the length as 70 mm has the best motion transmission performance. However, the length of the distal part affects the radius of the curvature of deflection. A longer length of the distal part of the steerable catheter may have a challenge to pass pathways that have an intersection shape.

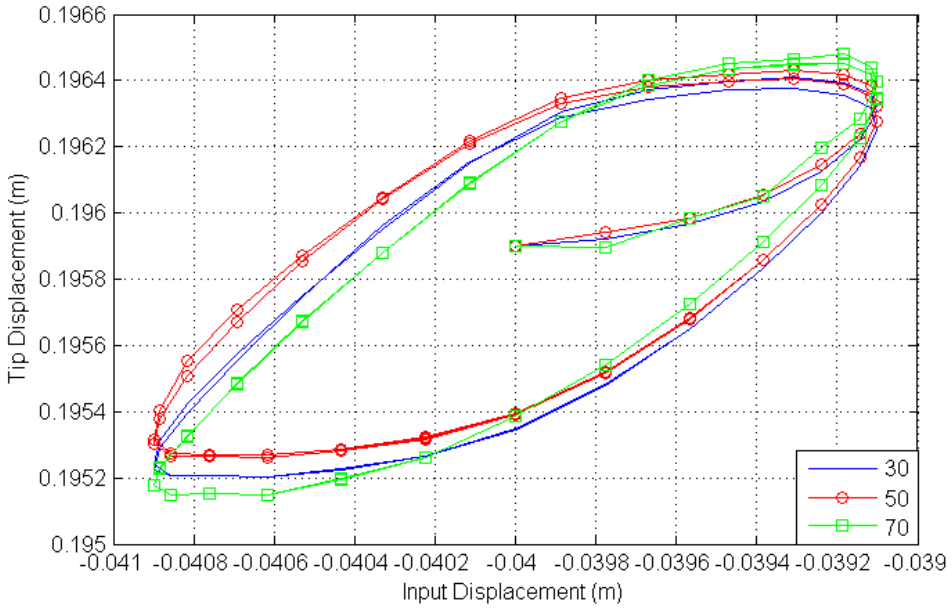

Figure 6.6. Comparison of motion transmission among different lengths of the distal tip of the steerable catheter

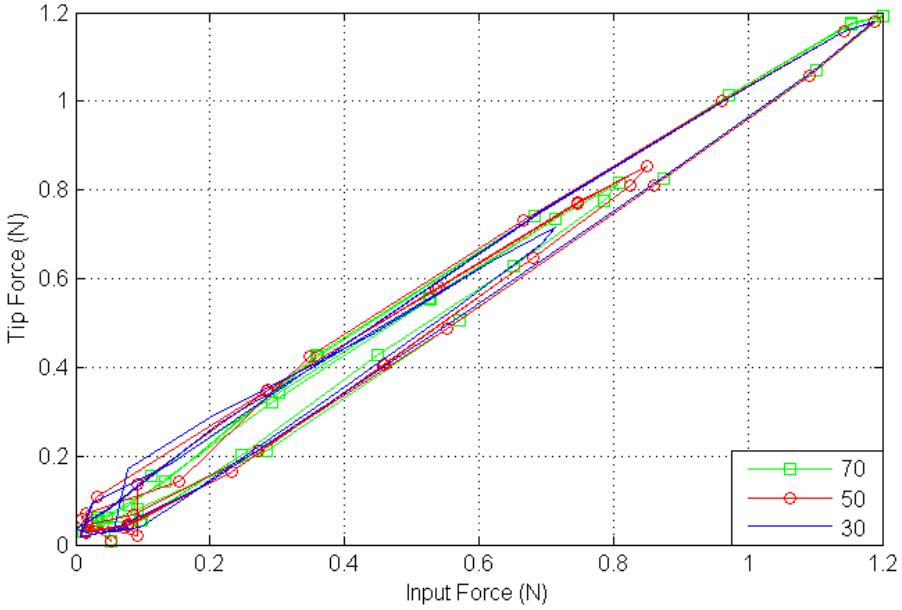

Figure 6.7. Comparison of force transmission among different lengths of the distal tip of the steerable catheter

6.5 Conclusion

In this chapter, the maximal contact force between the steerable catheter and the inner wall of pathway was analysed. Then, the structures of steerable catheter with different bending stiffness and different lengths of the distal part were analysed in terms of the force and motion transmission from the proximal end to the distal tip of catheter. Both the bending rigidity and the length of the distal part of the steerable catheter significantly affect the interaction force between the catheter and the pathway, force and motion transmission. These two parameters thus need to be carefully determined in design of the steerable catheter. The maximal contact force between the catheter and the pathway may occur in around the area of the CP of the catheter or the tip of the distal part of the catheter. The forces at these two areas should be monitored for a MIS procedure and as well as be taken as a critical force to evaluate the design of the catheter.

CHAPTER 7 CONCLUSIONS AND FUTURE WORK

7.1 Overview and conclusions

The steerable catheters/manipulators have demonstrated many advantages in the MIS. The motion and force transmission from the proximal tips to the distal tips of the catheter have significant effect to the efficiency and safety in the MIS. While the force information can be obtained by mounting sensors on the distal tip of the catheter, this idea would be quite intrusive and less reliable. In addition, this idea is also restricted by the difficulty of putting a sensor there due to the small diameter of the catheter. The other way to get the force information is to infer the force information with a kinetic model from the information on the catheter outside the human body. For this latter idea to work, there is a need of the kinetic model. Poor availability of an accurate kinetic model of the steerable catheter became a motivation of the study presented in this dissertation.

The overall objective of the study presented in this dissertation is to develop a much more accurate kinematic model of the steerable catheter. The following specific objectives were thus defined, which are re-visited here:

(1) To develop a kinetic model for the steerable catheter to describe the motion and force transmission of the catheter in its pathway by considering (1) the geometrical non-linear behavior of the catheter in motion, (2) the deformable pathway, (3) the friction between the catheter and the pathyway, and (4) the contact between the catheter and pathway. It is noted that the driving force applied by the physician is obtained by the force sensor mounted at the proximal end of the catheter which is outside the human body.

(2) To set up an experimental test-bed to validate the kinetic model. This objective can be further divided into two sub-objectives: (2a) to set up a test-bed to estimate the parameters of the kinetic model; (2b) to set up a test-bed which can measure all the required information to

validate the model.

(3) To explore the application of the kinetic model to the optimal design and operation of the steerable catheter.

After the elaboration of the research objectives in Chapter 1, Chapter 2 presented a literature review on the classification various steerable catheters and kinetic models of them, providing the understanding of the background of steerable catheters and the challenges in constructing a kinetic model. This chapter also elaborated on the suitability of taking the finite element method as a tool for constructing the kinetic model of steerable catheters.

Chapter 3 presented the development of a kinetic model of the steerable catheter and the pathway by considering their interaction. The movement of a steerable catheter in a pathway is a complex engineering phenonmenon, involving many factors such as the structure and stiffness and damping of the catheter of itself, the structure and stiffness and damping of the pathway, interaction between the catheter and the pathway (friction and contact mechanics). All these factors have been captured in the kinetic model as developed in this dissertation.

Chapter 4 presented the experimental validation of the kinetic model of the steerable catheter. An experimental test-bed of the steerable catheter was developed. The parameters in the model of the catheter as well as the model of the pathway were determined by the experiments. Several groups of experiments and simulations were performed to validate the developed kinetic model. The validity and reliability of the model were discussed as well.

Chapter 5 presented the analysis of the kinetic model of the steerable catheter with the aim to give the rationale for the development of the kinetic model (in Chapter 3), including (1) the number of finite elements used to model the whole catheter and (2) the choice of a proper friction model.

Chapter 6 presented the application of the kinetic model of the steerable catheter, particularly studying three important parameters that would affect the motion and force transmission signficiantly and the safety of the MIS. These parameters are: (1) the maximal contact force between the steerable catheter and the inner wall of the pathway was analysed; (2) the structure of

the steerable catheter with different bending rigidities and different lengths of the distal part.

The following conclusions can be drawn from this study:

(1) The geometrically non-linear FEM based kinetic model of the steerable catheter with the consideration of interactions between the catheter and the pathway with friction behavior is quite accurate and a unique one in the literature to the best of my knowledge.

(2) The Dahl friction model, the LuGre friction model and the simplified LuGre friction model are able to capture the friction behavior between the catheter and the pathway. The Coulomb friction model is not suitable in this case, as it cannot capture the hysteresis property which has a significant influence on the behavior of the catheter.

(3) The kinetic model of the steerable catheter, as developed in this dissertation, has a potential to be used to optimize the design and operation of steerable catheters with several salient points included: (1) the maximal contact force between the catheter and the pathway likely occurs on the tip of the distal part or the CP of the catheter and (2) the rigidity and length of the distal part are crucial structural parameters that will affect the motion and force transmission.

7.2 Contributions

In the field of the steerable catheter, biomechanics and bio-instrumentation, the contributions are summarized in the following:

(1) The approach to develop the kinetic model of the steerable catheter in a complex work environment is useful to model other similar compliant medical devices, such as endoscope.

(2) The kinetic model of the steerable catheter can provide the force information to improve the efficiency and safety of MIS and to realize the “doctor-assisted” catheter-based MIS procedure.

(3) The kinetic model can provide accurate data for developing other simplified models for the steerable catheters in their corresponding work environments for realizing the robotic-based fully automated MIS procedure.

(4) The kinetic model of the steerable catheter and the test-bed with the corresponding instruments and methods for the kinetic and kinematic measurements are a useful design

validation in the steerable catheter technology as well as for the training of physicians to perform the catheter-based interventional procedure by adding more complex anatomic phantoms.

In the field of continuum manipulator and continuum robots, the approach to develop the kinetic model is useful to model other manipulators and robots, such as snake-like robots.

7.3 Limitations and future work

The work presented in this dissertation has some limitations and several future studies are expected to improve the current work further.

First, the planar model of the steerable catheter was used to study the motion and force transmission. Extension of the plannar model of the steerable catheter to the spatial model is worth investigation in the future. The spatial model will be very relastic to the real situation. The spatial system can be extended from the planar system from a point of view of modeling; that is, a 2D beam element can be extended to a 3D beam element with SPACAR (Jonker, 1997, Aarts et al., 2011). The 2D pathway can be straightforwardly extended to the 3D pathway.

Second, the experimental test-bed can be extended to a 3D test-bed and improved by considering more complicated medical applications. A variety of anatomic phantoms, e.g., vascular, gastrointestinal tract, airway phantoms, should be considered, which is closer to the real situation of surgeries. This can expand the range of the applications of the test-bed, and the reliability for the medical training purpose.

Third, considering the applications, more complicated forces should be considered in the model. For example, the hydrodynamic drag force caused by the blood should be taken into account when the steerable catheter is used in vascular system. This can further improve the accuracy of the model.

Finally, the kinetic model of the steerable catheter developed in this dissertation will serve two proposed projects as future work. They are as follows:

(i) A new approach of "doctor-assisted" catheter-based surgery to improve the efficiency and safety

A completed catheter-based interventional surgery is composed of two parts: insertion and operation. During insertion, the catheter is driven by input force applied at the proximal end of the catheter by the physician. The application of force to the pathway and its anatomic attachments can be painful and excessive force can lead to perforation, in particular, pathological tissues. The perforation is the most serious complication during the insertion of catheter. The perforation may then require additional surgery for possible repair and embolization of the bleeding, even leading to the failure of a MIS procedure. The perforation is particularly due to the occurrence of an excessive contact pressure on the tissue. When the distal tip of the catheter reaches the target site, it requires a certain range of contact forces between the distal tip of the catheter and the tissue to maintain the stability and efficiency during operation. A large force can cause injury and perforation, while a small force can reduce the efficiency, even leading to the failure of a MIS procedure. The force sensor mounted at the proximal end of the catheter can only provide a physician with real-time feedback on the force applied during surgery, but it is not able to provide a reading of the contact pressure on the tissue. However, the kinetic model of the steerable catheter enables provision of the information of the forces being exerted against tissue. Therefore, the kinetic model of the steerable catheter provides the best solution for overcoming these problems. That is to say, physicians will receive a warning when the contact force on any particular section approaches the threshold of tissue perforation.

Furthermore, a friendly and straightforward human/device interface should be designed to achieve the goal of force monitoring and warning. In order to achieve real-time or short-time feedback of the force information, the model has to be refined to improve the computational efficiency. A simplified model is possible to be developed based on the predicted results by the kinetic model of the steerable catheter.

(ii) Application of the kinetic model to design new steerable catheters

The diversity of the medical applications with their specific requirements provides a wide research

ground for the design of steerable catheter with its end-effector. The main concerns of design of the steerable catheter are the miniaturization, workspace, maneuverability and stability which are physically related to its diameter, stiffness, actuation sections and length of each actuation segment. In other words, the design of steerable catheter is the trade-off among these four design parameters. Most of the current design methods of the steerable catheters are empirical and ad hoc. For this reason, the optimization of steerable catheters needs to be done. Optimization puts a high demand on accuracy of the model for kinetics, and therefore, development of a more accurate model for steerable catheters is an emerging research area. This kinetic model of the steerable catheter is able to provide reference and evaluation tool for the design of new steerable catheters. Based on this model, the optimization of the design and operation of steerable catheters is a promising research area.

REFERENCES

[1] Aagaard, P., Natale, A., & Di Biase, L. (2015). Robotic navigation for catheter ablation: benefits and challenges. Expert Review of Medical Devices, 12(4), 457-469.

[2] Aarts, R. G. K. M., Meijaard, J. P., & Jonker, J. B. (2011). SPACAR User Manual (2011 Edition). Department of Mechanical Engineering, University of Twente, the Netherlands. Available at: https://www.utwente.nl/ctw/wa/software/spacar/2012/manual/man2011.pdf.

[3] Abayazid, M., Roesthuis, R. J., Reilink, R., & Misra, S. (2013). Integrating deflection models and image feedback for real-time flexible needle steering. IEEE Transactions on Robotics, 29(2), 542-553.

[4] Abolhassani, N., Patel, R., & Moallem, M. (2007). Needle insertion into soft tissue: A survey. Medical Engineering & Physics, 29(4), 413-431.

[5] Adhikari, S. (2001). Damping models for structural vibration. Doctoral dissertation, University of Cambridge, Cambridge, United Kingdom.

[6] Alici, G., Mui, B., & Cook, C. (2006). Bending modeling and its experimental verification for conducting polymer actuators dedicated to manipulation applications. Sensors and Actuators A: Physical, 126(2), 396-404.

[7] Alterovitz, R., Branicky, M., & Goldberg, K. (2008). Motion planning under uncertainty for image-guided medical needle steering. The International Journal of Robotics Research, 27(11-12), 1361-1374.

[8] Alterovitz, R., Goldberg, K., & Okamura, A. (2005). Planning for steerable bevel-tip needle insertion through 2D soft tissue with obstacles. Proceedings of the 2005 IEEE International Conference on Robotics and Automation, pp. 1640-1645.

[9] Antman, S. S. (1995). Nonlinear Problems of Elasticity. New York, Springer Verlag.

[10] Arabagi, V., Gosline, A., Wood, R. J., & Dupont, P. E. (2013). Simultaneous soft sensing of tissue contact angle and force for millimeter-scale medical robots. 2013 IEEE International Conference on Robotics and Automation (ICRA), pp. 4396-4402.

[11] Attaway, S. W. (1999). The mechanics of friction in rope rescue. In International Technical Rescue Symposium, pp. 1-16.

[12] Bailly, Y., & Amirat, Y. (2005). Modeling and control of a hybrid continuum active catheter for aortic aneurysm treatment. Proceedings of the 2005 IEEE International Conference on Robotics and Automation, pp. 924-929.

[13] Bailly, Y., Amirat, Y., & Fried, G. (2011). Modeling and control of a continuum style microrobot for endovascular surgery. IEEE Transactions on Robotics, 27(5), 1024-1030.

[14] Bathe, K. J., (1996). Finite element procedures. New Jersey, Prentice Hall.

[15] Bedell, C., Lock, J., Gosline, A., & Dupont, P. E. (2011, May). Design optimization of concentric tube robots based on task and anatomical constraints. 2011 IEEE International Conference on Robotics and Automation (ICRA), pp. 398-403.

[16] Bi, Z. M., Zhang, W. J., Chen, I. M., & Lang, S. Y. T. (2007). Automated geneartion of the D–H parameters for configuration design of modular manipulators. Robotics and Computer-Integrated Manufacturing, 23(5), 553-562.

[17] Biosense Webster Inc. (2016). Carto® Thermocool Smarttouch® Catheter. Available at: https://www.biosensewebster.com/products/carto-3/smarttouch-catheter.aspx.

[18] Bismuth, J., Kashef, E., Cheshire, N., & Lumsden, A. B. (2011). Feasibility and safety of remote endovascular catheter navigation in a porcine model. Journal of Endovascular Therapy, 18(2), 243-249.

[19] Bismuth, J., Duran, C., Stankovic, M., Gersak, B., & Lumsden, A. B. (2013). A first-in-man study of the role of flexible robotics in overcoming navigation challenges in the iliofemoral arteries. Journal of Vascular Surgery, 57(2), 14S-19S.

[20] Boston Scientific Inc. (2016). Electrophysiology Products, Corporate Overview. Available at: https://www.bostonscientific.com/content/dam/bostonscientific/Rhythm%20Managem-ent/general/Presentation%20Resources/EP-222901-AA_BSC_EP_Corporate_Overview-FINAL%20(2).pdf.

[21] Bonet, J., Wood, R. D. (2008). Nonlinear continuum mechanics for finite element analysis (2nd Edition). Cambridge University Press, Cambridge, UK.

[22] Burgner, J., Swaney, P. J., Lathrop, R. A., Weaver, K. D., & Webster, R. J. (2013). Debulking from within: a robotic steerable cannula for intracerebral hemorrhage evacuation. IEEE Transactions on Biomedical Engineering, 60(9), 2567-2575.

[23] Burgner, J., Rucker, D. C., Gilbert, H. B., Swaney, P. J., Russell, P. T., Weaver, K. D., & Webster, R. J. (2014). A telerobotic system for transnasal surgery. IEEE/ASME Transactions on Mechatronics, 19(3), 996-1006.

[24] Butler, E. J., Hammond-Oakley, R., Chawarski, S., Gosline, A. H., Codd, P., Anor, T., & Lock, J. (2012). Robotic neuro-emdoscope with concentric tube augmentation. 2012 IEEE/RSJ International Conference on Intelligent Robots and Systems (IROS), pp. 2941-2946.

[25] Camarillo, D. B., Carlson, C. R., & Salisbury, J. K. (2009). Configuration tracking for continuum manipulators with coupled tendon drive. IEEE Transactions on Robotics, 25(4), 798-808.

[26] Camarillo, D. B. (2008a). Mechanics and control of tendon driven continuum manipulators. PhD Thesis, Stanford University, Stanford, USA.

[27] Camarillo, D. B., Milne, C. F., Carlson, C. R., Zinn, M. R., & Salisbury, J. K. (2008b). Mechanics modeling of tendon-driven continuum manipulators. IEEE Transactions on Robotics, 24(6), 1262-1273.

[28] Canudas de Wit, C., Olsson, H., Astrom, K. J., & Lischinsky, P. (1995). A new model for control of systems with friction. IEEE Transactions on Automatic Control, 40(3), 419-425.

[29] Carlson, C. R., & Barbagli, F. (2013). Robotic catheter systems and methods. U.S. Patent No. 8,391,957. Washington, DC: U.S. Patent and Trademark Office.

[30] Carroll, S., Santoianni, D., Thibault, B., Wittenberger, D., Aubert, M. P., & Marcotte, M. A. (2011). Defined deflection structure. U.S. Patent No. 7,955,298. Washington, DC: U.S. Patent and Trademark Office.

[31] Cheng, W. B. (2014). Development of a Kinetic Model for Loop-Free Colonoscopy Technology. Doctoral Dissertation, University of Saskatchewan, Saskatoon, Canada.

[32] Cheng, W. B., Di, Y. Y., Zhang, E. M., Moser, M. A., Kanagaratnam, S., Korman, L. Y., & Zhang, W. J. (2013). Modeling and In Vitro Experimental Validation for Kinetics of the Colonoscope in Colonoscopy. Annals of Biomedical Engineering, 1-10.

[33] Chentanez, N., Alterovitz, R., Ritchie, D., Cho, L., Hauser, K. K., Goldberg, K., & O'Brien, J. F., (2009). Interactive simulation of surgical needle insertion and steering. Computer Graphics Proceeding, Annual Conference Series, Vol. 28, No. 3, pp: 1-10.

[34] Chowdhury, I., & Dasgupta, S. P. (2003). Computation of Rayleigh damping coefficients for large systems. The Electronic Journal of Geotechnical Engineering, 8(0), pp: 1-11.

[35] Chun, K. J., Wissner, E., Koektuerk, B., Konstantinidou, M., Schmidt, B., Zerm, T., & Kuck, K. H. (2010). Remote-controlled magnetic pulmonary vein isolation using a new irrigated-tip catheter in patients with atrial fibrillation. Circulation: Arrhythmia and Electrophysiology, 3(5), 458-464.

[36] Cotin, S., Duriez, C., Lenoir, J., Neumann, P., & Dawson, S. (2005). New approaches to catheter navigation for interventional radiology simulation. In Medical Image Computing and Computer-Assisted Intervention–MICCAI 2005, Springer Berlin Heidelberg, pp. 534-542.

[37] Da, L., Zhang, D., & Wang, T. (2008). Overview of the vascular interventional robot. The International Journal of Medical Robotics and Computer Assisted Surgery, 4(4), 289-294.

[38] Dario, P., Carrozza, M. C., Marcacci, M., D'Attanasio, S., Magnami, B., Tonet, O., & Megali, G. (2000). A novel mechatronic tool for computer-assisted arthroscopy. IEEE Transactions on Information Technology in Biomedicine, 4(1), 15-29.

[39] De Greef, A., Lambert, P., & Delchambre, A. (2009). Towards flexible medical instruments: Review of flexible fluidic actuators. Precision Engineering, 33(4), 311-321.

[40] Degani, A., Choset, H., Wolf, A., Ota, T., & Zenati, M. A. (2006). Percutaneous intrapericardial interventions using a highly articulated robotic probe. The First IEEE/RAS-EMBS International Conference on Biomedical Robotics and Biomechatronics, pp. 7-12.

[41] Della Santa, A., Mazzoldi, A., & De Rossi, D. (1996). Steerable microcatheters actuated by embedded conducting polymer structures. Journal of Intelligent Material Systems and Structures, 7(3), 292-300.

[42] Dequidt, J., Marchal, M., Duriez, C., Kerien, E., & Cotin, S. (2008). Interactive simulation of embolization coils: Modeling and experimental validation. In Medical Image Computing and Computer-Assisted Intervention–MICCAI 2008, pp. 695-702.

[43] Di Biase, L., Wang, Y. A. N., Horton, R., Gallinghouse, G. J., Mohanty, P., Sanchez, J., & Natale, A. (2009a). Ablation of Atrial Fibrillation Utilizing Robotic Catheter Navigation in Comparison to Manual Navigation and Ablation: Single-Center Experience. Journal of cardiovascular electrophysiology, 20(12), 1328-1335.

[44] Di Biase, L., Natale, A., Barrett, C., Tan, C., Elayi, C. S., Ching, C. K., & Wisnoskey, B. J.

(2009b). Relationship between catheter forces, lesion characteristics, “popping” and char formation: experience with robotic navigation system. Journal of cardiovascular electrophysiology, 20(4), 436-440.

[45] Duerig, T. W., Pelton, A., & Stöckel, D. (1999). An overview of nitinol medical applications. Materials Science and Engineering: A, 273, 149-160.

[46] Duindam, V., Xu, J., Alterovitz, R., Sastry, S., & Goldberg, K. (2010). Three-dimensional motion planning algorithms for steerable needles using inverse kinematics. The International Journal of Robotics Research, 29(7), 789-800.

[47] Dupont, P. E., Armstrong, B., & Hayward, V. (2000). Elasto-plastic friction model: contact compliance and stiction. In Proceedings of the American control conference, Vol. 2, pp. 1072-1077.

[48] Dupont, P. E., Lock, J., Itkowitz, B., & Butler, E. (2010). Design and control of concentric-tube robots. IEEE Transactions on Robotics, 26(2), 209-225.

[49] Duriez, C., Cotin, S., Lenoir, J., & Neumann, P. (2006). New approaches to catheter navigation for interventional radiology simulation. Computer Aided Surgery, 11(6), 300-308.

[50] Ernst, S., Ouyang, F., Linder, C., Hertting, K., Stahl, F., Chun, J., & Kuck, K. H. (2004). Initial experience with remote catheter ablation using a novel magnetic navigation system magnetic remote catheter ablation. Circulation, 109(12), 1472-1475.

[51] Erni, S., Schürle, S., Fakhraee, A., Kratochvil, B. E., & Nelson, B. J. (2013). Comparison, optimization, and limitations of magnetic manipulation systems. Journal of Micro-Bio Robotics, 1-14.

[52] Faddis, M. N., Blume, W., Finney, J., Hall, A., Rauch, J., Sell, J., & Lindsay, B. (2002). Novel, magnetically guided catheter for endocardial mapping and radiofrequency catheter ablation. Circulation, 106(23), 2980-2985.

[53] Fang, B. K., Ju, M. S., & Lin, C. C. K. (2009, January). Development of Active Guide-wire for Cardiac Catheterization by Using Ionic Polymer-Metal Composites. In 13th International Conference on Biomedical Engineering, Springer Berlin Heidelberg, pp. 340-343.

[54] Filgueiras-Rama, D., Estrada, A., Shachar, J., Castrejón, S., Doiny, D., Ortega, M. & Merino, J. L. (2013). Remote Magnetic Navigation for Accurate, Real-time Catheter

Positioning and Ablation in Cardiac Electrophysiology Procedures. Journal of visualized experiments: JoVE, (74).Ganji, Y., & Janabi-Sharifi, F. (2009). Catheter kinematics for intracardiac navigation. IEEE Transactions on Biomedical Engineering, 56(3), 621-632.

[55] Ganji, Y., & Janabi-Sharifi, F. (2007). Kinematic characterization of a cardiac ablation catheter. 2007 IEEE/RSJ International Conference on Intelligent Robots and Systems, pp. 1876-1881.

[56] Ganji, Y., & Janabi-Sharifi, F. (2009). Catheter kinematics for intracardiac navigation. IEEE Transactions on Biomedical Engineering, 56(3), 621-632.

[57] Ghali, B. (2008). Algorithms for nonlinear finite element-based modeling of soft-tissue deformation and cutting. Master Thesis, McMaster University, Hamilton, Canada.

[58] Gilbert, H. B., Rucker, D. C., & Webster III, R. J. (2013). Concentric tube robots: The state of the art and future directions. 2013 International Symposium on Robotics Research, 1-16.

[59] Glozman, D., & Shoham, M. (2007). Image-guided robotic flexible needle steering. IEEE Transactions on Robotics, 23(3), 459-467.

[60] Gosline, A. H., Vasilyev, N. V., Butler, E. J., Folk, C., Cohen, A., Chen, R., ... & Dupont, P. E. (2012). Percutaneous intracardiac beating-heart surgery using metal MEMS tissue approximation tools. The International Journal of Robotics Research, 31(9), 1081-1093.

[61] Gosselin, F. P., Lalande, V., & Martel, S. (2011). Characterization of the deflections of a catheter steered using a magnetic resonance imaging system. Medical physics, 38, 4994-5002.

[62] Govari, A., Altmann, A. C., Ephrath, Y., & Beeckler, C. T. (2011). ROBOTIC DRIVE FOR CATHETER. U.S. Patent No. 20,110,040,150. Washington, DC: U.S. Patent and Trademark Office.

[63] Guo, S.X., Fukuda, T., Kosuge, K., Arai, F., Oguro, K., & Negoro, M. (1995). Micro catheter system with active guide wire. 1995 IEEE International Conference on Robotics and Automation, Vol. 1, pp. 79-84.

[64] Guo, X., Tegg, T. T., & Stehr, R. E. (2011). Deflectable catheter with distal deflectable segment. U.S. Patent No. 7,985,215. Washington, DC: U.S. Patent and Trademark Office.

[65] Guo, Y., Xu, W., Fu, Y., & Zhang, W. (2010). Comparison studies on dynamic packaging properties of corrugated paperboard pads. Engineering, 2(05), 378-386.

[66] Haga, Y., Esashi, M., & Maeda, S. (2000). Bending, torsional and extending active catheter

assembled using electroplating. In Micro Electro Mechanical Systems. 2000 The Thirteenth Annual International Conference on MEMS, IEEE, pp. 181-186.

[67] Haga, Y., Mineta, T., & Esashi, M. (2002). Active catheter, active guide wire and related sensor systems. 2002 Proceedings of the 5th Biannual World on Automation Congress, IEEE, Vol. 14, pp. 291-296.

[68] Haga, Y., Tanahashi, Y., & Esashi, M. (1998). Small diameter active catheter using shape memory alloy. Micro Electro Mechanical Systems. 1998 Proceedings of the Eleventh Annual International Workshop on MEMS, IEEE, pp. 419-424.

[69] Hannan, M. W., & Walker, I. D. (2003). Kinematics and the implementation of an elephant's trunk manipulator and other continuum style robots. Journal of Robotic Systems, 20(2), 45-63.

[70] Hansen Medical Inc. (2016a). Artisan® Extend Control Catheter. Available at: http://www.hansenmedical.com/us/en/cardiac-arrhythmia/artisan-extend-catheter/product-overview.

[71] Hansen Medical Inc. (2016b). Magellan™ Robotic System. Available at: http://www.hansenmedical.com/us/en/vascular/magellan-robotic-system/product-overview.

[72] Harada, K., Bo, Z., Enosawa, S., Chiba, T., & Fujie, M. G. (2007). Bending laser manipulator for intrauterine surgery and viscoelastic model of fetal rat tissue. 2007 IEEE International Conference on Robotics and Automation, pp. 611-616.

[73] Hetts, S. W., Saeed, M., Martin, A. J., Evans, L., Bernhardt, A. F., Malba, V., ... & Sincic, R. (2013). Endovascular catheter for magnetic navigation under MR imaging guidance: evaluation of safety in vivo at 1.5 T. American Journal of Neuroradiology, 34(11), 2083-2091.

[74] Howell, L. L. (2001). Compliant mechanisms. John Wiley & Sons.

[75] Ikeuchi, M., & Ikuta, K. (2009). Development of pressure-driven micro active catheter using membrane micro emboss following excimer laser ablation (MeME-X) process. 2009 IEEE International Conference on Robotics and Automation (ICRA'09), pp. 4469-4472.

[76] Ikuta, K., Matsuda, M., Yajima, D., & Ota, Y. (2012). Pressure Pulse Drive: A Control Method for the Precise Bending of Hydraulic Active Catheters. IEEE/ASME Transactions on Mechatronics, 17(5), 876-883.

[77] Jayender, J., Azizian, M., & Patel, R. V. (2008). Autonomous image-guided robot-assisted

active catheter insertion. IEEE Transactions on Robotics, 24(4), 858-871.

[78] Jayender, J., Patel, R. V., & Nikumb, S. (2009). Robot-assisted active catheter insertion: algorithms and experiments. The International Journal of Robotics Research, 28(9), 1101-1117.

[79] Jeon, S. M., & Jang, G. H. (2012). Precise Steering and Unclogging Motions of a Catheter With a Rotary Magnetic Drill Tip Actuated by a Magnetic Navigation System. IEEE Transactions on Magnetics, 48(11), 4062-4065.

[80] Jones, B. A., Gray, R. L., & Turlapati, K. (2009). Three dimensional statics for continuum robotics. 2009 IEEE/RSJ International Conference on Intelligent Robots and Systems, pp. 2659-2664.

[81] Jonker, J. B. (1997). Dynamics of machines: A finite element approach. Lecture notes, Department of Mechanical Engineering, University of Twente, Netherlands.

[82] Jung, J., Penning, R. S., Ferrier, N. J., & Zinn, M. R. (2011). A modeling approach for continuum robotic manipulators: effects of nonlinear internal device friction. 2011 IEEE/RSJ International Conference on Intelligent Robots and Systems (IROS), pp. 5139-5146.

[83] Jung, J., Penning, R. S., & Zinn, M. R. (2014). A modeling approach for robotic catheters: effects of nonlinear internal device friction. Advanced Robotics, 28(8), 557-572.

[84] Kanagaratnam, P., Koa-Wing, M., Wallace, D. T., Goldenberg, A. S., Peters, N. S., & Davies, D. W. (2008). Experience of robotic catheter ablation in humans using a novel remotely steerable catheter sheath. Journal of Interventional Cardiac Electrophysiology, 21(1), 19-26.

[85] Kang, D. (2007). Modeling of the piezoelectric-driven stick-slip actuators. Master dissertation, University of Saskatchewan, Saskatoon, Canada.

[86] Kautzner, J., Peichl, P., ČIHÁK, R., Wichterle, D., & MLČOCHOVÁ, H. (2009). Early experience with robotic navigation for catheter ablation of paroxysmal atrial fibrillation. Pacing and Clinical Electrophysiology, 32(s1), S163-S166.

[87] Kesner, S. B., & Howe, R. D. (2011). Position control of motion compensation cardiac catheters. IEEE Transactions on Robotics, 27(6), 1045-1055.

[88] Khatait, J. P., Brouwer, D. M., Aarts, R. G., & Herder, J. L. (2013). Modeling of a flexible instrument to study its sliding behavior inside a curved endoscope. Journal of

Computational and Nonlinear Dynamics, 8(3), 031002-1:10.

[89] Khatait, J. P., Brouwer, D. M., Meijaard, J. P., Aarts, R. G., & Herder, J. L. (2014). Flexible Multibody Modeling of a Surgical Instrument inside an Endoscope. Journal of Computational and Nonlinear Dynamics, 9(1), 011018-1:11.

[90] Khoshnam, M., Azizian, M., & Patel, R. V. (2012). Modeling of a steerable catheter based on beam theory. 2012 IEEE International Conference on Robotics and Automation (ICRA), pp. 4681-4686.

[91] Khoshnam, M., Skanes, A. C., & Patel, R. V. (2015). Modeling and estimation of tip contact force for steerable ablation catheters. IEEE Transactions on Biomedical Engineering, 62(5), 1404-1415.

[92] Kim, A. M., Turakhia, M., Lu, J., Badhwar, N., Lee, B. K., Lee, R. J., & Olgin, J. E. (2008). Impact of remote magnetic catheter navigation on ablation fluoroscopy and procedure time. Pacing and Clinical Electrophysiology, 31(11), 1399-1404.

[93] Kotoyama, K., Nakagawa, H., Shah, D. C., Lambert., H., Leo, G., Aeby, N., Ikeda, A., Pitha, J. V., Sharma, T., Lazzara, R., & Jackman, W. M. (2008). Novel Contact Force Sensor Incorporated in Irrigated Radiofrequency Ablation Catheter Predicts Lesion Size and Incidence of Steam Pop and Thrombus. Circulation: Arrhythmia and Electrophysiology. 1: 354-362.

[94] Kutzer, M. D. M., Segreti, S. M., Brown, C. Y., Armand, M., Taylor, R. H., & Mears, S. C. (2011). Design of a new cable-driven manipulator with a large open lumen: Preliminary applications in the minimally-invasive removal of osteolysis. 2011 IEEE International Conference on Robotics and Automation (ICRA), pp. 2913-2920.

[95] Lenoir, J., Cotin, S., Duriez, C., & Neumann, P. (2006). Interactive physically-based simulation of catheter and guidewire. Computers & Graphics, 30(3), 416-422.

[96] Lim, G., Minami, K., Sugihara, M., Uchiyama, M., & Esashi, M. (1995). Active catheter with multi-link structure based on silicon micromachining. 1995 IEEE Proceedings on Micro Electro Mechanical Systems, pp. 116-121.

[97] Lim, G., Park, K., Sugihara, M., Minami, K., & Esashi, M. (1996). Future of active catheters. Sensors and Actuators A: Physical, 56(1), 113-121.

[98] Liu, T., & Cavusoglu, M. C. (2014). Three dimensional modeling of an MRI actuated steerable catheter system. 2014 IEEE International Conference on Robotics and

Automation (ICRA), pp. 4393-4398.

[99] Liu, Y. F., Li, J., Zhang, Z. M., Hu, X. H., & Zhang, W. J. (2015). Experimental comparison of five friction models on the same test-bed of the micro stick-slip motion system. Mechanical Sciences, 6(1), 15-28.

[100] Mahvash, M., & Dupont, P. E. (2011). Stiffness control of surgical continuum manipulators. IEEE Transactions on Robotics, 27(2), 334-345.

[101] Miyazaki, S., Nault, I., Haissaguerre, M., & Hocini, M. (2010). Atrial fibrillation ablation by aortic retrograde approach using a magnetic navigation system. Journal of Cardiovascular Electrophysiology, 21(4), 455-457.

[102] Morgan, N. B. (2004). Medical shape memory alloy applications - the market and its products. Materials Science and Engineering: A, 378(1), 16-23.

[103] Murphy, R. J., Moses, M. S., Kutzer, M. D., Chirikjian, G. S., & Armand, M. (2013). Constrained workspace generation for snake-like manipulators with applications to minimally invasive surgery. 2013 IEEE International Conference on Robotics and Automation (ICRA), pp. 5341-5347.

[104] Murray, R. M., Li, Z., Sastry, S. S., & Sastry, S. S. (1994). A mathematical introduction to robotic manipulation. Boca Raton, CRC press.

[105] Nguyen, B. L., Merino, J. L., & Gang, E. S. (2010). Remote navigation for ablation procedures–A new step forward in the treatment of cardiac arrhythmias. Eur Cardiol, 6, 50-56.

[106] Oguro, K., Asaka, K., & Takenaka, H. (1993). Polymer film actuator driven by a low voltage. In Proceedings of 4th International Symposium on Micro Machine and Human Science, pp. 39-40.

[107] Olsson, H., Åström, K. J., De Wit, C. C., Gäfvert, M., & Lischinsky, P. (1998). Friction models and friction compensation. European journal of control, 4(3), 176-195.

[108] Oppenheim, A. V., Schafer, R. W., & Buck, J. R. (1989). Discrete-time signal processing (Vol. 2). Englewood Cliffs: Prentice-hall.

[109] Pappone, C., Vicedomini, G., Manguso, F., Gugliotta, F., Mazzone, P., Gulletta, S., & Santinelli, V. (2006). Robotic magnetic navigation for atrial fibrillation ablation. Journal of the American College of Cardiology, 47(7), 1390-1400.

[110] Proietti, R., Pecoraro, V., Di Biase, L., Natale, A., Santangeli, P., Viecca, M., & Tagliabue,

L. (2013). Remote magnetic with open-irrigated catheter vs. manual navigation for ablation of atrial fibrillation: a systematic review and meta-analysis. Europace.

[111] Reed, K. B., Okamura, A. M., & Cowan, N. J. (2009). Modeling and control of needles with torsional friction. IEEE Transactions on Biomedical Engineering, 56(12), 2905-2916.

[112] Riga, C. V., Bicknell, C. D., Hamady, M. S., & Cheshire, N. J. (2011). Evaluation of robotic endovascular catheters for arch vessel cannulation. Journal of Vascular Surgery, 54(3), 799-809.

[113] Robinson, G., & Davies, J. B. C. (1999). Continuum robots-a state of the art. Proceedings of 1999 IEEE International Conference on Robotics and Automation, Vol. 4, pp. 2849-2854.

[114] Rucker, D. C., Jones, B. A., & Webster, R. J. (2010a). A geometrically exact model for externally loaded concentric-tube continuum robots. IEEE Transactions on Robotics, 26(5), 769-780.

[115] Rucker, D. C., & Webster, R. J. (2009). Parsimonious evaluation of concentric-tube continuum robot equilibrium conformation. IEEE Transactions on Biomedical Engineering, 56(9), 2308-2311.

[116] Rucker, D. C., & Webster, R. J. (2011). Statics and dynamics of continuum robots with general tendon routing and external loading. IEEE Transactions on Robotics, 27(6), 1033-1044.

[117] Rucker, D. C., Webster, R. J., Chirikjian, G. S., & Cowan, N. J. (2010b). Equilibrium conformations of concentric-tube continuum robots. The International Journal of Robotics Research, pp, 1-18. DOI: 10.1177/0278364910367543.

[118] Ruzzu, A., Bade, K., Fahrenberg, J., & Maas, D. (1998). Positioning system for catheter tips based on an active microvalve system. Journal of Micromechanics and Microengineering, 8(2), pp, 161-164.

[119] Saliba, W., Cummings, J. E., Oh, S., Zhang, Y., Mazgalev, T. N., Schweikert, R. A., & Natale, A. (2006). Novel robotic catheter remote control system: feasibility and safety of transseptal puncture and endocardial catheter navigation. Journal of cardiovascular electrophysiology, 17(10), 1102-1105.

[120] Sears, P., & Dupont, P. (2006). A steerable needle technology using curved concentric tubes. 2006 IEEE/RSJ International Conference on Intelligent Robots and Systems, pp. 2850-2856.

[121] Segreti, S. M., Kutzer, M. D., Murphy, R. J., & Armand, M. (2012). Cable length estimation

for a compliant surgical manipulator. 2012 IEEE International Conference on Robotics and Automation (ICRA), pp. 701-708.

[122] Sewa, S., Onishi, K., Asaka, K., Fujiwara, N., & Oguro, K. (1998). Polymer actuator driven by ion current at low voltage, applied to catheter system. 1998 Proceedings of The Eleventh Annual International Workshop on MEMS, pp. 148-153.

[123] Simaan, N., Xu, K., Wei, W., Kapoor, A., Kazanzides, P., Taylor, R., & Flint, P. (2009). Design and integration of a telerobotic system for minimally invasive surgery of the throat. The International Journal of Robotics Research, 28(9), 1134-1153.

[124] Smela, E. (2003). Conjugated polymer actuators for biomedical applications. Advanced Materials, 15(6), 481-494.

[125] Stereotaxis Inc. (2016). NIOBE® Magnetic Navigation System. Available at: http://www.stereotaxis.com/products/.

[126] Su, H. J. (2009). A pseudorigid-body 3R model for determining large deflection of cantilever beams subject to tip loads. Journal of Mechanisms and Robotics, 1(2), pp. 021008-1 - 021008-9.

[127] Swevers, J., Al-Bender, F., Ganseman, C. G., & Projogo, T. (2000). An integrated friction model structure with improved presliding behavior for accurate friction compensation. IEEE Transactions on Automatic Control, 45(4), 675-686.

[128] Szewczyk, J., Marchandise, E., Flaud, P., Royon, L., & Blanc, R. (2011). Active catheters for neuroradiology. Journal of Robotics and Mechatronics, 23(1), 105.

[129] Takizawa, H., Tosaka, H., Ohta, R., Kaneko, S., & Ueda, Y. (1999). Development of a microfine active bending catheter equipped with MIF tactile sensors. 1999 Twelfth IEEE International Conference on MEMS, pp. 412-417.

[130] Tang, W., Wan, T. R., Gould, D. A., How, T., & John, N. W. (2012). A stable and real-time nonlinear elastic approach to simulating guidewire and catheter insertions based on Cosserat rod. IEEE Transactions on Biomedical Engineering, 59(8), 2211-2218.

[131] ten Hoff, H. (1993). Scanning mechanisms for intravascular ultrasound imaging: a flexible approach. Doctoral Dissertation, Erasmus MC: University Medical Center Rotterdam, Rotterdam, Netherlands.

[132] Tunay, I. (2004). Modeling magnetic catheters in external fields. 2004 26th Annual International Conference of the IEEE on Engineering in Medicine and Biology Society, Vol.

1, pp. 2006-2009.

[133] Tunay, I. (2011). Distributed parameter statics of magnetic catheters. 2011 Annual International Conference of the IEEE on Engineering in Medicine and Biology Society, EMBC, pp. 8344-8347.

[134] Tung, A. T., Park, B. H., Niemeyer, G., & Liang, D. H. (2007). Laser-machined shape memory alloy actuators for active catheters. IEEE/ASME Transactions on Mechatronics, 12(4), 439-446.

[135] Ullah, W., Hunter, R. J., Haldar, S., Mclean, A., Dhinoja, M., Sporton, S. & Schilling, R. J. (2014). Comparison of robotic and manual persistent AF ablation using catheter contact force sensing: an international multicenter registry study. Pacing and Clinical Electrophysiology, 37(11), 1427-1435.

[136] Van der Werff, K. (1977). Kinematic and dynamic analysis of mechanisms, a finite element approach. Doctoral dissertation, Delft University of Technology, Netherlands.

[137] Venkiteswaran, V. K., & Su, H. J. (2015). A parameter optimization framework for determining the pseudo-rigid-body model of cantilever-beams. Precision Engineering, 40, 46-54.

[138] Wang, K. D., & Yan, G. Z. (2009). Research on measurement and modeling of the gastro intestine's frictional characteristics. Measurement Science and Technology, 20(1), 015803.

[139] Walker, I. D. (2013). Continuous backbone “continuum” robot manipulators. International Scholarly Research Notices (ISRN) Robotics, vol. 2013, pp. 1-19.

[140] Watson, J. R. (2013). Asymmetric dual directional steerable catheter sheath. U.S. Patent No. 8,500,733. Washington, DC: U.S. Patent and Trademark Office.

[141] Webster, R. J., & Jones, B. A. (2010). Design and kinematic modeling of constant curvature continuum robots: A review. The International Journal of Robotics Research, 29(13), 1661-1683.

[142] Webster, R. J., Kim, J. S., Cowan, N. J., Chirikjian, G. S., & Okamura, A. M. (2006). Nonholonomic modeling of needle steering. The International Journal of Robotics Research, 25(5-6), 509-525.

[143] Webster, R. J., Memisevic, J., & Okamura, A. M. (2005). Design considerations for robotic needle steering. Proceedings of the 2005 IEEE International Conference on Robotics and Automation, pp. 3588-3594.

[144] Webster, R. J., Romano, J. M., & Cowan, N. J. (2009). Mechanics of precurved-tube continuum robots. IEEE Transactions on Robotics, 25(1), 67-78.

[145] Wood, M. A., Orlov, M., Ramaswamy, K., Haffajee, C., & Ellenbogen, K. (2008). Remote magnetic versus manual catheter navigation for ablation of supraventricular tachycardias: a randomized, multicenter trial. Pacing and clinical electrophysiology, 31(10), 1313-1321.

[146] Worthington-Kirsch, R. L., Andrews, R. T., Siskin, G. P., Shlansky-Goldberg, R., Lipman, J. C., Goodwin, S. C., & Hovsepian, D. M. (2002). II. Uterine fibroid embolization: technical aspects. Techniques in vascular and interventional radiology, 5(1), 17-34.

[147] Xu, K., & Simaan, N. (2008). An investigation of the intrinsic force sensing capabilities of continuum robots. IEEE Transactions on Robotics, 24(3), 576-587.

[148] Xu, K., & Simaan, N. (2010). Intrinsic wrench estimation and its performance index for multisegment continuum robots. IEEE Transactions on Robotics, 26(3), 555-561.

[149] Xu, R., Asadian, A., Naidu, A. S., & Patel, R. V. (2013). Position control of concentric-tube continuum robots using a modified Jacobian-based approach. 2013 IEEE International Conference on Robotics and Automation (ICRA), pp. 5813-5818.

[150] Xu, R., & Patel, R. V. (2012). A fast torsionally compliant kinematic model of concentric-tube robots. 2012 Annual International Conference of the IEEE on Engineering in Medicine and Biology Society (EMBC), pp. 904-907.

[151] Yokoyama, K., Nakagawa., H., Shah, D. C., Lambert, H., Leo, M., Aeby, N., Ikeda, A., Pitha, J. V., Sharma, T., Lazzara, R., & Jackman, W. M. (2008). Novel Contact Force Sensor Incorporated in Irrigated Radiofrequency Ablation Catheter Predicts Lesion Size and Incidence of Steam Pop and Thrombus. Circulation: Arrhythmia and Electrophysiology. 1: 354-362.

[152] Zhang, B., Kobayashi, Y., Chiba, T., & Fujie, M. G. (2009). Robotic patch-stabilizer using wire driven mechanism for minimally invasive fetal surgery. 2009 Annual International Conference of the IEEE on Engineering in Medicine and Biology Society, pp. 5076-5079.

[153] Zhang, Q. S., Chen, X. B., Yang, Q., & Zhang, W. J. (2012). Development and characterization of a novel piezoelectric-driven stick-slip actuator with anisotropic-friction surfaces. The International Journal of Advanced Manufacturing Technology, 61(9-12), 1029-1034.

[154] Zhang, W. J., Ouyang, P. R., & Sun, Z. H. (2010). A novel hybridization design principle

for intelligent mechatronics systems. In Proceedings of International Conference on Advanced Mechatronics (ICAM2010), pp. 4-6.

[155] Zhang, W. J., & van der Werff, K. (1998). Automatic communication from a neutral object model of mechanism to mechanism analysis programs based on a finite element approach in a software environment for CADCAM of mechanisms. Finite Elements in Analysis and Design, 28(3), 209-239.

APPENDIX A COPYRIGHT PERMISSIONS

A.1 Permission for figures from IEEE publications

Thesis / Dissertation Reuse

The IEEE does not require individuals working on a thesis to obtain a formal reuse license, however, you may print out this statement to be used as a permission grant:

Requirements to be followed when using any portion (e.g., figure, graph, table, or textual material) of an IEEE copyrighted paper in a thesis:

1) In the case of textual material (e.g., using short quotes or referring to the work within these papers) users must give full credit to the original source (author, paper, publication) followed by the IEEE copyright line © 2011 IEEE.
2) In the case of illustrations or tabular material, we require that the copyright line © [Year of original publication] IEEE appear prominently with each reprinted figure and/or table.
3) If a substantial portion of the original paper is to be used, and if you are not the senior author, also obtain the senior author's approval.

Requirements to be followed when using an entire IEEE copyrighted paper in a thesis:

1) The following IEEE copyright/ credit notice should be placed prominently in the references: © [year of original publication] IEEE. Reprinted, with permission, from [author names, paper title, IEEE publication title, and month/year of publication]
2) Only the accepted version of an IEEE copyrighted paper can be used when posting the paper or your thesis on-line.
3) In placing the thesis on the author's university website, please display the following message in a prominent place on the website: In reference to IEEE copyrighted material which is used with permission in this thesis, the IEEE does not endorse any of [university/educational entity's name goes here]'s products or services. Internal or personal use of this material is permitted. If interested in reprinting/republishing IEEE copyrighted material for advertising or promotional purposes or for creating new collective works for resale or redistribution, please go tohttp://www.ieee.org/publications_standards/publications/rights/rights_link.html to learn how to obtain a License from RightsLink.

If applicable, University Microfilms and/or ProQuest Library, or the Archives of Canada may supply single copies of the dissertation.

A.2 Permission for Figure 2.8

ELSEVIER LICENSE
TERMS AND CONDITIONS

Mar 31, 2016

This is a License Agreement between Xiaohua Hu ("You") and Elsevier ("Elsevier") provided by Copyright Clearance Center ("CCC"). The license consists of your order details, the terms and conditions provided by Elsevier, and the payment terms and conditions.

All payments must be made in full to CCC. For payment instructions, please see information listed at the bottom of this form.

Supplier	Elsevier Limited The Boulevard,Langford Lane Kidlington,Oxford,OX5 1GB,UK
Registered Company Number	1982084
Customer name	Xiaohua Hu
Customer address	Division of Biomedical Engineering, 57 Campus Dr. Saskatoon, SK S7N 5A9
License number	3839171085824
License date	Mar 31, 2016
Licensed content publisher	Elsevier
Licensed content publication	Sensors and Actuators A: Physical
Licensed content title	Laser-machined shape memory alloy sensors for position feedback in active catheters
Licensed content author	Alexander T. Tung,Byong-Ho Park,David H. Liang,Günter Niemeyer
Licensed content date	15 September 2008
Licensed content volume number	147
Licensed content issue number	1
Number of pages	10
Start Page	83
End Page	92
Type of Use	reuse in a thesis/dissertation
Portion	figures/tables/illustrations
Number of figures/tables/illustrations	1

Format	both print and electronic
Are you the author of this Elsevier article?	No
Will you be translating?	No
Original figure numbers	Fig. 3
Title of your thesis/dissertation	DEVELOPMENT OF A KINETIC MODEL FOR THE STEERABLE CATEHTERS FOR MINIMALLY INVASIVE SURGERY
Expected completion date	Aug 2016
Estimated size (number of pages)	240
Elsevier VAT number	GB 494 6272 12
Permissions price	0.00 CAD
VAT/Local Sales Tax	0.00 CAD / 0.00 GBP
Total	0.00 CAD

APPENDIX B NATURAL FREQUENCY OF THE CATHETER BODY AND DISTAL DEFLECTION PART OF STEERABL CATHETER AND THE TUBE

```
% to caculate the natrual frequency of catheter body
  clc;
  clear all;

%%  input parameters of catheter body
    r = 1.2;                    % radius of catheter(mm)
    I = pi*r^4/4;                % moment of inertia
    A = pi*(r^2);                % cross-sectional A  (mm^2)
    lbeam = 150;                % length (mm)
    EI = 734.4;              % flexural stiffness (N*mm^2 ) of tube
    E = 1000*EI/I;              % modulus of elasticity (mN/mm^2=1000Mpa )
    mass = 0.00753*150/1000;    % mass of catheter (kg)
    density = mass/(lbeam*A);   % unit: (kg/mm^3)
    num_elements = 10;

%%  input parameters of distal deflection part of catheter
    r = 1.2;                    % radius of catheter(mm)
    I = pi*r^4/4;                % moment of inertia
    A = pi*(r^2);                % cross-sectional A  (mm^2)
    lbeam = 50;                % length (mm)
    EI = 171.2363;              % flexural stiffness (N*mm^2 ) of tube
    E = 1000*EI/I;              % modulus of elasticity (mN/mm^2=1000Mpa )
    mass = 0.03*50/1000;    % mass of catheter (kg)
    density = mass/(lbeam*A);   % unit: (kg/mm^3)
    num_elements = 10;

%%  input parameters of tube
    D = 3.3;
    R = D/2;
    d = 2.6;
    r = d/2;                    % radius of tube (mm)
    I = pi*(R^4-r^4)/4;             % moment of inertia
    A = pi*(R^2-r^2);               % cross-sectional A  (mm^2)
    lbeam = 100;                % length of the colonoscope unit: (mm)
    EI = 1621.563;              % flexural stiffness (N*mm^2 ) of tube
    E = 1000*EI/I;              % modulus of elasticity (mN/mm^2=1000Mpa )
    mass = 0.694/1000;    % mass of tube (kg)
    density = mass/(lbeam*A);   % unit: (kg/mm^3)
    num_elements = 10;
```

The following codes refer to (Guo et al. 2010).

```
%   define length of each element, uniform lengths
    l = lbeam/num_elements;
%   define whether or not to do Guyan Reduction
    guyan = input('enter "1" to do Guyan elimination of rotations, "enter" to
not do Guyan ...  ');
    if (isempty(guyan))
        guyan = 0;
    else
```

```
    end

    if  guyan == 0
        num_plot_max = 2*num_elements;

        num_plot_default = num_elements;
    else
        num_plot_max = num_elements;
         num_plot_default = num_elements;
    end
    num_plot = input(['enter the number of modes to plot, max
',num2str(num_plot_max),', default ',num2str(num_plot_default),' ...  ']);
    if (isempty(num_plot))
        num_plot = 9;
    else
    end
%   define length of each element, uniform lengths
    l = lbeam/num_elements;
%   define length vector for plotting, right-to-left numbering
    lvec = 0:l:lbeam;
%   define the node numbers
    n = 1:num_elements+1;
%   number the nodes for the elements
    node1 = 1:num_elements;
    node2 = 2:num_elements+1;
%   size the stiffness and mass matrices to have 2 times the number of nodes
%   to allow for translation and rotation dof's for each node, including
built-
%   in end
    max_node1 = max(node1);
    max_node2 = max(node2);
    max_node_used = max([max_node1 max_node2]);
    mnu = max_node_used;
    k = zeros(2*mnu);
    m = zeros(2*mnu);
%   now build up the global stiffness and consistent mass matrices, element by
element
    mpl = density*A;
    for  i = 1:num_elements
        dof1 = 2*node1(i)-1;
        dof2 = 2*node1(i);
        dof3 = 2*node2(i)-1;
        dof4 = 2*node2(i);
        k(dof1,dof1) = k(dof1,dof1)+(12*E*I/l^3);
        k(dof2,dof1) = k(dof2,dof1)+(6*E*I/l^2);
        k(dof3,dof1) = k(dof3,dof1)+(-12*E*I/l^3);
        k(dof4,dof1) = k(dof4,dof1)+(6*E*I/l^2);
        k(dof1,dof2) = k(dof1,dof2)+(6*E*I/l^2);
        k(dof2,dof2) = k(dof2,dof2)+(4*E*I/l);
        k(dof3,dof2) = k(dof3,dof2)+(-6*E*I/l^2);
        k(dof4,dof2) = k(dof4,dof2)+(2*E*I/l);
        k(dof1,dof3) = k(dof1,dof3)+(-12*E*I/l^3);
        k(dof2,dof3) = k(dof2,dof3)+(-6*E*I/l^2);
        k(dof3,dof3) = k(dof3,dof3)+(12*E*I/l^3);
        k(dof4,dof3) = k(dof4,dof3)+(-6*E*I/l^2);
        k(dof1,dof4) = k(dof1,dof4)+(6*E*I/l^2);
```

```
        k(dof2,dof4) = k(dof2,dof4)+(2*E*I/l);
        k(dof3,dof4) = k(dof3,dof4)+(-6*E*I/l^2);
        k(dof4,dof4) = k(dof4,dof4)+(4*E*I/l);
        m(dof1,dof1) = m(dof1,dof1)+(mpl/420)*(156*l);
        m(dof2,dof1) = m(dof2,dof1)+(mpl/420)*(22*l^2);
        m(dof3,dof1) = m(dof3,dof1)+(mpl/420)*(54*l);
        m(dof4,dof1) = m(dof4,dof1)+(mpl/420)*(-13*l^2);
        m(dof1,dof2) = m(dof1,dof2)+(mpl/420)*(22*l^2);
        m(dof2,dof2) = m(dof2,dof2)+(mpl/420)*(4*l^3);
        m(dof3,dof2) = m(dof3,dof2)+(mpl/420)*(13*l^2);
        m(dof4,dof2) = m(dof4,dof2)+(mpl/420)*(-3*l^3);
        m(dof1,dof3) = m(dof1,dof3)+(mpl/420)*(54*l);
        m(dof2,dof3) = m(dof2,dof3)+(mpl/420)*(13*l^2);
        m(dof3,dof3) = m(dof3,dof3)+(mpl/420)*(156*l);
        m(dof4,dof3) = m(dof4,dof3)+(mpl/420)*(-22*l^2);
        m(dof1,dof4) = m(dof1,dof4)+(mpl/420)*(-13*l^2);
        m(dof2,dof4) = m(dof2,dof4)+(mpl/420)*(-3*l^3);
        m(dof3,dof4) = m(dof3,dof4)+(mpl/420)*(-22*l^2);
        m(dof4,dof4) = m(dof4,dof4)+(mpl/420)*(4*l^3);
    end
%   now that stiffness and mass matrices are defined for all dof's, including
%   constrained dof's, need to delete rows and columns of the matrices that
%   correspond to constrained dof's, in the left-to-right case, the first two
%   rows and columns
    k(1:2,:) = [];  % translation/rotation of node 1
    k(:,1:2) = [];
    m(1:2,:) = [];
    m(:,1:2) = [];
    if  guyan == 1
%   Guyan Reduction - reduce out the rotation dof's, leaving displacement
dof's
%   re-order the matrices
%   re-order the columns of k
    kr = zeros(2*(mnu-1));
    krr = zeros(2*(mnu-1));
%   rearrange columns, rotation and then displacement dof's
    mkrcolcnt = 0;
    for  mkcolcnt = 2:2:2*(mnu-1)
        mkrcolcnt = mkrcolcnt + 1;
        kr(:,mkrcolcnt) = k(:,mkcolcnt);
        mr(:,mkrcolcnt) = m(:,mkcolcnt);
    end
    mkrcolcnt = num_elements;
    for  mkcolcnt = 1:2:2*(mnu-1)
        mkrcolcnt = mkrcolcnt + 1;
        kr(:,mkrcolcnt) = k(:,mkcolcnt);
        mr(:,mkrcolcnt) = m(:,mkcolcnt);
    end
%   rearrange rows, rotation and then displacement dof's
    mkrrowcnt = 0;
    for  mkrowcnt = 2:2:2*(mnu-1)
        mkrrowcnt = mkrrowcnt + 1;
        krr(mkrrowcnt,:) = kr(mkrowcnt,:);
        mrr(mkrrowcnt,:) = mr(mkrowcnt,:);
    end
    mkrrowcnt = num_elements;
    for  mkrowcnt = 1:2:2*(mnu-1)
```

```
        mkrrowcnt = mkrrowcnt + 1;
        krr(mkrrowcnt,:) = kr(mkrowcnt,:);
        mrr(mkrrowcnt,:) = mr(mkrowcnt,:);
    end
%   define sub-matrices and transformation matrix T
    kaa = krr(1:num_elements,1:num_elements);
    kab = krr(1:num_elements,num_elements+1:2*num_elements);
    T = [-inv(kaa)*kab
            eye(num_elements,num_elements)]
%   calculate reduced mass and stiffness matrices
    kbb = T'*krr*T
    mbb = T'*mrr*T
    else
    kbb = k;
    mbb = m;
    end
%   define the number of dof for state-space version, 2 times dof left after
%   removing constrained dof's
    [dof,dof] = size(kbb);
%   define the sizes of mass and stiffness matrices for state-space
    ssdof = 2*dof;
    aud = zeros(ssdof);     % creates a ssdof x ssdof null matrix
%   divide the negative of the stiffness matrix by the mass matrix
    ksm = inv(mbb)*(-kbb);
%   now expand to state space size
%   fill out unit values in mass and stiffness matrices
    for  row = 1:2:ssdof
        aud(row,row+1) = 1;
    end
%   fill out mass and stiffness terms from m and k
    for  row = 2:2:ssdof
        for  col = 2:2:ssdof
            aud(row,col-1) = ksm(row/2,col/2);
        end
    end
%   calculate the eigenvalues/eigenvectors of the undamped matrix for plotting
%   and for calculating the damping matrix c
    [evec1,evalu] = eig(aud);
    evalud = diag(evalu);
    evaludhz = evalud/(2*pi);
    num_modes = length(evalud)/2;
%   now reorder the eigenvalues and eigenvectors from low to high freq
    [evalorder,indexhz] = sort(abs((evalud)));
    for  cnt = 1:length(evalud)
        eval(cnt,1) = evalud(indexhz(cnt));
        evalhzr(cnt,1) = round(evaludhz(indexhz(cnt)));
        evec(:,cnt) = evec1(:,indexhz(cnt));
    end
%   now check for any imaginary eigenvectors and convert to real
    for  cnt = 1:length(evalud)
        if  (imag(evec(1,cnt)) & imag(evec(3,cnt)) & imag(evec(5,cnt))) ~= 0
            evec(:,cnt) = imag(evec(:,cnt));
        else
        end
    end
    if  guyan == 0
%   now separate the displacement and rotations in the eigenvectors
```

```
%   for plotting mode shapes
    evec_disp = zeros(ceil(dof/2),ssdof);
    rownew = 0;
    for  row = 1:4:ssdof
        rownew = rownew+1;
        evec_disp(rownew,:) = evec(row,:);
    end
    evec_rotation = zeros(ceil(dof/2),ssdof);
    rownew = 0;
    for  row = 3:4:ssdof
        rownew = rownew+1;
        evec_rotation(rownew,:) = evec(row,:);
    end
    else
    evec_disp = zeros(ceil(dof/4),ssdof);
    rownew = 0;
    for  row = 1:2:ssdof
        rownew = rownew+1;
        evec_disp(rownew,:) = evec(row,:);
    end
    end
%   normalize the displacement eigenvectors wrt one for plotting
    for  col = 1:ssdof
        evec_disp(:,col) = evec_disp(:,col)/max(abs(real(evec_disp(:,col))));
        if  evec_disp(floor(dof/2),col) >= 0
            evec_disp(:,col) = -evec_disp(:,col);
        else
        end
    end
%   list eigenvalues, hz
    format long e
    evaludhz_list = sort(evaludhz(1:2:2*num_modes))
    format short
%   list displacement (not velocity) eigenvectors
    evec_disp(:,1:2:2*num_plot)
    if  guyan == 0
%   plot mode shapes
    for  mode_cnt = 1:num_plot
        evec_cnt = 2*mode_cnt -1;
        plot(lvec,[0; evec_disp(:,evec_cnt)],'ko-')
        title(['Cantilever Beam, Mode ', ...
            num2str(mode_cnt),': ',num2str(abs(evalhzr(evec_cnt))),' hz']);
        xlabel('Distance From Built-In End')
        ylabel('Normalized Y-Displacement')
        axis([0 lbeam -1.5 1.5])
        grid on
    disp('execution paused to display figure, "enter" to continue'); pause
    end
    else
%   plot mode shapes, Guyan Reduced
    for  mode_cnt = 1:num_plot
        evec_cnt = 2*mode_cnt -1;
        plot(lvec,[0; evec_disp(:,evec_cnt)],'ko-')
        title(['Cantilever Beam, Mode ', ...
            num2str(mode_cnt),': ',num2str(abs(evalhzr(evec_cnt))),' hz']);
        xlabel('Distance From Built-In End')
        ylabel('Normalized Y-Displacement')
```

```
        axis([0 lbeam -1.5 1.5])
        grid on
    disp('execution paused to display figure, "enter" to continue'); pause
    end
    end
%   normalization with respect to mass on a filled (not diagonal) mass matrix
%   calculate the displacement (displacement and rotation) eigenvectors
%   to be used for the modal model eigenvectors
    xm = zeros(dof);
    col = 0;
    for  mode = 1:2:ssdof
        col = col + 1;
        row = 0;
        for  ndof = 1:2:ssdof
            row = row + 1;
            xm(row,col) = evec(ndof,mode);
        end
    end
%   normalize with respect to mass
    for  mode = 1:dof
        xn(:,mode) = xm(:,mode)/sqrt(xm(:,mode)'*mbb*xm(:,mode));
    end
%   calculate the normalized mass and stiffness matrices for checking
    mm = xn'*mbb*xn;
    km = xn'*kbb*xn;
%   check that the sqrt of diagonal elements of km are eigenvalues
    p = (diag(km)).^0.5;
    row = 0;
    for cnt = 1:2:ssdof
        row = row + 1;
        evalrad(row) = abs((eval(cnt)));
    end
    [p evalrad']/(2*pi)
    evalhz = evalrad/(2*pi);
    semilogy(evalhz)
    title('Resonant Frequencies, Hz')
    xlabel('Mode Number')
    ylabel('Frequency, hz')
    grid
    disp('execution paused to display figure, "enter" to continue'); pause
```

APPENDIX C MATLAB CODES FOR THE SIMULATION OF THE KINETIC MODEL OF STEERABLE CATHETER DURING INSERION

The kinetic model of the steerable catheter interacting with the pathway was implemented in the SPACAR program through several user-defined routines in MATLAB environment. The main program was defined in SPACAR by defining the initial kinetic information and dynamic information of the steerable catheter, and intergrator (Appendix C.1). The contact situation and friction between the catheter and pathway were defined through user-defined routines (Appendix C.2). The time, displacement, deformation and velocity information in the main program can be updated and transferred to Appendix C.2 in each step, while the force information in Appendix C.2 can be updated and transferred to the main program in each step. The detail information of using SPACAR can be found in (Aarts et al. 2011).

C.1 Spacar data for the kinetic model of the steerable catheter

```
PLBEAM  1   1   2   3   4
PLBEAM  2   3   4   5   6
PLBEAM  3   5   6   7   8
PLBEAM  4   7   8   9   10
PLBEAM  5   9   10  11  12
PLBEAM  6   11  12  13  14
PLBEAM  7   13  14  15  16
PLBEAM  8   15  16  17  18
PLBEAM  9   17  18  19  20
PLBEAM  10  19  20  21  22
PLBEAM  11  21  22  23  24
PLBEAM  12  23  24  25  26

X   1   0   0
X   3   0   -0.0167
X   5   0   -0.0334
X   7   0   -0.050
X   9   0   -0.080
X   11  0   -0.110
X   13  0   -0.150
X   15  0   -0.190
X   17  0   -0.230
X   19  0   -0.270
X   21  0   -0.310
X   23  0   -0.360
X   25  0   -0.400

DYNX    1   1
```

```
DYNX    2
DYNX    3   1
DYNX    4
DYNX    5   1
DYNX    6
DYNX    7   1
DYNX    8
DYNX    9   1
DYNX    10
DYNX    11  1
DYNX    12
DYNX    13  1
DYNX    14
DYNX    15  1
DYNX    16
DYNX    17  1
DYNX    18
DYNX    19  1
DYNX    20
DYNX    21  1
DYNX    22
DYNX    23  1
DYNX    24
DYNX    25  1
INPUTX  25  2

FIX 26

RLSE    1   2   3
RLSE    2   2   3
RLSE    3   2   3
RLSE    4   2   3
RLSE    5   2   3
RLSE    6   2   3
RLSE    7   2   3
RLSE    8   2   3
RLSE    9   2   3
RLSE    10  2   3
RLSE    11  2   3
RLSE    12  2   3

END
HALT

EM  1   0.00753
EM  2   0.00753
EM  3   0.00753
EM  4   0.00753
EM  5   0.00753
EM  6   0.00753
EM  7   0.00753
EM  8   0.00753
EM  9   0.00753
EM  10  0.00753
EM  11  0.00753
EM  12  0.00753
```

```
ESTIFF  1   0   0.0001712363
ESTIFF  2   0   0.0001712363
ESTIFF  3   0   0.0001712363
ESTIFF  4   0   0.0007344
ESTIFF  5   0   0.0007344
ESTIFF  6   0   0.0007344
ESTIFF  7   0   0.0007344
ESTIFF  8   0   0.0007344
ESTIFF  9   0   0.0007344
ESTIFF  10  0   0.0007344
ESTIFF  11  0   0.0007344
ESTIFF  12  0   0.0007344

%EDAMP   1   0.015011
%EDAMP   2   0.015011
%EDAMP   3   0.014962
%EDAMP   4   0.352807
%EDAMP   5   0.352807
%EDAMP   6   0.353388
%EDAMP   7   0.353388
%EDAMP   8   0.354551
%EDAMP   9   0.354551
%EDAMP   10  0.355713
%EDAMP   11  0.355713
%EDAMP   12  0.356875

% XF    1   0.01   -0.01
% XF  13  0   0.01
USERSIG FORCE
% USERINP MOTION
TIMESTEP    36   36
INPUTX 25 2 -0.400 0.01  0.00

INTEGRAT    155 0.00001  % It effects the stability of the system.
ERROR   0.00000005  0.00000005  % It effects the stability of the system.
END
END
```

C.2 Codes for the user defined contact situation

```
                %% User defined interaction force %%
% %%%%%%%%%%%%%%%%%%%%%%%%%%%%%%%%%%%%%%%%%%%%%%%%%%%%%%%%%%%%%%%%%%%%%%%%%%%
% USERSIG: Name of the MATLAB M-file with user functions with forces and
stresses.
%
% function [time, sig, f] = pushsig(t, ne, le, e, ep, nx, lnp, x, xp);
%
% Three columns should be provided with
% 1. The element number (e) or the node number (x).
% 2. The deformation mode number (e) or the coordinate number (x).
% 3. The current value of the stress or force component.
%
% Two more columns can be provided, which specify the diagonal elements of the
stiffness
% and damping matrices, respectively, corresponding to the stress or force
component.
%
% sig: user defined generalized stress resultants;
% f: user defined nodal forces fx;
% t: time;
% ne: number of deformation parameters;
% le: location matrix for the elements;
% e: generalized deformations;
% ep: velocity;
% nx: number of coordinates;
% lnp: location matrix for the nodes;
% x: coordinates (nodal displacements);
% xp: velocity (Only one row vector with the current values of the velocities
are passed on to the subroutine as input parameters);
% nxp: number of fixed, calculable, input, dynamic and kinematic coordinates
% nep: number of fixed, calculable, input, dynamic and kinematic deformation
parameters
% %%%%%%%%%%%%%%%%%%%%%%%%%%%%%%%%%%%%%%%%%%%%%%%%%%%%%%%%%%%%%%%%%%%%%%%%%%%

function [time, sig, f] = FORCE(t, ne, le, e, ep, nx, lnp, x, xp);
%% initial condition
global z1p
global z3p
global z5p
global z7p
global z9p
global z11p
global z13p
global z15p
global z17p
global z19p
global z21p
global z23p
global z25p

z1p = 0.0000;
z3p = 0.0000;
z5p = 0.0000;
z7p = 0.0000;
```

```
z9p = 0.0000;
z11p = 0.0000;
z13p = 0.0000;
z15p = 0.0000;
z17p = 0.0000;
z19p = 0.0000;
z21p = 0.0000;
z23p = 0.0000;
z25p = 0.0000;

time = t;
sig = [];

R = 0.2; % radius of tube curve
L = (2*pi*R)/4; % the length of the 1/4 ciclar curve.
r = 0.0013; % the inner radius of the tube is 2mm.
r0 = 0.0012; % catheter radius
Ox = R;
Oy = 0.05;

M = 0.00694*(L+0.01); %0.694/100 g/mm=0.00694kg/m
Kv = 622.68; % stiffness of tube N/m, 2*10^4 in Kohatait thesis
Cv = 11.4701*M+0.000185*Kv; % C=11.4701M+0.000185Kv; 10 Ns/m^2 in Khatait
thesis % 0.016 in experiment
a = r-r0+0.002;
b = a+0.0005; % the original transit zone is 0.5mm
u = 0.1204; % friction coefficient
sigma0 = 300000; %0.07 N/mm in Ref. (Jung J, 2014)
sigma1 = 3;
% sigma2 = 1.5;
dt = 0.00001; %0.0001;

%% Caculate the contact force Fn and friction force Ff on each node
% Node 1
x1 = x(1,lnp(1,1)); % the x coordinate of the node 1;
y1 = x(1,lnp(1,2)); % the y coordinate of the node 1;
v1 = xp(1,lnp(1,1));
phi1 = x(1,lnp(2,1));

if y1>=0.05; % caculate the contact force Fn.
   Rj1 = sqrt((x1-Ox)^2+(y1-Oy)^2);
   alpha1 = asin((y1-0.05)/Rj1); % rad
   if Rj1>=R
      xn1 = Rj1-R; % Distance between the node and centerline of tube;
      Vn1 = v1*sin(phi1+alpha1-pi/2); % Velocity of catheter in normal
direction;
      Vt1 = v1*cos(phi1+alpha1-pi/2);
      beta1 = (xn1-a)/(b-a);
      contact=0;
      if xn1>b;
      contact=1;
      Fn1 = Kv*(b-a)*(beta1-1/2)+Cv*Vn1;
      else if a<=xn1&xn1<=b;
              contact=1;
              Fn1 = (Kv/2)*(b-a)*beta1^2+Cv*(3-2*beta1)*beta1^2*Vn1;
           else xn1<a;
```

```
                contact=0;
                Fn1 = 0;
            end
        end
        Fn1x = Fn1*cos(alpha1);
        Fn1y = -Fn1*sin(alpha1);
        % caculate the Ff
        if Fn1 == 0;
           Ff1 = 0;
           Ff1x = 0;
           Ff1y = 0;
        else
            Fc1 = u*Fn1; % caculate the friction force.
            z1 = Vt1*(1-sigma0*sign(Vt1)*z1p/abs(Fc1))*dt+z1p
            %dotz1 = (z1-z1p)/dt;
            Ff1 = sigma0*z1+sigma1*Vt1;
            z1p = z1;
            Ff1x = -Ff1*sin(alpha1);
            Ff1y = -Ff1*cos(alpha1);
        end
    else Rj1<R
        xn1 = R-Rj1; % Distance between the node and centerline of tube;
        Vn1 = v1*sin(-phi1-alpha1+pi/2); % Velocity of catheter in normal
direction;
        Vt1 = v1*cos(-phi1-alpha1+pi/2);
        beta1 = (xn1-a)/(b-a);
        contact=0;
        if xn1>b;
        contact=1;
        Fn1 = Kv*(b-a)*(beta1-1/2)+Cv*Vn1;
        else if a<=xn1&xn1<=b;
                contact=1;
                Fn1 = (Kv/2)*(b-a)*beta1^2+Cv*(3-2*beta1)*beta1^2*Vn1;
             else xn1<a;
                  contact=0;
                  Fn1 = 0;
            end
        end
        Fn1x = -Fn1*cos(alpha1);
        Fn1y = Fn1*sin(alpha1);
        % caculate the Ff
        if Fn1 == 0;
           Ff1 = 0;
           Ff1x = 0;
           Ff1y = 0;
        else
            Fc1 = u*Fn1; % caculate the friction force.
            z1 = Vt1*(1-sigma0*sign(Vt1)*z1p/abs(Fc1))*dt+z1p
            %dotz1 = (z1-z1p)/dt;
            Ff1 = sigma0*z1+sigma1*Vt1;
            z1p = z1
            Ff1x = -Ff1*sin(alpha1);
            Ff1y = -Ff1*cos(alpha1);
        end
    end

else 0<=y1&y1<0.05; % the catheter's x-displacement should be restrained.
```

```
Rj1 = sqrt((x1-Ox)^2);
if Rj1>=R
   xn1 = Rj1-R; % Distance between the node and centerline of tube;
   Vn1 = v1*sin(phi1-pi/2); % Velocity of catheter in normal direction;
   Vt1 = v1*cos(phi1-pi/2);
   beta1 = (xn1-a)/(b-a);
   if xn1>b;
      Fn1 = Kv*(b-a)*(beta1-1/2)+Cv*Vn1;
   else if a<=xn1&xn1<=b;
           Fn1 = (Kv/2)*(b-a)*beta1^2+Cv*(3-2*beta1)*beta1^2*Vn1;
        else xn1<a;
             Fn1 = 0;
        end
   end
   Fn1x = Fn1;
   Fn1y = 0;

   if Fn1 == 0;
      Ff1 = 0;
      Ff1x = 0;
      Ff1y = 0;
   else
       Fc1 = u*Fn1; % caculate the friction force.
       z1 = Vt1*(1-sigma0*sign(Vt1)*z1p/abs(Fc1))*dt+z1p
       %dotz1 = (z1-z1p)/dt;
       Ff1 = sigma0*z1+sigma1*Vt1;
       z1p = z1
       Ff1x = 0;
       Ff1y = Ff1;
   end

   % caculate the Ff

else Rj1<R;
     xn1 = R-Rj1; % Distance between the node and centerline of tube;
     Vn1 = v1*cos(phi1); % Velocity of catheter in normal direction;
     Vt1 = v1*sin(phi1);
     beta1 = (xn1-a)/(b-a);
     if xn1>b;
        Fn1 = Kv*(b-a)*(beta1-1/2)+Cv*Vn1;
     else if a<=xn1&xn1<=b;
             Fn1 = (Kv/2)*(b-a)*beta1^2+Cv*(3-2*beta1)*beta1^2*Vn1;
          else xn1<a;
               Fn1 = 0;
         end
     end
     Fn1x = -Fn1;
     Fn1y = 0;
   if Fn1 == 0;
       Ff1 = 0;
       Ff1x = 0;
       Ff1y = 0;
   else
       Fc1 = u*Fn1; % caculate the friction force.
       z1 = Vt1*(1-sigma0*sign(Vt1)*z1p/abs(Fc1))*dt+z1p
       %dotz1 = (z1-z1p)/dt;
```

```
          Ff1 = sigma0*z1+sigma1*Vt1;
          z1p = z1
          Ff1x = 0;
          Ff1y = Ff1;
      end

   end
end

F1x = Fn1x+Ff1x;
F1y = Fn1y+Ff1y;

%% Node 3
x3 = x(1,lnp(3,1)); % the x coordinate of the node 1;
y3 = x(1,lnp(3,2)); % the y coordinate of the node 1;
v3 = xp(1,lnp(3,1));
phi3 = x(1,lnp(4,1));

if y3>=0.05; % caculate the contact force Fn.
   Rj3 = sqrt((x3-Ox)^2+(y3-Oy)^2);
   alpha3 = asin((y3-0.05)/Rj3); % rad
   if Rj3>=R
      xn3 = Rj3-R; % Distance between the node and centerline of tube;
      Vn3 = v3*sin(phi3+alpha3-pi/2); % Velocity of catheter in normal
direction;
      Vt3 = v3*cos(phi3+alpha3-pi/2);
      beta3 = (xn3-a)/(b-a);
      contact=0;
      if xn3>b;
      contact=1;
      Fn3 = Kv*(b-a)*(beta3-1/2)+Cv*Vn3;
      else if a<=xn3&xn3<=b;
              contact=1;
              Fn3 = (Kv/2)*(b-a)*beta3^2+Cv*(3-2*beta3)*beta3^2*Vn3;
           else xn3<a;
                contact=0;
                Fn3 = 0;
          end
      end
      Fn3x = Fn3*cos(alpha3);
      Fn3y = -Fn3*sin(alpha3);
      % caculate the Ff
      if Fn3 == 0;
         Ff3 = 0;
         Ff3x = 0;
         Ff3y = 0;
      else
          Fc3 = u*Fn3; % caculate the friction force.
          z3 = Vt3*(1-sigma0*sign(Vt3)*z3p/abs(Fc3))*dt+z3p
          %dotz3 = (z3-z3p)/dt;
          Ff3 = sigma0*z3+sigma1*Vt3;
          z3p = z3
          Ff3x = -Ff3*sin(alpha3);
          Ff3y = -Ff3*cos(alpha3);
      end
   else Rj3<R
```

```
      xn3 = R-Rj3; % Distance between the node and centerline of tube;
      Vn3 = v3*sin(-phi3-alpha3+pi/2); % Velocity of catheter in normal
direction;
      Vt3 = v3*cos(-phi3-alpha3+pi/2);
      beta3 = (xn3-a)/(b-a);
      contact=0;
      if xn3>b;
      contact=1;
      Fn3 = Kv*(b-a)*(beta3-1/2)+Cv*Vn3;
      else if a<=xn3&xn3<=b;
              contact=1;
              Fn3 = (Kv/2)*(b-a)*beta3^2+Cv*(3-2*beta3)*beta3^2*Vn3;
           else xn3<a;
                contact=0;
                Fn3 = 0;
          end
      end
      Fn3x = -Fn3*cos(alpha3);
      Fn3y = Fn3*sin(alpha3);
      % caculate the Ff
      if Fn3 == 0;
         Ff3 = 0;
         Ff3x = 0;
         Ff3y = 0;
      else
          Fc3 = u*Fn3; % caculate the friction force.
          z3 = Vt3*(1-sigma0*sign(Vt3)*z3p/abs(Fc3))*dt+z3p
          %dotz3 = (z3-z3p)/dt;
          Ff3 = sigma0*z3+sigma1*Vt3;
          z3p = z3
          Ff3x = -Ff3*sin(alpha3);
          Ff3y = -Ff3*cos(alpha3);
      end
   end

else 0<=y3&y3<0.05; % the catheter's x-displacement should be restrained.
   Rj3 = sqrt((x3-Ox)^2);
   if Rj3>=R
      xn3 = Rj3-R; % Distance between the node and centerline of tube;
      Vn3 = v3*sin(phi3-pi/2); % Velocity of catheter in normal direction;
      Vt3 = v3*cos(phi3-pi/2);
      beta3 = (xn3-a)/(b-a);
      if xn3>b;
         Fn3 = Kv*(b-a)*(beta3-1/2)+Cv*Vn3;
      else if a<=xn3&xn3<=b;
              Fn3 = (Kv/2)*(b-a)*beta3^2+Cv*(3-2*beta3)*beta3^2*Vn3;
           else xn3<a;
                Fn3 = 0;
           end
      end
      Fn3x = Fn3;
      Fn3y = 0;

      if Fn3 == 0;
         Ff3 = 0;
         Ff3x = 0;
```

```
         Ff3y = 0;
      else
          Fc3 = u*Fn3; % caculate the friction force.
          z3 = Vt3*(1-sigma0*sign(Vt3)*z3p/abs(Fc3))*dt+z3p
          %dotz3 = (z3-z3p)/dt;
          Ff3 = sigma0*z3+sigma1*Vt3;
          z3p = z3
          Ff3x = 0;
          Ff3y = Ff3;
      end

      % caculate the Ff

   else Rj3<R;
        xn3 = R-Rj3; % Distance between the node and centerline of tube;
        Vn3 = v3*cos(phi3); % Velocity of catheter in normal direction;
        Vt3 = v3*sin(phi3);
        beta3 = (xn3-a)/(b-a);
        if xn3>b;
           Fn3 = Kv*(b-a)*(beta3-1/2)+Cv*Vn3;
        else if a<=xn3&xn3<=b;
                Fn3 = (Kv/2)*(b-a)*beta3^2+Cv*(3-2*beta3)*beta3^2*Vn3;
             else xn3<a;
                  Fn3 = 0;
            end
        end
        Fn3x = -Fn3;
        Fn3y = 0;
      if Fn3 == 0;
          Ff3 = 0;
          Ff3x = 0;
          Ff3y = 0;
      else
          Fc3 = u*Fn3; % caculate the friction force.
          z3 = Vt3*(1-sigma0*sign(Vt3)*z3p/abs(Fc3))*dt+z3p
          %dotz3 = (z3-z3p)/dt;
          Ff3 = sigma0*z3+sigma1*Vt3;
          z3p = z3
          Ff3x = 0;
          Ff3y = Ff3;
      end

   end
end

F3x = Fn3x+Ff3x;
F3y = Fn3y+Ff3y;

%% Node 5
x5 = x(1,lnp(5,1)); % the x coordinate of the node 1;
y5 = x(1,lnp(5,2)); % the y coordinate of the node 1;
v5 = xp(1,lnp(5,1));
phi5 = x(1,lnp(6,1));

if y5>=0.05; % caculate the contact force Fn.
   Rj5 = sqrt((x5-Ox)^2+(y5-Oy)^2);
```

```
   alpha5 = asin((y5-0.05)/Rj5); % rad
   if Rj5>=R
      xn5 = Rj5-R; % Distance between the node and centerline of tube;
      Vn5 = v5*sin(phi5+alpha5-pi/2); % Velocity of catheter in normal
direction;
      Vt5 = v5*cos(phi5+alpha5-pi/2);
      beta5 = (xn5-a)/(b-a);
      contact=0;
      if xn5>b;
      contact=1;
      Fn5 = Kv*(b-a)*(beta5-1/2)+Cv*Vn5;
      else if a<=xn5&xn5<=b;
              contact=1;
              Fn5 = (Kv/2)*(b-a)*beta5^2+Cv*(3-2*beta5)*beta5^2*Vn5;
           else xn5<a;
                contact=0;
                Fn5 = 0;
          end
      end
      Fn5x = Fn5*cos(alpha5);
      Fn5y = -Fn5*sin(alpha5);
      % caculate the Ff
      if Fn5 == 0;
         Ff5 = 0;
         Ff5x = 0;
         Ff5y = 0;
      else
          Fc5 = u*Fn5; % caculate the friction force.
          z5 = Vt5*(1-sigma0*sign(Vt5)*z5p/abs(Fc5))*dt+z5p
          %dotz5 = (z5-z5p)/dt;
          Ff5 = sigma0*z5+sigma1*Vt5;
          z5p = z5
          Ff5x = -Ff5*sin(alpha5);
          Ff5y = -Ff5*cos(alpha5);
      end
   else Rj5<R
      xn5 = R-Rj5; % Distance between the node and centerline of tube;
      Vn5 = v5*sin(-phi5-alpha5+pi/2); % Velocity of catheter in normal
direction;
      Vt5 = v5*cos(-phi5-alpha5+pi/2);
      beta5 = (xn5-a)/(b-a);
      contact=0;
      if xn5>b;
      contact=1;
      Fn5 = Kv*(b-a)*(beta5-1/2)+Cv*Vn5;
      else if a<=xn5&xn5<=b;
              contact=1;
              Fn5 = (Kv/2)*(b-a)*beta5^2+Cv*(3-2*beta5)*beta5^2*Vn5;
           else xn5<a;
                contact=0;
                Fn5 = 0;
          end
      end
      Fn5x = -Fn5*cos(alpha5);
      Fn5y = Fn5*sin(alpha5);
      % caculate the Ff
      if Fn5 == 0;
```

```
         Ff5 = 0;
         Ff5x = 0;
         Ff5y = 0;
      else
          Fc5 = u*Fn5; % caculate the friction force.
          z5 = Vt5*(1-sigma0*sign(Vt5)*z5p/abs(Fc5))*dt+z5p
          %dotz5 = (z5-z5p)/dt;
          Ff5 = sigma0*z5+sigma1*Vt5;
          z5p = z5
          Ff5x = -Ff5*sin(alpha5);
          Ff5y = -Ff5*cos(alpha5);
      end
   end

else 0<=y5&y5<0.05; % the catheter's x-displacement should be restrained.
   Rj5 = sqrt((x5-Ox)^2);
   if Rj5>=R
      xn5 = Rj5-R; % Distance between the node and centerline of tube;
      Vn5 = v5*sin(phi5-pi/2); % Velocity of catheter in normal direction;
      Vt5 = v5*cos(phi5-pi/2);
      beta5 = (xn5-a)/(b-a);
      if xn5>b;
         Fn5 = Kv*(b-a)*(beta5-1/2)+Cv*Vn5;
      else if a<=xn5&xn5<=b;
              Fn5 = (Kv/2)*(b-a)*beta5^2+Cv*(3-2*beta5)*beta5^2*Vn5;
           else xn5<a;
                Fn5 = 0;
           end
      end
      Fn5x = Fn5;
      Fn5y = 0;

      if Fn5 == 0;
         Ff5 = 0;
         Ff5x = 0;
         Ff5y = 0;
      else
          Fc5 = u*Fn5; % caculate the friction force.
          z5 = Vt5*(1-sigma0*sign(Vt5)*z5p/abs(Fc5))*dt+z5p
          %dotz5 = (z5-z5p)/dt;
          Ff5 = sigma0*z5+sigma1*Vt5;
          z5p = z5
          Ff5x = 0;
          Ff5y = Ff5;
      end

      % caculate the Ff

   else Rj5<R;
        xn5 = R-Rj5; % Distance between the node and centerline of tube;
        Vn5 = v5*cos(phi5); % Velocity of catheter in normal direction;
        Vt5 = v5*sin(phi5);
        beta5 = (xn5-a)/(b-a);
        if xn5>b;
           Fn5 = Kv*(b-a)*(beta5-1/2)+Cv*Vn5;
        else if a<=xn5&xn5<=b;
```

```
                Fn5 = (Kv/2)*(b-a)*beta5^2+Cv*(3-2*beta5)*beta5^2*Vn5;
             else xn5<a;
                  Fn5 = 0;
            end
        end
        Fn5x = -Fn5;
        Fn5y = 0;
      if Fn5 == 0;
          Ff5 = 0;
          Ff5x = 0;
          Ff5y = 0;
      else
          Fc5 = u*Fn5; % caculate the friction force.
          z5 = Vt5*(1-sigma0*sign(Vt5)*z5p/abs(Fc5))*dt+z5p
          %dotz5 = (z5-z5p)/dt;
          Ff5 = sigma0*z5+sigma1*Vt5;
          z5p = z5
          Ff5x = 0;
          Ff5y = Ff5;
      end

   end
end

F5x = Fn5x+Ff5x;
F5y = Fn5y+Ff5y;

%% Node 7
x7 = x(1,lnp(7,1)); % the x coordinate of the node 1;
y7 = x(1,lnp(7,2)); % the y coordinate of the node 1;
v7 = xp(1,lnp(7,1));
phi7 = x(1,lnp(8,1));

if y7>=0.05; % caculate the contact force Fn.
   Rj7 = sqrt((x7-Ox)^2+(y7-Oy)^2);
   alpha7 = asin((y7-0.05)/Rj7); % rad
   if Rj7>=R
      xn7 = Rj7-R; % Distance between the node and centerline of tube;
      Vn7 = v7*sin(phi7+alpha7-pi/2); % Velocity of catheter in normal
direction;
      Vt7 = v7*cos(phi7+alpha7-pi/2);
      beta7 = (xn7-a)/(b-a);
      contact=0;
      if xn7>b;
      contact=1;
      Fn7 = Kv*(b-a)*(beta7-1/2)+Cv*Vn7;
      else if a<=xn7&xn7<=b;
              contact=1;
              Fn7 = (Kv/2)*(b-a)*beta7^2+Cv*(3-2*beta7)*beta7^2*Vn7;
           else xn7<a;
                contact=0;
                Fn7 = 0;
          end
      end
      Fn7x = Fn7*cos(alpha7);
      Fn7y = -Fn7*sin(alpha7);
```

```
      % caculate the Ff
      if Fn7 == 0;
         Ff7 = 0;
         Ff7x = 0;
         Ff7y = 0;
      else
          Fc7 = u*Fn7; % caculate the friction force.
          z7 = Vt7*(1-sigma0*sign(Vt7)*z7p/abs(Fc7))*dt+z7p
          %dotz7 = (z7-z7p)/dt;
          Ff7 = sigma0*z7+sigma1*Vt7;
          z7p = z7
          Ff7x = -Ff7*sin(alpha7);
          Ff7y = -Ff7*cos(alpha7);
      end
   else Rj7<R
      xn7 = R-Rj7; % Distance between the node and centerline of tube;
      Vn7 = v7*sin(-phi7-alpha7+pi/2); % Velocity of catheter in normal
direction;
      Vt7 = v7*cos(-phi7-alpha7+pi/2);
      beta7 = (xn7-a)/(b-a);
      contact=0;
      if xn7>b;
      contact=1;
      Fn7 = Kv*(b-a)*(beta7-1/2)+Cv*Vn7;
      else if a<=xn7&xn7<=b;
              contact=1;
              Fn7 = (Kv/2)*(b-a)*beta7^2+Cv*(3-2*beta7)*beta7^2*Vn7;
           else xn7<a;
                contact=0;
                Fn7 = 0;
          end
      end
      Fn7x = -Fn7*cos(alpha7);
      Fn7y = Fn7*sin(alpha7);
      % caculate the Ff
      if Fn7 == 0;
         Ff7 = 0;
         Ff7x = 0;
         Ff7y = 0;
      else
          Fc7 = u*Fn7; % caculate the friction force.
          z7 = Vt7*(1-sigma0*sign(Vt7)*z7p/abs(Fc7))*dt+z7p
          %dotz7 = (z7-z7p)/dt;
          Ff7 = sigma0*z7+sigma1*Vt7;
          z7p = z7
          Ff7x = -Ff7*sin(alpha7);
          Ff7y = -Ff7*cos(alpha7);
      end
   end

else 0<=y7&y7<0.05; % the catheter's x-displacement should be restrained.
   Rj7 = sqrt((x7-Ox)^2);
   if Rj7>=R
      xn7 = Rj7-R; % Distance between the node and centerline of tube;
      Vn7 = v7*sin(phi7-pi/2); % Velocity of catheter in normal direction;
      Vt7 = v7*cos(phi7-pi/2);
      beta7 = (xn7-a)/(b-a);
```

```
   if xn7>b;
      Fn7 = Kv*(b-a)*(beta7-1/2)+Cv*Vn7;
   else if a<=xn7&xn7<=b;
           Fn7 = (Kv/2)*(b-a)*beta7^2+Cv*(3-2*beta7)*beta7^2*Vn7;
        else xn7<a;
             Fn7 = 0;
        end
   end
   Fn7x = Fn7;
   Fn7y = 0;

   if Fn7 == 0;
      Ff7 = 0;
      Ff7x = 0;
      Ff7y = 0;
   else
       Fc7 = u*Fn7; % caculate the friction force.
       z7 = Vt7*(1-sigma0*sign(Vt7)*z7p/abs(Fc7))*dt+z7p
       %dotz7 = (z7-z7p)/dt;
       Ff7 = sigma0*z7+sigma1*Vt7;
       z7p = z7
       Ff7x = 0;
       Ff7y = Ff7;
   end

   % caculate the Ff

else Rj7<R;
     xn7 = R-Rj7; % Distance between the node and centerline of tube;
     Vn7 = v7*cos(phi7); % Velocity of catheter in normal direction;
     Vt7 = v7*sin(phi7);
     beta7 = (xn7-a)/(b-a);
     if xn7>b;
        Fn7 = Kv*(b-a)*(beta7-1/2)+Cv*Vn7;
     else if a<=xn7&xn7<=b;
              Fn7 = (Kv/2)*(b-a)*beta7^2+Cv*(3-2*beta7)*beta7^2*Vn7;
          else xn7<a;
               Fn7 = 0;
          end
     end
     Fn7x = -Fn7;
     Fn7y = 0;
   if Fn7 == 0;
       Ff7 = 0;
       Ff7x = 0;
       Ff7y = 0;
   else
       Fc7 = u*Fn7; % caculate the friction force.
       z7 = Vt7*(1-sigma0*sign(Vt7)*z7p/abs(Fc7))*dt+z7p
       %dotz7 = (z7-z7p)/dt;
       Ff7 = sigma0*z7+sigma1*Vt7;
       z7p = z7
       Ff7x = 0;
       Ff7y = Ff7;
   end
```

```
   end
end

F7x = Fn7x+Ff7x;
F7y = Fn7y+Ff7y;

%% Node 9
x9 = x(1,lnp(9,1)); % the x coordinate of the node 1;
y9 = x(1,lnp(9,2)); % the y coordinate of the node 1;
v9 = xp(1,lnp(9,1));
phi9 = x(1,lnp(10,1));

if y9>=0.05; % caculate the contact force Fn.
   Rj9 = sqrt((x9-Ox)^2+(y9-Oy)^2);
   alpha9 = asin((y9-0.05)/Rj9); % rad
   if Rj9>=R
      xn9 = Rj9-R; % Distance between the node and centerline of tube;
      Vn9 = v9*sin(phi9+alpha9-pi/2); % Velocity of catheter in normal
direction;
      Vt9 = v9*cos(phi9+alpha9-pi/2);
      beta9 = (xn9-a)/(b-a);
      contact=0;
      if xn9>b;
      contact=1;
      Fn9 = Kv*(b-a)*(beta9-1/2)+Cv*Vn9;
      else if a<=xn9&xn9<=b;
              contact=1;
              Fn9 = (Kv/2)*(b-a)*beta9^2+Cv*(3-2*beta9)*beta9^2*Vn9;
           else xn9<a;
                contact=0;
                Fn9 = 0;
          end
      end
      Fn9x = Fn9*cos(alpha9);
      Fn9y = -Fn9*sin(alpha9);
      % caculate the Ff
      if Fn9 == 0;
         Ff9 = 0;
         Ff9x = 0;
         Ff9y = 0;
      else
          Fc9 = u*Fn9; % caculate the friction force.
          z9 = Vt9*(1-sigma0*sign(Vt9)*z9p/abs(Fc9))*dt+z9p
          %dotz9 = (z9-z9p)/dt;
          Ff9 = sigma0*z9+sigma1*Vt9;
          z9p = z9
          Ff9x = -Ff9*sin(alpha9);
          Ff9y = -Ff9*cos(alpha9);
      end
   else Rj9<R
      xn9 = R-Rj9; % Distance between the node and centerline of tube;
      Vn9 = v9*sin(-phi9-alpha9+pi/2); % Velocity of catheter in normal
direction;
      Vt9 = v9*cos(-phi9-alpha9+pi/2);
      beta9 = (xn9-a)/(b-a);
      contact=0;
```

```
      if xn9>b;
      contact=1;
      Fn9 = Kv*(b-a)*(beta9-1/2)+Cv*Vn9;
      else if a<=xn9&xn9<=b;
              contact=1;
              Fn9 = (Kv/2)*(b-a)*beta9^2+Cv*(3-2*beta9)*beta9^2*Vn9;
           else xn9<a;
                contact=0;
                Fn9 = 0;
          end
      end
      Fn9x = -Fn9*cos(alpha9);
      Fn9y = Fn9*sin(alpha9);
      % caculate the Ff
      if Fn9 == 0;
         Ff9 = 0;
         Ff9x = 0;
         Ff9y = 0;
      else
          Fc9 = u*Fn9; % caculate the friction force.
          z9 = Vt9*(1-sigma0*sign(Vt9)*z9p/abs(Fc9))*dt+z9p;
          %dotz9 = (z9-z9p)/dt;
          Ff9 = sigma0*z9+sigma1*Vt9;
          z9p = z9
          Ff9x = -Ff9*sin(alpha9);
          Ff9y = -Ff9*cos(alpha9);
      end
   end

else 0<=y9&y9<0.05; % the catheter's x-displacement should be restrained.
   Rj9 = sqrt((x9-Ox)^2);
   if Rj9>=R
      xn9 = Rj9-R; % Distance between the node and centerline of tube;
      Vn9 = v9*sin(phi9-pi/2); % Velocity of catheter in normal direction;
      Vt9 = v9*cos(phi9-pi/2);
      beta9 = (xn9-a)/(b-a);
      if xn9>b;
         Fn9 = Kv*(b-a)*(beta9-1/2)+Cv*Vn9;
      else if a<=xn9&xn9<=b;
              Fn9 = (Kv/2)*(b-a)*beta9^2+Cv*(3-2*beta9)*beta9^2*Vn9;
           else xn9<a;
                Fn9 = 0;
           end
      end
      Fn9x = Fn9;
      Fn9y = 0;

      if Fn9 == 0;
         Ff9 = 0;
         Ff9x = 0;
         Ff9y = 0;
      else
          Fc9 = u*Fn9; % caculate the friction force.
          z9 = Vt9*(1-sigma0*sign(Vt9)*z9p/abs(Fc9))*dt+z9p;
          %dotz9 = (z9-z9p)/dt;
          Ff9 = sigma0*z9+sigma1*Vt9;
```

```
          z9p = z9
          Ff9x = 0;
          Ff9y = Ff9;
      end

      % caculate the Ff

   else Rj9<R;
        xn9 = R-Rj9; % Distance between the node and centerline of tube;
        Vn9 = v9*cos(phi9); % Velocity of catheter in normal direction;
        Vt9 = v9*sin(phi9);
        beta9 = (xn9-a)/(b-a);
        if xn9>b;
           Fn9 = Kv*(b-a)*(beta9-1/2)+Cv*Vn9;
        else if a<=xn9&xn9<=b;
                Fn9 = (Kv/2)*(b-a)*beta9^2+Cv*(3-2*beta9)*beta9^2*Vn9;
             else xn9<a;
                  Fn9 = 0;
            end
        end
        Fn9x = -Fn9;
        Fn9y = 0;
      if Fn9 == 0;
          Ff9 = 0;
          Ff9x = 0;
          Ff9y = 0;
      else
          Fc9 = u*Fn9; % caculate the friction force.
          z9 = Vt9*(1-sigma0*sign(Vt9)*z9p/abs(Fc9))*dt+z9p;
          %dotz9 = (z9-z9p)/dt;
          Ff9 = sigma0*z9+sigma1*Vt9;
          z9p = z9
          Ff9x = 0;
          Ff9y = Ff9;
      end

   end
end

F9x = Fn9x+Ff9x;
F9y = Fn9y+Ff9y;

%% Node 11
x11 = x(1,lnp(11,1)); % the x coordinate of the node 1;
y11 = x(1,lnp(11,2)); % the y coordinate of the node 1;
v11 = xp(1,lnp(11,1));
phi11 = x(1,lnp(12,1));

if y11>=0.05; % caculate the contact force Fn.
   Rj11 = sqrt((x11-Ox)^2+(y11-Oy)^2);
   alpha11 = asin((y11-0.05)/Rj11); % rad
   if Rj11>=R
      xn11 = Rj11-R; % Distance between the node and centerline of tube;
      Vn11 = v11*sin(phi11+alpha11-pi/2); % Velocity of catheter in normal
direction;
      Vt11 = v11*cos(phi11+alpha11-pi/2);
```

```
      beta11 = (xn11-a)/(b-a);
      contact=0;
      if xn11>b;
      contact=1;
      Fn11 = Kv*(b-a)*(beta11-1/2)+Cv*Vn11;
      else if a<=xn11&xn11<=b;
              contact=1;
              Fn11 = (Kv/2)*(b-a)*beta11^2+Cv*(3-2*beta11)*beta11^2*Vn11;
           else xn11<a;
                contact=0;
                Fn11 = 0;
          end
      end
      Fn11x = Fn11*cos(alpha11);
      Fn11y = -Fn11*sin(alpha11);
      % caculate the Ff
      if Fn11 == 0;
         Ff11 = 0;
         Ff11x = 0;
         Ff11y = 0;
      else
          Fc11 = u*Fn11; % caculate the friction force.
          z11 = Vt11*(1-sigma0*sign(Vt11)*z11p/abs(Fc11))*dt+z11p;
          %dotz11 = (z11-z11p)/dt;
          Ff11 = sigma0*z11+sigma1*Vt11;
          z11p = z11
          Ff11x = -Ff11*sin(alpha11);
          Ff11y = -Ff11*cos(alpha11);
      end
   else Rj11<R
      xn11 = R-Rj11; % Distance between the node and centerline of tube;
      Vn11 = v11*sin(-phi11-alpha11+pi/2); % Velocity of catheter in normal
direction;
      Vt11 = v11*cos(-phi11-alpha11+pi/2);
      beta11 = (xn11-a)/(b-a);
      contact=0;
      if xn11>b;
      contact=1;
      Fn11 = Kv*(b-a)*(beta11-1/2)+Cv*Vn11;
      else if a<=xn11&xn11<=b;
              contact=1;
              Fn11 = (Kv/2)*(b-a)*beta11^2+Cv*(3-2*beta11)*beta11^2*Vn11;
           else xn11<a;
                contact=0;
                Fn11 = 0;
          end
      end
      Fn11x = -Fn11*cos(alpha11);
      Fn11y = Fn11*sin(alpha11);
      % caculate the Ff
      if Fn11 == 0;
         Ff11 = 0;
         Ff11x = 0;
         Ff11y = 0;
      else
          Fc11 = u*Fn11; % caculate the friction force.
          z11 = Vt11*(1-sigma0*sign(Vt11)*z11p/abs(Fc11))*dt+z11p;
```

```
            %dotz11 = (z11-z11p)/dt;
            Ff11 = sigma0*z11+sigma1*Vt11;
            z11p = z11
            Ff11x = -Ff11*sin(alpha11);
            Ff11y = -Ff11*cos(alpha11);
         end
      end

else 0<=y11&y11<0.05; % the catheter's x-displacement should be restrained.
      Rj11 = sqrt((x11-Ox)^2);
      if Rj11>=R
         xn11 = Rj11-R; % Distance between the node and centerline of tube;
         Vn11 = v11*sin(phi11-pi/2); % Velocity of catheter in normal direction;
         Vt11 = v11*cos(phi11-pi/2);
         beta11 = (xn11-a)/(b-a);
         if xn11>b;
            Fn11 = Kv*(b-a)*(beta11-1/2)+Cv*Vn11;
         else if a<=xn11&xn11<=b;
                 Fn11 = (Kv/2)*(b-a)*beta11^2+Cv*(3-2*beta11)*beta11^2*Vn11;
              else xn11<a;
                   Fn11 = 0;
              end
         end
         Fn11x = Fn11;
         Fn11y = 0;

         if Fn11 == 0;
            Ff11 = 0;
            Ff11x = 0;
            Ff11y = 0;
         else
             Fc11 = u*Fn11; % caculate the friction force.
             z11 = Vt11*(1-sigma0*sign(Vt11)*z11p/abs(Fc11))*dt+z11p;
             %dotz11 = (z11-z11p)/dt;
             Ff11 = sigma0*z11+sigma1*Vt11;
             z11p = z11
             Ff11x = 0;
             Ff11y = Ff11;
         end

         % caculate the Ff

      else Rj11<R;
           xn11 = R-Rj11; % Distance between the node and centerline of tube;
           Vn11 = v11*cos(phi11); % Velocity of catheter in normal direction;
           Vt11 = v11*sin(phi11);
           beta11 = (xn11-a)/(b-a);
           if xn11>b;
              Fn11 = Kv*(b-a)*(beta11-1/2)+Cv*Vn11;
           else if a<=xn11&xn11<=b;
                   Fn11 = (Kv/2)*(b-a)*beta11^2+Cv*(3-2*beta11)*beta11^2*Vn11;
                else xn11<a;
                     Fn11 = 0;
                end
           end
           Fn11x = -Fn11;
```

```
        Fn11y = 0;
      if Fn11 == 0;
          Ff11 = 0;
          Ff11x = 0;
          Ff11y = 0;
      else
          Fc11 = u*Fn11; % caculate the friction force.
          z11 = Vt11*(1-sigma0*sign(Vt11)*z11p/abs(Fc11))*dt+z11p;
          %dotz11 = (z11-z11p)/dt;
          Ff11 = sigma0*z11+sigma1*Vt11;
          z11p = z11
          Ff11x = 0;
          Ff11y = Ff11;
      end

   end
end

F11x = Fn11x+Ff11x;
F11y = Fn11y+Ff11y;

%% Node 13
x13 = x(1,lnp(13,1)); % the x coordinate of the node 1;
y13 = x(1,lnp(13,2)); % the y coordinate of the node 1;
v13 = xp(1,lnp(13,1));
phi13 = x(1,lnp(14,1));

if y13>=0.05; % caculate the contact force Fn.
   Rj13 = sqrt((x13-Ox)^2+(y13-Oy)^2);
   alpha13 = asin((y13-0.05)/Rj13); % rad
   if Rj13>=R
      xn13 = Rj13-R; % Distance between the node and centerline of tube;
      Vn13 = v13*sin(phi13+alpha13-pi/2); % Velocity of catheter in normal
direction;
      Vt13 = v13*cos(phi13+alpha13-pi/2);
      beta13 = (xn13-a)/(b-a);
      contact=0;
      if xn13>b;
      contact=1;
      Fn13 = Kv*(b-a)*(beta13-1/2)+Cv*Vn13;
      else if a<=xn13&xn13<=b;
              contact=1;
              Fn13 = (Kv/2)*(b-a)*beta13^2+Cv*(3-2*beta13)*beta13^2*Vn13;
           else xn13<a;
                contact=0;
                Fn13 = 0;
          end
      end
      Fn13x = Fn13*cos(alpha13);
      Fn13y = -Fn13*sin(alpha13);
      % caculate the Ff
      if Fn13 == 0;
         Ff13 = 0;
         Ff13x = 0;
         Ff13y = 0;
      else
```

```
          Fc13 = u*Fn13; % caculate the friction force.
          z13 = Vt13*(1-sigma0*sign(Vt13)*z13p/abs(Fc13))*dt+z13p;
          %dotz13 = (z13-z13p)/dt;
          Ff13 = sigma0*z13+sigma1*Vt13;
          z13p = z13
          Ff13x = -Ff13*sin(alpha13);
          Ff13y = -Ff13*cos(alpha13);
      end
   else Rj13<R
      xn13 = R-Rj13; % Distance between the node and centerline of tube;
      Vn13 = v13*sin(-phi13-alpha13+pi/2); % Velocity of catheter in normal
direction;
      Vt13 = v13*cos(-phi13-alpha13+pi/2);
      beta13 = (xn13-a)/(b-a);
      contact=0;
      if xn13>b;
      contact=1;
      Fn13 = Kv*(b-a)*(beta13-1/2)+Cv*Vn13;
      else if a<=xn13&xn13<=b;
              contact=1;
              Fn13 = (Kv/2)*(b-a)*beta13^2+Cv*(3-2*beta13)*beta13^2*Vn13;
           else xn13<a;
                contact=0;
                Fn13 = 0;
          end
      end
      Fn13x = -Fn13*cos(alpha13);
      Fn13y = Fn13*sin(alpha13);
      % caculate the Ff
      if Fn13 == 0;
         Ff13 = 0;
         Ff13x = 0;
         Ff13y = 0;
      else
          Fc13 = u*Fn13; % caculate the friction force.
          z13 = Vt13*(1-sigma0*sign(Vt13)*z13p/abs(Fc13))*dt+z13p;
          %dotz13 = (z13-z13p)/dt;
          Ff13 = sigma0*z13+sigma1*Vt13;
          z13p = z13
          Ff13x = -Ff13*sin(alpha13);
          Ff13y = -Ff13*cos(alpha13);
      end
   end

else 0<=y13&y13<0.05; % the catheter's x-displacement should be restrained.
   Rj13 = sqrt((x13-Ox)^2);
   if Rj13>=R
      xn13 = Rj13-R; % Distance between the node and centerline of tube;
      Vn13 = v13*sin(phi13-pi/2); % Velocity of catheter in normal direction;
      Vt13 = v13*cos(phi13-pi/2);
      beta13 = (xn13-a)/(b-a);
      if xn13>b;
         Fn13 = Kv*(b-a)*(beta13-1/2)+Cv*Vn13;
      else if a<=xn13&xn13<=b;
              Fn13 = (Kv/2)*(b-a)*beta13^2+Cv*(3-2*beta13)*beta13^2*Vn13;
           else xn13<a;
                Fn13 = 0;
```

```
          end
      end
      Fn13x = Fn13;
      Fn13y = 0;

      if Fn13 == 0;
         Ff13 = 0;
         Ff13x = 0;
         Ff13y = 0;
      else
          Fc13 = u*Fn13; % caculate the friction force.
          z13 = Vt13*(1-sigma0*sign(Vt13)*z13p/abs(Fc13))*dt+z13p;
          %dotz13 = (z13-z13p)/dt;
          Ff13 = sigma0*z13+sigma1*Vt13;
          z13p = z13
          Ff13x = 0;
          Ff13y = Ff13;
      end

      % caculate the Ff

   else Rj13<R;
        xn13 = R-Rj13; % Distance between the node and centerline of tube;
        Vn13 = v13*cos(phi13); % Velocity of catheter in normal direction;
        Vt13 = v13*sin(phi13);
        beta13 = (xn13-a)/(b-a);
        if xn13>b;
           Fn13 = Kv*(b-a)*(beta13-1/2)+Cv*Vn13;
        else if a<=xn13&xn13<=b;
                Fn13 = (Kv/2)*(b-a)*beta13^2+Cv*(3-2*beta13)*beta13^2*Vn13;
             else xn13<a;
                  Fn13 = 0;
            end
        end
        Fn13x = -Fn13;
        Fn13y = 0;
      if Fn13 == 0;
          Ff13 = 0;
          Ff13x = 0;
          Ff13y = 0;
      else
          Fc13 = u*Fn13; % caculate the friction force.
          z13 = Vt13*(1-sigma0*sign(Vt13)*z13p/abs(Fc13))*dt+z13p;
          %dotz13 = (z13-z13p)/dt;
          Ff13 = sigma0*z13+sigma1*Vt13;
          z13p = z13
          Ff13x = 0;
          Ff13y = Ff13;
      end

   end
end

F13x = Fn13x+Ff13x;
F13y = Fn13y+Ff13y;
```

```
%% Node 15
x15 = x(1,lnp(15,1)); % the x coordinate of the node 1;
y15 = x(1,lnp(15,2)); % the y coordinate of the node 1;
v15 = xp(1,lnp(15,1));
phi15 = x(1,lnp(16,1));

if y15>=0.05; % caculate the contact force Fn.
   Rj15 = sqrt((x15-Ox)^2+(y15-Oy)^2);
   alpha15 = asin((y15-0.05)/Rj15); % rad
   if Rj15>=R
      xn15 = Rj15-R; % Distance between the node and centerline of tube;
      Vn15 = v15*sin(phi15+alpha15-pi/2); % Velocity of catheter in normal
direction;
      Vt15 = v15*cos(phi15+alpha15-pi/2);
      beta15 = (xn15-a)/(b-a);
      contact=0;
      if xn15>b;
      contact=1;
      Fn15 = Kv*(b-a)*(beta15-1/2)+Cv*Vn15;
      else if a<=xn15&xn15<=b;
              contact=1;
              Fn15 = (Kv/2)*(b-a)*beta15^2+Cv*(3-2*beta15)*beta15^2*Vn15;
           else xn15<a;
                contact=0;
                Fn15 = 0;
          end
      end
      Fn15x = Fn15*cos(alpha15);
      Fn15y = -Fn15*sin(alpha15);
      % caculate the Ff
      if Fn15 == 0;
         Ff15 = 0;
         Ff15x = 0;
         Ff15y = 0;
      else
          Fc15 = u*Fn15; % caculate the friction force.
          z15 = Vt15*(1-sigma0*sign(Vt15)*z15p/abs(Fc15))*dt+z15p;
          %dotz15 = (z15-z15p)/dt;
          Ff15 = sigma0*z15+sigma1*Vt15;
          z15p = z15
          Ff15x = -Ff15*sin(alpha15);
          Ff15y = -Ff15*cos(alpha15);
      end
   else Rj15<R
      xn15 = R-Rj15; % Distance between the node and centerline of tube;
      Vn15 = v15*sin(-phi15-alpha15+pi/2); % Velocity of catheter in normal
direction;
      Vt15 = v15*cos(-phi15-alpha15+pi/2);
      beta15 = (xn15-a)/(b-a);
      contact=0;
      if xn15>b;
      contact=1;
      Fn15 = Kv*(b-a)*(beta15-1/2)+Cv*Vn15;
      else if a<=xn15&xn15<=b;
              contact=1;
              Fn15 = (Kv/2)*(b-a)*beta15^2+Cv*(3-2*beta15)*beta15^2*Vn15;
           else xn15<a;
```

```
                contact=0;
                Fn15 = 0;
            end
        end
        Fn15x = -Fn15*cos(alpha15);
        Fn15y = Fn15*sin(alpha15);
        % caculate the Ff
        if Fn15 == 0;
           Ff15 = 0;
           Ff15x = 0;
           Ff15y = 0;
        else
            Fc15 = u*Fn15; % caculate the friction force.
            z15 = Vt15*(1-sigma0*sign(Vt15)*z15p/abs(Fc15))*dt+z15p;
            %dotz15 = (z15-z15p)/dt;
            Ff15 = sigma0*z15+sigma1*Vt15;
            z15p = z15
            Ff15x = -Ff15*sin(alpha15);
            Ff15y = -Ff15*cos(alpha15);
        end
    end

else 0<=y15&y15<0.05; % the catheter's x-displacement should be restrained.
    Rj15 = sqrt((x15-Ox)^2);
    if Rj15>=R
        xn15 = Rj15-R; % Distance between the node and centerline of tube;
        Vn15 = v15*sin(phi15-pi/2); % Velocity of catheter in normal direction;
        Vt15 = v15*cos(phi15-pi/2);
        beta15 = (xn15-a)/(b-a);
        if xn15>b;
           Fn15 = Kv*(b-a)*(beta15-1/2)+Cv*Vn15;
        else if a<=xn15&xn15<=b;
                Fn15 = (Kv/2)*(b-a)*beta15^2+Cv*(3-2*beta15)*beta15^2*Vn15;
             else xn15<a;
                  Fn15 = 0;
             end
        end
        Fn15x = Fn15;
        Fn15y = 0;

        if Fn15 == 0;
           Ff15 = 0;
           Ff15x = 0;
           Ff15y = 0;
        else
            Fc15 = u*Fn15; % caculate the friction force.
            z15 = Vt15*(1-sigma0*sign(Vt15)*z15p/abs(Fc15))*dt+z15p;
            %dotz15 = (z15-z15p)/dt;
            Ff15 = sigma0*z15+sigma1*Vt15;
            z15p = z15
            Ff15x = 0;
            Ff15y = Ff15;
        end

        % caculate the Ff
```

```
   else Rj15<R;
        xn15 = R-Rj15; % Distance between the node and centerline of tube;
        Vn15 = v15*cos(phi15); % Velocity of catheter in normal direction;
        Vt15 = v15*sin(phi15);
        beta15 = (xn15-a)/(b-a);
        if xn15>b;
           Fn15 = Kv*(b-a)*(beta15-1/2)+Cv*Vn15;
        else if a<=xn15&xn15<=b;
                Fn15 = (Kv/2)*(b-a)*beta15^2+Cv*(3-2*beta15)*beta15^2*Vn15;
             else xn15<a;
                  Fn15 = 0;
            end
        end
        Fn15x = -Fn15;
        Fn15y = 0;
      if Fn15 == 0;
          Ff15 = 0;
          Ff15x = 0;
          Ff15y = 0;
      else
          Fc15 = u*Fn15; % caculate the friction force.
          z15 = Vt15*(1-sigma0*sign(Vt15)*z15p/abs(Fc15))*dt+z15p;
          %dotz15 = (z15-z15p)/dt;
          Ff15 = sigma0*z15+sigma1*Vt15;
          z15p = z15
          Ff15x = 0;
          Ff15y = Ff15;
      end

   end
end

F15x = Fn15x+Ff15x;
F15y = Fn15y+Ff15y;

%% Node 17
x17 = x(1,lnp(17,1)); % the x coordinate of the node 1;
y17 = x(1,lnp(17,2)); % the y coordinate of the node 1;
v17 = xp(1,lnp(17,1));
phi17 = x(1,lnp(18,1));

if y17>=0.05; % caculate the contact force Fn.
   Rj17 = sqrt((x17-Ox)^2+(y17-Oy)^2);
   alpha17 = asin((y17-0.05)/Rj17); % rad
   if Rj17>=R
      xn17 = Rj17-R; % Distance between the node and centerline of tube;
      Vn17 = v17*sin(phi17+alpha17-pi/2); % Velocity of catheter in normal
direction;
      Vt17 = v17*cos(phi17+alpha17-pi/2);
      beta17 = (xn17-a)/(b-a);
      contact=0;
      if xn17>b;
      contact=1;
      Fn17 = Kv*(b-a)*(beta17-1/2)+Cv*Vn17;
      else if a<=xn17&xn17<=b;
              contact=1;
```

```
            Fn17 = (Kv/2)*(b-a)*beta17^2+Cv*(3-2*beta17)*beta17^2*Vn17;
         else xn17<a;
              contact=0;
              Fn17 = 0;
        end
     end
     Fn17x = Fn17*cos(alpha17);
     Fn17y = -Fn17*sin(alpha17);
     % caculate the Ff
     if Fn17 == 0;
        Ff17 = 0;
        Ff17x = 0;
        Ff17y = 0;
     else
         Fc17 = u*Fn17; % caculate the friction force.
         z17 = Vt17*(1-sigma0*sign(Vt17)*z17p/abs(Fc17))*dt+z17p;
         %dotz17 = (z17-z17p)/dt;
         Ff17 = sigma0*z17+sigma1*Vt17;
         z17p = z17
         Ff17x = -Ff17*sin(alpha17);
         Ff17y = -Ff17*cos(alpha17);
     end
  else Rj17<R
     xn17 = R-Rj17; % Distance between the node and centerline of tube;
     Vn17 = v17*sin(-phi17-alpha17+pi/2); % Velocity of catheter in normal
direction;
     Vt17 = v17*cos(-phi17-alpha17+pi/2);
     beta17 = (xn17-a)/(b-a);
     contact=0;
     if xn17>b;
     contact=1;
     Fn17 = Kv*(b-a)*(beta17-1/2)+Cv*Vn17;
     else if a<=xn17&xn17<=b;
             contact=1;
             Fn17 = (Kv/2)*(b-a)*beta17^2+Cv*(3-2*beta17)*beta17^2*Vn17;
          else xn17<a;
              contact=0;
              Fn17 = 0;
         end
     end
     Fn17x = -Fn17*cos(alpha17);
     Fn17y = Fn17*sin(alpha17);
     % caculate the Ff
     if Fn17 == 0;
        Ff17 = 0;
        Ff17x = 0;
        Ff17y = 0;
     else
         Fc17 = u*Fn17; % caculate the friction force.
         z17 = Vt17*(1-sigma0*sign(Vt17)*z17p/abs(Fc17))*dt+z17p;
         %dotz17 = (z17-z17p)/dt;
         Ff17 = sigma0*z17+sigma1*Vt17;
         z17p = z17
         Ff17x = -Ff17*sin(alpha17);
         Ff17y = -Ff17*cos(alpha17);
     end
  end
```

```
else 0<=y17&y17<0.05; % the catheter's x-displacement should be restrained.
   Rj17 = sqrt((x17-Ox)^2);
   if Rj17>=R
      xn17 = Rj17-R; % Distance between the node and centerline of tube;
      Vn17 = v17*sin(phi17-pi/2); % Velocity of catheter in normal direction;
      Vt17 = v17*cos(phi17-pi/2);
      beta17 = (xn17-a)/(b-a);
      if xn17>b;
         Fn17 = Kv*(b-a)*(beta17-1/2)+Cv*Vn17;
      else if a<=xn17&xn17<=b;
              Fn17 = (Kv/2)*(b-a)*beta17^2+Cv*(3-2*beta17)*beta17^2*Vn17;
           else xn17<a;
                Fn17 = 0;
           end
      end
      Fn17x = Fn17;
      Fn17y = 0;

      if Fn17 == 0;
         Ff17 = 0;
         Ff17x = 0;
         Ff17y = 0;
      else
          Fc17 = u*Fn17; % caculate the friction force.
          z17 = Vt17*(1-sigma0*sign(Vt17)*z17p/abs(Fc17))*dt+z17p;
          %dotz17 = (z17-z17p)/dt;
          Ff17 = sigma0*z17+sigma1*Vt17;
          z17p = z17
          Ff17x = 0;
          Ff17y = Ff17;
      end

      % caculate the Ff

   else Rj17<R;
        xn17 = R-Rj17; % Distance between the node and centerline of tube;
        Vn17 = v17*cos(phi17); % Velocity of catheter in normal direction;
        Vt17 = v17*sin(phi17);
        beta17 = (xn17-a)/(b-a);
        if xn17>b;
           Fn17 = Kv*(b-a)*(beta17-1/2)+Cv*Vn17;
        else if a<=xn17&xn17<=b;
                Fn17 = (Kv/2)*(b-a)*beta17^2+Cv*(3-2*beta17)*beta17^2*Vn17;
             else xn17<a;
                  Fn17 = 0;
            end
        end
        Fn17x = -Fn17;
        Fn17y = 0;
      if Fn17 == 0;
          Ff17 = 0;
          Ff17x = 0;
          Ff17y = 0;
      else
          Fc17 = u*Fn17; % caculate the friction force.
```

```
          z17 = Vt17*(1-sigma0*sign(Vt17)*z17p/abs(Fc17))*dt+z17p;
          %dotz17 = (z17-z17p)/dt;
          Ff17 = sigma0*z17+sigma1*Vt17;
          z17p = z17
          Ff17x = 0;
          Ff17y = Ff17;
      end

   end
end

F17x = Fn17x+Ff17x;
F17y = Fn17y+Ff17y;

%% Node 19
x19 = x(1,lnp(19,1)); % the x coordinate of the node 1;
y19 = x(1,lnp(19,2)); % the y coordinate of the node 1;
v19 = xp(1,lnp(19,1));
phi19 = x(1,lnp(20,1));

if y19>=0.05; % caculate the contact force Fn.
   Rj19 = sqrt((x19-Ox)^2+(y19-Oy)^2);
   alpha19 = asin((y19-0.05)/Rj19); % rad
   if Rj19>=R
      xn19 = Rj19-R; % Distance between the node and centerline of tube;
      Vn19 = v19*sin(phi19+alpha19-pi/2); % Velocity of catheter in normal
direction;
      Vt19 = v19*cos(phi19+alpha19-pi/2);
      beta19 = (xn19-a)/(b-a);
      contact=0;
      if xn19>b;
      contact=1;
      Fn19 = Kv*(b-a)*(beta19-1/2)+Cv*Vn19;
      else if a<=xn19&xn19<=b;
              contact=1;
              Fn19 = (Kv/2)*(b-a)*beta19^2+Cv*(3-2*beta19)*beta19^2*Vn19;
           else xn19<a;
                contact=0;
                Fn19 = 0;
          end
      end
      Fn19x = Fn19*cos(alpha19);
      Fn19y = -Fn19*sin(alpha19);
      % caculate the Ff
      if Fn19 == 0;
         Ff19 = 0;
         Ff19x = 0;
         Ff19y = 0;
      else
          Fc19 = u*Fn19; % caculate the friction force.
          z19 = Vt19*(1-sigma0*sign(Vt19)*z19p/abs(Fc19))*dt+z19p;
          %dotz19 = (z19-z19p)/dt;
          Ff19 = sigma0*z19+sigma1*Vt19;
          z19p = z19
          Ff19x = -Ff19*sin(alpha19);
          Ff19y = -Ff19*cos(alpha19);
```

```
      end
   else Rj19<R
      xn19 = R-Rj19; % Distance between the node and centerline of tube;
      Vn19 = v19*sin(-phi19-alpha19+pi/2); % Velocity of catheter in normal
direction;
      Vt19 = v19*cos(-phi19-alpha19+pi/2);
      beta19 = (xn19-a)/(b-a);
      contact=0;
      if xn19>b;
      contact=1;
      Fn19 = Kv*(b-a)*(beta19-1/2)+Cv*Vn19;
      else if a<=xn19&xn19<=b;
             contact=1;
             Fn19 = (Kv/2)*(b-a)*beta19^2+Cv*(3-2*beta19)*beta19^2*Vn19;
           else xn19<a;
                contact=0;
                Fn19 = 0;
          end
      end
      Fn19x = -Fn19*cos(alpha19);
      Fn19y = Fn19*sin(alpha19);
      % caculate the Ff
      if Fn19 == 0;
         Ff19 = 0;
         Ff19x = 0;
         Ff19y = 0;
      else
          Fc19 = u*Fn19; % caculate the friction force.
          z19 = Vt19*(1-sigma0*sign(Vt19)*z19p/abs(Fc19))*dt+z19p;
          %dotz19 = (z19-z19p)/dt;
          Ff19 = sigma0*z19+sigma1*Vt19;
          z19p = z19
          Ff19x = -Ff19*sin(alpha19);
          Ff19y = -Ff19*cos(alpha19);
      end
   end

else 0<=y19&y19<0.05; % the catheter's x-displacement should be restrained.
   Rj19 = sqrt((x19-Ox)^2);
   if Rj19>=R
      xn19 = Rj19-R; % Distance between the node and centerline of tube;
      Vn19 = v19*sin(phi19-pi/2); % Velocity of catheter in normal direction;
      Vt19 = v19*cos(phi19-pi/2);
      beta19 = (xn19-a)/(b-a);
      if xn19>b;
         Fn19 = Kv*(b-a)*(beta19-1/2)+Cv*Vn19;
      else if a<=xn19&xn19<=b;
             Fn19 = (Kv/2)*(b-a)*beta19^2+Cv*(3-2*beta19)*beta19^2*Vn19;
           else xn19<a;
                Fn19 = 0;
           end
      end
      Fn19x = Fn19;
      Fn19y = 0;

      if Fn19 == 0;
```

```
         Ff19 = 0;
         Ff19x = 0;
         Ff19y = 0;
      else
          Fc19 = u*Fn19; % caculate the friction force.
          z19 = Vt19*(1-sigma0*sign(Vt19)*z19p/abs(Fc19))*dt+z19p;
          %dotz19 = (z19-z19p)/dt;
          Ff19 = sigma0*z19+sigma1*Vt19;
          z19p = z19
          Ff19x = 0;
          Ff19y = Ff19;
      end

      % caculate the Ff

   else Rj19<R;
        xn19 = R-Rj19; % Distance between the node and centerline of tube;
        Vn19 = v19*cos(phi19); % Velocity of catheter in normal direction;
        Vt19 = v19*sin(phi19);
        beta19 = (xn19-a)/(b-a);
        if xn19>b;
           Fn19 = Kv*(b-a)*(beta19-1/2)+Cv*Vn19;
        else if a<=xn19&xn19<=b;
                Fn19 = (Kv/2)*(b-a)*beta19^2+Cv*(3-2*beta19)*beta19^2*Vn19;
             else xn19<a;
                  Fn19 = 0;
            end
        end
        Fn19x = -Fn19;
        Fn19y = 0;
      if Fn19 == 0;
          Ff19 = 0;
          Ff19x = 0;
          Ff19y = 0;
      else
          Fc19 = u*Fn19; % caculate the friction force.
          z19 = Vt19*(1-sigma0*sign(Vt19)*z19p/abs(Fc19))*dt+z19p;
          %dotz19 = (z19-z19p)/dt;
          Ff19 = sigma0*z19+sigma1*Vt19;
          z19p = z19
          Ff19x = 0;
          Ff19y = Ff19;
      end

   end
end

F19x = Fn19x+Ff19x;
F19y = Fn19y+Ff19y;

%% Node 21
x21 = x(1,lnp(21,1)); % the x coordinate of the node 1;
y21 = x(1,lnp(21,2)); % the y coordinate of the node 1;
v21 = xp(1,lnp(21,1));
phi21 = x(1,lnp(22,1));
```

```
if y21>=0.05; % caculate the contact force Fn.
   Rj21 = sqrt((x21-Ox)^2+(y21-Oy)^2);
   alpha21 = asin((y21-0.05)/Rj21); % rad
   if Rj21>=R
      xn21 = Rj21-R; % Distance between the node and centerline of tube;
      Vn21 = v21*sin(phi21+alpha21-pi/2); % Velocity of catheter in normal
direction;
      Vt21 = v21*cos(phi21+alpha21-pi/2);
      beta21 = (xn21-a)/(b-a);
      contact=0;
      if xn21>b;
      contact=1;
      Fn21 = Kv*(b-a)*(beta21-1/2)+Cv*Vn21;
      else if a<=xn21&xn21<=b;
              contact=1;
              Fn21 = (Kv/2)*(b-a)*beta21^2+Cv*(3-2*beta21)*beta21^2*Vn21;
           else xn21<a;
                contact=0;
                Fn21 = 0;
          end
      end
      Fn21x = Fn21*cos(alpha21);
      Fn21y = -Fn21*sin(alpha21);
      % caculate the Ff
      if Fn21 == 0;
         Ff21 = 0;
         Ff21x = 0;
         Ff21y = 0;
      else
          Fc21 = u*Fn21; % caculate the friction force.
          z21 = Vt21*(1-sigma0*sign(Vt21)*z21p/abs(Fc21))*dt+z21p;
          %dotz21 = (z21-z21p)/dt;
          Ff21 = sigma0*z21+sigma1*Vt21;
          z21p = z21
          Ff21x = -Ff21*sin(alpha21);
          Ff21y = -Ff21*cos(alpha21);
      end
   else Rj21<R
      xn21 = R-Rj21; % Distance between the node and centerline of tube;
      Vn21 = v21*sin(-phi21-alpha21+pi/2); % Velocity of catheter in normal
direction;
      Vt21 = v21*cos(-phi21-alpha21+pi/2);
      beta21 = (xn21-a)/(b-a);
      contact=0;
      if xn21>b;
      contact=1;
      Fn21 = Kv*(b-a)*(beta21-1/2)+Cv*Vn21;
      else if a<=xn21&xn21<=b;
              contact=1;
              Fn21 = (Kv/2)*(b-a)*beta21^2+Cv*(3-2*beta21)*beta21^2*Vn21;
           else xn21<a;
                contact=0;
                Fn21 = 0;
          end
      end
      Fn21x = -Fn21*cos(alpha21);
      Fn21y = Fn21*sin(alpha21);
```

```
      % caculate the Ff
      if Fn21 == 0;
         Ff21 = 0;
         Ff21x = 0;
         Ff21y = 0;
      else
          Fc21 = u*Fn21; % caculate the friction force.
          z21 = Vt21*(1-sigma0*sign(Vt21)*z21p/abs(Fc21))*dt+z21p;
          %dotz21 = (z21-z21p)/dt;
          Ff21 = sigma0*z21+sigma1*Vt21;
          z21p = z21
          Ff21x = -Ff21*sin(alpha21);
          Ff21y = -Ff21*cos(alpha21);
      end
   end

else 0<=y21&y21<0.05; % the catheter's x-displacement should be restrained.
   Rj21 = sqrt((x21-Ox)^2);
   if Rj21>=R
      xn21 = Rj21-R; % Distance between the node and centerline of tube;
      Vn21 = v21*sin(phi21-pi/2); % Velocity of catheter in normal direction;
      Vt21 = v21*cos(phi21-pi/2);
      beta21 = (xn21-a)/(b-a);
      if xn21>b;
         Fn21 = Kv*(b-a)*(beta21-1/2)+Cv*Vn21;
      else if a<=xn21&xn21<=b;
              Fn21 = (Kv/2)*(b-a)*beta21^2+Cv*(3-2*beta21)*beta21^2*Vn21;
           else xn21<a;
                Fn21 = 0;
           end
      end
      Fn21x = Fn21;
      Fn21y = 0;

      if Fn21 == 0;
         Ff21 = 0;
         Ff21x = 0;
         Ff21y = 0;
      else
          Fc21 = u*Fn21; % caculate the friction force.
          z21 = Vt21*(1-sigma0*sign(Vt21)*z21p/abs(Fc21))*dt+z21p;
          %dotz21 = (z21-z21p)/dt;
          Ff21 = sigma0*z21+sigma1*Vt21;
          z21p = z21
          Ff21x = 0;
          Ff21y = Ff21;
      end

      % caculate the Ff

   else Rj21<R;
        xn21 = R-Rj21; % Distance between the node and centerline of tube;
        Vn21 = v21*cos(phi21); % Velocity of catheter in normal direction;
        Vt21 = v21*sin(phi21);
        beta21 = (xn21-a)/(b-a);
        if xn21>b;
```

```
           Fn21 = Kv*(b-a)*(beta21-1/2)+Cv*Vn21;
        else if a<=xn21&xn21<=b;
                Fn21 = (Kv/2)*(b-a)*beta21^2+Cv*(3-2*beta21)*beta21^2*Vn21;
             else xn21<a;
                  Fn21 = 0;
            end
        end
        Fn21x = -Fn21;
        Fn21y = 0;
      if Fn21 == 0;
          Ff21 = 0;
          Ff21x = 0;
          Ff21y = 0;
      else
          Fc21 = u*Fn21; % caculate the friction force.
          z21 = Vt21*(1-sigma0*sign(Vt21)*z21p/abs(Fc21))*dt+z21p;
          %dotz21 = (z21-z21p)/dt;
          Ff21 = sigma0*z21+sigma1*Vt21;
          z21p = z21
          Ff21x = 0;
          Ff21y = Ff21;
      end

   end
end

F21x = Fn21x+Ff21x;
F21y = Fn21y+Ff21y;

%% Node 23
x23 = x(1,lnp(23,1)); % the x coordinate of the node 1;
y23 = x(1,lnp(23,2)); % the y coordinate of the node 1;
v23 = xp(1,lnp(23,1));
phi23 = x(1,lnp(24,1));

if y23>=0.05; % caculate the contact force Fn.
   Rj23 = sqrt((x23-Ox)^2+(y23-Oy)^2);
   alpha23 = asin((y23-0.05)/Rj23); % rad
   if Rj23>=R
      xn23 = Rj23-R; % Distance between the node and centerline of tube;
      Vn23 = v23*sin(phi23+alpha23-pi/2); % Velocity of catheter in normal
direction;
      Vt23 = v23*cos(phi23+alpha23-pi/2);
      beta23 = (xn23-a)/(b-a);
      contact=0;
      if xn23>b;
      contact=1;
      Fn23 = Kv*(b-a)*(beta23-1/2)+Cv*Vn23;
      else if a<=xn23&xn23<=b;
              contact=1;
              Fn23 = (Kv/2)*(b-a)*beta23^2+Cv*(3-2*beta23)*beta23^2*Vn23;
           else xn23<a;
                contact=0;
                Fn23 = 0;
          end
      end
```

```
      Fn23x = Fn23*cos(alpha23);
      Fn23y = -Fn23*sin(alpha23);
      % caculate the Ff
      if Fn23 == 0;
         Ff23 = 0;
         Ff23x = 0;
         Ff23y = 0;
      else
          Fc23 = u*Fn23; % caculate the friction force.
          z23 = Vt23*(1-sigma0*sign(Vt23)*z23p/abs(Fc23))*dt+z23p;
          %dotz23 = (z23-z23p)/dt;
          Ff23 = sigma0*z23+sigma1*Vt23;
          z23p = z23
          Ff23x = -Ff23*sin(alpha23);
          Ff23y = -Ff23*cos(alpha23);
      end
   else Rj23<R
      xn23 = R-Rj23; % Distance between the node and centerline of tube;
      Vn23 = v23*sin(-phi23-alpha23+pi/2); % Velocity of catheter in normal
direction;
      Vt23 = v23*cos(-phi23-alpha23+pi/2);
      beta23 = (xn23-a)/(b-a);
      contact=0;
      if xn23>b;
      contact=1;
      Fn23 = Kv*(b-a)*(beta23-1/2)+Cv*Vn23;
      else if a<=xn23&xn23<=b;
              contact=1;
              Fn23 = (Kv/2)*(b-a)*beta23^2+Cv*(3-2*beta23)*beta23^2*Vn23;
           else xn23<a;
                contact=0;
                Fn23 = 0;
          end
      end
      Fn23x = -Fn23*cos(alpha23);
      Fn23y = Fn23*sin(alpha23);
      % caculate the Ff
      if Fn23 == 0;
         Ff23 = 0;
         Ff23x = 0;
         Ff23y = 0;
      else
          Fc23 = u*Fn23; % caculate the friction force.
          z23 = Vt23*(1-sigma0*sign(Vt23)*z23p/abs(Fc23))*dt+z23p;
          %dotz23 = (z23-z23p)/dt;
          Ff23 = sigma0*z23+sigma1*Vt23;
          z23p = z23
          Ff23x = -Ff23*sin(alpha23);
          Ff23y = -Ff23*cos(alpha23);
      end
   end

else 0<=y23&y23<0.05; % the catheter's x-displacement should be restrained.
   Rj23 = sqrt((x23-Ox)^2);
   if Rj23>=R
      xn23 = Rj23-R; % Distance between the node and centerline of tube;
      Vn23 = v23*sin(phi23-pi/2); % Velocity of catheter in normal direction;
```

```
   Vt23 = v23*cos(phi23-pi/2);
   beta23 = (xn23-a)/(b-a);
   if xn23>b;
      Fn23 = Kv*(b-a)*(beta23-1/2)+Cv*Vn23;
   else if a<=xn23&xn23<=b;
           Fn23 = (Kv/2)*(b-a)*beta23^2+Cv*(3-2*beta23)*beta23^2*Vn23;
        else xn23<a;
             Fn23 = 0;
        end
   end
   Fn23x = Fn23;
   Fn23y = 0;

   if Fn23 == 0;
      Ff23 = 0;
      Ff23x = 0;
      Ff23y = 0;
   else
       Fc23 = u*Fn23; % caculate the friction force.
       z23 = Vt23*(1-sigma0*sign(Vt23)*z23p/abs(Fc23))*dt+z23p;
       %dotz23 = (z23-z23p)/dt;
       Ff23 = sigma0*z23+sigma1*Vt23;
       z23p = z23
       Ff23x = 0;
       Ff23y = Ff23;
   end

   % caculate the Ff

else Rj23<R;
     xn23 = R-Rj23; % Distance between the node and centerline of tube;
     Vn23 = v23*cos(phi23); % Velocity of catheter in normal direction;
     Vt23 = v23*sin(phi23);
     beta23 = (xn23-a)/(b-a);
     if xn23>b;
        Fn23 = Kv*(b-a)*(beta23-1/2)+Cv*Vn23;
     else if a<=xn23&xn23<=b;
             Fn23 = (Kv/2)*(b-a)*beta23^2+Cv*(3-2*beta23)*beta23^2*Vn23;
          else xn23<a;
               Fn23 = 0;
         end
     end
     Fn23x = -Fn23;
     Fn23y = 0;
   if Fn23 == 0;
       Ff23 = 0;
       Ff23x = 0;
       Ff23y = 0;
   else
       Fc23 = u*Fn23; % caculate the friction force.
       z23 = Vt23*(1-sigma0*sign(Vt23)*z23p/abs(Fc23))*dt+z23p;
       %dotz23 = (z23-z23p)/dt;
       Ff23 = sigma0*z23+sigma1*Vt23;
       z23p = z23
       Ff23x = 0;
       Ff23y = Ff23;
```

```
      end

   end
end

F23x = Fn23x+Ff23x;
F23y = Fn23y+Ff23y;

%% Node 25
x25 = x(1,lnp(25,1)); % the x coordinate of the node 1;
y25 = x(1,lnp(25,2)); % the y coordinate of the node 1;
v25 = xp(1,lnp(25,1));
phi25 = x(1,lnp(26,1));

if y25>=0.05; % caculate the contact force Fn.
   Rj25 = sqrt((x25-Ox)^2+(y25-Oy)^2);
   alpha25 = asin((y25-0.05)/Rj25); % rad
   if Rj25>=R
      xn25 = Rj25-R; % Distance between the node and centerline of tube;
      Vn25 = v25*sin(phi25+alpha25-pi/2); % Velocity of catheter in normal
direction;
      Vt25 = v25*cos(phi25+alpha25-pi/2);
      beta25 = (xn25-a)/(b-a);
      contact=0;
      if xn25>b;
      contact=1;
      Fn25 = Kv*(b-a)*(beta25-1/2)+Cv*Vn25;
      else if a<=xn25&xn25<=b;
              contact=1;
              Fn25 = (Kv/2)*(b-a)*beta25^2+Cv*(3-2*beta25)*beta25^2*Vn25;
           else xn25<a;
                contact=0;
                Fn25 = 0;
          end
      end
      Fn25x = Fn25*cos(alpha25);
      Fn25y = -Fn25*sin(alpha25);
      % caculate the Ff
      if Fn25 == 0;
         Ff25 = 0;
         Ff25x = 0;
         Ff25y = 0;
      else
          Fc25 = u*Fn25; % caculate the friction force.
          z25 = Vt25*(1-sigma0*sign(Vt25)*z25p/abs(Fc25))*dt+z25p;
          %dotz25 = (z25-z25p)/dt;
          Ff25 = sigma0*z25+sigma1*Vt25;
          z25p = z25
          Ff25x = -Ff25*sin(alpha25);
          Ff25y = -Ff25*cos(alpha25);
      end
   else Rj25<R
      xn25 = R-Rj25; % Distance between the node and centerline of tube;
      Vn25 = v25*sin(-phi25-alpha25+pi/2); % Velocity of catheter in normal
direction;
      Vt25 = v25*cos(-phi25-alpha25+pi/2);
```

```
      beta25 = (xn25-a)/(b-a);
      contact=0;
      if xn25>b;
      contact=1;
      Fn25 = Kv*(b-a)*(beta25-1/2)+Cv*Vn25;
      else if a<=xn25&xn25<=b;
              contact=1;
              Fn25 = (Kv/2)*(b-a)*beta25^2+Cv*(3-2*beta25)*beta25^2*Vn25;
           else xn25<a;
                contact=0;
                Fn25 = 0;
          end
      end
      Fn25x = -Fn25*cos(alpha25);
      Fn25y = Fn25*sin(alpha25);
      % caculate the Ff
      if Fn25 == 0;
         Ff25 = 0;
         Ff25x = 0;
         Ff25y = 0;
      else
          Fc25 = u*Fn25; % caculate the friction force.
          z25 = Vt25*(1-sigma0*sign(Vt25)*z25p/abs(Fc25))*dt+z25p;
          %dotz25 = (z25-z25p)/dt;
          Ff25 = sigma0*z25+sigma1*Vt25;
          z25p = z25
          Ff25x = -Ff25*sin(alpha25);
          Ff25y = -Ff25*cos(alpha25);
      end
   end

else 0<=y25&y25<0.05; % the catheter's x-displacement should be restrained.
   Rj25 = sqrt((x25-Ox)^2);
   if Rj25>=R
      xn25 = Rj25-R; % Distance between the node and centerline of tube;
      Vn25 = v25*sin(phi25-pi/2); % Velocity of catheter in normal direction;
      Vt25 = v25*cos(phi25-pi/2);
      beta25 = (xn25-a)/(b-a);
      if xn25>b;
         Fn25 = Kv*(b-a)*(beta25-1/2)+Cv*Vn25;
      else if a<=xn25&xn25<=b;
              Fn25 = (Kv/2)*(b-a)*beta25^2+Cv*(3-2*beta25)*beta25^2*Vn25;
           else xn25<a;
                Fn25 = 0;
           end
      end
      Fn25x = Fn25;
      Fn25y = 0;

      if Fn25 == 0;
         Ff25 = 0;
         Ff25x = 0;
         Ff25y = 0;
      else
          Fc25 = u*Fn25; % caculate the friction force.
          z25 = Vt25*(1-sigma0*sign(Vt25)*z25p/abs(Fc25))*dt+z25p;
```

```
          %dotz25 = (z25-z25p)/dt;
          Ff25 = sigma0*z25+sigma1*Vt25;
          z25p = z25
          Ff25x = 0;
          Ff25y = Ff25;
      end

      % caculate the Ff

   else Rj25<R;
        xn25 = R-Rj25; % Distance between the node and centerline of tube;
        Vn25 = v25*cos(phi25); % Velocity of catheter in normal direction;
        Vt25 = v25*sin(phi25);
        beta25 = (xn25-a)/(b-a);
        if xn25>b;
           Fn25 = Kv*(b-a)*(beta25-1/2)+Cv*Vn25;
        else if a<=xn25&xn25<=b;
                Fn25 = (Kv/2)*(b-a)*beta25^2+Cv*(3-2*beta25)*beta25^2*Vn25;
             else xn25<a;
                  Fn25 = 0;
            end
        end
        Fn25x = -Fn25;
        Fn25y = 0;
      if Fn25 == 0;
          Ff25 = 0;
          Ff25x = 0;
          Ff25y = 0;
      else
          Fc25 = u*Fn25; % caculate the friction force.
          z25 = Vt25*(1-sigma0*sign(Vt25)*z25p/abs(Fc25))*dt+z25p;
          %dotz25 = (z25-z25p)/dt;
          Ff25 = sigma0*z25+sigma1*Vt25;
          z25p = z25
          Ff25x = 0;
          Ff25y = Ff25;
      end

   end
end

F25x = Fn25x+Ff25x;
F25y = Fn25y+Ff25y;


%% Apply Fn and Ff to each node.
f = [1  1   F1x
     1  2   F1y
     3  1   F3x
     3  2   F3y
     5  1   F5x
     5  2   F5y
     7  1   F7x
     7  2   F7y
     9  1   F9x
     9  2   F9y
```

```
11  1   F11x
11  2   F11y
13  1   F13x
13  2   F13y
15  1   F15x
15  2   F15y
17  1   F17x
17  2   F17y
19  1   F19x
19  2   F19y
21  1   F21x
21  2   F21y
23  1   F23x
23  2   F23y
25  1   F25x
25  2   F25y]
```

APPENDIX D MATLAB CODES FOR THE SIMULATION OF THE KINETIC MODEL OF STEERABLE CATHETER DURING OPERATION

D.1 Spacar data for the kinetic model of the steerable catheter

```
PLBEAM  1   1   2   3   4
PLBEAM  2   3   4   5   6
PLBEAM  3   5   6   7   8
PLBEAM  4   7   8   9   10
PLBEAM  5   9   10  11  12
PLBEAM  6   11  12  13  14
PLBEAM  7   13  14  15  16
PLBEAM  8   15  16  17  18
PLBEAM  9   17  18  19  20
PLBEAM  10  19  20  21  22
PLBEAM  11  21  22  23  24
PLBEAM  12  23  24  25  26

X   1   0.1959  0.2503
X   3   0.1792  0.2489
X   5   0.1627  0.2468
X   7   0.1466  0.2429
X   9   0.1231  0.2343
X   11  0.1006  0.2233
X   13  0.0757  0.2067
X   15  0.0536  0.1865
X   17  0.0294    0.1547
X   19  0.0123    0.1186
X   21  0.0014    0.0699
X   23  -0.0003    0.0200
X   25  -0.0002   -0.0400

%FIX 1
%FIX 2
FIX 26

DYNX    1   1
DYNX    2
DYNX    3   1
DYNX    4
DYNX    5   1
DYNX    6
DYNX    7   1
DYNX    8
DYNX    9   1
DYNX    10
DYNX    11  1
DYNX    12
DYNX    13  1
DYNX    14
DYNX    15  1
DYNX    16
```

```
DYNX    17  1
DYNX    18
DYNX    19  1
DYNX    20
DYNX    21  1
DYNX    22
DYNX    23  1
DYNX    24
DYNX    25  1
INPUTX  25  2

RLSE    1   2   3
RLSE    2   2   3
RLSE    3   2   3
RLSE    4   2   3
RLSE    5   2   3
RLSE    6   2   3
RLSE    7   2   3
RLSE    8   2   3
RLSE    9   2   3
RLSE    10  2   3
RLSE    11  2   3
RLSE    12  2   3

END
HALT

% M=0.00753g/mm=0.00753kg/m
EM  1   0.00753
EM  2   0.00753
EM  3   0.00753
EM  4   0.00753
EM  5   0.00753
EM  6   0.00753
EM  7   0.00753
EM  8   0.00753
EM  9   0.00753
EM  10  0.00753
EM  11  0.00753
EM  12  0.00753

ESTIFF  1   0   0.0001712363
ESTIFF  2   0   0.0001712363
ESTIFF  3   0   0.0001712363
ESTIFF  4   0   0.0007344
ESTIFF  5   0   0.0007344
ESTIFF  6   0   0.0007344
ESTIFF  7   0   0.0007344
ESTIFF  8   0   0.0007344
ESTIFF  9   0   0.0007344
ESTIFF  10  0   0.0007344
ESTIFF  11  0   0.0007344
ESTIFF  12  0   0.0007344

EDAMP   1   0.015011
EDAMP   2   0.015011
```

```
EDAMP   3   0.014962
EDAMP   4   0.352807
EDAMP   5   0.352807
EDAMP   6   0.353388
EDAMP   7   0.353388
EDAMP   8   0.354551
EDAMP   9   0.354551
EDAMP   10  0.355713
EDAMP   11  0.355713
EDAMP   12  0.356875

% ESIG    1   -0.0070
ESIG    1   0
ESIG    2   -0.085
ESIG    3   -0.0112
ESIG    4   -0.0213
ESIG    5   -0.0248
ESIG    6   -0.0257
ESIG    7   -0.0262
ESIG    8   -0.0261
ESIG    9   -0.0261
ESIG    10  -0.0248
ESIG    11  -0.0193
% ESIG    12  -0.0172
ESIG    12  0

% XF   25   0   2
USERSIG FORCE
USERINP MOTION
TIMESTEP    1   100
%INPUTX 25  2   -0.0400 0.000000000 0.0005

INTEGRAT    155 0.0001  % It effects the stability of the system.
ERROR   0.000000005 0.000000005  % It effects the stability of the system.
END
END
```

D.2 Codes for the user defined contact situation

```
                %% User defined interaction force %%
function [time, sig, f] = FORCE(t, ne, le, e, ep, nx, lnp, x, xp);
%% initial condition
global z1p
global z3p
global z5p
global z7p
global z9p
global z11p
global z13p
global z15p
global z17p
global z19p
global z21p
global z23p
global z25p

z1p = 0.0000;
z3p = 0.0000;
z5p = 0.0000;
z7p = 0.0000;
z9p = 0.0000;
z11p = 0.0000;
z13p = 0.0000;
z15p = 0.0000;
z17p = 0.0000;
z19p = 0.0000;
z21p = 0.0000;
z23p = 0.0000;
z25p = 0.0000;

time = t;
sig = [];

R = 0.2; % radius of tube curve
L = (2*pi*R)/4; % the length of the 1/4 ciclar curve.
r = 0.0013; % the inner radius of the tube is 2mm.
r0 = 0.0012; % catheter radius
Ox = R;
Oy = 0.05;

M = 0.00694*(L+0.01); %0.694/100 g/mm=0.00694kg/m
Kv = 622.68; % stiffness of tube N/m, 2*10^4 in Kohatait thesis
Cv = 11.4701*M+0.000185*Kv; % C=11.4701M+0.000185Kv; 10 Ns/m^2 in Khatait
thesis % 0.016 in experiment
a = r-r0;
b = a+0.0005; % the original transit zone is 0.5mm
u = 0.1204; % friction coefficient
sigma0 = 300000; %0.07 N/mm in Ref. (Jung J, 2014)
sigma1 = 1;
% sigma2 = 1.5;
dt = 0.00001; %0.0001;
```

```
%% Caculate the contact force Fn and friction force Ff on each node

%% Node 3
x3 = x(1,lnp(3,1)); % the x coordinate of the node 1;
y3 = x(1,lnp(3,2)); % the y coordinate of the node 1;
v3 = xp(1,lnp(3,1));
phi3 = x(1,lnp(4,1));

if y3>=0.05; % caculate the contact force Fn.
   Rj3 = sqrt((x3-Ox)^2+(y3-Oy)^2);
   alpha3 = asin((y3-0.05)/Rj3); % rad
   if Rj3>=R
      xn3 = Rj3-R; % Distance between the node and centerline of tube;
      Vn3 = v3*sin(phi3+alpha3-pi/2); % Velocity of catheter in normal
direction;
      Vt3 = v3*cos(phi3+alpha3-pi/2);
      beta3 = (xn3-a)/(b-a);
      contact=0;
      if xn3>b;
      contact=1;
      Fn3 = Kv*(b-a)*(beta3-1/2)+Cv*Vn3;
      else if a<=xn3&xn3<=b;
              contact=1;
              Fn3 = (Kv/2)*(b-a)*beta3^2+Cv*(3-2*beta3)*beta3^2*Vn3;
           else xn3<a;
                contact=0;
                Fn3 = 0;
          end
      end
      Fn3x = Fn3*cos(alpha3);
      Fn3y = -Fn3*sin(alpha3);
      % caculate the Ff
      if Fn3 == 0;
         Ff3 = 0;
         Ff3x = 0;
         Ff3y = 0;
      else
          Fc3 = u*Fn3; % caculate the friction force.
          z3 = Vt3*(1-sigma0*sign(Vt3)*z3p/abs(Fc3))*dt+z3p
          %dotz3 = (z3-z3p)/dt;
          Ff3 = sigma0*z3+sigma1*Vt3;
          z3p = z3
          Ff3x = -Ff3*sin(alpha3);
          Ff3y = -Ff3*cos(alpha3);
      end
   else Rj3<R
      xn3 = R-Rj3; % Distance between the node and centerline of tube;
      Vn3 = v3*sin(-phi3-alpha3+pi/2); % Velocity of catheter in normal
direction;
      Vt3 = v3*cos(-phi3-alpha3+pi/2);
      beta3 = (xn3-a)/(b-a);
      contact=0;
      if xn3>b;
      contact=1;
      Fn3 = Kv*(b-a)*(beta3-1/2)+Cv*Vn3;
```

```
      else if a<=xn3&xn3<=b;
              contact=1;
              Fn3 = (Kv/2)*(b-a)*beta3^2+Cv*(3-2*beta3)*beta3^2*Vn3;
           else xn3<a;
                contact=0;
                Fn3 = 0;
          end
      end
      Fn3x = -Fn3*cos(alpha3);
      Fn3y = Fn3*sin(alpha3);
      % caculate the Ff
      if Fn3 == 0;
         Ff3 = 0;
         Ff3x = 0;
         Ff3y = 0;
      else
          Fc3 = u*Fn3; % caculate the friction force.
          z3 = Vt3*(1-sigma0*sign(Vt3)*z3p/abs(Fc3))*dt+z3p
          %dotz3 = (z3-z3p)/dt;
          Ff3 = sigma0*z3+sigma1*Vt3;
          z3p = z3
          Ff3x = -Ff3*sin(alpha3);
          Ff3y = -Ff3*cos(alpha3);
      end
   end

else 0<=y3&y3<0.05; % the catheter's x-displacement should be restrained.
   Rj3 = sqrt((x3-Ox)^2);
   if Rj3>=R
      xn3 = Rj3-R; % Distance between the node and centerline of tube;
      Vn3 = v3*sin(phi3-pi/2); % Velocity of catheter in normal direction;
      Vt3 = v3*cos(phi3-pi/2);
      beta3 = (xn3-a)/(b-a);
      if xn3>b;
         Fn3 = Kv*(b-a)*(beta3-1/2)+Cv*Vn3;
      else if a<=xn3&xn3<=b;
              Fn3 = (Kv/2)*(b-a)*beta3^2+Cv*(3-2*beta3)*beta3^2*Vn3;
           else xn3<a;
                Fn3 = 0;
           end
      end
      Fn3x = Fn3;
      Fn3y = 0;

      if Fn3 == 0;
         Ff3 = 0;
         Ff3x = 0;
         Ff3y = 0;
      else
          Fc3 = u*Fn3; % caculate the friction force.
          z3 = Vt3*(1-sigma0*sign(Vt3)*z3p/abs(Fc3))*dt+z3p
          %dotz3 = (z3-z3p)/dt;
          Ff3 = sigma0*z3+sigma1*Vt3;
          z3p = z3
          Ff3x = 0;
          Ff3y = Ff3;
```

```
      end

      % caculate the Ff

   else Rj3<R;
        xn3 = R-Rj3; % Distance between the node and centerline of tube;
        Vn3 = v3*cos(phi3); % Velocity of catheter in normal direction;
        Vt3 = v3*sin(phi3);
        beta3 = (xn3-a)/(b-a);
        if xn3>b;
           Fn3 = Kv*(b-a)*(beta3-1/2)+Cv*Vn3;
        else if a<=xn3&xn3<=b;
                Fn3 = (Kv/2)*(b-a)*beta3^2+Cv*(3-2*beta3)*beta3^2*Vn3;
             else xn3<a;
                  Fn3 = 0;
            end
        end
        Fn3x = -Fn3;
        Fn3y = 0;
      if Fn3 == 0;
          Ff3 = 0;
          Ff3x = 0;
          Ff3y = 0;
      else
          Fc3 = u*Fn3; % caculate the friction force.
          z3 = Vt3*(1-sigma0*sign(Vt3)*z3p/abs(Fc3))*dt+z3p
          %dotz3 = (z3-z3p)/dt;
          Ff3 = sigma0*z3+sigma1*Vt3;
          z3p = z3
          Ff3x = 0;
          Ff3y = Ff3;
      end

   end
end

F3x = Fn3x+Ff3x;
F3y = Fn3y+Ff3y;

%% Node 5
x5 = x(1,lnp(5,1)); % the x coordinate of the node 1;
y5 = x(1,lnp(5,2)); % the y coordinate of the node 1;
v5 = xp(1,lnp(5,1));
phi5 = x(1,lnp(6,1));

if y5>=0.05; % caculate the contact force Fn.
   Rj5 = sqrt((x5-Ox)^2+(y5-Oy)^2);
   alpha5 = asin((y5-0.05)/Rj5); % rad
   if Rj5>=R
      xn5 = Rj5-R; % Distance between the node and centerline of tube;
      Vn5 = v5*sin(phi5+alpha5-pi/2); % Velocity of catheter in normal
direction;
      Vt5 = v5*cos(phi5+alpha5-pi/2);
      beta5 = (xn5-a)/(b-a);
      contact=0;
      if xn5>b;
```

```
      contact=1;
      Fn5 = Kv*(b-a)*(beta5-1/2)+Cv*Vn5;
      else if a<=xn5&xn5<=b;
              contact=1;
              Fn5 = (Kv/2)*(b-a)*beta5^2+Cv*(3-2*beta5)*beta5^2*Vn5;
           else xn5<a;
                contact=0;
                Fn5 = 0;
          end
      end
      Fn5x = Fn5*cos(alpha5);
      Fn5y = -Fn5*sin(alpha5);
      % caculate the Ff
      if Fn5 == 0;
         Ff5 = 0;
         Ff5x = 0;
         Ff5y = 0;
      else
          Fc5 = u*Fn5; % caculate the friction force.
          z5 = Vt5*(1-sigma0*sign(Vt5)*z5p/abs(Fc5))*dt+z5p
          %dotz5 = (z5-z5p)/dt;
          Ff5 = sigma0*z5+sigma1*Vt5;
          z5p = z5
          Ff5x = -Ff5*sin(alpha5);
          Ff5y = -Ff5*cos(alpha5);
      end
   else Rj5<R
      xn5 = R-Rj5; % Distance between the node and centerline of tube;
      Vn5 = v5*sin(-phi5-alpha5+pi/2); % Velocity of catheter in normal
direction;
      Vt5 = v5*cos(-phi5-alpha5+pi/2);
      beta5 = (xn5-a)/(b-a);
      contact=0;
      if xn5>b;
      contact=1;
      Fn5 = Kv*(b-a)*(beta5-1/2)+Cv*Vn5;
      else if a<=xn5&xn5<=b;
              contact=1;
              Fn5 = (Kv/2)*(b-a)*beta5^2+Cv*(3-2*beta5)*beta5^2*Vn5;
           else xn5<a;
                contact=0;
                Fn5 = 0;
          end
      end
      Fn5x = -Fn5*cos(alpha5);
      Fn5y = Fn5*sin(alpha5);
      % caculate the Ff
      if Fn5 == 0;
         Ff5 = 0;
         Ff5x = 0;
         Ff5y = 0;
      else
          Fc5 = u*Fn5; % caculate the friction force.
          z5 = Vt5*(1-sigma0*sign(Vt5)*z5p/abs(Fc5))*dt+z5p
          %dotz5 = (z5-z5p)/dt;
          Ff5 = sigma0*z5+sigma1*Vt5;
          z5p = z5
```

```
            Ff5x = -Ff5*sin(alpha5);
            Ff5y = -Ff5*cos(alpha5);
         end
      end

else 0<=y5&y5<0.05; % the catheter's x-displacement should be restrained.
      Rj5 = sqrt((x5-Ox)^2);
      if Rj5>=R
         xn5 = Rj5-R; % Distance between the node and centerline of tube;
         Vn5 = v5*sin(phi5-pi/2); % Velocity of catheter in normal direction;
         Vt5 = v5*cos(phi5-pi/2);
         beta5 = (xn5-a)/(b-a);
         if xn5>b;
            Fn5 = Kv*(b-a)*(beta5-1/2)+Cv*Vn5;
         else if a<=xn5&xn5<=b;
                 Fn5 = (Kv/2)*(b-a)*beta5^2+Cv*(3-2*beta5)*beta5^2*Vn5;
              else xn5<a;
                   Fn5 = 0;
              end
         end
         Fn5x = Fn5;
         Fn5y = 0;

         if Fn5 == 0;
            Ff5 = 0;
            Ff5x = 0;
            Ff5y = 0;
         else
             Fc5 = u*Fn5; % caculate the friction force.
             z5 = Vt5*(1-sigma0*sign(Vt5)*z5p/abs(Fc5))*dt+z5p
             %dotz5 = (z5-z5p)/dt;
             Ff5 = sigma0*z5+sigma1*Vt5;
             z5p = z5
             Ff5x = 0;
             Ff5y = Ff5;
         end

         % caculate the Ff

      else Rj5<R;
           xn5 = R-Rj5; % Distance between the node and centerline of tube;
           Vn5 = v5*cos(phi5); % Velocity of catheter in normal direction;
           Vt5 = v5*sin(phi5);
           beta5 = (xn5-a)/(b-a);
           if xn5>b;
              Fn5 = Kv*(b-a)*(beta5-1/2)+Cv*Vn5;
           else if a<=xn5&xn5<=b;
                   Fn5 = (Kv/2)*(b-a)*beta5^2+Cv*(3-2*beta5)*beta5^2*Vn5;
                else xn5<a;
                     Fn5 = 0;
                end
           end
           Fn5x = -Fn5;
           Fn5y = 0;
         if Fn5 == 0;
             Ff5 = 0;
```

```
          Ff5x = 0;
          Ff5y = 0;
      else
          Fc5 = u*Fn5; % caculate the friction force.
          z5 = Vt5*(1-sigma0*sign(Vt5)*z5p/abs(Fc5))*dt+z5p
          %dotz5 = (z5-z5p)/dt;
          Ff5 = sigma0*z5+sigma1*Vt5;
          z5p = z5
          Ff5x = 0;
          Ff5y = Ff5;
      end

   end
end

F5x = Fn5x+Ff5x;
F5y = Fn5y+Ff5y;

%% Node 7
x7 = x(1,lnp(7,1)); % the x coordinate of the node 1;
y7 = x(1,lnp(7,2)); % the y coordinate of the node 1;
v7 = xp(1,lnp(7,1));
phi7 = x(1,lnp(8,1));

if y7>=0.05; % caculate the contact force Fn.
   Rj7 = sqrt((x7-Ox)^2+(y7-Oy)^2);
   alpha7 = asin((y7-0.05)/Rj7); % rad
   if Rj7>=R
      xn7 = Rj7-R; % Distance between the node and centerline of tube;
      Vn7 = v7*sin(phi7+alpha7-pi/2); % Velocity of catheter in normal
direction;
      Vt7 = v7*cos(phi7+alpha7-pi/2);
      beta7 = (xn7-a)/(b-a);
      contact=0;
      if xn7>b;
      contact=1;
      Fn7 = Kv*(b-a)*(beta7-1/2)+Cv*Vn7;
      else if a<=xn7&xn7<=b;
              contact=1;
              Fn7 = (Kv/2)*(b-a)*beta7^2+Cv*(3-2*beta7)*beta7^2*Vn7;
           else xn7<a;
                contact=0;
                Fn7 = 0;
          end
      end
      Fn7x = Fn7*cos(alpha7);
      Fn7y = -Fn7*sin(alpha7);
      % caculate the Ff
      if Fn7 == 0;
         Ff7 = 0;
         Ff7x = 0;
         Ff7y = 0;
      else
          Fc7 = u*Fn7; % caculate the friction force.
          z7 = Vt7*(1-sigma0*sign(Vt7)*z7p/abs(Fc7))*dt+z7p
          %dotz7 = (z7-z7p)/dt;
```

```
          Ff7 = sigma0*z7+sigma1*Vt7;
          z7p = z7
          Ff7x = -Ff7*sin(alpha7);
          Ff7y = -Ff7*cos(alpha7);
      end
   else Rj7<R
      xn7 = R-Rj7; % Distance between the node and centerline of tube;
      Vn7 = v7*sin(-phi7-alpha7+pi/2); % Velocity of catheter in normal
direction;
      Vt7 = v7*cos(-phi7-alpha7+pi/2);
      beta7 = (xn7-a)/(b-a);
      contact=0;
      if xn7>b;
      contact=1;
      Fn7 = Kv*(b-a)*(beta7-1/2)+Cv*Vn7;
      else if a<=xn7&xn7<=b;
              contact=1;
              Fn7 = (Kv/2)*(b-a)*beta7^2+Cv*(3-2*beta7)*beta7^2*Vn7;
           else xn7<a;
                contact=0;
                Fn7 = 0;
          end
      end
      Fn7x = -Fn7*cos(alpha7);
      Fn7y = Fn7*sin(alpha7);
      % caculate the Ff
      if Fn7 == 0;
         Ff7 = 0;
         Ff7x = 0;
         Ff7y = 0;
      else
          Fc7 = u*Fn7; % caculate the friction force.
          z7 = Vt7*(1-sigma0*sign(Vt7)*z7p/abs(Fc7))*dt+z7p
          %dotz7 = (z7-z7p)/dt;
          Ff7 = sigma0*z7+sigma1*Vt7;
          z7p = z7
          Ff7x = -Ff7*sin(alpha7);
          Ff7y = -Ff7*cos(alpha7);
      end
   end

else 0<=y7&y7<0.05; % the catheter's x-displacement should be restrained.
   Rj7 = sqrt((x7-Ox)^2);
   if Rj7>=R
      xn7 = Rj7-R; % Distance between the node and centerline of tube;
      Vn7 = v7*sin(phi7-pi/2); % Velocity of catheter in normal direction;
      Vt7 = v7*cos(phi7-pi/2);
      beta7 = (xn7-a)/(b-a);
      if xn7>b;
         Fn7 = Kv*(b-a)*(beta7-1/2)+Cv*Vn7;
      else if a<=xn7&xn7<=b;
              Fn7 = (Kv/2)*(b-a)*beta7^2+Cv*(3-2*beta7)*beta7^2*Vn7;
           else xn7<a;
                Fn7 = 0;
           end
      end
      Fn7x = Fn7;
```

```
      Fn7y = 0;

      if Fn7 == 0;
         Ff7 = 0;
         Ff7x = 0;
         Ff7y = 0;
      else
          Fc7 = u*Fn7; % caculate the friction force.
          z7 = Vt7*(1-sigma0*sign(Vt7)*z7p/abs(Fc7))*dt+z7p
          %dotz7 = (z7-z7p)/dt;
          Ff7 = sigma0*z7+sigma1*Vt7;
          z7p = z7
          Ff7x = 0;
          Ff7y = Ff7;
      end

      % caculate the Ff

   else Rj7<R;
        xn7 = R-Rj7; % Distance between the node and centerline of tube;
        Vn7 = v7*cos(phi7); % Velocity of catheter in normal direction;
        Vt7 = v7*sin(phi7);
        beta7 = (xn7-a)/(b-a);
        if xn7>b;
           Fn7 = Kv*(b-a)*(beta7-1/2)+Cv*Vn7;
        else if a<=xn7&xn7<=b;
                Fn7 = (Kv/2)*(b-a)*beta7^2+Cv*(3-2*beta7)*beta7^2*Vn7;
             else xn7<a;
                  Fn7 = 0;
            end
        end
        Fn7x = -Fn7;
        Fn7y = 0;
      if Fn7 == 0;
          Ff7 = 0;
          Ff7x = 0;
          Ff7y = 0;
      else
          Fc7 = u*Fn7; % caculate the friction force.
          z7 = Vt7*(1-sigma0*sign(Vt7)*z7p/abs(Fc7))*dt+z7p
          %dotz7 = (z7-z7p)/dt;
          Ff7 = sigma0*z7+sigma1*Vt7;
          z7p = z7
          Ff7x = 0;
          Ff7y = Ff7;
      end

   end
end

F7x = Fn7x+Ff7x;
F7y = Fn7y+Ff7y;

%% Node 9
x9 = x(1,lnp(9,1)); % the x coordinate of the node 1;
y9 = x(1,lnp(9,2)); % the y coordinate of the node 1;
```

```
v9 = xp(1,lnp(9,1));
phi9 = x(1,lnp(10,1));

if y9>=0.05; % caculate the contact force Fn.
   Rj9 = sqrt((x9-Ox)^2+(y9-Oy)^2);
   alpha9 = asin((y9-0.05)/Rj9); % rad
   if Rj9>=R
      xn9 = Rj9-R; % Distance between the node and centerline of tube;
      Vn9 = v9*sin(phi9+alpha9-pi/2); % Velocity of catheter in normal
direction;
      Vt9 = v9*cos(phi9+alpha9-pi/2);
      beta9 = (xn9-a)/(b-a);
      contact=0;
      if xn9>b;
      contact=1;
      Fn9 = Kv*(b-a)*(beta9-1/2)+Cv*Vn9;
      else if a<=xn9&xn9<=b;
              contact=1;
              Fn9 = (Kv/2)*(b-a)*beta9^2+Cv*(3-2*beta9)*beta9^2*Vn9;
           else xn9<a;
                contact=0;
                Fn9 = 0;
          end
      end
      Fn9x = Fn9*cos(alpha9);
      Fn9y = -Fn9*sin(alpha9);
      % caculate the Ff
      if Fn9 == 0;
         Ff9 = 0;
         Ff9x = 0;
         Ff9y = 0;
      else
          Fc9 = u*Fn9; % caculate the friction force.
          z9 = Vt9*(1-sigma0*sign(Vt9)*z9p/abs(Fc9))*dt+z9p
          %dotz9 = (z9-z9p)/dt;
          Ff9 = sigma0*z9+sigma1*Vt9;
          z9p = z9
          Ff9x = -Ff9*sin(alpha9);
          Ff9y = -Ff9*cos(alpha9);
      end
   else Rj9<R
      xn9 = R-Rj9; % Distance between the node and centerline of tube;
      Vn9 = v9*sin(-phi9-alpha9+pi/2); % Velocity of catheter in normal
direction;
      Vt9 = v9*cos(-phi9-alpha9+pi/2);
      beta9 = (xn9-a)/(b-a);
      contact=0;
      if xn9>b;
      contact=1;
      Fn9 = Kv*(b-a)*(beta9-1/2)+Cv*Vn9;
      else if a<=xn9&xn9<=b;
              contact=1;
              Fn9 = (Kv/2)*(b-a)*beta9^2+Cv*(3-2*beta9)*beta9^2*Vn9;
           else xn9<a;
                contact=0;
                Fn9 = 0;
          end
```

```
      end
      Fn9x = -Fn9*cos(alpha9);
      Fn9y = Fn9*sin(alpha9);
      % caculate the Ff
      if Fn9 == 0;
         Ff9 = 0;
         Ff9x = 0;
         Ff9y = 0;
      else
          Fc9 = u*Fn9; % caculate the friction force.
          z9 = Vt9*(1-sigma0*sign(Vt9)*z9p/abs(Fc9))*dt+z9p;
          %dotz9 = (z9-z9p)/dt;
          Ff9 = sigma0*z9+sigma1*Vt9;
          z9p = z9
          Ff9x = -Ff9*sin(alpha9);
          Ff9y = -Ff9*cos(alpha9);
      end
   end

else 0<=y9&y9<0.05; % the catheter's x-displacement should be restrained.
   Rj9 = sqrt((x9-Ox)^2);
   if Rj9>=R
      xn9 = Rj9-R; % Distance between the node and centerline of tube;
      Vn9 = v9*sin(phi9-pi/2); % Velocity of catheter in normal direction;
      Vt9 = v9*cos(phi9-pi/2);
      beta9 = (xn9-a)/(b-a);
      if xn9>b;
         Fn9 = Kv*(b-a)*(beta9-1/2)+Cv*Vn9;
      else if a<=xn9&xn9<=b;
              Fn9 = (Kv/2)*(b-a)*beta9^2+Cv*(3-2*beta9)*beta9^2*Vn9;
           else xn9<a;
                Fn9 = 0;
           end
      end
      Fn9x = Fn9;
      Fn9y = 0;

      if Fn9 == 0;
         Ff9 = 0;
         Ff9x = 0;
         Ff9y = 0;
      else
          Fc9 = u*Fn9; % caculate the friction force.
          z9 = Vt9*(1-sigma0*sign(Vt9)*z9p/abs(Fc9))*dt+z9p;
          %dotz9 = (z9-z9p)/dt;
          Ff9 = sigma0*z9+sigma1*Vt9;
          z9p = z9
          Ff9x = 0;
          Ff9y = Ff9;
      end

      % caculate the Ff

   else Rj9<R;
        xn9 = R-Rj9; % Distance between the node and centerline of tube;
        Vn9 = v9*cos(phi9); % Velocity of catheter in normal direction;
```

```
        Vt9 = v9*sin(phi9);
        beta9 = (xn9-a)/(b-a);
        if xn9>b;
           Fn9 = Kv*(b-a)*(beta9-1/2)+Cv*Vn9;
        else if a<=xn9&xn9<=b;
                Fn9 = (Kv/2)*(b-a)*beta9^2+Cv*(3-2*beta9)*beta9^2*Vn9;
             else xn9<a;
                  Fn9 = 0;
            end
        end
        Fn9x = -Fn9;
        Fn9y = 0;
      if Fn9 == 0;
          Ff9 = 0;
          Ff9x = 0;
          Ff9y = 0;
      else
          Fc9 = u*Fn9; % caculate the friction force.
          z9 = Vt9*(1-sigma0*sign(Vt9)*z9p/abs(Fc9))*dt+z9p;
          %dotz9 = (z9-z9p)/dt;
          Ff9 = sigma0*z9+sigma1*Vt9;
          z9p = z9
          Ff9x = 0;
          Ff9y = Ff9;
      end

   end
end

F9x = Fn9x+Ff9x;
F9y = Fn9y+Ff9y;

%% Node 11
x11 = x(1,lnp(11,1)); % the x coordinate of the node 1;
y11 = x(1,lnp(11,2)); % the y coordinate of the node 1;
v11 = xp(1,lnp(11,1));
phi11 = x(1,lnp(12,1));

if y11>=0.05; % caculate the contact force Fn.
   Rj11 = sqrt((x11-Ox)^2+(y11-Oy)^2);
   alpha11 = asin((y11-0.05)/Rj11); % rad
   if Rj11>=R
      xn11 = Rj11-R; % Distance between the node and centerline of tube;
      Vn11 = v11*sin(phi11+alpha11-pi/2); % Velocity of catheter in normal
direction;
      Vt11 = v11*cos(phi11+alpha11-pi/2);
      beta11 = (xn11-a)/(b-a);
      contact=0;
      if xn11>b;
      contact=1;
      Fn11 = Kv*(b-a)*(beta11-1/2)+Cv*Vn11;
      else if a<=xn11&xn11<=b;
              contact=1;
              Fn11 = (Kv/2)*(b-a)*beta11^2+Cv*(3-2*beta11)*beta11^2*Vn11;
           else xn11<a;
                contact=0;
```

```
                Fn11 = 0;
            end
        end
        Fn11x = Fn11*cos(alpha11);
        Fn11y = -Fn11*sin(alpha11);
        % caculate the Ff
        if Fn11 == 0;
           Ff11 = 0;
           Ff11x = 0;
           Ff11y = 0;
        else
            Fc11 = u*Fn11; % caculate the friction force.
            z11 = Vt11*(1-sigma0*sign(Vt11)*z11p/abs(Fc11))*dt+z11p;
            %dotz11 = (z11-z11p)/dt;
            Ff11 = sigma0*z11+sigma1*Vt11;
            z11p = z11
            Ff11x = -Ff11*sin(alpha11);
            Ff11y = -Ff11*cos(alpha11);
        end
    else Rj11<R
        xn11 = R-Rj11; % Distance between the node and centerline of tube;
        Vn11 = v11*sin(-phi11-alpha11+pi/2); % Velocity of catheter in normal
direction;
        Vt11 = v11*cos(-phi11-alpha11+pi/2);
        beta11 = (xn11-a)/(b-a);
        contact=0;
        if xn11>b;
        contact=1;
        Fn11 = Kv*(b-a)*(beta11-1/2)+Cv*Vn11;
        else if a<=xn11&xn11<=b;
                contact=1;
                Fn11 = (Kv/2)*(b-a)*beta11^2+Cv*(3-2*beta11)*beta11^2*Vn11;
             else xn11<a;
                  contact=0;
                  Fn11 = 0;
            end
        end
        Fn11x = -Fn11*cos(alpha11);
        Fn11y = Fn11*sin(alpha11);
        % caculate the Ff
        if Fn11 == 0;
           Ff11 = 0;
           Ff11x = 0;
           Ff11y = 0;
        else
            Fc11 = u*Fn11; % caculate the friction force.
            z11 = Vt11*(1-sigma0*sign(Vt11)*z11p/abs(Fc11))*dt+z11p;
            %dotz11 = (z11-z11p)/dt;
            Ff11 = sigma0*z11+sigma1*Vt11;
            z11p = z11
            Ff11x = -Ff11*sin(alpha11);
            Ff11y = -Ff11*cos(alpha11);
        end
    end

else 0<=y11&y11<0.05; % the catheter's x-displacement should be restrained.
    Rj11 = sqrt((x11-Ox)^2);
```

```
if Rj11>=R
   xn11 = Rj11-R; % Distance between the node and centerline of tube;
   Vn11 = v11*sin(phi11-pi/2); % Velocity of catheter in normal direction;
   Vt11 = v11*cos(phi11-pi/2);
   beta11 = (xn11-a)/(b-a);
   if xn11>b;
      Fn11 = Kv*(b-a)*(beta11-1/2)+Cv*Vn11;
   else if a<=xn11&xn11<=b;
           Fn11 = (Kv/2)*(b-a)*beta11^2+Cv*(3-2*beta11)*beta11^2*Vn11;
        else xn11<a;
             Fn11 = 0;
        end
   end
   Fn11x = Fn11;
   Fn11y = 0;

   if Fn11 == 0;
      Ff11 = 0;
      Ff11x = 0;
      Ff11y = 0;
   else
       Fc11 = u*Fn11; % caculate the friction force.
       z11 = Vt11*(1-sigma0*sign(Vt11)*z11p/abs(Fc11))*dt+z11p;
       %dotz11 = (z11-z11p)/dt;
       Ff11 = sigma0*z11+sigma1*Vt11;
       z11p = z11
       Ff11x = 0;
       Ff11y = Ff11;
   end

   % caculate the Ff

else Rj11<R;
     xn11 = R-Rj11; % Distance between the node and centerline of tube;
     Vn11 = v11*cos(phi11); % Velocity of catheter in normal direction;
     Vt11 = v11*sin(phi11);
     beta11 = (xn11-a)/(b-a);
     if xn11>b;
        Fn11 = Kv*(b-a)*(beta11-1/2)+Cv*Vn11;
     else if a<=xn11&xn11<=b;
             Fn11 = (Kv/2)*(b-a)*beta11^2+Cv*(3-2*beta11)*beta11^2*Vn11;
          else xn11<a;
               Fn11 = 0;
         end
     end
     Fn11x = -Fn11;
     Fn11y = 0;
   if Fn11 == 0;
       Ff11 = 0;
       Ff11x = 0;
       Ff11y = 0;
   else
       Fc11 = u*Fn11; % caculate the friction force.
       z11 = Vt11*(1-sigma0*sign(Vt11)*z11p/abs(Fc11))*dt+z11p;
       %dotz11 = (z11-z11p)/dt;
       Ff11 = sigma0*z11+sigma1*Vt11;
```

```
          z11p = z11
          Ff11x = 0;
          Ff11y = Ff11;
      end

   end
end

F11x = Fn11x+Ff11x;
F11y = Fn11y+Ff11y;

%% Node 13
x13 = x(1,lnp(13,1)); % the x coordinate of the node 1;
y13 = x(1,lnp(13,2)); % the y coordinate of the node 1;
v13 = xp(1,lnp(13,1));
phi13 = x(1,lnp(14,1));

if y13>=0.05; % caculate the contact force Fn.
   Rj13 = sqrt((x13-Ox)^2+(y13-Oy)^2);
   alpha13 = asin((y13-0.05)/Rj13); % rad
   if Rj13>=R
      xn13 = Rj13-R; % Distance between the node and centerline of tube;
      Vn13 = v13*sin(phi13+alpha13-pi/2); % Velocity of catheter in normal
direction;
      Vt13 = v13*cos(phi13+alpha13-pi/2);
      beta13 = (xn13-a)/(b-a);
      contact=0;
      if xn13>b;
      contact=1;
      Fn13 = Kv*(b-a)*(beta13-1/2)+Cv*Vn13;
      else if a<=xn13&xn13<=b;
              contact=1;
              Fn13 = (Kv/2)*(b-a)*beta13^2+Cv*(3-2*beta13)*beta13^2*Vn13;
           else xn13<a;
                contact=0;
                Fn13 = 0;
          end
      end
      Fn13x = Fn13*cos(alpha13);
      Fn13y = -Fn13*sin(alpha13);
      % caculate the Ff
      if Fn13 == 0;
         Ff13 = 0;
         Ff13x = 0;
         Ff13y = 0;
      else
          Fc13 = u*Fn13; % caculate the friction force.
          z13 = Vt13*(1-sigma0*sign(Vt13)*z13p/abs(Fc13))*dt+z13p;
          %dotz13 = (z13-z13p)/dt;
          Ff13 = sigma0*z13+sigma1*Vt13;
          z13p = z13
          Ff13x = -Ff13*sin(alpha13);
          Ff13y = -Ff13*cos(alpha13);
      end
   else Rj13<R
      xn13 = R-Rj13; % Distance between the node and centerline of tube;
```

```
      Vn13 = v13*sin(-phi13-alpha13+pi/2); % Velocity of catheter in normal
direction;
      Vt13 = v13*cos(-phi13-alpha13+pi/2);
      beta13 = (xn13-a)/(b-a);
      contact=0;
      if xn13>b;
      contact=1;
      Fn13 = Kv*(b-a)*(beta13-1/2)+Cv*Vn13;
      else if a<=xn13&xn13<=b;
              contact=1;
              Fn13 = (Kv/2)*(b-a)*beta13^2+Cv*(3-2*beta13)*beta13^2*Vn13;
           else xn13<a;
                contact=0;
                Fn13 = 0;
          end
      end
      Fn13x = -Fn13*cos(alpha13);
      Fn13y = Fn13*sin(alpha13);
      % caculate the Ff
      if Fn13 == 0;
         Ff13 = 0;
         Ff13x = 0;
         Ff13y = 0;
      else
          Fc13 = u*Fn13; % caculate the friction force.
          z13 = Vt13*(1-sigma0*sign(Vt13)*z13p/abs(Fc13))*dt+z13p;
          %dotz13 = (z13-z13p)/dt;
          Ff13 = sigma0*z13+sigma1*Vt13;
          z13p = z13
          Ff13x = -Ff13*sin(alpha13);
          Ff13y = -Ff13*cos(alpha13);
      end
   end

else 0<=y13&y13<0.05; % the catheter's x-displacement should be restrained.
   Rj13 = sqrt((x13-Ox)^2);
   if Rj13>=R
      xn13 = Rj13-R; % Distance between the node and centerline of tube;
      Vn13 = v13*sin(phi13-pi/2); % Velocity of catheter in normal direction;
      Vt13 = v13*cos(phi13-pi/2);
      beta13 = (xn13-a)/(b-a);
      if xn13>b;
         Fn13 = Kv*(b-a)*(beta13-1/2)+Cv*Vn13;
      else if a<=xn13&xn13<=b;
              Fn13 = (Kv/2)*(b-a)*beta13^2+Cv*(3-2*beta13)*beta13^2*Vn13;
           else xn13<a;
                Fn13 = 0;
           end
      end
      Fn13x = Fn13;
      Fn13y = 0;

      if Fn13 == 0;
         Ff13 = 0;
         Ff13x = 0;
         Ff13y = 0;
```

```
      else
          Fc13 = u*Fn13; % caculate the friction force.
          z13 = Vt13*(1-sigma0*sign(Vt13)*z13p/abs(Fc13))*dt+z13p;
          %dotz13 = (z13-z13p)/dt;
          Ff13 = sigma0*z13+sigma1*Vt13;
          z13p = z13
          Ff13x = 0;
          Ff13y = Ff13;
      end

      % caculate the Ff

   else Rj13<R;
        xn13 = R-Rj13; % Distance between the node and centerline of tube;
        Vn13 = v13*cos(phi13); % Velocity of catheter in normal direction;
        Vt13 = v13*sin(phi13);
        beta13 = (xn13-a)/(b-a);
        if xn13>b;
           Fn13 = Kv*(b-a)*(beta13-1/2)+Cv*Vn13;
        else if a<=xn13&xn13<=b;
                Fn13 = (Kv/2)*(b-a)*beta13^2+Cv*(3-2*beta13)*beta13^2*Vn13;
             else xn13<a;
                  Fn13 = 0;
            end
        end
        Fn13x = -Fn13;
        Fn13y = 0;
      if Fn13 == 0;
          Ff13 = 0;
          Ff13x = 0;
          Ff13y = 0;
      else
          Fc13 = u*Fn13; % caculate the friction force.
          z13 = Vt13*(1-sigma0*sign(Vt13)*z13p/abs(Fc13))*dt+z13p;
          %dotz13 = (z13-z13p)/dt;
          Ff13 = sigma0*z13+sigma1*Vt13;
          z13p = z13
          Ff13x = 0;
          Ff13y = Ff13;
      end

   end
end

F13x = Fn13x+Ff13x;
F13y = Fn13y+Ff13y;

%% Node 15
x15 = x(1,lnp(15,1)); % the x coordinate of the node 1;
y15 = x(1,lnp(15,2)); % the y coordinate of the node 1;
v15 = xp(1,lnp(15,1));
phi15 = x(1,lnp(16,1));

if y15>=0.05; % caculate the contact force Fn.
   Rj15 = sqrt((x15-Ox)^2+(y15-Oy)^2);
   alpha15 = asin((y15-0.05)/Rj15); % rad
```

```
   if Rj15>=R
      xn15 = Rj15-R; % Distance between the node and centerline of tube;
      Vn15 = v15*sin(phi15+alpha15-pi/2); % Velocity of catheter in normal
direction;
      Vt15 = v15*cos(phi15+alpha15-pi/2);
      beta15 = (xn15-a)/(b-a);
      contact=0;
      if xn15>b;
      contact=1;
      Fn15 = Kv*(b-a)*(beta15-1/2)+Cv*Vn15;
      else if a<=xn15&xn15<=b;
              contact=1;
              Fn15 = (Kv/2)*(b-a)*beta15^2+Cv*(3-2*beta15)*beta15^2*Vn15;
           else xn15<a;
                contact=0;
                Fn15 = 0;
          end
      end
      Fn15x = Fn15*cos(alpha15);
      Fn15y = -Fn15*sin(alpha15);
      % caculate the Ff
      if Fn15 == 0;
         Ff15 = 0;
         Ff15x = 0;
         Ff15y = 0;
      else
          Fc15 = u*Fn15; % caculate the friction force.
          z15 = Vt15*(1-sigma0*sign(Vt15)*z15p/abs(Fc15))*dt+z15p;
          %dotz15 = (z15-z15p)/dt;
          Ff15 = sigma0*z15+sigma1*Vt15;
          z15p = z15
          Ff15x = -Ff15*sin(alpha15);
          Ff15y = -Ff15*cos(alpha15);
      end
   else Rj15<R
      xn15 = R-Rj15; % Distance between the node and centerline of tube;
      Vn15 = v15*sin(-phi15-alpha15+pi/2); % Velocity of catheter in normal
direction;
      Vt15 = v15*cos(-phi15-alpha15+pi/2);
      beta15 = (xn15-a)/(b-a);
      contact=0;
      if xn15>b;
      contact=1;
      Fn15 = Kv*(b-a)*(beta15-1/2)+Cv*Vn15;
      else if a<=xn15&xn15<=b;
              contact=1;
              Fn15 = (Kv/2)*(b-a)*beta15^2+Cv*(3-2*beta15)*beta15^2*Vn15;
           else xn15<a;
                contact=0;
                Fn15 = 0;
          end
      end
      Fn15x = -Fn15*cos(alpha15);
      Fn15y = Fn15*sin(alpha15);
      % caculate the Ff
      if Fn15 == 0;
         Ff15 = 0;
```

```
         Ff15x = 0;
         Ff15y = 0;
      else
          Fc15 = u*Fn15; % caculate the friction force.
          z15 = Vt15*(1-sigma0*sign(Vt15)*z15p/abs(Fc15))*dt+z15p;
          %dotz15 = (z15-z15p)/dt;
          Ff15 = sigma0*z15+sigma1*Vt15;
          z15p = z15
          Ff15x = -Ff15*sin(alpha15);
          Ff15y = -Ff15*cos(alpha15);
      end
   end

else 0<=y15&y15<0.05; % the catheter's x-displacement should be restrained.
   Rj15 = sqrt((x15-Ox)^2);
   if Rj15>=R
      xn15 = Rj15-R; % Distance between the node and centerline of tube;
      Vn15 = v15*sin(phi15-pi/2); % Velocity of catheter in normal direction;
      Vt15 = v15*cos(phi15-pi/2);
      beta15 = (xn15-a)/(b-a);
      if xn15>b;
         Fn15 = Kv*(b-a)*(beta15-1/2)+Cv*Vn15;
      else if a<=xn15&xn15<=b;
              Fn15 = (Kv/2)*(b-a)*beta15^2+Cv*(3-2*beta15)*beta15^2*Vn15;
           else xn15<a;
                Fn15 = 0;
           end
      end
      Fn15x = Fn15;
      Fn15y = 0;

      if Fn15 == 0;
         Ff15 = 0;
         Ff15x = 0;
         Ff15y = 0;
      else
          Fc15 = u*Fn15; % caculate the friction force.
          z15 = Vt15*(1-sigma0*sign(Vt15)*z15p/abs(Fc15))*dt+z15p;
          %dotz15 = (z15-z15p)/dt;
          Ff15 = sigma0*z15+sigma1*Vt15;
          z15p = z15
          Ff15x = 0;
          Ff15y = Ff15;
      end

      % caculate the Ff

   else Rj15<R;
        xn15 = R-Rj15; % Distance between the node and centerline of tube;
        Vn15 = v15*cos(phi15); % Velocity of catheter in normal direction;
        Vt15 = v15*sin(phi15);
        beta15 = (xn15-a)/(b-a);
        if xn15>b;
           Fn15 = Kv*(b-a)*(beta15-1/2)+Cv*Vn15;
        else if a<=xn15&xn15<=b;
                Fn15 = (Kv/2)*(b-a)*beta15^2+Cv*(3-2*beta15)*beta15^2*Vn15;
```

```
             else xn15<a;
                  Fn15 = 0;
            end
        end
        Fn15x = -Fn15;
        Fn15y = 0;
      if Fn15 == 0;
          Ff15 = 0;
          Ff15x = 0;
          Ff15y = 0;
      else
          Fc15 = u*Fn15; % caculate the friction force.
          z15 = Vt15*(1-sigma0*sign(Vt15)*z15p/abs(Fc15))*dt+z15p;
          %dotz15 = (z15-z15p)/dt;
          Ff15 = sigma0*z15+sigma1*Vt15;
          z15p = z15
          Ff15x = 0;
          Ff15y = Ff15;
      end

   end
end

F15x = Fn15x+Ff15x;
F15y = Fn15y+Ff15y;

%% Node 17
x17 = x(1,lnp(17,1)); % the x coordinate of the node 1;
y17 = x(1,lnp(17,2)); % the y coordinate of the node 1;
v17 = xp(1,lnp(17,1));
phi17 = x(1,lnp(18,1));

if y17>=0.05; % caculate the contact force Fn.
   Rj17 = sqrt((x17-Ox)^2+(y17-Oy)^2);
   alpha17 = asin((y17-0.05)/Rj17); % rad
   if Rj17>=R
      xn17 = Rj17-R; % Distance between the node and centerline of tube;
      Vn17 = v17*sin(phi17+alpha17-pi/2); % Velocity of catheter in normal
direction;
      Vt17 = v17*cos(phi17+alpha17-pi/2);
      beta17 = (xn17-a)/(b-a);
      contact=0;
      if xn17>b;
      contact=1;
      Fn17 = Kv*(b-a)*(beta17-1/2)+Cv*Vn17;
      else if a<=xn17&xn17<=b;
              contact=1;
              Fn17 = (Kv/2)*(b-a)*beta17^2+Cv*(3-2*beta17)*beta17^2*Vn17;
           else xn17<a;
                contact=0;
                Fn17 = 0;
           end
      end
      Fn17x = Fn17*cos(alpha17);
      Fn17y = -Fn17*sin(alpha17);
      % caculate the Ff
```

```
      if Fn17 == 0;
         Ff17 = 0;
         Ff17x = 0;
         Ff17y = 0;
      else
          Fc17 = u*Fn17; % caculate the friction force.
          z17 = Vt17*(1-sigma0*sign(Vt17)*z17p/abs(Fc17))*dt+z17p;
          %dotz17 = (z17-z17p)/dt;
          Ff17 = sigma0*z17+sigma1*Vt17;
          z17p = z17
          Ff17x = -Ff17*sin(alpha17);
          Ff17y = -Ff17*cos(alpha17);
      end
   else Rj17<R
      xn17 = R-Rj17; % Distance between the node and centerline of tube;
      Vn17 = v17*sin(-phi17-alpha17+pi/2); % Velocity of catheter in normal
direction;
      Vt17 = v17*cos(-phi17-alpha17+pi/2);
      beta17 = (xn17-a)/(b-a);
      contact=0;
      if xn17>b;
      contact=1;
      Fn17 = Kv*(b-a)*(beta17-1/2)+Cv*Vn17;
      else if a<=xn17&xn17<=b;
              contact=1;
              Fn17 = (Kv/2)*(b-a)*beta17^2+Cv*(3-2*beta17)*beta17^2*Vn17;
           else xn17<a;
                contact=0;
                Fn17 = 0;
          end
      end
      Fn17x = -Fn17*cos(alpha17);
      Fn17y = Fn17*sin(alpha17);
      % caculate the Ff
      if Fn17 == 0;
         Ff17 = 0;
         Ff17x = 0;
         Ff17y = 0;
      else
          Fc17 = u*Fn17; % caculate the friction force.
          z17 = Vt17*(1-sigma0*sign(Vt17)*z17p/abs(Fc17))*dt+z17p;
          %dotz17 = (z17-z17p)/dt;
          Ff17 = sigma0*z17+sigma1*Vt17;
          z17p = z17
          Ff17x = -Ff17*sin(alpha17);
          Ff17y = -Ff17*cos(alpha17);
      end
   end

else 0<=y17&y17<0.05; % the catheter's x-displacement should be restrained.
   Rj17 = sqrt((x17-Ox)^2);
   if Rj17>=R
      xn17 = Rj17-R; % Distance between the node and centerline of tube;
      Vn17 = v17*sin(phi17-pi/2); % Velocity of catheter in normal direction;
      Vt17 = v17*cos(phi17-pi/2);
      beta17 = (xn17-a)/(b-a);
      if xn17>b;
```

```
      Fn17 = Kv*(b-a)*(beta17-1/2)+Cv*Vn17;
   else if a<=xn17&xn17<=b;
           Fn17 = (Kv/2)*(b-a)*beta17^2+Cv*(3-2*beta17)*beta17^2*Vn17;
        else xn17<a;
             Fn17 = 0;
        end
   end
   Fn17x = Fn17;
   Fn17y = 0;

   if Fn17 == 0;
      Ff17 = 0;
      Ff17x = 0;
      Ff17y = 0;
   else
       Fc17 = u*Fn17; % caculate the friction force.
       z17 = Vt17*(1-sigma0*sign(Vt17)*z17p/abs(Fc17))*dt+z17p;
       %dotz17 = (z17-z17p)/dt;
       Ff17 = sigma0*z17+sigma1*Vt17;
       z17p = z17
       Ff17x = 0;
       Ff17y = Ff17;
   end

   % caculate the Ff

else Rj17<R;
     xn17 = R-Rj17; % Distance between the node and centerline of tube;
     Vn17 = v17*cos(phi17); % Velocity of catheter in normal direction;
     Vt17 = v17*sin(phi17);
     beta17 = (xn17-a)/(b-a);
     if xn17>b;
        Fn17 = Kv*(b-a)*(beta17-1/2)+Cv*Vn17;
     else if a<=xn17&xn17<=b;
             Fn17 = (Kv/2)*(b-a)*beta17^2+Cv*(3-2*beta17)*beta17^2*Vn17;
          else xn17<a;
               Fn17 = 0;
          end
     end
     Fn17x = -Fn17;
     Fn17y = 0;
   if Fn17 == 0;
       Ff17 = 0;
       Ff17x = 0;
       Ff17y = 0;
   else
       Fc17 = u*Fn17; % caculate the friction force.
       z17 = Vt17*(1-sigma0*sign(Vt17)*z17p/abs(Fc17))*dt+z17p;
       %dotz17 = (z17-z17p)/dt;
       Ff17 = sigma0*z17+sigma1*Vt17;
       z17p = z17
       Ff17x = 0;
       Ff17y = Ff17;
   end

end
```

```
end

F17x = Fn17x+Ff17x;
F17y = Fn17y+Ff17y;

%% Node 19
x19 = x(1,lnp(19,1)); % the x coordinate of the node 1;
y19 = x(1,lnp(19,2)); % the y coordinate of the node 1;
v19 = xp(1,lnp(19,1));
phi19 = x(1,lnp(20,1));

if y19>=0.05; % caculate the contact force Fn.
   Rj19 = sqrt((x19-Ox)^2+(y19-Oy)^2);
   alpha19 = asin((y19-0.05)/Rj19); % rad
   if Rj19>=R
      xn19 = Rj19-R; % Distance between the node and centerline of tube;
      Vn19 = v19*sin(phi19+alpha19-pi/2); % Velocity of catheter in normal
direction;
      Vt19 = v19*cos(phi19+alpha19-pi/2);
      beta19 = (xn19-a)/(b-a);
      contact=0;
      if xn19>b;
      contact=1;
      Fn19 = Kv*(b-a)*(beta19-1/2)+Cv*Vn19;
      else if a<=xn19&xn19<=b;
              contact=1;
              Fn19 = (Kv/2)*(b-a)*beta19^2+Cv*(3-2*beta19)*beta19^2*Vn19;
           else xn19<a;
                contact=0;
                Fn19 = 0;
          end
      end
      Fn19x = Fn19*cos(alpha19);
      Fn19y = -Fn19*sin(alpha19);
      % caculate the Ff
      if Fn19 == 0;
         Ff19 = 0;
         Ff19x = 0;
         Ff19y = 0;
      else
          Fc19 = u*Fn19; % caculate the friction force.
          z19 = Vt19*(1-sigma0*sign(Vt19)*z19p/abs(Fc19))*dt+z19p;
          %dotz19 = (z19-z19p)/dt;
          Ff19 = sigma0*z19+sigma1*Vt19;
          z19p = z19
          Ff19x = -Ff19*sin(alpha19);
          Ff19y = -Ff19*cos(alpha19);
      end
   else Rj19<R
      xn19 = R-Rj19; % Distance between the node and centerline of tube;
      Vn19 = v19*sin(-phi19-alpha19+pi/2); % Velocity of catheter in normal
direction;
      Vt19 = v19*cos(-phi19-alpha19+pi/2);
      beta19 = (xn19-a)/(b-a);
      contact=0;
      if xn19>b;
```

```
      contact=1;
      Fn19 = Kv*(b-a)*(beta19-1/2)+Cv*Vn19;
      else if a<=xn19&xn19<=b;
              contact=1;
              Fn19 = (Kv/2)*(b-a)*beta19^2+Cv*(3-2*beta19)*beta19^2*Vn19;
           else xn19<a;
                contact=0;
                Fn19 = 0;
          end
      end
      Fn19x = -Fn19*cos(alpha19);
      Fn19y = Fn19*sin(alpha19);
      % caculate the Ff
      if Fn19 == 0;
         Ff19 = 0;
         Ff19x = 0;
         Ff19y = 0;
      else
          Fc19 = u*Fn19; % caculate the friction force.
          z19 = Vt19*(1-sigma0*sign(Vt19)*z19p/abs(Fc19))*dt+z19p;
          %dotz19 = (z19-z19p)/dt;
          Ff19 = sigma0*z19+sigma1*Vt19;
          z19p = z19
          Ff19x = -Ff19*sin(alpha19);
          Ff19y = -Ff19*cos(alpha19);
      end
   end

else 0<=y19&y19<0.05; % the catheter's x-displacement should be restrained.
   Rj19 = sqrt((x19-Ox)^2);
   if Rj19>=R
      xn19 = Rj19-R; % Distance between the node and centerline of tube;
      Vn19 = v19*sin(phi19-pi/2); % Velocity of catheter in normal direction;
      Vt19 = v19*cos(phi19-pi/2);
      beta19 = (xn19-a)/(b-a);
      if xn19>b;
         Fn19 = Kv*(b-a)*(beta19-1/2)+Cv*Vn19;
      else if a<=xn19&xn19<=b;
              Fn19 = (Kv/2)*(b-a)*beta19^2+Cv*(3-2*beta19)*beta19^2*Vn19;
           else xn19<a;
                Fn19 = 0;
           end
      end
      Fn19x = Fn19;
      Fn19y = 0;

      if Fn19 == 0;
         Ff19 = 0;
         Ff19x = 0;
         Ff19y = 0;
      else
          Fc19 = u*Fn19; % caculate the friction force.
          z19 = Vt19*(1-sigma0*sign(Vt19)*z19p/abs(Fc19))*dt+z19p;
          %dotz19 = (z19-z19p)/dt;
          Ff19 = sigma0*z19+sigma1*Vt19;
          z19p = z19
```

```
          Ff19x = 0;
          Ff19y = Ff19;
      end

      % caculate the Ff

   else Rj19<R;
        xn19 = R-Rj19; % Distance between the node and centerline of tube;
        Vn19 = v19*cos(phi19); % Velocity of catheter in normal direction;
        Vt19 = v19*sin(phi19);
        beta19 = (xn19-a)/(b-a);
        if xn19>b;
           Fn19 = Kv*(b-a)*(beta19-1/2)+Cv*Vn19;
        else if a<=xn19&xn19<=b;
                Fn19 = (Kv/2)*(b-a)*beta19^2+Cv*(3-2*beta19)*beta19^2*Vn19;
             else xn19<a;
                  Fn19 = 0;
            end
        end
        Fn19x = -Fn19;
        Fn19y = 0;
      if Fn19 == 0;
          Ff19 = 0;
          Ff19x = 0;
          Ff19y = 0;
      else
          Fc19 = u*Fn19; % caculate the friction force.
          z19 = Vt19*(1-sigma0*sign(Vt19)*z19p/abs(Fc19))*dt+z19p;
          %dotz19 = (z19-z19p)/dt;
          Ff19 = sigma0*z19+sigma1*Vt19;
          z19p = z19
          Ff19x = 0;
          Ff19y = Ff19;
      end

   end
end

F19x = Fn19x+Ff19x;
F19y = Fn19y+Ff19y;

%% Node 21
x21 = x(1,lnp(21,1)); % the x coordinate of the node 1;
y21 = x(1,lnp(21,2)); % the y coordinate of the node 1;
v21 = xp(1,lnp(21,1));
phi21 = x(1,lnp(22,1));

if y21>=0.05; % caculate the contact force Fn.
   Rj21 = sqrt((x21-Ox)^2+(y21-Oy)^2);
   alpha21 = asin((y21-0.05)/Rj21); % rad
   if Rj21>=R
      xn21 = Rj21-R; % Distance between the node and centerline of tube;
      Vn21 = v21*sin(phi21+alpha21-pi/2); % Velocity of catheter in normal
direction;
      Vt21 = v21*cos(phi21+alpha21-pi/2);
      beta21 = (xn21-a)/(b-a);
```

```
      contact=0;
      if xn21>b;
      contact=1;
      Fn21 = Kv*(b-a)*(beta21-1/2)+Cv*Vn21;
      else if a<=xn21&xn21<=b;
              contact=1;
              Fn21 = (Kv/2)*(b-a)*beta21^2+Cv*(3-2*beta21)*beta21^2*Vn21;
           else xn21<a;
                contact=0;
                Fn21 = 0;
          end
      end
      Fn21x = Fn21*cos(alpha21);
      Fn21y = -Fn21*sin(alpha21);
      % caculate the Ff
      if Fn21 == 0;
         Ff21 = 0;
         Ff21x = 0;
         Ff21y = 0;
      else
          Fc21 = u*Fn21; % caculate the friction force.
          z21 = Vt21*(1-sigma0*sign(Vt21)*z21p/abs(Fc21))*dt+z21p;
          %dotz21 = (z21-z21p)/dt;
          Ff21 = sigma0*z21+sigma1*Vt21;
          z21p = z21
          Ff21x = -Ff21*sin(alpha21);
          Ff21y = -Ff21*cos(alpha21);
      end
   else Rj21<R
      xn21 = R-Rj21; % Distance between the node and centerline of tube;
      Vn21 = v21*sin(-phi21-alpha21+pi/2); % Velocity of catheter in normal
direction;
      Vt21 = v21*cos(-phi21-alpha21+pi/2);
      beta21 = (xn21-a)/(b-a);
      contact=0;
      if xn21>b;
      contact=1;
      Fn21 = Kv*(b-a)*(beta21-1/2)+Cv*Vn21;
      else if a<=xn21&xn21<=b;
              contact=1;
              Fn21 = (Kv/2)*(b-a)*beta21^2+Cv*(3-2*beta21)*beta21^2*Vn21;
           else xn21<a;
                contact=0;
                Fn21 = 0;
          end
      end
      Fn21x = -Fn21*cos(alpha21);
      Fn21y = Fn21*sin(alpha21);
      % caculate the Ff
      if Fn21 == 0;
         Ff21 = 0;
         Ff21x = 0;
         Ff21y = 0;
      else
          Fc21 = u*Fn21; % caculate the friction force.
          z21 = Vt21*(1-sigma0*sign(Vt21)*z21p/abs(Fc21))*dt+z21p;
          %dotz21 = (z21-z21p)/dt;
```

```
            Ff21 = sigma0*z21+sigma1*Vt21;
            z21p = z21
            Ff21x = -Ff21*sin(alpha21);
            Ff21y = -Ff21*cos(alpha21);
         end
      end

   else 0<=y21&y21<0.05; % the catheter's x-displacement should be restrained.
      Rj21 = sqrt((x21-Ox)^2);
      if Rj21>=R
         xn21 = Rj21-R; % Distance between the node and centerline of tube;
         Vn21 = v21*sin(phi21-pi/2); % Velocity of catheter in normal direction;
         Vt21 = v21*cos(phi21-pi/2);
         beta21 = (xn21-a)/(b-a);
         if xn21>b;
            Fn21 = Kv*(b-a)*(beta21-1/2)+Cv*Vn21;
         else if a<=xn21&xn21<=b;
                 Fn21 = (Kv/2)*(b-a)*beta21^2+Cv*(3-2*beta21)*beta21^2*Vn21;
              else xn21<a;
                   Fn21 = 0;
              end
         end
         Fn21x = Fn21;
         Fn21y = 0;

         if Fn21 == 0;
            Ff21 = 0;
            Ff21x = 0;
            Ff21y = 0;
         else
             Fc21 = u*Fn21; % caculate the friction force.
             z21 = Vt21*(1-sigma0*sign(Vt21)*z21p/abs(Fc21))*dt+z21p;
             %dotz21 = (z21-z21p)/dt;
             Ff21 = sigma0*z21+sigma1*Vt21;
             z21p = z21
             Ff21x = 0;
             Ff21y = Ff21;
         end

         % caculate the Ff

      else Rj21<R;
           xn21 = R-Rj21; % Distance between the node and centerline of tube;
           Vn21 = v21*cos(phi21); % Velocity of catheter in normal direction;
           Vt21 = v21*sin(phi21);
           beta21 = (xn21-a)/(b-a);
           if xn21>b;
              Fn21 = Kv*(b-a)*(beta21-1/2)+Cv*Vn21;
           else if a<=xn21&xn21<=b;
                   Fn21 = (Kv/2)*(b-a)*beta21^2+Cv*(3-2*beta21)*beta21^2*Vn21;
                else xn21<a;
                     Fn21 = 0;
                end
           end
           Fn21x = -Fn21;
           Fn21y = 0;
```

```
      if Fn21 == 0;
          Ff21 = 0;
          Ff21x = 0;
          Ff21y = 0;
      else
          Fc21 = u*Fn21; % caculate the friction force.
          z21 = Vt21*(1-sigma0*sign(Vt21)*z21p/abs(Fc21))*dt+z21p;
          %dotz21 = (z21-z21p)/dt;
          Ff21 = sigma0*z21+sigma1*Vt21;
          z21p = z21
          Ff21x = 0;
          Ff21y = Ff21;
      end

   end
end

F21x = Fn21x+Ff21x;
F21y = Fn21y+Ff21y;

%% Node 23
x23 = x(1,lnp(23,1)); % the x coordinate of the node 1;
y23 = x(1,lnp(23,2)); % the y coordinate of the node 1;
v23 = xp(1,lnp(23,1));
phi23 = x(1,lnp(24,1));

if y23>=0.05; % caculate the contact force Fn.
   Rj23 = sqrt((x23-Ox)^2+(y23-Oy)^2);
   alpha23 = asin((y23-0.05)/Rj23); % rad
   if Rj23>=R
      xn23 = Rj23-R; % Distance between the node and centerline of tube;
      Vn23 = v23*sin(phi23+alpha23-pi/2); % Velocity of catheter in normal
direction;
      Vt23 = v23*cos(phi23+alpha23-pi/2);
      beta23 = (xn23-a)/(b-a);
      contact=0;
      if xn23>b;
      contact=1;
      Fn23 = Kv*(b-a)*(beta23-1/2)+Cv*Vn23;
      else if a<=xn23&xn23<=b;
              contact=1;
              Fn23 = (Kv/2)*(b-a)*beta23^2+Cv*(3-2*beta23)*beta23^2*Vn23;
           else xn23<a;
                contact=0;
                Fn23 = 0;
          end
      end
      Fn23x = Fn23*cos(alpha23);
      Fn23y = -Fn23*sin(alpha23);
      % caculate the Ff
      if Fn23 == 0;
         Ff23 = 0;
         Ff23x = 0;
         Ff23y = 0;
      else
          Fc23 = u*Fn23; % caculate the friction force.
```

```
          z23 = Vt23*(1-sigma0*sign(Vt23)*z23p/abs(Fc23))*dt+z23p;
          %dotz23 = (z23-z23p)/dt;
          Ff23 = sigma0*z23+sigma1*Vt23;
          z23p = z23
          Ff23x = -Ff23*sin(alpha23);
          Ff23y = -Ff23*cos(alpha23);
      end
   else Rj23<R
      xn23 = R-Rj23; % Distance between the node and centerline of tube;
      Vn23 = v23*sin(-phi23-alpha23+pi/2); % Velocity of catheter in normal
direction;
      Vt23 = v23*cos(-phi23-alpha23+pi/2);
      beta23 = (xn23-a)/(b-a);
      contact=0;
      if xn23>b;
      contact=1;
      Fn23 = Kv*(b-a)*(beta23-1/2)+Cv*Vn23;
      else if a<=xn23&xn23<=b;
             contact=1;
             Fn23 = (Kv/2)*(b-a)*beta23^2+Cv*(3-2*beta23)*beta23^2*Vn23;
           else xn23<a;
                contact=0;
                Fn23 = 0;
          end
      end
      Fn23x = -Fn23*cos(alpha23);
      Fn23y = Fn23*sin(alpha23);
      % caculate the Ff
      if Fn23 == 0;
         Ff23 = 0;
         Ff23x = 0;
         Ff23y = 0;
      else
          Fc23 = u*Fn23; % caculate the friction force.
          z23 = Vt23*(1-sigma0*sign(Vt23)*z23p/abs(Fc23))*dt+z23p;
          %dotz23 = (z23-z23p)/dt;
          Ff23 = sigma0*z23+sigma1*Vt23;
          z23p = z23
          Ff23x = -Ff23*sin(alpha23);
          Ff23y = -Ff23*cos(alpha23);
      end
   end

else 0<=y23&y23<0.05; % the catheter's x-displacement should be restrained.
   Rj23 = sqrt((x23-Ox)^2);
   if Rj23>=R
      xn23 = Rj23-R; % Distance between the node and centerline of tube;
      Vn23 = v23*sin(phi23-pi/2); % Velocity of catheter in normal direction;
      Vt23 = v23*cos(phi23-pi/2);
      beta23 = (xn23-a)/(b-a);
      if xn23>b;
         Fn23 = Kv*(b-a)*(beta23-1/2)+Cv*Vn23;
      else if a<=xn23&xn23<=b;
             Fn23 = (Kv/2)*(b-a)*beta23^2+Cv*(3-2*beta23)*beta23^2*Vn23;
           else xn23<a;
                Fn23 = 0;
           end
```

```
      end
      Fn23x = Fn23;
      Fn23y = 0;

      if Fn23 == 0;
         Ff23 = 0;
         Ff23x = 0;
         Ff23y = 0;
      else
          Fc23 = u*Fn23; % caculate the friction force.
          z23 = Vt23*(1-sigma0*sign(Vt23)*z23p/abs(Fc23))*dt+z23p;
          %dotz23 = (z23-z23p)/dt;
          Ff23 = sigma0*z23+sigma1*Vt23;
          z23p = z23
          Ff23x = 0;
          Ff23y = Ff23;
      end

      % caculate the Ff

   else Rj23<R;
        xn23 = R-Rj23; % Distance between the node and centerline of tube;
        Vn23 = v23*cos(phi23); % Velocity of catheter in normal direction;
        Vt23 = v23*sin(phi23);
        beta23 = (xn23-a)/(b-a);
        if xn23>b;
           Fn23 = Kv*(b-a)*(beta23-1/2)+Cv*Vn23;
        else if a<=xn23&xn23<=b;
                Fn23 = (Kv/2)*(b-a)*beta23^2+Cv*(3-2*beta23)*beta23^2*Vn23;
             else xn23<a;
                  Fn23 = 0;
            end
        end
        Fn23x = -Fn23;
        Fn23y = 0;
      if Fn23 == 0;
          Ff23 = 0;
          Ff23x = 0;
          Ff23y = 0;
      else
          Fc23 = u*Fn23; % caculate the friction force.
          z23 = Vt23*(1-sigma0*sign(Vt23)*z23p/abs(Fc23))*dt+z23p;
          %dotz23 = (z23-z23p)/dt;
          Ff23 = sigma0*z23+sigma1*Vt23;
          z23p = z23
          Ff23x = 0;
          Ff23y = Ff23;
      end

   end
end

F23x = Fn23x+Ff23x;
F23y = Fn23y+Ff23y;

%% Node 25
```

```
x25 = x(1,lnp(25,1)); % the x coordinate of the node 1;
y25 = x(1,lnp(25,2)); % the y coordinate of the node 1;
v25 = xp(1,lnp(25,1));
phi25 = x(1,lnp(26,1));

if y25>=0.05; % caculate the contact force Fn.
   Rj25 = sqrt((x25-Ox)^2+(y25-Oy)^2);
   alpha25 = asin((y25-0.05)/Rj25); % rad
   if Rj25>=R
      xn25 = Rj25-R; % Distance between the node and centerline of tube;
      Vn25 = v25*sin(phi25+alpha25-pi/2); % Velocity of catheter in normal
direction;
      Vt25 = v25*cos(phi25+alpha25-pi/2);
      beta25 = (xn25-a)/(b-a);
      contact=0;
      if xn25>b;
      contact=1;
      Fn25 = Kv*(b-a)*(beta25-1/2)+Cv*Vn25;
      else if a<=xn25&xn25<=b;
              contact=1;
              Fn25 = (Kv/2)*(b-a)*beta25^2+Cv*(3-2*beta25)*beta25^2*Vn25;
           else xn25<a;
                contact=0;
                Fn25 = 0;
          end
      end
      Fn25x = Fn25*cos(alpha25);
      Fn25y = -Fn25*sin(alpha25);
      % caculate the Ff
      if Fn25 == 0;
         Ff25 = 0;
         Ff25x = 0;
         Ff25y = 0;
      else
          Fc25 = u*Fn25; % caculate the friction force.
          z25 = Vt25*(1-sigma0*sign(Vt25)*z25p/abs(Fc25))*dt+z25p;
          %dotz25 = (z25-z25p)/dt;
          Ff25 = sigma0*z25+sigma1*Vt25;
          z25p = z25
          Ff25x = -Ff25*sin(alpha25);
          Ff25y = -Ff25*cos(alpha25);
      end
   else Rj25<R
      xn25 = R-Rj25; % Distance between the node and centerline of tube;
      Vn25 = v25*sin(-phi25-alpha25+pi/2); % Velocity of catheter in normal
direction;
      Vt25 = v25*cos(-phi25-alpha25+pi/2);
      beta25 = (xn25-a)/(b-a);
      contact=0;
      if xn25>b;
      contact=1;
      Fn25 = Kv*(b-a)*(beta25-1/2)+Cv*Vn25;
      else if a<=xn25&xn25<=b;
              contact=1;
              Fn25 = (Kv/2)*(b-a)*beta25^2+Cv*(3-2*beta25)*beta25^2*Vn25;
           else xn25<a;
                contact=0;
```

```
                Fn25 = 0;
            end
        end
        Fn25x = -Fn25*cos(alpha25);
        Fn25y = Fn25*sin(alpha25);
        % caculate the Ff
        if Fn25 == 0;
           Ff25 = 0;
           Ff25x = 0;
           Ff25y = 0;
        else
            Fc25 = u*Fn25; % caculate the friction force.
            z25 = Vt25*(1-sigma0*sign(Vt25)*z25p/abs(Fc25))*dt+z25p;
            %dotz25 = (z25-z25p)/dt;
            Ff25 = sigma0*z25+sigma1*Vt25;
            z25p = z25
            Ff25x = -Ff25*sin(alpha25);
            Ff25y = -Ff25*cos(alpha25);
        end
    end

else 0<=y25&y25<0.05; % the catheter's x-displacement should be restrained.
    Rj25 = sqrt((x25-Ox)^2);
    if Rj25>=R
        xn25 = Rj25-R; % Distance between the node and centerline of tube;
        Vn25 = v25*sin(phi25-pi/2); % Velocity of catheter in normal direction;
        Vt25 = v25*cos(phi25-pi/2);
        beta25 = (xn25-a)/(b-a);
        if xn25>b;
           Fn25 = Kv*(b-a)*(beta25-1/2)+Cv*Vn25;
        else if a<=xn25&xn25<=b;
                Fn25 = (Kv/2)*(b-a)*beta25^2+Cv*(3-2*beta25)*beta25^2*Vn25;
             else xn25<a;
                  Fn25 = 0;
             end
        end
        Fn25x = Fn25;
        Fn25y = 0;

        if Fn25 == 0;
           Ff25 = 0;
           Ff25x = 0;
           Ff25y = 0;
        else
            Fc25 = u*Fn25; % caculate the friction force.
            z25 = Vt25*(1-sigma0*sign(Vt25)*z25p/abs(Fc25))*dt+z25p;
            %dotz25 = (z25-z25p)/dt;
            Ff25 = sigma0*z25+sigma1*Vt25;
            z25p = z25
            Ff25x = 0;
            Ff25y = Ff25;
        end

        % caculate the Ff

    else Rj25<R;
```

```
        xn25 = R-Rj25; % Distance between the node and centerline of tube;
        Vn25 = v25*cos(phi25); % Velocity of catheter in normal direction;
        Vt25 = v25*sin(phi25);
        beta25 = (xn25-a)/(b-a);
        if xn25>b;
           Fn25 = Kv*(b-a)*(beta25-1/2)+Cv*Vn25;
        else if a<=xn25&xn25<=b;
                Fn25 = (Kv/2)*(b-a)*beta25^2+Cv*(3-2*beta25)*beta25^2*Vn25;
             else xn25<a;
                  Fn25 = 0;
            end
        end
        Fn25x = -Fn25;
        Fn25y = 0;
      if Fn25 == 0;
          Ff25 = 0;
          Ff25x = 0;
          Ff25y = 0;
      else
          Fc25 = u*Fn25; % caculate the friction force.
          z25 = Vt25*(1-sigma0*sign(Vt25)*z25p/abs(Fc25))*dt+z25p;
          %dotz25 = (z25-z25p)/dt;
          Ff25 = sigma0*z25+sigma1*Vt25;
          z25p = z25
          Ff25x = 0;
          Ff25y = Ff25;
      end

   end
end

F25x = Fn25x+Ff25x;
F25y = Fn25y+Ff25y;

%% Apply Fn and Ff to each node.
f = [3  1   F3x
     3  2   F3y
     5  1   F5x
     5  2   F5y
     7  1   F7x
     7  2   F7y
     9  1   F9x
     9  2   F9y
     11  1   F11x
     11  2   F11y
     13  1   F13x
     13  2   F13y
     15  1   F15x
     15  2   F15y
     17  1   F17x
     17  2   F17y
     19  1   F19x
     19  2   F19y
     21  1   F21x
     21  2   F21y
     23  1   F23x
```

```
23  2   F23y
25  1   F25x
25  2   F25y]
```

D.3 Codes for the user defined input motion

```
function [t,e, x]=MOTION(t, is)
t = t;
time = t;
e = [];
A = 0.0009;
w = 8*pi;
x1 = A.*sin(w.*t)-0.04;
v1 = A.*w.*cos(w.*t);
a1 = -A.*w.*w.*sin(w.*t);
x = [25 2 x1 v1 a1]
```